Evaluation of geno- and phenotypic alterations in Luminal B breast cancer using tumor mice (TM) and humanized tumor mice (HTM)

Dissertation
zur Erlangung des Doktorgrades
der Biomedizinischen Wissenschaften
(Dr. rer. physiol.)

der
Fakultät für Medizin
der Universität Regensburg

vorgelegt von
Eva-Maria Rom-Jurek
aus
Weiden i.d.Opf.

im Jahr
2020

Dekan:	Prof. Dr. Dr. Torsten E. Reichert
Betreuer:	Prof. Dr. med. vet. Anja-Katrin Wege
Tag der mündlichen Prüfung:	

Für meine Eltern Elisabeth und Werner Rom, meine Kinder Jonathan und Nicolas und meinen Mann Ben

Parts of this work have already been published in peer-reviewed journals in an open-access format:

Rom-Jurek, E.-M., Kirchhammer, N., Ugocsai, P., Ortmann, O., Wege, A.K. and Brockhoff, G. (2018), “Regulation of Programmed Death Ligand 1 (PD-L1) Expression in Breast Cancer Cell Lines In Vitro and in Immunodeficient and Humanized Tumor Mice”, *International journal of molecular sciences*, Vol. 19 No. 2.

The content of this thesis is unpublished but in preparation:

Rom-Jurek E.-M., Wege, Brockhoff, Denkert, Jank, Trumpp, Klein, Irlbeck, Pfarr, Weichert, et al: “MDM2 gene amplification in Luminal B tumors is associated with increased aggressiveness and metastatic potential in humanized tumor mice (HTM).” *(in preparation)*

Table of content

Zusammenfassung **6**
Summary **9**
1. Introduction **11**
1.1 From breast physiology to the pathophysiology of Luminal B breast cancer 11
1.1.1 Different cell types involved in breast (cancer) physiology 11
1.1.2 Breast cancer etiology 12
1.1.3 Classification of breast cancer and breast cancer subentities 13
1.1.4 Luminal breast cancer 14
1.2 Breast cancer metastases 15
1.2.1 Metastatic sites in breast cancer 15
1.2.2 EMT and MET in breast cancer metastases 16
1.2.3 Stem cells traits and their relevance in EMT-MET and breast cancer metastases 17
1.2.4 Disseminated tumor cells (DTCs) 20
1.3 The role of genetic aberrations in breast cancer 20
1.4 TILs and immune checkpoints in breast cancer 21
1.5 PDX models and humanized PDX models in breast cancer research 22
1.6 Aim of the thesis 26
2. Material **27**
2.1 Consumables 27
2.2 Buffers and Solutions 27
2.3 Buffers 28
2.4 Culture Media 29
2.5 Cell lines 29
2.6 Anesthesia 29
2.7 Antibodies Flow Cytometry 30
2.8 Antibody Immunohistochemical Staining 31
2.9 Kits 31
2.10 siRNA 32
2.11 Reagents and chemicals 32
2.12 Devices 33
2.13 Software 33
3 Methods **34**
3.1 Human sample preparation 34
3.1.1 Isolation of tumor cells from serous effusions 34
3.1.2 Primary tumor tissue 35

3.1.3 Isolation of hematopoietic stem cells from cord blood 35
3.2 Animal Experiments 37
3.2.1 Experimental Design 37
3.2.2 Generation of tumor mice (TM) 39
3.2.3 Generation of humanized tumor mice (HTM) 41
3.2.4 Preparation of blood, organs and tumor tissue 42
3.3 Flow cytometry 44
3.3.1 Phenotypic Analysis 44
3.3.2 Apoptosis 45
3.3.3 S-phase fraction 46
3.4 Human -Mouse PCR 46
3.4.1 DNA extraction and quantitative real-time PCR 46
3.5 Immunohistochemical Staining 50
3.6 Analysis of Lung metastases 51
3.7 Fluorescence in-situ-hybridisation (FISH) 51
3.8 Cell culture and cryopreservation 52
3.9 Protein biochemical analysis 53
3.9.1 Protein isolation 53
3.9.2.BCA Assay 53
3.9.3. Western Blotting 54
3.10 Breast cancer cell line treatments and assays 55
3.10.1 Experimental Design 55
3.10.2 MDM2 siRNA Knockdown 56
3.10.3 AMG232 treatment 57
3.10.4 Wound Healing Assay 57
3.11 Bone Marrow DTC (disseminated cancer cell) single-cell analysis (Cooperation with Christoph Klein and Christoph Irlbeck UKR) 58
3.11.1 PDX BM staining for DTC detection 58
3.11.2 Single cells isolation and whole genome amplification (WGA) performed by Christoph Irlbeck 58
3.11.3 Control and quality PCR of WGA product 59
3.11.4 Gel electrophoresis 60
3.11.5 Reamplification 61
3.11.6 Low pass-sequencing for copy number alteration profiling (performed by Christoph Irlbeck) 61
3.11.7 Preparation of Ref Sequ files and analysis by progenetix software 62
3.12 Panel Sequencing (Performed by Nicole Pfarr and Wilko Weichert TUM) 62
3.12.1 DNA Isolation of FFPE tissue 62
3.12.2 Sequencing Panels 63

3.12.3 Massive parallel sequencing....63
3.12.4 Data analysis and prediction of copy number variations....64
3.13 Statistical analyses....64
4 Results....66
4.1 Primary tumor patient samples....66
4.2 Characterization of the primary tumor specimen....70
4.2.1 Phenotypical characterization of patient Luminal A and B tumor cells using (stem cell FACS) SCF panel....70
4.2.2 Immune cell infiltration in primary Luminal patient tumors....72
4.2.3 T cell phenotyping of TILs in the primary tumors of Luminal patients....74
4.2.4 Tumor cell phenotyping and immune cell characterization in solid tumors compared to effusions (metastases) of Luminal B patients....76
4.2.5 Primary tumor culturing....78
4.3 Characterization of all Luminal B tumor mice (TM)....79
4.3.1 Engraftment success of primary tumors in TM (tumor mice)....79
4.3.2 Total engraftment numbers of tumors in TM and HTM....80
4.3.3 Characterization of human origin in PDX tumors....81
4.3.4 The immunohistochemical phenotype of the PDX tumor is congruent with the patients' primary tumor....81
4.4 MDM2 /TP53 /MDM4 alterations in Luminal B breast cancer PDX....84
4.4.1 Uncovered alterations in Luminal B breast cancer by Panel Sequencing....84
4.4.2 Classification of PDX models according to chromosomal aberrations of MDM2 and p53....87
4.4.3 Classification of PDX models according to the MDM2 and p53 protein levels....88
4.4.4 MDM2 amplification increased tumor weight and tumor volume over time, decreased the disease-free survival but did not alter the overall survival....89
4.4.5 Phenotypic differences and alterations in the MIC population ($CD44^+/cMET^+/CD47^+$) between TM MDM2 amplified tumors and TM MDM2 WT tumors....90
4.4.6 MDM2 amplified tumors promote lung metastases and differ phenotypically from the corresponding tumor....93
4.4.7 MDM2 amplification decreases T-cell infiltration in HTM....94
4.4.8 Effect of MDM2 amplification in Luminal B humanized PDX mice....96
4.4.9 HTM MDM2 amplified tumors promote lung metastases that differ phenotypically from the corresponding tumor....97
4.4.11 Copy number variation low pass-sequencing of the Luminal B HTM P and TM P PDX model....99
4.4.12 Metastatic potential of generated PDX and the genetic aberrations of HTM and TM tumors....102
4.5 The relevance of immune checkpoints (PD-L1) in Luminal breast cancer....102
4.6 Targeting MDM2 in ZR-75-1 breast cancer cell line *in vitro*....105

4.6.1 Effect of MDM2 knockdown on apoptosis, S-phase fraction, and cell number 105
4.6.2 Effect of AMG232 inhibition on apoptosis, S-phase fraction, and cell number.....108
4.6.3 MDM2 knockdown increases apoptosis *via* the p53 pathway 110
5. Discussion 112
5.1. Luminal B breast cancer PDX models and Luminal B primary tumor cell culturing ...112
5.2. Genomic and phenotypic markers that could identify a high-risk Luminal B tumor ...117
5.2.1 Genomic markers 117
5.2.2 Phenotypic markers.....120
5.3 Immune cell interactions and immune cell checkpoint relevance in Luminal B breast cancer.....122
5.4 Genotypic differences between the primary tumor and bone marrow DTCs 125
5.5 Organotropism in Luminal B breast cancer due to genetic alterations 127
5.6 Conclusion.....128
References.....129
List of abbreviations 144
List of tables.....146
List of figures 147
Acknowledgements.....149
Selbständigkeitserklärung.....151
Curriculum vitae.....152

Zusammenfassung

Luminal B Brustkrebs tritt bei 20 % aller diagnostizierten Mammakarzinome auf. Jedoch haben Patientinnen bei dieser Diagnose nur eine 50 prozentige Überlebenswahrscheinlichkeit für die nächsten 5 Jahre. Hierbei zählt vor allem ein Rückfall oder die spätere Metastasierung nach wie vor zu den häufigsten Todesursachen, auch wenn es zwischenzeitlich einige Fortschritte in deren Behandlung gibt. Dennoch stellt vor allem die Risikoeinschätzung, die ein potentielles Rezidiv und/oder die Manifestierung von Fernmetastasen vorhersagt, ein Problem dar. Die gängigen Marker die hierzu verwendet werden, wie der Hormonrezeptor Status, die Proliferationsindizes, die Zelldifferenzierung und genetischen „Assays“ reichen nicht aus, um Luminal B Patientinnen in „Hoch und „Niedrig-Risikogruppen“ einzuteilen. Deshalb war die Zielsetzung dieses Projekts Marker zu identifizieren, die eine Einteilung der hoch aggressiven Luminal B Tumoren ermöglichen und Tumorzelldisseminierung und Metastasierung vorhersagen. Diese sollen es erleichtern eine Therapieentscheidung zu treffen und zusätzlich die Frage beantworten, ob eine Luminal B Brustkrebspatientin Chemotherapie benötigt oder nicht.

Um diese Fragen zu beantworten, wurden die Primärtumore der Luminal B Patientinnen phänotypisch untersucht. Gleichzeitig wurden aus den Primärtumoren sogenannte Luminal B Xenotransplantations-Modelle generiert (Tumormäuse TM) und analysiert. Zudem sollte auch der Einfluss des humanen Immunsystems auf Luminal B Tumoren analysiert werden, was durch das Generieren der humanisierten Tumormäuse (HTM) ermöglicht wurde. Phänotypisch zeigte sich, dass man Luminal B Tumoren anhand der erhöhten **CD24** Expression im Vergleich zu Luminal A ermitteln kann. Zudem zeigte sich bei den primären Luminal B Hoch-Risikotumoren (definiert durch Todesfall der Patientin, Rückfall oder Metastasierung, und durch das Anwachsen eines Luminal B Tumors als Xenotransplantations-Model) ein erhöhtes Vorkommen der Co-expression von **CD44/cMET/CD47** der sogenannten Metastasierungs-initiierenden Zellpopulation im Vergleich zu Luminal B Niedrig-Risikotumoren (alle Patientinnen, die überlebt haben; keinen Rückfall erlitten und bei welchen der Tumor nicht im Xenograftmodel angewachsen ist). Zusätzlich konnte beim phänotypischen Vergleich von Luminal B Primärtumoren und der zugehörigen Metastase eine erhöhte Expression von **cMET** und **CD44** nachgewiesen werden. Dies

zeigte sich sowohl beim Vergleich von TM oder HTM Tumoren mit der dazugehörigen Lungenmetastase, als auch bei den Primärtumoren der Patientinnen die mit Luminal B Aszites Präparaten oder Pleuraergüssen verglichen wurden. Es konnte auch ein erhöhtes **CD4/CD8** Verhältnis auf Immunzellen, die den Tumor infiltrieren, in Luminal B Hoch-Risikotumoren nachgewiesen werden. Eine der wichtigsten Entdeckungen dieser Arbeit stellte dabei das vermehrte Auftreten einer MDM2 Amplifikation in Luminalen Tumoren dar. Diese zeigte sich mit erhöhter Tumoraggressivität und einer hohen Metastasierungswahrscheinlichkeit in Luminal B TM und HTM. In TM und HTM wiesen **MDM2 amplifizierte** Tumore zudem häufig Lungenmetastasen und disseminierte Zellen im Knochenmark auf. Diese Ergebnisse wurden in Zellkulturversuchen durch eine Herunterregulierung von MDM2 validiert und zeigten dabei einen p53 abhängigen Mechanismus, der die Proliferation und Apoptose der Tumorzellen steuert. Im Einklang mit diesen Ergebnissen stand auch die Behandlung der Zellen mit einem MDM2 Inhibitor (AMG232) und liefert dadurch einen klinisch relevanten Ansatz zur Therapie von MDM2 amplifizierten Tumoren. Zudem wurden genetische **TP53 Mutationen** in Luminal B Tumoren mit erhöhter Disseminierung von Tumorzellen ins Knochenmark in Verbindung gebracht. Die **Amplifikation von MDM4** in Luminal B Tumoren zeigte in der TM hingegen sogar eine Metastasierung des Tumors in multiple Organe wie der Lunge, der Leber, des Gehirns, und des Knochenmarks. Interessanterweise regulieren sich alle entdeckten genomischen Aberrationen (MDM2/P53/MDM4) gegenseitig und gehören zum gleichen Signalweg. Das wiederum deutet auf eine wichtige Rolle von MDM2, p53 und MDM4 beim aggressiven Luminal B Mammakarzinom hin. Auffallend hierbei sind nicht nur die Aggressivität der Tumore, sondern auch die aberrationsabhängige Metastasierung in bestimmte Organe. Ein weiterer Teil dieser Arbeit beschäftigte sich mit den genetischen Unterschieden zwischen Einzelzellen aus dem Primärtumor und disseminierten Tumorzellen im Knochenmark in der TM und HTM. Hierbei konnte gezeigt werden, dass die Tumorzellen aus dem Primärtumor (TM und HTM) und die disseminierten Tumorzellen aus dem Knochenmark unterschiedliche Cluster bilden und damit unterschiedliche genetische Modifikationen aufweisen. Interessanterweise differenzierten sich zudem disseminierte Tumorzellen aus dem Knochenmark von HTM von allen anderen Tumorzellen und auch den disseminierten Zellen aus der TM. Dies deutet auf einen möglichen Selektionsdruck auf Zellen mit bestimmter genetischer Ausstattung hin, der in der Peripherie von humanen Immunzellen

verursacht wird. Zudem kann dies aber auch auf Knochenmarksnischen-bedingte Selektion, die durch humane Immunzellen verändert wird, zurückgeführt werden. Insgesamt zeigte sich in diesen Experimenten die generell geringe Immunogenität von Luminal B Tumoren sowohl auf Patientenebene als auch in der HTM. Somit spiegelt das HTM Xenotransplantations-Modell die Situation im Luminal B Patienten erfolgreich wider und ist damit auch ein Modell für zukünftige Therapiestudien für dieses Patientenkollektiv.

Zusammenfassend zeigte sich, dass Luminal B Xenotransplantations-Modelle und humanisierte Luminal B Xenotransplantations-Modelle ein geeignetes System zur Identifizierung von phäno- und genotypischen Veränderungen sind, die mit einem erhöhten Metastasierungspotential und einer erhöhten Aggressivität einhergehen. Zurzeit werden MDM2 Amplifikationen und Expressionen im Zusammenhang mit dem (tumorfreien) Überleben an einem größeren Patientenkollektiv in unserem Labor untersucht. Weitere klinische Studien könnten dann zeigen, ob Luminal B Brustkrebspatientinnen mit Tumoren, die eine MDM2/MDM4/TP53 Veränderungen aufweisen, zusätzlich von einer Chemotherapie oder eventuell von einer zielgerichteten Inhibition von MDM2 profitieren würden.

Summary

The breast cancer subtype Luminal B is diagnosed in 20% of all breast cancer cases whereas only 50 % of the patients are still alive 5 years after the first diagnosis. Despite the advances in treatment, patients suffering from Luminal B breast cancer frequently experience a relapse or develop distant metastases. Besides the current strategy of hormone-receptor-positivity, proliferation indices, grading, and gene signature assays to categorize the Luminal breast cancer patients into high and low-risk groups, there is still a lack of appropriate markers that reliably predict events of recurrence. Overall, this thesis aims to identify biomarkers that are associated with aggressivity, cell dissemination and/or metastases formation. Importantly these markers might contribute to the therapy decision if Luminal B breast cancer patients need a chemotherapeutic intervention or not.

Therefore, the primary Luminal B patient samples were analyzed and PDX models were generated by the transplantation of primary Luminal B patient samples into NSG mice, the so-called tumor mouse (TM). Additionally, humanized Luminal B tumor mice (HTM) were generated and assessed under the influence of the human immune system. The phenotypic analysis of the primary patient samples revealed that a high expression of **CD24** in Luminal B breast cancer patients differs from Luminal A breast cancer patients**.** The occurrence of MICs **($CD44^+/cMET^+/CD47^+$)** in the high-risk Luminal B tumors (patients that died, suffered from a relapse, or when the PDX model was successful) compared with low-risk Luminal B tumors (patients that are alive, without a relapse, and where the PDX model failed) could serve as a marker for the identification of high-risk Luminal B breast cancer patients. Remarkably, tumor cells of lung metastases differed phenotypically to those of the primary tumor, showing an increased **CD44** and **cMET** expression in the TM, as well as in the patient metastases (e.g. pleural effusion and ascites). Enhanced expression of cMET and CD44 in Luminal B metastases were determined to be independent of the absence or the presence of a human immune system. Moreover, an increased **CD4/CD8** ratio was determined as an indicator of a high-risk Luminal B tumor. However, the most important finding was the dependence of **MDM2** amplification to form highly aggressive tumors accompanied by the high probability for metastatic spread in Luminal B TM and HTM. When MDM2 was amplified in tumors, the metastases preferentially were found in the lung of the PDX model, and DTCs in the bone marrow. This means that an amplification of MDM2 in

Summary

Luminal breast cancer characterizes the patients as high-risk patients. These findings were confirmed *in vitro* by a MDM2 knockdown experiment, showing a p53 mediated mechanism of apoptosis and cell proliferation. Targeting MDM2 by AMG232 inhibition revealed increased apoptosis and reduced proliferation, which demonstrated the potential clinical relevance. **TP53** mutation was also detected as a high-risk marker in Luminal B TM as this alteration in the primary tumor promoted BM DTCs. **MDM4** amplification was verified to promote metastatic spread into various organs, such as the lung, the liver, the brain, and the BM, and subclassifies the tumor as a high-risk tumor. All the determined genomic alterations of MDM2, p53, and MDM4 regulate each other, which shows the importance of the pathway for high-risk Luminal B breast cancer.

Single cell sequencing revealed one cluster formation of primary tumor with specific genomic losses and gains and another cluster mainly formed by DTCs. The differences in copy number profiles were preferentially shown by DTCs that derived from HTM PDX but not from TM, implicating a selection pressure in the periphery potentially evoked by human immune cells. Moreover, a selection determined by the bone marrow niche, which is altered by human immune cells in the HTM, could enable DTCs with a special genetic profile to colonize. The low immunogenicity of Luminal B tumors was demonstrated in primary patient samples and in the HTM, rendering the Luminal B HTM PDX as an adequate model to analyze Luminal B breast cancer. These models could be useful for preclinical immune-modulatory studies in Luminal B breast cancer in the future.

In summary, we showed the suitability of Luminal B PDX and humanized PDX models that are able to identify geno- and phenotypic markers that predict a high potential for metastatic spread and aggressiveness of the tumor. However, prospectively further studies on MDM2 amplification and MDM2 expression in Luminal B breast cancer have to be validated in large patient cohorts. Further clinical studies should determine if breast cancer patients with genetic MDM2/MDM4/TP53 predisposition might additionally benefit from cytotoxic intervention or from specific MDM2 targeting (e.g., by MDM2 inhibitors).

1. Introduction

Suffering from breast cancer metastases is the final and fatal step in the progression of Luminal B breast cancer. Despite the stratification of hormone receptor-positive Luminal B tumors by means of molecular intrinsic marker like the proliferation index (> 14%), the grading, and molecular assays for risk assessment, there is still a lack of appropriate markers to identify the high-risk Luminal B tumors, that might metastasize. While Luminal A (low-risk) tumors can be treated efficiently, Luminal B high-risk tumors have an unfavorable outcome of disease. The worse prognosis is mainly determined by therapy resistance and the development of distant metastases after a long latency. Therefore, it is important to understand the biology of Luminal B breast cancer as well as the metastatic driver molecules. Moreover, the influence of human immune cells should be taken into account to detect appropriate markers for the better identification of Luminal B high-risk breast cancer.

1.1 From breast physiology to the pathophysiology of Luminal B breast cancer

1.1.1 Different cell types involved in breast (cancer) physiology

Before birth, until puberty, in the reproductive phase, during pregnancy and after menopause, the mammary gland is subjected to continuous remodeling processes that are due to the hormonal changes (Macias and Hinck, 2012). The adult female mammary gland consists of branching trees of ducts that radially extend from the nipple and terminate in the lobules that comprise clusters of alveoli. The mammary alveolus is built up of the basement membrane, containing the basal cells referred to as myoepithelial cells, and the inner layer composed of luminal cells (Figure 1). The multipotent stem cells give rise to luminal epithelial stem cells and basal stem cells that further divide into luminal and basal progenitor cells. However, the luminal progenitor cells differentiate into two types of hormone receptor-negative cells and one hormone receptor-positive cell type (Cristea and Polyak, 2018). The basal layer is embedded in breast stroma containing adipocytes, fibroblasts, and immune cells (macrophages and lymphocytes), blood and lymph vessels (Pellacani *et al.*, 2019).

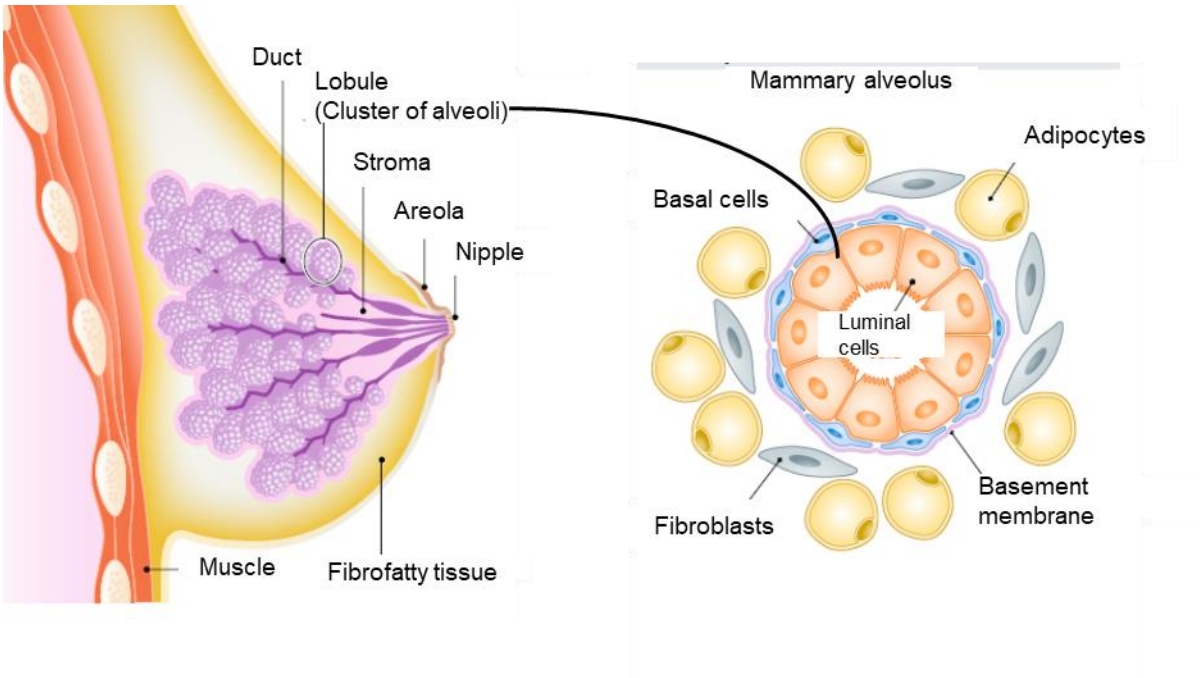

Figure 1: Anatomy of the human mammary gland
Each lactiferous duct in the mammary gland originates from the nipple and branches into ducts that end in the alveoli. Those mammary alveoli comprise the basal cells on the outside and an inner layer of luminal cells. The alveoli are embedded in the mammary stroma containing fibroblasts and adipocytes. The picture is adapted and modified from Pellacani 2019.

During the reproductive phase of a female, the mammary gland is susceptible to restructure the tissue due to the monthly menstrual cycle that is orchestrated by the uterus and pituitary hormones like estrogen and progesterone resulting in the continuous reorganization of the mammary gland (Ramakrishnan *et al.*, 2002). In the case of pregnancy, the luminal epithelial layer is able to produce and secrete milk upon hormonal stimulus. Furthermore, the luminal layer is characterized by its high epithelial cell adhesion molecule (EpCAM), cytokeratin (CK) 18, and CK 8 expression. In contrast, the basal cells express EpCAM very low and could be identified by CK 14 staining. In normal mammary tissue, approximately 7 % of the epithelial cells in the mammary gland are hormone receptor-positive, whereas 87 % of the cells are luminal epithelial cells or occupied an intermediate position in the duct wall (Petersen *et al.*, 1987). These distinct expression patterns are not only helpful to identify the different cell types in healthy mammary tissue but are also responsible for the different entities in breast malignancies.

1.1.2 Breast cancer etiology

In the mammary gland, the cells grow and divide and are strictly controlled through homeostatic regulation between proliferation and death. However, an imbalance between proliferation and cell death could lead to the development of breast cancer,

whereas the reasons for carcinogenesis are not fully understood. There are several risk factors that promote the formation of breast malignancies like the genetic predisposition, race or ethnicity, childlessness, non-breastfeeding, hormone receptor replacement therapy after menopause, excessive alcohol consumption, smoking, or obesity (Feng *et al.*, 2018). Besides the so-called acquired risk factors for breast cancer, only 5-10 % of breast cancer malignancies are due to inherited reasons like BRCA1/2 mutations or TP53 mutations (Duda and Schulz-Wendtland, 2017; Feng *et al.*, 2018).

1.1.3 Classification of breast cancer and breast cancer subentities

One of the most common types of breast cancer is the non-invasive or pre-invasive intraductal carcinoma in situ (DCIS) which develops inside the normal ducts. DCIS itself is not invasive but in situ carcinomas have a high potential to become invasive. In contrast, invasive breast cancer invades and spread outside the normal breast lobules and ducts and grows into the surrounding tissues. The invasive breast cancer cells derive either from the epithelial cells of the mammary ducts (ductal) or from the mammary lobules (lobular). The invasive ductal carcinoma (70-80 %), as well as the invasive lobular carcinoma (10 %), represents the highest proportion of mammary malignancies and derives from early lesions (carcinoma in situ). About 90 % of breast cancer cases are invasive (Feng *et al.*, 2018). Besides this histological classification, the classification of breast cancer is performed according to the pTNM staging. This staging considers the size of the primary tumor (T), the lymph node involvement (N), and the presence of distant metastases (M), as it represents important information for therapy and prognosis of the carcinoma (Duda and Schulz-Wendtland, 2017). The grading system which is scaled into three stages (G1-G3), provides additional information on the degree of malignancy, thereby including the formation of tubular gland structures, the nuclear atypia, and the frequency of mitosis (Elston and Ellis, 1991). The higher the grading the worse is the prognosis. Accordingly, Grade 1 proliferates slowly and is well-differentiated, Grade 2 is moderately differentiated, and Grade 3 propagates fast and is poorly differentiated (Klöppel *et al.*, 2013). However, an additional important low prognostic but highly predictive factor is the hormone receptor status. The nuclear estrogen receptor alpha (ER) expression and the nuclear progesterone receptor expression (PR) expression is determined by immunohistochemical staining and calculated according to the Remmele Score (Remmele and Stegner, 1987). The score comprises the staining intensity and the

percentage of the stained nuclei which are summarized in an immune reactive score (0-12). The chief markers to subcategorize breast cancer are not only ER and PR but also the oncogene human epidermal growth factor receptor 2 (Her2). The combination of these markers allows the assignment of individual cases to specific categories, namely Luminal breast cancer ER^+ ($ER^+/HER2^-$), $HER2^+$ breast cancer ($ER^-/HER2^+$), triple-negative breast cancer (TNBC; $ER^-/PR^-/HER2^-$), and Luminal B /$Her2^+$ breast cancer ($ER^+/PR(^+/_-)/HER2^+$) (Bertos and Park, 2011).

1.1.4 Luminal breast cancer

Luminal breast cancer is the predominant type of breast cancer with an incidence of 70-80%. This tumor entity can further be subdivided into Luminal A (low-risk) and Luminal B (high-risk) tumors (Sørlie *et al.*, 2001; Perou *et al.*, 2000). According to St. Gallen conference 2011, the proliferation capacity of these tumors is characterized by Ki67 < 14 % and Ki67 > 14 %, respectively (Goldhirsch *et al.*, 2011; Cheang *et al.*, 2009). This classification is a guidance value for therapy decisions. In matters of a high proliferation capacity, the decision for Luminal B breast cancer patients is in favor of chemotherapy treatment, whereas this therapy approach is disputable when the proliferation threshold is close to 14 %. Luminal A tumors with a low proliferation capacity do not necessarily benefit from cytostatic drugs and receive only endocrine therapy in most cases. It is known that the response of an anti-hormonal therapy is more efficient in Luminal A breast cancer patients compared to Luminal B breast cancer patients (Rouzier *et al.*, 2005; Hayes *et al.*, 2007; Goldhirsch *et al.*, 2011). However, the differentiation between high and low-risk Liminal B tumors remains crucial. Another step towards risk stratification in Luminal breast cancer are the gene expression tests that are able to predict a risk assessment for recurrence or the development of distant metastases and therefore help to estimate the need for chemotherapeutic intervention. Oncotype DX (21 gene assay) and EndoPredict (11 gene assay) were both prognostic for the risk of distant recurrence (Narain and Adcock, 2017). Mammaprint (Agendia) assesses the risk of recurrence through the determination of 70 genes. The Prosigna (PAM50; 55 gene assay) assay has been validated as a prognosticator in clinically low-risk, postmenopausal patients with ER^+ early-stage breast cancer treated with endocrine therapy (Narain and Adcock, 2017). The test separates the high and low-risk Luminal B patients by a risk of recurrence score. However, the prediction of variable gene expression tests is still unsatisfying as the tests are not interchangeable and reveal different results for the same patients

(Alvarado *et al.*, 2015). Luminal B tumors also tend to metastasize into various organs including the bone marrow and are therefore associated with a poorer prognosis. However, if Luminal B breast cancer patients profit from chemotherapy is still disputed (Goldhirsch *et al.*, 2011; Lønning, 2012).

1.2 Breast cancer metastases

One of the major problems of suffering from breast cancer is still not the primary tumor but the development of distant metastases. Although approximately 6 % of the newly diagnoses patients harbor metastases, about 30 % of the women with breast cancer will develop distant metastases (O'Shaughnessy, 2005). The frequency did not change in the last decades, which is referable to the fact that the biology of metastatic processes and adequate prevention is less understood.

1.2.1 Metastatic sites in breast cancer

Breast cancer metastases are frequently found in the distant lymph nodes, the liver, the lung, the bone marrow, and the brain (Wu *et al.*, 2017). However, there are differences between breast cancer subentities and metastatic sites. Luminal B tumors show preferentially metastases in the liver, the lung, and the distant lymph nodes. If the Luminal B tumors additionally overexpress Her2, the brain, and the bone marrow are frequent sites of metastatic colonization (Chen *et al.*, 2018). Still, 70 % of the metastases are determined in the bone and is, therefore, the most prominent target site in breast cancer (Weilbaecher *et al.*, 2011). This so-called organotropism was shown to be driven by the different breast cancer subentities, different gene signatures, and different signaling pathways of metastatic tumor cells, and the crosstalk with the host (immune) microenvironment, (Chen *et al.*, 2018). This phenomenon is supported by the hypothesis of “seed and soil” that was claimed by Paget decades ago. The tumor cells (seed) can only grow in a distant organ (soil) if it is “planted” in the appropriate microenvironment (Paget, 1889). The chemical attraction is one of the key modulators to successfully colonize at distant organs. Multiple factors like cytokines, bone sialoprotein, or osteopontin expression in the microenvironment are implicated to play a major role in metastases formation (Ibrahim *et al.*, 2000). Nevertheless, the distinct drivers for breast cancer metastasis organotropism are still not fully understood.

1.2.2 EMT and MET in breast cancer metastases

Metastases development is a multifactorial process that requires several factors to enable the cancer cell to spread. In each step, the cancer cell could be eliminated by the failure of adaption or due to immune cell eradication. Therefore, only a few cells that are adjusted will succeed in the colonization of distant organs (Fidler, 2003; Valastyan and Weinberg, 2011). The stepwise cascade from the primary tumor to the adaptation to foreign tissue microenvironments comprises (1) the local invasion of primary tumor cells through surrounding extracellular matrix (ECM) and stromal cell layers accompanied by the intravasation of the tumor cell into the blood vessels, (2) the survival as a circulating tumor cell (CTC) in the vasculature periphery, (3) the arresting at distant organ sites, (4) the adherence to the vessel wall and the extravasation into the distant tissues, (5) the persistence in the foreign microenvironment, and (6) the proliferation to form micrometastases in the distant organ (Valastyan and Weinberg, 2011; Fidler, 2003; Bill and Christofori, 2015).

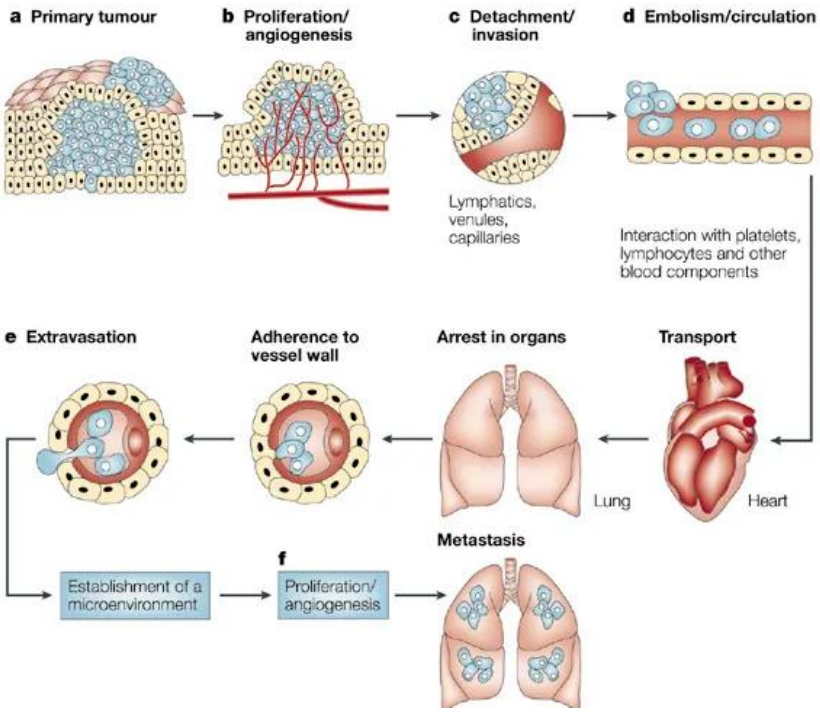

Figure 2: Schematic description of the development of distant metastases
A) The initial step requires progressive tumor growth. **B)** The tumor needs extensive vascularisation to allow the tumor cells to **C)** detach and invade the blood vessels. **D)** The tumor cells are then circulating in the peripheral blood where they have to survive. Next, the cells arrest in an organ by the adherence to the vessel wall. **E)** The extravasation is followed by the adaptation to the new microenvironment. **F)** The proliferation and the angiogenesis completes the metastatic process to form solid metastases. This figure is adapted and modified from Fidler 2003.

These multiple processes require an adaptation of the tumor cell to the physiology of a certain location. Epithelial to mesenchymal transition (EMT) is a reversible process that attains the tumor cells a mesenchymal phenotype in order to exit the primary tumor site and allows them to metastasize to distant organs (Kotiyal and Bhattacharya, 2014). In contrast, mesenchymal to epithelial transition (MET) is required after colonization of an organ to build a new malignant tumor growth the so-called metastasis. In terms of EMT, the TGFbeta and RTK/ Ras signaling, EMT transcription factors, and pathways such as Wnt, Notch, and Hedgehog are known to contribute to that process (Bill and Christofori, 2015; Felipe Lima *et al.*, 2016). The reduced expression of E-cadherin, as a cell-cell adhesion molecule, regulated by the transcription factors Snail and Twist seems to be one of the crucial steps that drive EMT (Huber *et al.*, 2005). Cancer stemness has been associated with an enhanced capacity for EMT. Breast cancer stem cells exhibit cellular plasticity as they are able to reversibly transit between the mesenchymal and the epithelial state. This tumor cell plasticity and the evolvement of breast cancer stem cells (CSC) are associated with EMT that typically goes along with altered expression or activity of cytokeratin, vimentin, CD24, Claudin, ALDH, SLUG, and SNAIL and consequently with an increased capacity of self-renewal, tumor initiation, and recurrence (Al-Hajj *et al.*, 2003; Liu and Wicha, 2010).

1.2.3 Stem cells traits and their relevance in EMT-MET and breast cancer metastases

To date, it remains still challenging to detect all tumor cells in the periphery e.g. as DTCs in the BM or circulating tumor cells (CTCs) in the peripheral blood. The DTC and CTCs are a prognostic factor for patient survival and metastatic spread (Braun *et al.*, 2005). The established method for CTC detection in the blood is the *CellSearch*® system that is able to quantify the tumor cells in seven ml blood due to the expression of **EpCAM** on the surface of the tumor cells. EpCAM as epithelial cell adhesion molecule is only expressed on epithelial cells and thereby this method excludes the mesenchymal and hematopoietic cells (Gires and Stoecklein, 2014). EpCAM plays a major role in embryonic development and is located at the basolateral membrane in normal epithelial tissue (Gires, 2011). Besides the expression in normal tissue EpCAM is expressed in a variety of malignancies including breast cancer. Preferentially EpCAM is found on luminal cells (Visvader and Stingl, 2014). However, its regulation is rather dynamic. While EpCAM is highly expressed in the primary tumor, the expression of EpCAM can be downregulated in the CTC (Gires and Stoecklein, 2014).

This fact shows that CTC capturing through EpCAM expression might not detect all tumor cells. EpCAM is highly expressed especially in $Her2^+$ Luminal B breast cancer and associated with a rather unfavorable prognosis (Soysal *et al.*, 2013). Additionally, EpCAM expression in the primary breast cancer tumor is associated with increased bone marrow metastases and increased stem cell capacity of the tumor cells (Hiraga *et al.*, 2016; Huber *et al.*, 2015). Not only EpCAM as a cell adhesion molecule but also CD44 and CD24 play a pivotal role in breast cancer stemness and metastases. **CD44** is necessary for the communication and adhesion between adjacent cells and between cells and the extracellular matrix and was shown to contribute to metastasis formation (Naor *et al.*, 2002). It can interact with a variety of effectors such as the hyaluronic acid – an abundant compound of the extracellular matrix (Toole, 2009; Louderbough and Schroeder, 2011) and is expressed by a multitude of carcinoma cells especially on cancer-initiating ones (Zöller, 2011; Wang *et al.*, 2018b). Moreover, it plays a major role in cell adhesion, cell proliferation, migration, invasiveness, chemoresistance and metastasis initiation (Baccelli *et al.*, 2013; Zöller, 2011; Naor *et al.*, 2008; Williams *et al.*, 2013). **CD24** is a heavily glycosylated mucin-like glycosylphosphatidyl-inositol-linked cell surface protein and is expressed in a wide variety of human malignancies (Jaggupilli and Elkord, 2012). The high CD24 expression levels are associated with enhanced proliferation (Baumann *et al.*, 2005), clonogenicity *in vitro* (Smith *et al.*, 2006), and metastases (Friederichs *et al.*, 2000). However, the expression of $CD44^{high}$ /$CD24^{low}$ was determined previously to be the tumor-initiating phenotype for breast cancer stem cells whereas the multitude of cells within the same tumor exhibit $CD44^{low}$ / $CD24^{high}$ (Al-Hajj *et al.*, 2003; Mani *et al.*, 2008). It was also shown that the $CD44^{high}$ /$CD24^{low}$ phenotype is frequently expressed in highly aggressive TNBC and $Her2^+$ breast cancer (Honeth *et al.*, 2008). **CD47** is an integrin associated transmembrane protein and known for its interaction with the SIRP alpha receptor to prevent phagocytosis by macrophages or dendritic cells. The expression of CD47 as “Don’t eat me signal”, therefore, enables the cancer cell to be eradicated by immune cells (Nagahara *et al.*, 2010). High expression of CD47 in CTCs and DTCs was associated with decreased DFS in breast cancer patients (Nagahara *et al.*, 2010). Additionally, high CD47 and CD44 co-expression were shown previously to be a prognosticator for limited survival in Luminal breast cancer (Baccelli *et al.*, 2014). Another important biomarker is **cMET** also called HGFR (hepatocyte growth factor receptor). This receptor tyrosine kinase activates, upon hepatocyte growth factor (HGF) binding,

diverse cellular functions that play an important role in organ development and cancer progression (Trusolino *et al.*, 2010). HGF is one of the factors that promote invasive tumor growth, metastases formation and induction of EMT (Christofori, 2006). By means of its role in metastasis initiation (Baccelli *et al.*, 2013) a high cMET expression has been shown to be associated with reduced survival and an aggressive phenotype in breast cancer patients (Ho-Yen *et al.*, 2015). In addition, cMET has also been determined to inversely correlate with tumor size in breast cancer (Ho-Yen *et al.*, 2014). Interestingly, the HGF induced activation of cMET stimulated the CD44 signal transduction and stabilized the androgen receptor functions in prostate cancer (Ghatak *et al.*, 2010). However, the co-expression of $EpCAM^+$/ $CD44^+$/ $CD47^+$/$cMET^+$ was demonstrated by Baccelli to be the prominent phenotype in CTCs to initiate metastases (metastases initiating cells (MIC)) in breast cancer (Baccelli *et al.*, 2013) further showing the potential of CD47 and cMET as CSC biomarkers. Another important oncogene in breast cancer is **Her2**. Her2 as receptor tyrosine kinase is overexpressed in 20 - 25 % of invasive breast cancer and predicts a poor clinical outcome (Slamon *et al.*, 1987). The overexpression of Her2 is in most cases due to the amplification of the Her2 gene. The constitutive kinase activity in $Her2^+$ breast cancer, therefore, promotes increased proliferation and invasion of the tumor cells (Olayioye, 2001). Despite the prognostic and predictive value of Her2 in breast cancer, it is also implicated as a driver for breast cancer stemness as $Her2^+$ breast cancer cells showed an increased mammosphere formation due to increased clonogenicity (Korkaya *et al.*, 2008; Korkaya and Wicha, 2009; Magnifico *et al.*, 2009). Other researchers reported the detection of $Her2^+$ DTCs that arose from Her2- breast cancer tumor, suggesting a small subpopulation of Her2 overexpressing tumor cells in the primary tumor that might be missed by routine diagnostic of the primary tumor (Pantel and Alix-Panabières, 2014). The prognosis of Her2 breast cancer is poor as those tumors often tend to generate distant metastases. However, it is possible to treat $Her2^+$ breast cancer adequately with the monoclonal antibody Trastuzumab (Herceptin) in combination with chemotherapy. This therapeutic intervention targets Her2 and therefore efficiently diminish the proliferation and increases disease-free survival (Piccart-Gebhart *et al.*, 2005). Even though several biomarkers are known to be regulated in breast cancer and breast cancer metastases, it still remains to be elucidated which additional factor might play a pivotal role in breast cancer stemness and metastases formation.

1.2.4 Disseminated tumor cells (DTCs)

During the way of the tumor cells through the periphery (e.g. the blood or the lymph vessels) the cells referred to CTC, whereas after extravasation and colonization the tumor cells are termed as disseminated tumor cells (DTC). The DTCs can be detected in the mesenchymal tissue due to their epithelial origin thereby expressing cytokeratins such as CK8, CK18, and CK19 (Braun *et al.*, 2005). The occurrence of DTCs in the bone marrow of breast cancer patients is a risk factor for the development of distant metastases (Wiedswang *et al.*, 2003). Moreover, the DTC persistence correlates with diminished disease-free survival (DFS) and reduced overall survival (OS) (Janni *et al.*, 2011). However, the time at which dissemination takes place is still disputed. There are two well-known theories when dissemination occurs. The first one is that the cancer cells were shown to disseminate at late stages (Koscielny *et al.*, 1984), and the second one is the well-accepted theory of parallel progression of tumor cell dissemination and tumor growth (Klein, 2009). Moreover, tumor cell dissemination can occur even in the absence of a detectable tumor as so-called cancer of unknown primary(van de Wouw *et al.*, 2002). Surprisingly, epidemiologic studies revealed that metastases could be initiated already five to seven years before the primary tumor is diagnosed (Engel *et al.*, 2003). Supporting the early dissemination hypothesis it was shown that DTCs from breast cancer patients harbor fewer aberrations than the primary tumor cells at an advanced state, indicating a slow progression of DTCs (Schmidt-Kittler *et al.*, 2003). However, there are some studies that demonstrated a genomic congruency of DTCs and primary tumor cells in breast cancer (Mathiesen *et al.*, 2012; Stoecklein *et al.*, 2008). Interestingly, the recurrence and metastases in breast cancer take a long period of time after primary tumor detection indicating that DTCs could somehow transform/switch in a state of dormancy. To date, there are two types of dormancy known. One state of dormancy is defined by the potential of the cancer cell to stay in an arrested cell cycle phase (G0/G1) that is reversible (Hayat, 2013) and the other state is called tumor mass dormancy where the equilibrium of cell death and self-renewal of the cancer cell (Kareva, 2016). However, the fate of the disseminated cell is supposed to be triggered by several intrinsic and extrinsic factors that contribute to dormancy or active proliferation (Osisami and Keller, 2013).

1.3 The role of genetic aberrations in breast cancer

Despite Her2, there are several other aberrations that are frequently altered in breast cancer. Inherited BRCA1 and BRCA2 mutations or mutations in the TP53 gene are

detected frequently. The latter is preferentially found in very aggressive tumor types such as TNBC and Her2$^+$ breast cancer (Abubakar *et al.*, 2019) and is associated with poor clinical outcome. P53 as a product of the TP53 tumor suppressor gene is not expressed in healthy cells or rather to a low degree. If stressors like DNA damages, hypoxia, or activation of oncogenes occur in healthy cells, p53 turns on transcriptional target genes to send the cell in cell cycle arrest in order to prevent DNA lesions. However, if the DNA damages are irreparable the p53 upregulation promotes apoptosis (Shi and Gu, 2012). P53 also induces the transcription of mouse double minute protein 2 (MDM2), an E3-ligase, which serves as a negative feedback regulator. It ubiquitinylates p53 for its degradation on the proteasome. MDM2 deregulations frequently occur in Luminal B breast cancer (31%) and in Her2$^+$ breast cancer (30%) (Network, 2012) and were shown to promote invasiveness, EMT, and metastases in breast cancer (Haupt *et al.*, 2017). In contrast, TP53 mutations are predominantly detected in TNBC and Her2$^+$ breast cancer.

1.4 TILs and immune checkpoints in breast cancer

The evaluation of tumor-infiltrating lymphocytes (TIL) is gaining more and more clinical relevance in breast cancer as they were shown to have a potential prognostic and predictive value (Salgado *et al.*, 2015). The most TILs can be found in in TNBC with an average of 20 % infiltration (range: 4 % - 37 %) and in Her2$^+$ breast cancer with an average of 16 % (range: 11 % - 24 %). In both subtypes/entities, increased infiltration is associated with a survival benefit (Stanton *et al.*, 2016). Furthermore, all breast cancer subtypes with TILs predicted response to neoadjuvant chemotherapeutic intervention. The same study described increased immune cell infiltration as an adverse prognostic factor for the outcome in Luminal-HER2- breast cancer patients, (Denkert *et al.*, 2018). Even though the TNBC and Her2$^+$ subtypes are immunogenic, Luminal breast cancer is rather escaping immunosurveillance and is only low infiltrated with an average of 6 % (range: 3 % - 12 %) (Stanton *et al.*, 2016). Nevertheless, Luminal B Her2$^+$ breast cancer is infiltrated with TILs to a greater extent (9 %) compared to Luminal A/B Her2- breast cancer (1%) (Pruneri *et al.*, 2017). The **CD8** infiltration inversely correlated with the ER-alpha and PR expression whereas the presence of CD8$^+$ immune cells predicted a favorable outcome for the patient (Mahmoud *et al.*, 2011). The infiltration of **CD4$^+$** cells was shown to be increased preferentially in aggressive tumor types such as TNBC and Her2$^+$ breast cancer (Meng *et al.*, 2018). However, CD8$^+$ and CD4$^+$ immune cells and various other immune cells

like T regs or B cells play a prognostic role in different stages of the mamma carcinoma (early breast cancer, neoadjuvant or adjuvant situation, metastasized) (DeNardo and Coussens, 2007; Emens, 2012). Not only the immune cell infiltration but also the tumor-immune cell interactions play a pivotal role. This interaction involves tumor cell elimination, tumor-immune cell equilibrium, but also the escape of tumor cells from the immunological defense. This could be achieved, besides other mechanisms, by the expression of inhibitory immune checkpoint molecules (Mittal *et al.*, 2014). Therapeutic strategies designed to stimulate the patient's inherent immunological tumor defense e.g., by targeting immune checkpoints are considered to enhance conventional treatment regimens. A prominent target that contributes to tumor cell evasion is the immune checkpoint programmed death-ligand 1 (PD-L1). If expressed by tumor cells (Blank *et al.*, 2005), the interaction of PD-L1 with its counterpart, the programmed death receptor 1 (PD-1) leads to T-cell anergy or apoptosis (Keir *et al.*, 2008). Triple-negative breast cancer (TNBC) specimens showed the highest level of PD-L1 expression, followed by Her2 overexpressing subtypes, and lastly the Luminal (Luminal A and Luminal B) entities (Ali *et al.*, 2015; Ghebeh *et al.*, 2006). However, PD-L1 expression on tumor cells has repeatedly been associated with a worse outcome (Wang *et al.*, 2016). Still, the relevance of PD-L1 and PD-1 expression in breast cancer is discussed controversially (Stovgaard *et al.*, 2019).

1.5 PDX models and humanized PDX models in breast cancer research

Mice are still the most common animals for usage as a model organism because of high genetic homology, easy genetic manipulation, a fully sequenced genome, low cost in breeding and quick reproduction cycles (Perlman, 2016). The understanding of the genomic landscape, the metastatic spread and the biology of breast cancer still remains challenging. The development of patient-derived xenografts (PDX) opened up new possibilities, thus, the breast cancer tumor engrafted in mice properly, reflected the heterogeneity of the primary tumor, the tumor behavior, and also the metastatic properties. Moreover, it was possible to detect new breast cancer targets and the PDX model was susceptible to predict treatment response which was a big step towards personalized medicine (Whittle *et al.*, 2015; Landis *et al.*, 2013). Different ways of primary tumor transplantations were used for the generation of breast cancer PDX models. In most cases, the tumors were transplanted orthotopic, hence, into the mammary fat pad of the mice (Al-Hajj *et al.*, 2003; DeRose *et al.*, 2011; Zhang and Lewis, 2013; Kabos *et al.*, 2012). Other methods like subcutaneous, under the

subrenal capsule, intraductal or interscapular transplantations were also successful (Marangoni *et al.*, 2009; Cottu *et al.*, 2012; Reyal *et al.*, 2012; Fiche *et al.*, 2019; Eirew *et al.*, 2015; Bergamaschi *et al.*, 2009). It was shown that successful engraftment is also determined by breast cancer subentity and their molecular traits. TNBC and $Her2^+$ breast cancer and metastatic breast cancer showed higher engraftment rates compared with the Luminal hormone receptor-positive entities (Landis *et al.*, 2013; Baccelli *et al.*, 2013). However, several improvements contributed to increased PDX take rates like the supplementation of estradiol as a subcutaneous transplanted pellet in hormone receptor-positive tumors (Al-Hajj *et al.*, 2003; Marangoni *et al.*, 2007), the use of Matrigel (Fleming *et al.*, 2010; Kabos *et al.*, 2012), the supplementations of human mesenchymal stem cell, (DeRose *et al.*, 2011) or the use of highly immunosuppressed mice (Oakes *et al.*, 2012; Zhang *et al.*, 2013; Kabos *et al.*, 2012). Highly immunosuppressed mice like NOD-SCID IL2Rγnull (NSG) mice have no T, B, or natural killer cells and a reduced myeloid cell function (Shultz *et al.*, 2005). The enhanced life span of these mice of over 1.5 years is an advantage due to the prolonged engraftment duration of a primary breast cancer tumor of approximately six months up to one year. Additionally, the NSG mouse strain exhibited the highest engraftment rates (Carreno *et al.*, 2009). A list of the most important breast cancer PDX studies, different breast cancer entities, mouse strains, transplantation sites and the overall success rate of engraftment is provided in Table 1. Various studies with breast cancer PDX models were shown to display the patients tumor heterogeneity, the metastatic behavior of the tumor, the patients disease outcome (DeRose *et al.*, 2011; Valdez *et al.*, 2011), and the concordance of drug response in patients (Marangoni *et al.*, 2007; Cottu *et al.*, 2012; Cottu *et al.*, 2014). The EurOPDX consortium was founded to enable translational knowledge in oncology by providing access to a multitude of PDX models. Hence, the EurOPDX harnesses the clinically relevant models in cancer, avoids the duplication of research efforts and improves drug development processes through interchanging data with other researchers. Nevertheless, the influence of the human immune system cannot be elucidated in these PDX models. The severe combined immune deficiency (SCID) mutation of the NSG mice additionally provides the opportunity to engraft human immune cells. This can be performed by the isolation of hematopoietic stem cells ($CD34^+$) from the human peripheral blood, the cord blood, the fetal liver cells from an abort, or the bone marrow, and can then be injected intravenously, intracardially, intraperitoneally, intrafemorally,

or intrahepatically using neonatal or adult immunodeficient mice (Wege, 2018). The humanized PDX model is another option of the humanized mouse model whereby the transplantation of primary breast cancer cells follows 12 weeks after humanization. These mouse models have been used in preclinical checkpoint inhibitor studies of TNBC humanized PDX mice that were treated with anti-PD-1 therapy. This resulted in a reduction of the tumor size whereby this reduction could be traced back to the inhibition of PD-1/$CD8^+$ cells (Wang *et al.*, 2018a). However, to date humanized PDX models in breast cancer research are used only rarely, which might be due to the fact that several factors like the availability of newborn mice, the immune system engraftment, primary tissue availability and toleration, and long latencies until tumor outgrowth that has to be combined in one experiment. Nevertheless, humanized breast cancer PDX models are a step towards a detailed understanding of breast cancer biology, metastasizing, and dissemination, under the influence of a human immune system. In addition, these mice can be used for preclinical studies in the area of immunomodulation.

Table 1: Overview of generated breast cancer PDX models

Study	**Breast cancer subtype**	**Mouse Strain**	**Transplantation site tissue/ single cells supplementation**	**Success rate overall**
(Visonneau *et al.*, 1998)	N.A.	SCID	s.c. tumor fragments	50 %
(Beckhove *et al.*, 2003)	N.A.	NOD/SCID	im tumor fragment matrigel	90 %
(Ma *et al.*, 2012)	TNBC	NOD/SCID	mfp single cells fibroblasts	N.A.
(Liu *et al.*, 2010; Al-Hajj *et al.*, 2003)	4 TNBC 2 $Her2^+$ 2 ER^+	NOD/SCID	thoracic mfp tissue fragments estradiol	N.A.
(Marangoni *et al.*, 2007; Cottu *et al.*, 2012; Reyal *et al.*, 2012)	15 TNBC,2 $Her2^+$, 1 ER^+, (Marangoni *et al.*, 2007), 22 TNBC, 8 ER^+ (Cottu *et al.*, 2012)	Swiss nude	interscapular fat pad tumor fragments estradiol	12.5 %
(Bergamaschi *et al.*, 2009)	1 TNBC, 1 ER^+	SCID	s.c. in the back pocket tumor fragments	20 %

			matrigel	
(DeRose *et al.*, 2011)	5 TNBC, 2 Her2$^+$, 2 ER$^+$,	NOD/SCID	cleared mfp tissue fragments, metastastic single cells estradiol	27 %
(Zhang *et al.*, 2013)	21 TNBC, 3 Her2$^+$, 3 ER$^+$	SCID beige, NSG	cleared mfp tumor fragments +/- fibroblasts, estradiol	30 %
(Kabos *et al.*, 2012)	1 TNBC, 5 ER$^+$	NOD/SCID, NSG	abdominal mfp tumor fragments matrigel	42 %
(Petrillo *et al.*, 2012)	4 TNBC, 1 Her2$^+$, 0 ER$^+$	NOD/SCID	s.c. dorsal flank tumor fragments estradiol	25 %
(Fleming *et al.*, 2010)	2 Her2$^+$, 2 ER$^+$	NOD/SCID	abdominal mfp pleural effusion cells estradiol, matrigel	N.A.
(Vaillant *et al.*, 2013; Oakes *et al.*, 2012)	17 TNBC, 13 ER$^+$, 2 ER-PR$^+$, 5 Her2$^+$,	NSG	inguinal mfp tumor fragments estradiol	23 %
(Eirew *et al.*, 2015)	6 TNBC, 5 ER$^+$, 4 Her2$^+$	NSG, NRG	mfp, s.c., sr	N.A.
(Fiche *et al.*, 2019)	21 ER$^+$	NSG	intraductal mfp single cells	N.A.

TNBC Triple-negative breast cancer, *ER* estrogen receptor, *Her2* human epidermal growth factor receptor, *NOD/SCID* non-obese diabetic / severe combined immune deficiency, *NSG* NOD-SCID IL2Rγnull, *NRG* NOD.Cg-Rag1^{tm1Mom} IL2rg^{tm1Wjl}, *mfp* mammary fat pad, *s.c.* subcutaneous, *id* intraductal, *sr* subrenal capsule, *im* intramuscular, *N.A:* not available

1.6 Aim of the thesis

The aim of this thesis, as part of the Deutsche Krebshilfe founded Luminal B consortium, was to determine markers for the heterogeneous Luminal B group to differentiate them into high and low-risk patients. Hence, the therapy decision could be facilitated if a Luminal B breast cancer patient might benefit from chemotherapeutic intervention or not. This goal should be realized by the generation and the analysis of patient-derived Luminal B xenografts in the so-called tumor mice (TM) or humanized tumor mice (HTM). These mice were generated by orthotopic transplantation and the subsequent expansion of primary tumor material from Luminal B patients in immunodeficient NSG mice. Finally, the expanded tumor material from these mice was further transplanted into mice which were neonatally reconstituted with human hematopoietic stem cells (HSC) derived from human cord blood. These mice developed a human immune system together with human tumor growth and allowed studies under human-like conditions. The main questions which should be addressed are:

(1.) the phenotypic differences of human high- and low-risk Luminal B
(2.) the evaluation of the capacity of Luminal B breast cancer to disseminate and to form metastases in TM and HTM (i.e., in the presence of a human immune system),
(3.) the identification of geno- and phenotypic patterns in primary Luminal B tumors that are associated with tumor outgrowth and cell dissemination (metastasis formation) and EMT / basal cell-like traits,
(4.) the analysis of phenotypical changes between the primary tumor and the corresponding metastases in the TM and HTM model, and
(5.) the assessment of human immune cell activity and invasion in correlation to tumor outgrowth, dissemination, and metastases.

Overall, the main goal of this thesis was to identify biomarkers that are associated with tumor outgrowth, cell dissemination and/or metastases formation using humanized PDX mice

2. Material

2.1 Consumables

12 % Mini Criterion TGX Stain-free gels	BioRad Laboratories, Munich, Germany
15 ml tube	Greiner Bio-One Bioscience, Frickenhausen, Germany
17ß-Estradiol pellets 0,18mg/90days	Innovative Research of America, Florida, USA
40 µm cell strainer	Corning, NY, USA
50 ml tube	Greiner Bio-One Bioscience, Frickenhausen, Germany
Adhesion slides	Carl Roth, Karlsruhe, Germany
BD Discardit II 2 ml, 5 ml, 10 ml, 20 ml (syringes)	BD Biosciences, Heidelberg, Germany
BD Microlance 3 20G, 22G, 27G (cannulas)	BD Biosciences, Heidelberg, Germany
BD SafetyGlide Insulin syringe	BD Biosciences, Heidelberg, Germany
Cell Scraper	Greiner, Solingen, Germany
Cord blood collection bag	Macopharma, Langen, Germany
Culture-Insert 2 Well in µ-Dish 35 mm	Ibidi, Gräfelfing, Germany
Cyro tubes	Greiner, Solingen, Germany
MACS separation LD columns	Miltenyi Biotech, Bergisch Gladbach,Germany
MACS separation MS columns	Miltenyi Biotech, Bergisch Gladbach,Germany
Medicon Einsatze unsteril	BD Biosciences, Heidelberg, Germany
Medimachine Medicon sterile	BD Biosciences, Heidelberg, Germany
Petri dish sterile	Sarstedt AG & Co., Nümbrecht, Germany
Round Bottom Polystyrene Test Tube (5ml)	Falcon, Heidelberg, Germany
SuperFrost Plus Slides	Menzel GmbH, Braunschweig, Germany
T25 tissue flask	Greiner Bio-One, Frickenhausen, Germany
Trimming blades	pfm medical AG, Cologne, Germany
Vicryl surgical sutures	Johnson & Johnson, New Brunswick, New Jersey, USA

2.2 Buffers and Solutions

AB serum, human	BioRad Laboratories, Munich, Germany
Accutase 100 ml	Sigma-Aldrich Chemie GmbH, Deisenhofen, Germany
Amphotericin B solution	Sigma-Aldrich Chemie GmbH, Deisenhofen, Germany
B27 supplement 50x minus Vitamin A	Life Technologies, Carlsbad, CA, USA
BSA 10x 10ml	BioRad Laboratories, Munich, Germany
Cell Lysis Buffer	Cell Signaling Technology, Inc., Beverly, MA, USA
Cholera Toxin 5ml	Sigma-Aldrich Chemie GmbH, Deisenhofen, Germany

Collagenase	Sigma-Aldrich Chemie GmbH, Deisenhofen, Germany
CryoStor® CS10	Stemcell Technologies, Vancouver, Canada
DAB plus substrate-chromogen solution	Dako, Santa Clara, CA United States
Dako REAL™ Peroxidase-Blocking Solution	DAKO, Hamburg, Germany
DAKO wash buffer 10x	DAKO, Hamburg, Germany
DMSO	Sigma-Aldrich Chemie GmbH, Deisenhofen, Germany
DNAse I	Sigma-Aldrich Chemie GmbH, Deisenhofen, Germany
EDTA	Thermo Scientific, Rockford, USA
EDTA-Lösung pH 8,0 (0,5M)	Applichem, Darmstadt, Germany
FCS	Gibco, Rockford, USA
HALT Protease Inhibitor	Thermo Fisher Scientific, Rockford, USA
HEPES solution	Sigma-Aldrich Chemie GmbH, Deisenhofen, Germany
Hyaluronidase	Sigma-Aldrich Chemie GmbH, Deisenhofen, Germany
Hydrocortison	Sigma-Aldrich Chemie GmbH, Deisenhofen, Germany
Insulin solution 5ml	Sigma-Aldrich Chemie GmbH, Deisenhofen, Germany
Matrigel (Cultrex PathClear Basement Membrane Extract)	R&D Systems, Inc., Minneapolis, USA
Methanol	Merck Millipore, Darmstadt, Germany
Pancoll human, density 1077g/ml	PAN Biotech GmbH, Aidenbach, Germany
PBS	Sigma-Aldrich Chemie GmbH, Deisenhofen, Germany
Penicillin/Streptomycin (10 U/µL)	PAN Biotech GmbH, Aidenbach, Germany
PMSF	AppliChem, Darmstadt, Germany
rh EGF 100µg	Immunotools, Friesoythe, Germany
rh FGF basic/FGF-2 50 µg	Immunotools, Friesoythe, Germany
RIPA buffer	Sigma-Aldrich Chemie GmbH, Deisenhofen, Germany
Trypsin with EDTA	PAN Biotech GmbH, Aidenbach, Germany
Türk's solution	Sigma-Aldrich Chemie GmbH, Deisenhofen, Germany

2.3 Buffers

Tris/Borate/EDTA (TBE) buffer 10x	539 g Tris 275 g Boric acid 37 g EDTA 5 l Demineralized water
FACS buffer	PBS 0.01 % NaN3 1 % FCS
Annexin binding buffer (10X)	0.1 M HEPES

	1.4 M NaCl 25mM CaCl2
PBS /EDTA 2mM	PBS EDTA 2mM
TAC buffer	TRIS: 170 mM, pH: 7.4 NH4Cl: 150mM pH: 7.4 Millipore H2O
Separation buffer	PBS BSA 0.5 % EDTA 2mM

2.4 Culture Media

Basal Medium	DMEM/F12 1 % HEPES (1M) 1 % Pen/Strep 1 % Amphotericin B
DMEM	Sigma-Aldrich Chemie GmbH, Deisenhofen, Germany
DMEM/F12	PAN Biotech, Aidenbach, Germany
RPMI-1640	PAN Biotech, Aidenbach, Germany

2.5 Cell lines

N1 = normal human skin fibroblasts (cloned but not immortalized)	Department of Clinical Chemistry, University of Regensburg
NIH/3T3 (primary mouse embryonic fibroblast cells)	ATCC number CRL-1658
JIMT 1	DSMZ ACC-number -589
BT474	ATCC number HTB-20
MDA-MB 231	ATCC number HTB-26
SK-BR-3	ATCC number HTB-30
ZR-75-1	ATCC number CRL-1500

2.6 Anesthesia

amount	**product name (concentration)**	**active component**	**dose**
10 ml (2 ml + 8 ml aqua dest.)	Dormicum (1 mg/ml)	Midazolam	5 mg/kg
2 ml	Fentanyl (0.05 mg/ml)	Fentanylcitrat	0.05 mg/kg
1 ml	Domitor (1 mg/ml)	Medetomidin	0.5 mg/kg

amount	**product name (concentration)**	**active component**	**dose**
5 ml	Anexate (0.1 mg/ml)	Flumazenil	0.5 mg/kg
0.5 ml	Antisedan (5 mg/ml)	Atipamezol	2.5 mg/kg
3 ml	Narcanti (0.4 mg/ml)	Naloxon	1.2 mg/kg

2.7 Antibodies Flow Cytometry

Antibody	Fluorochrome	Host	Company	Concentration µg/ml	Dilution	Clone
Her2	FITC	Mouse IgG1 κ	BioLegend®, San Diego, USA	400	1: 40	24D2
CD47	PE	Mouse IgG1 κ	BD Biosciences, Heidelberg	50	1:10	B6H12
CD44	PE/Cy7	Mouse IgG2bκ	BD Biosciences, Heidelberg	100	1:25	G44-26
cMET	APC	Mouse IgG1	R&D Systems, Inc., Minneapolis, USA	10	1:5	#95106
CD24	APC Vio 770	Mouse IgG2	Miltenyi Biotech, Bergisch Gladbach,Germany	50	1:10	32D12
CD45	BV510	Mouse IgG1, κ	BioLegend®, San Diego, USA	100	1:20	HI30
EpCAM	BV421	Mouse IgG2b, κ	BioLegend®, San Diego, USA	50	1:10	9C4
CD3	FITC	Mouse IgG1, κ	BD Biosciences, Heidelberg	100	1:3.6	SK7
CD19	PE	Mouse IgG1, κ	BD Biosciences, Heidelberg	N.A.	1:3.6	HIB19
CD33	PerCP CY5.5	Mouse IgG1, κ	BioLegend®, San Diego, USA	N.A.	1:6	WM53
CD45	APC	Mouse IgG1, κ	BD Biosciences, Heidelberg	N.A.	1:3.6	H130
CD3	FITC	Mouse BALB/c IgG1, κ	BD Biosciences, Heidelberg	100	1:10	UCHT1
CD127	PE	Mouse IgG1, κ	BioLegend®, San Diego, USA	100	1:20	A019D5
CD27	PE/Cy7	Mouse IgG1, κ	eBioscience Inc., San Diego, USA	50	1:17	O323
PD-1	AF647	Mouse IgG1, κ	BioLegend®, San Diego, USA	100	1:50	EH12.2 H7
CD4	APC-H7	Mouse IgG1, κ	BD Biosciences, Heidelberg	12	1:24	SK3
CD8a	BV510	Mouse IgG1, κ	BioLegend®, San Diego, USA	100	1:20	RPA-T8
CD45RA	BV421	Mouse IgG2b, κ	BioLegend®, San Diego, USA	6	1:12	HI100
CD34	PE	mouse IgG, κ	BioLegend®, San Diego, USA	N.A.	1:10	581
Isotype	FITC	Mouse IgG1 κ	eBioscience Inc., San Diego, USA	500	1:50	P3.6.2.8.1

Isotype	PE	Mouse IgG1 κ	eBioscience Inc., San Diego, USA	200	1:40	P3.6.2.8.1
Isotype	PE/Cy7	Mouse IgG2b, κ	eBioscience Inc., San Diego, USA	200	1:50	eBMG2b
Isotype	APC	Mouse IgG1 κ	BioLegend®, San Diego, USA	200	1:100	MOPC-21
Isotype	APC Vio770	Mouse IgG1 κ	Miltenyi Biotech, Bergisch Gladbach,Germany	200	1:10	X-56
Isotype	BV510	Mouse IgG1 κ	BioLegend®, San Diego, USA	100	1:20	MOPC-21
Isotype	BV421	Mouse IgG2b, κ	BioLegend®, San Diego, USA	50	1:10	MPC-11
Isotype	PE/Cy7	Mouse IgG1 κ	eBioscience Inc., San Diego, USA	200	1:66.7	P3.6.2.8.1
Isotype	AF647	mouse IgG1, κ	BioLegend®, San Diego, USA	100	1:50	MOPC-21

2.8 Antibody Immunohistochemical Staining

Antibody	**Supplier**	**Clone**	**Dilution**
CK 18	DAKO	DC10	1:50
ER	DAKO	6F11	1:35
PR	Novocastra	Clone 16	1:50
Her2	DAKO	Rab poly	1:250
Ki67	DAKO	MIB-1	1:200
EpCAM	DAKO	Ber-EP4	1:200
PD-L1	Abcam	[28-8]	2 µg/ml
MDM2	Calbiochem	IF2	1.5 µg/ml
CD44	cell signaling	156-3C11	1: 50
CD47	R&D	catalog number AF4670	1: 25
Cytokeratin A 45 B/B3 (CK 8, CK 18, CK 19)	Micromet, Munich	A 45 B/B3	1:100
Isotype IgG1 Kappa	Sigma	MOPC 21 M9269-1MG)	1:500

2.9 Kits

Ampli1TM LowPass Kit (SET A+Set B) 2 x 48 reactions	Menarini Silicon Biosystems, Castel Maggiore BO, Italy
Ampli1™ WGA (Menarini Silicon Biosystems, USA)	Menarini Silicon Biosystems, Castel Maggiore BO, Italy
Annexin V FITC	Immunotools, Friesoythe, Germany
AP conjugate Substrate Kit	BioRad Laboratories, Munich, Germany
BCA-Protein-Assay-Kit	Thermo Fisher Scientific, Rockford, USA
blood and cell culture DNA mini kit	Qiagen, Hilden, Germany

CD34 microbead kit, human	Miltenyi Biotech, Bergisch Gladbach, Germany
CD45 MicroBeads, human	Miltenyi Biotech, Bergisch Gladbach,Germany
iQ Sybr green supermix	Bio-Rad Laboratories GmbH, Munich, Germany
iView DAB detection kit	Ventana, Tucson, USA
SuperSignal™ West Pico PLUS Chemiluminescent Substrate	Thermo Fisher Scientific, Rockford, USA

2.10 siRNA

Dharmafect 1 (T-2001-02)	Horizon (Dharmacon), Lafayette, CO, USA
ON TargetPlus NON-Targeting Pool	Horizon (Dharmacon), Lafayette, CO, USA
Smart pool: ON TargetPlus MDM2 siRNA	Horizon (Dharmacon), Lafayette, CO, USA

2.11 Reagents and chemicals

1 kb Plus DNA Ladder + Dye	New England Biolabs, Massachusetts, USA
ß-Estardiol water soluble	Sigma-Aldrich Chemie GmbH, Deisenhofen, Germany
Agarose LE	Anprotec, Bruckberg, Germany
AMG232	Axon Medchem BV, Groningen, Netherlands
BSA 20 mg/ml	Roche Diagnostics, Basel, Switzerland
DAPI 50 µg/ml	Sigma-Aldrich Chemie GmbH, Deisenhofen, Germany
Entellan	Merck, Darmstadt, Germany
Eosin	Carl Roth, Karlsruhe, Germany
Ethidium Bromide Solution (10 mg/ml)	Sigma-Aldrich Chemie GmbH, Deisenhofen
Expand Long Templ.PCR Syst. 3600 U	Roche Diagnostics, Basel, Switzerland
FastStart Taq DNA Polymerase, dNTPack 5 U/µl	Roche Diagnostics, Basel, Switzerland
GeneRuler 100bp Plus DNA ladder	Thermo Fisher Scientific, Rockford, USA
Hematoxylin	Merck, Darmstadt, Germany
Heparin	Sigma-Aldrich Chemie GmbH, Deisenhofen, Germany
PCR-H_2O, Water for Chromatographie	VWR, Darmstadt, Germany
PI 1 mg/mL	Sigma-Aldrich Chemie GmbH, Deisenhofen, Germany
Precision plus protein Western C marker	Bio-Rad, Munich, Germany
Ribonuclease A (1 mg/mL)	Sigma-Aldrich Chemie GmbH, Deisenhofen, Germany
RNAse	Sigma-Aldrich Chemie GmbH, Deisenhofen, Germany
SuperSignal™ West Pico PLUS Chemiluminescent Substrate	Thermo Fisher Scientific, Rockford, USA
Trypan Blue Solution	Sigma-Aldrich Chemie GmbH, Deisenhofen, Germany

2.12 Devices

AxioImager Z1 microscope	Zeiss, Oberkochen, Germany
ELISA-Reader: EMax precision microtiter reader	Molecular Devices GmbH, Ismaning, Germany
FACSCanto-II flow cytometer	BD Biosciences, Heidelberg, Germany
ImageQuant LAS 4000 mini imager	GE Healthcare, Buckinghamshire, UK
MACS MultiStand	Miltenyi Biotech, Bergisch Gladbach, Germany
Medimachine System	BD Biosciences, Heidelberg, Germany
MidiMACS™	Miltenyi Biotech, Bergisch Gladbach, Germany
MiniMACS™	Miltenyi Biotech, Bergisch Gladbach, Germany
Thermolux heating plate	Witte + Sutor GmbH, Murrhardt, Germany
NanoDrop 2000c spectrophotometer	Peqlab Biotechnologie GmbH, Erlangen, Germany

2.13 Software

https://info.progenetix.org/uploader.html	University of Zurich, Switzerland
ImageQuant TL	GE Healthcare, Buckinghamshire, UK
AxioVision 4.8	Carl Zeiss Werk, Göttingen, Germany
Diva software Ver. 7.0	BD Biosciences, Heidelberg, Germany
ModFit LT 3.2 software	Verity Software House, Topsham, ME, USA
GraphPad Prism 5 software	GraphPad Software, San Diego, CA, USA

3 Methods

3.1 Human sample preparation

All patient samples included in the study were pre- or postmenopausal women diagnosed with primary or metastatic breast cancer and underwent surgery or therapeutic interventions at Caritas Hospital St. Josef Regensburg. Written informed consent was provided by every patient. Fresh, solid tumor material was removed under sterile conditions by a pathologist after the arrival at the institute of pathology at the University clinic Regensburg. The specimen were taken based on the permission of the Ethics Committee of the University of Regensburg (permission number: 14-101-0063 and 17-527-101). Table 20 shows all samples included in the study. The specimen number of the experiments conducted varies due to the fact of limited material of some samples.

3.1.1 Isolation of tumor cells from serous effusions

Pleural effusion or ascites samples were immediately shipped at room temperature after thoracentesis or laparocentesis. The tumor cells were isolated according to the protocol of DeRose 2013 (DeRose *et al.*, 2013). In brief, the fluid was transferred to a sterile falcon and centrifuged at 530 g for 5 min at 4 °C. The supernatant was discarded and red blood cells were lysed with the incubation of the cells in 10 ml TAC buffer gently agitating the suspension in a water bath at 37 °C for 10 min. After centrifugation at 530 g for 5 min at 4 °C, the lysis was repeated if red blood cells remained on the top layer of the tumor cell pellet. The tumor cell suspension was then counted under a light microscope with trypan blue staining using a hemocytometer. Occasionally, the suspension was cultured in basal medium (DMEM/F12 supplemented with 1 % 1M HEPES, 1 % Penicillin/Streptomycin (10 U/µL), and 1 % Amphotericin B) overnight until the next day. In order to get rid of remaining immune cells, the was suspension was depleted with CD45 MicroBeads (human) according to the manufacturers' protocol using manual separators for column-based cell isolation (Miltenyi Biotech). Therefore, the cell suspension was centrifuged at 300 g for 10 min at RT, the supernatant was aspirated and the pellet was resuspended in the appropriate amount of pre-cooled separation buffer (80 µl buffer per 10^7 total cells). Accordingly, 20 µl of CD45 Microbeads were added per 10^7 total cells, mixed and incubated for 15 min in the refrigerator. Afterward, the cells were washed by adding 1-2 ml of buffer per 10^7 cells

and centrifuged at 300g for 10 min. The supernatant was discarded and the pellet was resuspended in separation buffer (10^8 cells in 500 µl buffer). Before separation, the cell suspension was filtered through a 40 µm strainer. The magnetic separation columns were pre-rinsed with the appropriate amount of buffer depending on the column size (MS (500 µl) or LS (3 ml)). The cell suspension was applied to the column and the unlabeled cells that passed through were collected - that is the tumor cell fraction. The column was washed three times (3 x 3 ml) and the process was repeated with a fresh column to increase the purity of the tumor cell suspension. The column containing the $CD45^+$ cells was discarded and the flow containing the tumor cells was counted with trypan blue (1:2) using a hemocytometer. Occasionally, the cells were cultured in non-adherent Nunclon Sphera 6-well plates in basal medium until further use.

3.1.2 Primary tumor tissue

The solid tumor material was removed under sterile conditions under a laminar flow hood by a pathologist. The tumor was collected in prewarmed basal medium (DMEM/F12, 1 % HEPES (1M), 1 % Pen/Strep, 1 % Amphotericin B) in a petri dish and minced into fragments of 2 x 2 mm. The tumor fragments were either transplanted subsequently into NSG mice, cryopreserved or stored in basal medium until transplantation. Another method was the mechanical dissociation of the primary tumor under the laminar flow hood in prewarmed PBS using the Medimachine System with a sterile Medicon application. The cell suspension was filtered through a 40 µm strainer and centrifuged at RT for 2min at 210 g. The pellet was resuspended in DMEM and counted with trypan blue (1:100) using a hemocytometer. 1.5 x 10^6 tumor cells were used for flow cytometric analysis (SCF, RECON, and TCF see Table 4 and Table 5) and 2* 10^6 single cells were used for subcutaneous transplantation into NSG mice.

3.1.3 Isolation of hematopoietic stem cells from cord blood

Cord blood samples were obtained based on the approval given by the Ethics Committee of the University of Regensburg (permission number 17-527-10). All patients provided informed written consent. In order to humanize mice, $CD34^+$ hematopoietic stem cells (HSC) were isolated from the umbilical cord blood as described in the following:

Most of the samples were taken during a cesarean section to provide a high amount of umbilical cord blood. Immediately after cord blood puncture, the cord blood collection bags (Macopharma) were shipped at room temperature to our institute. The

isolation of $CD34^+$ cells was performed under sterile conditions. The content of the cord blood collection bag was mixed carefully to avoid blood agglutination, disinfected, and placed under the laminar flow hood. The blood was mixed with PBS (1:1) in 50 ml falcons (25 ml PBS and 25 ml cord blood). 50 ml falcons pre-filled with 15 ml Pancoll were overlayed with 30 ml of the PBS-blood mixture while holding the tube angular to avoid agitation. After gradient centrifugation without brake for 30 min at 600 rcf at RT, the yellow plasma layer was aspirated and the interphase (buffy coat) containing the mononuclear cells (MNCs) was pipetted with a 1000 µl pipette into a 50 ml tube pre-filled with 25 ml PBS / 2 mM EDTA solution (Figure 3). The bottom layer containing the Pancol layer, and a pellet of granulocytes and erythrocytes was discarded.

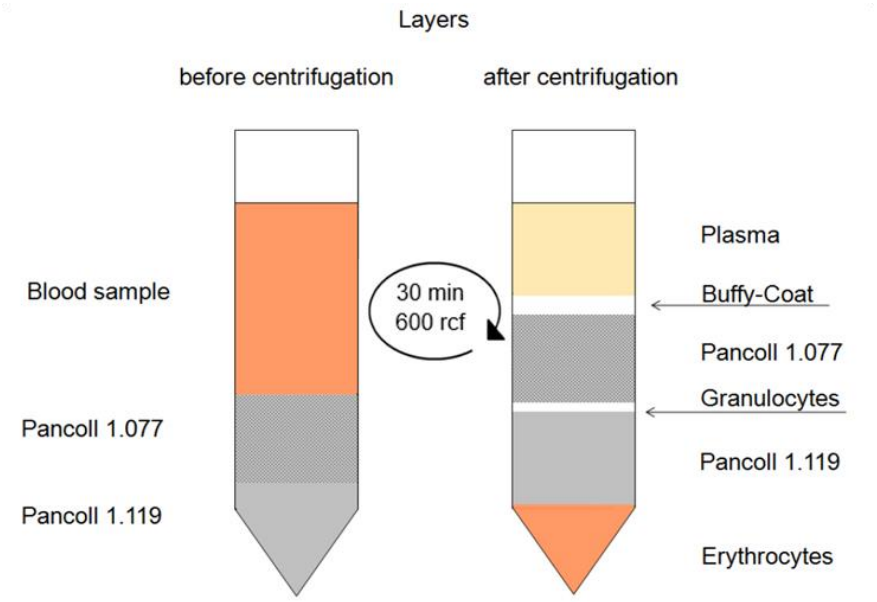

Figure 3: Graphic presentation of the different layers before and after the density gradient centrifugation
Adapted and modified from PAN Biotech GmbH, Aidenbach, Germany

The MNC cell suspension was then centrifuged at 300 rcf for 10 min at 4 °C. The supernatant was discarded, the pellet resuspended in 4 ml PBS/ EDTA and the cells were counted using a hemocytometer diluted 1:100 in trypan blue. All further steps were performed on ice under the laminar flow hood. The cells were centrifuged again for 10 min at 300 g at 4 °C, diluted in 300 µl separation buffer, 50 µl CD34 human MicroBeads, and 50 µl FcR Blocking reagent (Miltenyi) per 10^8 total cells. The suspension was incubated for 30 min at the refrigerator gently mixing the solution every 10 min. After centrifugation at 300 rcf for 10 min at 4 °C, the supernatant was aspirated, the pellet resuspended in 500 µl separation buffer per 10^8 total cells and the LS column placed in the magnetic MACS MultiStand with a 40 µm cell strainer on top. The latter

was pre-rinsed with 3 ml separation buffer and the bead labeled cells were pipetted through the cell strainer into the column. The flow-through containing the unlabeled cells was collected in a 15 ml tube. In order to increase the amount of $CD34^+$ cells, the flow-through was pipetted again into the column. Afterwards, the column was washed with the appropriate amount of separation buffer (3 x 3 ml), the column was removed from the separator out of the magnetic field and placed on a fresh 15 ml tube. 5 ml buffer were added and the $CD34^+$ labeled cells were collected by firmly pushing the plunger into the column. The cell suspension was stained with trypan blue (1:100), counted with a hemocytometer and 5 µl of the eluate were used to determine the purity of $CD34^+$ cells by flow cytometry. If the cells were not used immediately after separation the flow was cryopreserved in 50 % RPMI, 30 % FCS, and 20 % DMSO and the $CD34^+$ cells in 90 % FCS with 10 % DMSO until further use.

3.2 Animal Experiments

All animal experiments were performed according to the approval of the local veterinary of the district government of lower and upper Palatinate based on the national regulations of the German animal protection act and the European guidelines (permission number: 55.2 DMS-2532-2-422 and 54.2532.1-16/14). NOD-SCID IL2Rγnull (NSG) mice were obtained from Jackson Laboratories and bred and kept in a specialized pathogen-free facility at the University Clinic of Regensburg. The animals were housed in groups of 2 - 4 mice of the same sex (12 h light-dark-cycle, 22–24 °C) with access to water and food *ad libitum*. Breeding was performed by mating 1 - 2 females with one male and the offspring was weaned three or four weeks postpartum. The maintenance of the phenotype was verified regularly by NSG PCR of the breeding animals posthumously (Quadros *et al.*, 2016).

3.2.1 Experimental Design

In order to adapt the primary tumor specimen to the new NSG mouse microenvironment, the specimen were transplanted into NSG mice. After successful engraftment in the tumor mouse (TM), the tumors of the TM were used to generate humanized tumor mice (HTM) (Figure 4). All specimen were analyzed as described in the following:

Primary tumors were phenotypically analyzed for EpCAM, CD44, CD24, CD47, cMET, Her2 (stem cell marker) expression, TILs (CD45, CD3, CD19, CD33), and T-cell subsets CD4, CD8, CD45RA, CD27, PD-1, and CD127 (immune cell phenotyping).

Additionally, the tumor was embedded in paraffin for immunohistochemical staining, cryopreserved and cultured. Panel Sequencing of the tumor was performed by our cooperation partner in Munich. Tumor fragments were used for transplantation into NSG mice.

TM tumors were phenotypically analyzed on stem cell marker expression (EpCAM, CD44, CD24, CD47, cMET, Her2), cryopreserved, cultured and used for single-cell analysis. Additionally, the tumor was embedded in paraffin for immunohistochemical staining and fragments were flash-frozen for HuMo PCR and Western Blot analysis. Panel Sequencing of the tumor was performed by our cooperation partner in Munich. The lung, the liver, the brain, and the kidney were embedded in paraffin for immunohistochemical staining and analyzed phenotypically with the SCF on metastases. BM DTCs were characterized by SCF analysis, cultured and spotted on slides for single-cell analysis which was performed in cooperation with Christoph Irlbeck. TM tumors fragments were used for further transplantation into HTM.

HTM tumors were phenotypically analyzed on stem cell marker expression, TILs (RECON), and T-cell subsets (TCF). Furthermore, the tumor was embedded in paraffin for immunohistochemical staining, cryopreserved, cultured and used for single-cell analysis. The humanization was analyzed by RECON in the spleen, the blood, the BM and the LN. Additionally, the TCF was performed by flow cytometry in the spleen and the BM. For immunohistochemical analysis, the spleen was paraffin-embedded. The lung, the liver, the brain, and the kidney were embedded in paraffin for immunohistochemical staining and analyzed phenotypically with the SCF on metastases. BM DTCs were characterized by SCF analysis, cultured and spotted on slides for single-cell analysis which was performed in cooperation with Christoph Irlbeck.

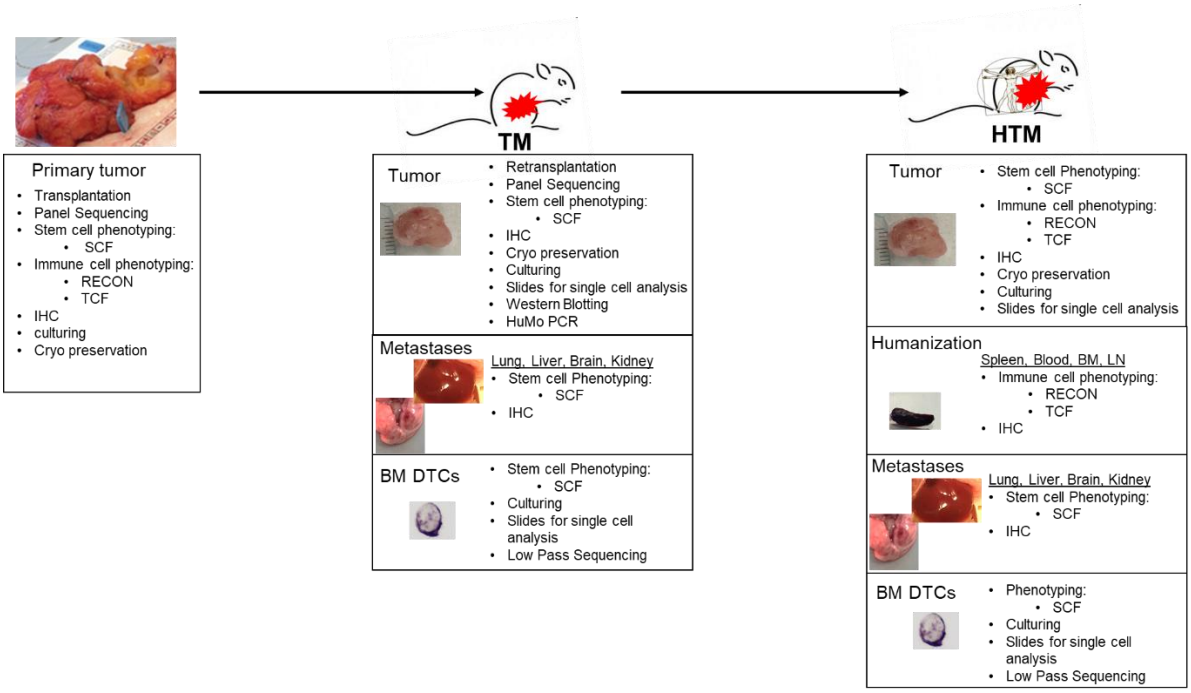

Figure 4: Schematic description of the workflow with Luminal B tumors in TM and HTM.
The graphic shows the transplantation flow from the primary tumor to the TM and from the TM to the HTM. All analyses of the different tissues and the used methods are described below each step.

3.2.2 Generation of tumor mice (TM)

33 primary or metastatic patient tumor samples were sent from Caritas Hospital St. Josef Regensburg to our laboratory in the institute of pathology at the University clinic Regensburg. The solid tumor material was removed under sterile conditions under a laminar flow hood by a pathologist. The tumors were collected in prewarmed basal medium (DMEM/F12, 1 % HEPES (1M), 1 % Pen/Strep, 1 % Amphotericin B) in a petri dish and minced into fragments of 2 x 2 mm. The transplantation was carried out in seven to eight weeks old, virgin, non-ovariectomized, female NSG mice according to the protocol of Al-Hajj (Al-Hajj *et al.*, 2003). More specifically, the mice received an antagonizable anesthesia intraperitoneally according to their weight and were placed under a laminar flow hood on a heating plate to ensure constant body temperature during the surgery (Table 2).

Table 2: List of the amount of anesthesia and antagonist required for the mouse according to the bodyweight

animal weight	anesthesia	antagonist
17 g	110 µl	180 µl
18 g	120 µl	190 µl
19 g	120 µl	200 µl
20 g	130 µl	210 µl
21 g	140 µl	230 µl

22 g	140 µl	240 µl
23 g	150 µl	250 µl
24 g	160 µl	260 µl
25 g	160 µl	260 µl
26 g	170 µl	275 µl

The mice received artificial tears in the form of cream on their eyes to protect them from drying. The mice were disinfected at the mammary fat pad (mfp) and through a small incision by the 4th or the 5th right mammary fat pad the tumor fragments were transplanted without clearing the fat pad beforehand. Additionally, the fragment transplanted was supplemented with 50 µl of Matrigel to allow nutritional content and enhance engraftment success. After closing the suture with Vicryl absorbable sewing material the animals received the antagonist and buprenorphine for analgesia (2 µl/g, s.c.) subcutaneously. The mice were placed on a heating plate to maintain the body temperature at 38 °C until the animals fully recovered. Long-term estrogen supplementation was achieved by a subcutaneous transplantation of a 17ß-estradiol pellet at a concentration of 0.18 mg that was administered simultaneously with tumor transplantation. To overcome long engraftment durations of the primary tumors, three already existing Luminal B PDX tumors from Dr. Marangoni (Institute Curie, Paris, France) were sent to our laboratory (HBCx3, HBCx22, HBCx34) and preprocessed as described above (Cottu *et al.*, 2012; Marangoni *et al.*, 2007; Reyal *et al.*, 2012; Cottu *et al.*, 2014)(Table 3). In addition two already existing Luminal B PDX models (; one derived from circulating tumor cells in the blood (CTC) (Baccelli *et al.*, 2013; Baccelli *et al.*, 2014) and the other from a pleural effusion (Bpe) of a Luminal B patient were provided by our cooperation partner (Prof. Trumpp, HI-Stem, Heidelberg, Germany) to generate TM and HTM in our laboratory. After the arrival of the CTC and Bpe tumors from our cooperation partner in Heidelberg, tumors were mechanically dissociated under the laminar flow hood in prewarmed PBS using the Medimachine System with a sterile Medicon application. The cell suspension was filtered through a 40 µm strainer and centrifuged at RT for 2 min at 210 g. The pellet was resuspended in DMEM and counted with trypan blue (1:100) using a hemocytometer. $2^* 10^6$ single cells were resuspended in a mixture of Matrigel and DMEM medium (10 µl + 20 µl) and transplanted subcutaneously into NSG mice (Table 3). In contrast, single-cell suspensions deriving from metastatic breast cancer patients effusions (AB model) $0.3^* 10^6$ tumor cells diluted in 50 µl DMEM were administered intraperitoneally into neonatal NSG mice (Table 3). In order to observe tumor engraftment and growth, the tumors

were palpated twice a week. The patient-derived xenograft (PDX) models were monitored for 12 months and euthanized beforehand if maximum tumor volume was reached or any signs of sickness occurred. If enough tissue was available the mice were transplanted in the left and the right mammary fat pad.

Table 3: Transplantation methods for the successfully established PDX models

PDX name	tumor	Derived from	Transplantation site
TM P	solid	Caritas Hospital St. Josef	orthotopic mfp fragments
TM AB	Pleural effusion	Caritas Hospital St. Josef	i.p. single cell suspension
TM X	solid	Caritas Hospital St. Josef	orthotopic mfp fragments
TM V	solid	Caritas Hospital St. Josef	orthotopic mfp fragments
TM U	pleural effusion	Caritas Hospital St. Josef	orthotopic single-cell suspension
TM CTC	solid	Prof. Trumpp, HI-Stem, Heidelberg, Germany (Baccelli *et al.*, 2013)	s.c. single-cell suspension /orthotopic mfp fragments
TM Bpe	solid	Prof. Trumpp HI-Stem, Heidelberg, Germany (unpublished)	s.c. single-cell suspension/ orthotopic mfp fragments
TM 3	solid	Dr. Elisabetta Marangoni, Institute Curie, Paris, France (Cottu *et al.*, 2012)	orthotopic mfp fragments
TM 22	solid	Dr. Elisabetta Marangoni, Institute Curie, Paris, France (Cottu *et al.*, 2012)	orthotopic mfp fragments
TM 34	solid	Dr. Elisabetta Marangoni, Institute Curie, Paris, France (Cottu *et al.*, 2012)	orthotopic mfp fragments

mfp mammary fat pad, *TM* tumor mouse, *s.c.* subcutaneous,

3.2.3 Generation of humanized tumor mice (HTM)

Humanized Tumor Mice (HTM) were generated as described previously (Wege *et al.*, 2011). In brief, newborn NSG mice were irradiated (1 Gy) within the first 48 h after delivery to clear the BM stem cell niche and allow successful settling of HSC to the BM. Three hours later the mice received an intrahepatic injection of 50 µl human $CD34^+$ cells (0.15 -0.2 x 10^6 in DMEM) together with a subcutaneous injection of 2 x 10^6 tumor

cells diluted in 20 µl DMEM and 10 µl Matrigel using a BD Safety Glide Insulin syringe (HTM CTC and HTM Bpe model). In the case of a tumor fragment transplantation, the mice were humanized beforehand and transplanted with tumor fragments into the mfp at the age of six to seven weeks (HTM P, HTM 3, HTM 22, HTM 34). The tumor fragments were taken either freshly isolated from a TM or from cryopreserved TM tissue. Avoiding any immune cell procrastinations of the HTM tumors into other mice the HTM tumors were never retransplanted as described in Figure 5. To determine the reconstitution of the HTM 12 weeks after humanization 50 µl peripheral blood was taken from the vena saphena, mixed with 20 µl 0.5 M EDTA to avoid clotting and analyzed by flow cytometry.

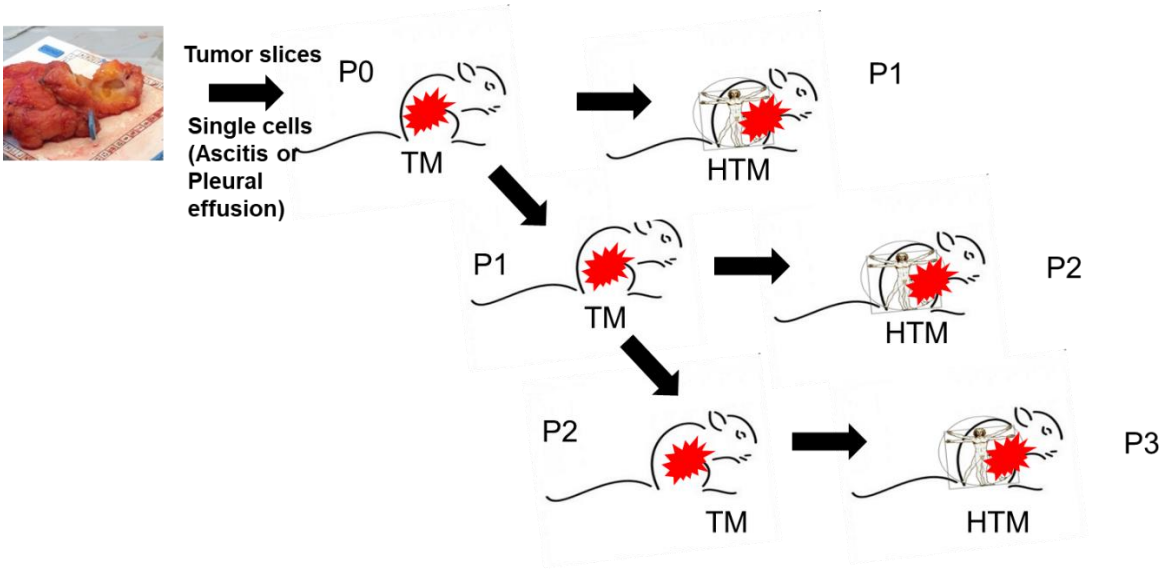

Figure 5: Schematic description of tumor passaging from TM to HTM.

3.2.4 Preparation of blood, organs and tumor tissue

TM or HTM were anesthetized and peripheral blood was taken retrobulbar with a capillary from HTM. The peripheral blood was collected in a 1.5 ml tube, allowed to coagulate at 4 °C and the supernatant containing the serum was transferred to a fresh cup after a 10 min centrifugation step (4 °C, 1300 rpm). Afterwards, the mice were sacrificed by cervical dislocation.

In the next step, 10 ml precooled PBS was injected using a 10 ml syringe with a 22G cannula into the peritoneum to isolate ascites cells. The isolated cell suspension was centrifuged at 300 rcf for 10 min at 4 °C, the supernatant discarded, the cells counted with a hemocytometer (trypan blue staining 1:100), and stored on ice until flow cytometric analysis, culturing, or paraffin embedding.

The liver, the lung, the lymph nodes (LN), and the spleen was removed and placed in PBS on ice. Approximately one half of each organ (liver, lung, spleen) was embedded in paraffin for histological staining while the other part was minced with PBS through a 40 µm cell strainer using the plunger of a 2 ml syringe. The cell suspensions were centrifuged (4 °C, 300 g, 10 min), the supernatant was discarded and the cells were resuspended in FACS buffer for flow cytometric analysis. Due to the size of the organ, the LN of HTM was just analyzed by flow cytometry.

The brain and the kidney were isolated and only embedded in paraffin for histological analysis.

The solid tumors (subcutaneous or from the mammary fat pad) were removed, pruned of fat tissue, weighed and measured. The volume of the tumor was calculated according to the formula (ellipsoid shaped tumors): volume = π / 6 x length x width x height (Tomayko and Reynolds, 1989). One part of the tumor was embedded in paraffin for histological analysis. Two small fragments were flash-frozen for protein isolation and DNA extraction at - 20 °C and – 80 °C. 4 fragments of 2 x 2 mm size were cryopreserved in 1.5 ml CryoStor Medium for future transplantations and the remaining tumor was used for single-cell analysis, flow cytometry, and cell culture. For single-cell preparation, the tumor was minced with PBS in the Medimachine System and filtered through a 40 µm cell strainer. The cell suspension was centrifuged at 230 rcf for 3 min at RT and the supernatant containing fat, fibroblasts, and immune cells were analyzed flow cytometrically on TILs (RECON) and T-cell subsets. The tumor cells were resuspended in PBS, counted with a hemocytometer (trypan blue 1:100), and 500.000 cells were pipetted on adhesion slides for single-cell analysis. The cells adhered on the slide within 90 min and the supernatant was discarded. The slides were dried overnight and stored at - 20 °C until further use. 500.000 tumor cells were used for flow cytometric analysis and the residual tumor cells were cultured in basal medium under two different conditions using adhesive or non-adhesive 6-well plates.

Additionally, the right and the left hind leg were taken for bone marrow (BM) collection. Therefore, the bones were pruned of muscles and the ends of the femur were clipped and flushed with PBS using a 10 ml syringe with a 27G needle until the bone appeared white. The cell suspension was centrifuged (10 min, 300 g, 4 °C) and the supernatant was aspirated. The pellet was resuspended in fresh PBS, filtered through a 40 µm cell strainer to remove remaining bone fragments and centrifuged again (10 min, 300 g, 4

°C). The supernatant was discarded, the cell pellet was diluted in PBS, and counted with Türk′s solution to haemolyse remaining erythrocytes. 500.000 cells were spotted on adhesion slides and tilted of PBS after 90 min of incubation time. The slides were dried overnight and stored at - 20 °C until single-cell analysis. 500.000 cells were analyzed by flow cytometry and the remaining BM cells were cultured in adherent conditions in 6-well plates in basal medium in order to enable the disseminated cells to grow for 4 -5 months.

3.3 Flow cytometry

3.3.1 Phenotypic Analysis

In order to determine phenotypic alterations, TILs, or reconstitution the organs were analyzed by flow cytometry using a FACS Canto-II flow cytometer run by the Diva software Ver. 7.0 (BD Biosciences, San Jose, USA). The Stem cell marker expression panel (stem cell marker FACS: SCF) was used for primary patient tumor, TM and HTM tumor, TM and HTM BM DTCs, TM and HTM lung and liver metastases and included CD44, CD47, MET, CD24, Her2, and CD45 (Table 4). In contrast, the T-cell subset panel (T cell marker FACS: TCF) comprised of CD3, CD4, CD8a, CD45RA, CD27, CD127, and PD-L1 and was determined on primary patient tumor samples or organs from HTM (tumor, spleen, BM)(Table 4). To verify the humanization in HTM (spleen, BM, LN) or TILs in the primary patient tumor or HTM tumor CD45, CD3, CD19 and CD33 (RECON) were analyzed (Table 4). The appropriate mouse immunoglobulin was used for each staining as control and is described in Table 5. A detailed description of the used staining for each organ and tumor is summarized in Figure 4.

Table 4: Antibody Staining

Laser	**Blue laser**			**Red laser**		**Violet laser**	
Fluorochrome	FITC	PE	PE/Cy7	APC AF647	APC Vio 770	BV510	BV421
SCF	Her2	CD47	CD44	c-MET	CD24	CD45	EpCAM
TCF	CD3	CD127	CD27	PD-1	CD4	CD8a	CD45RA
RECON	CD3	CD19	CD33	CD45	X	X	X

Table 5: Isotype Control

Laser	**Blue Laser**			**Red Laser**		**Violet Laser**	
	FITC	PE	PE/Cy7	APC AF647	APC Vio 770	BV510	BV421
SCF	Mouse IgG1 κ	Mouse IgG1 κ	Mouse IgG2b,κ	Mouse IgG1 κ	Mouse IgG1 κ	Mouse IgG1 κ	Mouse IgG2b, κ

TCF	CD3	Mouse IgG1 κ	Mouse IgG1 κ	mouse IgG1, κ	CD4	CD8a	Mouse IgG2b, κ
RECON	No isotype necessary						

Prior to transplantation of tumor material in mice, each primary tumor specimen was analyzed phenotypically on stem cell marker expression, TILs, and reconstitution. The tumors derived from TM were only analyzed on stem cell marker expression whereas the HTM tumors were additionally investigated on immune cell infiltration and the different T-cell subsets. The reconstitution of HTM with human immune cells was determined in the spleen, the BM, and the spleen of HTM.To identify metastases in liver or lung or disseminated cancer cells (DTCs) in the BM, the organs were analyzed using SCF staining whereas EpCAM (epithelial cell adhesion molecule) served as a surrogate marker for tumor cells. The existence and occurrence of EpCAM- tumor cells is possible but not included in the analysis. FACS staining procedure for all organs is described in the following. In order to reduce non-specific binding, 500.000 cells were incubated with 20 µl mouse serum on ice 10 min before specific antibody staining. The cells were stained then for 30 min with 50 µl FACS buffer including the appropriate amount of antibodies of the certain staining SCF, TCF, and RECON (Table 4). After a washing step with 1 ml FACS buffer, the cells were centrifuged (3 min, 300g, RT) and diluted in 300 µl FACS buffer.

3.3.2 Apoptosis

The apoptosis assay was used to analyze the treatment effects of tumor cells on cell death. Living cells are lacking a phosphatidylserine membrane flip to bind annexin V and their cell membrane is intact thereby prohibiting PI to enter the cell. Hence, living cells are negative for both, annexin V and PI. Cells in early apoptosis are annexin V positive but negative for PI at low concentrations, whereas annexin V and PI-positive cells reside in late apoptosis (Figure 6). In order to include the apoptotic cells in the measurement, the supernatant was pipetted into a 50 ml tube with 20 ml PBS. The adherent cells were washed, trypsinized, stopped with medium containing FCS and added to the tube with the supernatant in PBS. After centrifugation (3 min, 12000 rpm, 4 °C) the supernatant was discarded and the cells were resuspended in 75 µl AnnexinV-FITC solution containing 5 µl Annexin V FITC and 70 µl binding buffer. After 20 min of incubation on ice in the dark, the cells were resuspended in 200 µl binding buffer and transferred to a FACS tube. Prior to the measurement 10 µl of DAPI (stock concentration: 5 µg/ml) were added to the tube.

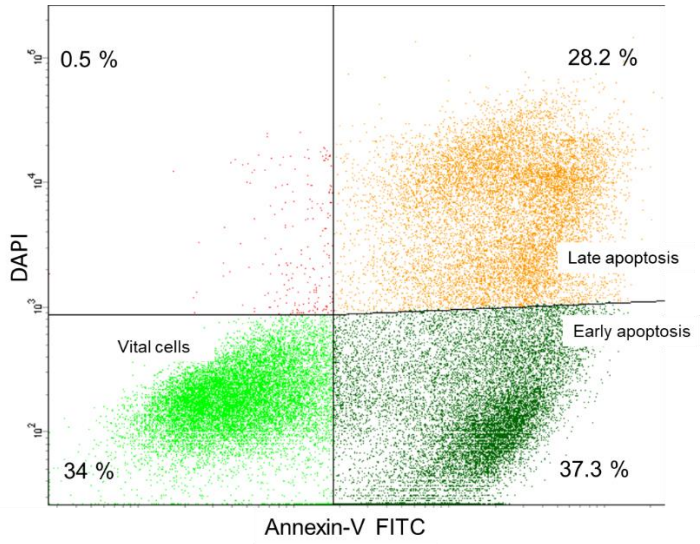

Figure 6: Example of apoptosis assay analyzed by flow cytometry
The staining is depicted as Annexin-V FITC versus DAPI. The percentage of vital cells, cells in early and late apoptosis are listed in each quadrant.

3.3.3 S-phase fraction

The S-phase fraction was analyzed to determine proliferative capacity after breast cancer cell line treatment. During cell proliferation, the cell enters different parts of the cell cycle which are subdivided in mitotic division (M-Phase) and the Interphase comprising gap 1 (G1), synthesis (S), and gap 2 (G2) phase. Due to the different chromosome sets of each phase, the cells can be analyzed on their proliferative capacity. Therefore, 500.000 cells were harvested, washed with PBS, and lysed with 500 µl 70 % methanol in a closed tube overnight in the fridge. The next day the cells were washed two times with 2 ml FACS buffer, centrifuged and resuspended in 440 µl FACS buffer with 50 µl RNAse. After 20 min incubation in a 37 °C water bath, 10 µl DAPI (50 µg/ml) were added and incubated on ice in the dark for 30 min. The distribution of the cells in different cell cycle phases was analyzed by flow cytometry and calculated by ModFit Software. For each treatment condition, the appropriate untreated control and solvent control was applied.

3.4 Human -Mouse PCR

3.4.1 DNA extraction and quantitative real-time PCR

To verify the human origin of the engrafted PDX tumors a quantitative RT PCR was performed according to the paper of Malek published in 2010 (Malek *et al.*, 2010). The DNA of the TM derived tumor fragment was extracted using blood and cell culture DNA mini kit according to the manufacturer's protocol. The DNA concentration was determined spectrophotometrically using a NanoDrop 2000c spectrophotometer. Each

RT-PCR comprised 8 µl of the template DNA (250 ng of total genomic DNA), 10 µl iQTM SYBR® Green Supermix (Bio-Rad), and 1 µl of each forward and reverse primer (human ß-actin or mouse ß-2-microglobin,10 µM stock concentration) (Table 6 and Table 7).

Table 6: HuMo PCR Master mix	
iQ™ SYBR® Green Supermix	10 µl
Forward-Primer	1 µl
Reverse-Primer	1 µl
Template	8 µl
Total	20 µl

Table 7: HuMo PCR Primer		
	Sequence	Amplicon length
human ß-actin 5’	5’-ctgttttgtggcttgttcag-3’	
human ß-actin 3’	5’-aggaaaccttccctcctcta-3’	122 bp
mouse ß-2-microglobin 5’	5’-ttggttgagaagcagaaaca-3’	
mouse ß-2-microglobin 3’	5’-cacacagtcaagttcccaaa-3’	181 bp

RT-PCR was run with the program described in Table 8

Table 8: RT-PCR program			
Description	Temperature	Duration	cycle
Initial melting	95 °C	05:00	
Melting	95 °C	00:45	
Annealing	59 °C	00:45	35
Elongation	72 °C	00:45	
Elongation	72 °C	05:00	
Melting Curve			
Cooling	40 °C		

The melting blots were analyzed to validate PCR specificity. To determine the coefficients for data analysis a standard curve was performed. Therefore, different amounts of human (N1 = adult skin of a healthy donor, cloned but not immortalized (Department of Clinical Chemistry, University of Regensburg)) and mouse (NIH/3T3 primary mouse embryonic fibroblast cells (ATCC® CRL-1658™)) genomic DNA were prepared as described in Table 9 in line 1 and 2. From the percentage of human DNA

in each mixture (line 3) the corresponding percentage of human cells was calculated (line 4) by adjusting the differences in mouse and human genome size with the formula:

% Human cells = (% HumanDNA/3.2)/(% HumanDNA/3.2 + % MouseDNA/2.7) x 100

RT-PCR was run for each DNA mixture with human- or mouse-specific primers in triplicates. From the results given as cycle threshold (Ct) (line 5 and line 6), the amplification ratio was calculated for each pair of RT-PCR using Amplification Ratio = 2(Ct [Human] – Ct [Mouse] (line 7) and was Log2 transformed (line 8). Input values (% human cells; line 4) and experimental results (Log2 amplification ratio; line 8) were fitted using the non-linear regression 3- parameter sigmoidal function f = a/(1+exp(-(x-x0)/b)) and the constants were determined to be a = 99,8213, b = 1,4232, and x_0 = -1,4401. Based on these constants, the percentage of human cells was re-calculated from log (2) amplification for each standard (line 9). The detection limit of human cells in mouse tissue was therefore determined as 1.4 % human cells in mouse tissue. The DNA content of the TM and HTM tumor probes was calculated with the constants derived from the sigmoidal standard curve. As a control different mixtures of human and mouse DNA (Hu:Mo -50 %:50 %; 0 %:100 %; 100 %:0%) and H_2O were applied to each run.

Table 9: Calculation of the standard curve for HuMo PCR

1	**Human DNA in ng**	250,00	249,88	249,51	249,02	248,05	246,09	242,19	234,37	218,75	187,5	125	62,5	31,25	15,62	7,81	3,91	1,95	0,98	0,49	0,12	0
2	**Mouse DNA in ng**	0	0,12	0,49	0,98	1,95	3,91	7,81	15,63	31,25	62,5	125	187,5	218,75	234,38	242,19	246,09	248,05	249,02	249,51	249,88	250
3	**Human DNA (%)**	100,000	99,951	99,805	99,609	99,219	98,438	96,875	93,750	87,500	75,000	50,000	25,000	12,500	6,250	3,125	1,563	0,781	0,391	0,195	0,049	0,000
4	**Human cells (%)**	100,000	99,942	99,769	99,537	99,075	98,153	96,318	92,677	85,520	71,681	45,763	21,951	10,757	5,325	2,650	1,322	0,660	0,330	0,165	0,041	0,000
qPCR results and calculations																						
5	**Ct with human primers**	20,688	20,677	20,677	20,682	20,676	20,649	20,700	20,728	20,831	21,027	21,674	22,638	23,601	24,425	25,394	25,977	26,394	26,816	27,166	26,706	26,493
6	**Ct with mouse primers**	30,000	30,000	28,078	26,988	26,117	25,046	24,018	22,959	21,982	20,980	19,934	19,355	19,181	19,052	19,028	18,929	18,908	18,897	18,895	18,856	18,894
7	**Amplification Ratio**	635,659	640,277	168,995	79,119	43,416	21,069	9,974	4,695	2,220	0,967	0,299	0,103	0,047	0,024	0,012	0,008	0,006	0,004	0,003	0,004	0,005
8	**Log(2) Amp Ratio**	9,312	9,323	7,401	6,306	5,440	4,397	3,318	2,231	1,150	-0,048	-1,740	-3,283	-4,420	-5,372	-6,365	-7,048	-7,487	-7,919	-8,272	-7,849	-7,599
Reverse calculation																						
9	**Human cells (%)**	99,769	99,769	99,622	99,391	99,034	98,196	96,416	92,787	85,904	72,548	44,667	21,462	10,948	5,926	3,040	1,904	1,406	1,041	0,815	1,093	1,300

3.5 Immunohistochemical Staining

Tissue samples of spleen, liver, lung, brain, pleural effusion, primary patient tumors or TM or HTM tumors were fixed in 4 % formalin, embedded in paraffin (FFPE) and cut into 1.5 µm slices as described previously (Rom-Jurek *et al.*, 2018). The specimens were stained automatically for CK18 (DC10, DAKO), ER (6F11, Novocastra), PR (Clone 16, Novocastra), Her2 (order number A0485, DAKO), Ki67 (MIB-1, DAKO), EpCAM (Ber-EP4, DAKO), PD-L1 (28-8, Abcam) by Ventana Nexes autostainer (Ventana, Tucson, USA). The autostainer was programmed based on the instructions given in the manual of the iView DAB detection kit (Ventana, Tucson, USA, #760–091). Additionally, each tumor slide was stained with hematoxylin and eosin (H&E) to verify tumor cell morphology. H&E staining was manually performed by incubation of the slide for 5 min in acetone at -20 °C and a 5 min step to airdry the slides at RT. This was followed by the rehydration of the slide in a descending alcohol gradient (99 %, 96 %, and 70 % ethanol, 1 min for each dilution) and a 20sec nuclei staining with hematoxylin. The slides were washed for 20 min in H_2O and counterstained with eosin for 20 sec with a subsequent washing step in H_2O for 20 min. Finally, the slides were dehydrated in descending alcohol gradient (70 %, 96 %, and 99 % ethanol, 1 min for each dilution), submerged in xylol and mounted with entellan. MDM2 ((IF2, Calbiochem), CD44 (156-3C11, cell signaling), and CD47 (catalog number AF4670, R&D) were also stained manually. In brief, the samples were deparaffinized followed by rehydration in a descending ethanol gradient (100%, 80%, 70%). Antigen retrieval was done with Tris/EDTA buffer (pH 9) at 121 °C for 5 min using the decloaking chamber. The slides were cooled down for 1 h in a water bath. After blocking endogenous peroxidase with Dako REAL™ Peroxidase-Blocking Solution the slides were washed with Dako wash buffer (dilution 1:10) for 5 min and the primary antibody MDM2 (IF2, Calbiochem), CD44 (156-3C11, cell signaling) and CD47 (catalog number AF4670, R&D) were applied in appropriate dilution (1.5 µg/ml / 1:50 / 1:25) for 45 min. Afterwards, the sections were washed with wash buffer and for CD47 antibody the slide was additionally incubated with Polink-2 Plus HRP Sheep for 10 min with three drops of reagent 1 and additional 10 min with three drops of reagent 2. CD47 slides were washed again and the secondary antibody was applied for 30 min at room temperature. CD47, MDM2, and CD44 sections were washed again and incubated for 10 min with DAB plus substrate-chromogen solution in appropriate dilution (1:10). The

specimens were rinsed with distilled water and counterstained with hematoxylin for 2 min. The sections were rinsed in tap water (5 min), distilled water (1 min), and dehydrated in ascending ethanol gradient (70 %, 80 %, 100 %). After 2 x 5 min cleaning steps the specimens were cover-slipped with xylene containing mounting medium. All histological specimens were imaged with an AxioImager Z1 microscope (Zeiss, Oberkochen, Germany). H&E, ER, PR, Her2, Ki67 stainings of the primary patient tumor and H&E and PD-L1 of TM and HTM tumor were analyzed in routine diagnostic at the institute of pathology at the University clinic Regensburg by a pathologist. To assess the PD-L1 staining an additional score was used as published previously (Brockhoff *et al.*, 2018) (Table 10).

Table 10: PD-L1 Score adapted from (Brockhoff *et al.*, 2018)

Score	% PD-L1
0	0
1	1 to 9
2	10 to 39
3	> 40

3.6 Analysis of Lung metastases

To quantify the metastatic properties of the different PDX models as well as the influence of the human immune system, the 1.5 µm lung slices were stained for CK 18 as described at 3.5 immunohistochemical staining. Three representative pictures of one lung slide for each animal were taken under the light microscope in 20-fold magnification. If minimum two of the three pictures contained lung micrometastases the general occurrence of lung metastases was considered as positive, otherwise the lung was recorded as negative for micrometastases.

3.7 Fluorescence in-situ-hybridisation (FISH)

Tumor tissue sections of the different TM PDX models (TM P, TM CTC, TM Bpe, TM 34, TM 22, TM 3) and a paraffin-embedded cell pellet section of TM AB were applied on charged SuperFrost Plus slides and Fluorescence in-situ hybridization (FISH) was performed using the directly labeled dual-color probe MDM2/CEN12 or CD274, PDCD1LG1/CEN9 (both ZytoVision Ltd., Bremerhaven, Germany). The MDM2 and PD-L1 specific probes were labeled with ZyGreen™ (absorption 530 nm, emission 528 nm) and the centromeric probes (CEN 12 and CEN 9) with ZyOrange™ (absorption 547 nm, emission 528 nm). The centromeric regions (CEN 12, CEN 9) were taken as a surrogate for the number of chromosome 12 and chromosome 9, respectively. The

dual marker probes enable it to interpret a potential gain of MDM2 or PD-L1 either as gene amplification or to chromosome 12 or 9 polysomy. The staining was performed as published previously (Rom-Jurek *et al.*, 2018).

3.8 Cell culture and cryopreservation

All cell culture work was performed under sterile conditions in a laminar flow hood, and the cells were cultured at 37 °C, 95 % O_2 and 5 % CO_2. The different cell lines required specific media as listed in Table 11. Before use, all media and solutions were pre-warmed to 37 °C and supplementations were added freshly. To avoid contaminations, the primary cell culture and cell line cell culture was handled in a separate laminar flow hood and in a separate incubator.

Table 11: Used cell lines and their corresponding media

NIH/3T3	DMEM + 5 % FCS
N1	DMEM + 10 % FCS
ZR-75-1	RPMI (phenol red) + 5 % FCS
BT474	DMEM + 5 % FCS
MDA-MB 231	DMEM + 5 % FCS
SK-BR-3	DMEM + 5 % FCS
JIMT 1	RPMI (phenol red) + 5 % FCS
Ascites of TM AB (primary culture)	DMEM rhEGF 20 ng/ml Insulin 5 µg/ml Amphotericin B 1 % Pen/Strep 1 % FCS 5 %
MNCs (primary culture)	RPMI + 10 % FCS
BM and primary culture isolated of different TM and HTM Primary patient tumors	DMEM/F12 Pen/Strep 1 % Amphotericin B 1 % FCS 5 % rhEGF 20 ng/ml Hydrocortisone 0.5 µg/ml Insulin 10 µg/ml ß-Estradiol 5 nM
3 D culturing	DMEM/F12 B27 diluted 1:50 rhEGF 10 ng/ml Pen/Strep 1 % Heparin 4 µg/ml rhFGF 10 ng/ml Amphotericin B 2.5 µg/ml

Before reaching full confluence, cells were passaged by washing them with PBS and treating them with accutase (primary cells) for 10 - 15 min or trypsin-EDTA (cell lines) for 5 min at 37 °C. Trypsin-EDTA reaction was stopped by adding cell-specific medium with FCS in surplus whereas no neutralization was required after accutase treatment. The flasks were agitated thoroughly to detach all the cells from the bottom of the flask. Then the cell suspension was collected in a 50 ml tube and centrifuged at room temperature for 3 min at 1200 rpm and resuspended in the corresponding medium. To determine the cell number, 10 µl of the cell suspension was mixed with the same volume of trypan blue solution, transferred to a Neubauer hemocytometer. The cells were counted (mean of 4 x 16 panel) and calculated by multiplying the mean with the dilution factor and the hemocytometer factor. For long-term storage of primary cells, approximately 1- 2 million cells were cryopreserved in 1.5 ml CryoStor Medium whereas cell lines were preserved in 10 % DMSO, 20 % FCS, and 70 % medium. Cryo-cups were frozen at – 80°C overnight and stored in liquid nitrogen until further use.

3.9 Protein biochemical analysis

3.9.1 Protein isolation

Cell line total protein lysates were performed according to the protocol published previously (Rom-Jurek *et al.*, 2018). For protein isolation out of flash-frozen tumor fragments 300 µl RIPA buffer supplemented with HALT protease inhibitor (1:100) and EDTA (1:100) were pipetted into a 1.5 ml cup and the tissue was homogenized with a pestle until the liquid was turbid. The tissue was stored on ice for 30 min, vortexed thoroughly in between, and centrifuged at 13000 rpm for 5 min at 4 °C. The supernatant was collected in a new tube and stored at – 20 °C until further use.

3.9.2.BCA Assay

The protein concentration was determined by bicinchoninic acid (BCA) assay according to manufacturers' instructions. This analytic method is based on the biuret reaction whereby divalent cuprous ions ($Cu2^{+}$) are reduced to monovalent cuprous ions ($Cu1^{+}$) in the presence of protein in an alkaline environment. BCA is capable of forming a purple complex with $Cu1^{+}$. The produced complex is stable for approximately 24h. The measured absorption at 562 nm is linear-proportional to protein concentrations over a range of 20 – 1200 µg/ml. The determination of protein concentrations was assigned in duplicates**.** Protein standard and probes (1:10) were pipetted in a 96 – well plate and blended with 200 µl of 0.08 % Cu (II) SO4 in

bicinchoninic acid. After 30 min incubation time at 37 °C, absorption was assigned at 562 nm with an ELISA reader. The final concentration of the samples was calculated *via* the standard curve method.

3.9.3. Western Blotting

20 µg protein per lane and an equivalent amount of 4 x loading dye were separated in 10 % SDS-Page under non-reduced conditions and plotted onto Polyvinylidene Difluoride (PVDF) membranes. According to the antibody, the blocking solution and the incubation time was different as listed in Table 12: **Primary antibody** below. In order to quantify the protein amount, either ß-actin or Rab11 were used as loading controls. The precision plus protein marker served as protein size standard**.** Finally, the membranes were hybridized with horseradish peroxidase (HRP)-conjugated antibodies according to the host of the primary antibody as listed in Table 13. The blots were visualized using the chemiluminescent western blotting detection system SuperSignal West Pico PLUS Chemiluminescent Substrate and were analyzed by ImageQuant LAS 4000 mini imager. For p53 and cMET antibody detection, 20 µg protein were separated in a 12 % Criterion TGX Stain-free gels. The analysis was performed using a stain-free total protein method whereby trihalo compounds bind to tryptophan residues in proteins when they are exposed to UV light. Hence, the proteins in the gel are fluorescent and can be visualized during electrophoresis or blotting. This offers the opportunity to normalize the band to total protein in each lane thereby circumventing the issue of using a loading control.

Table 12: Primary antibody

Antibody	Host and product size	Blocking solution	Dilution of the Antibody	Incubation time	Supplier
MDM2 (IF2)	Mouse - 54-90 kDa	5 % MMP in PBS/T	1:100 PBST+3 % non-fat dry milk	1 h at RT	Calbiochem
Rab 11	Rabbit 25 kDa	5 % BSA in TBS/T	1:1000 in TBS-T +5 % BSA	Overnight at 4 °C	Cell Signaling
Integrin ß1 Antikörper (N-20)	Goat 138 kDa	5 % BSA in TBS/T	1:1000 in TBS-T +5 % BSA	Overnight at 4 °C	Santa cruz
Phospho-FAK (Tyr397)	Rabbit 125 kDa	5 % MMP in TBS/T	1:1000 in TBS-T +5 % BSA	Overnight at 4 °C	cell signaling
ß-Actin	Rabbit 42 kDa	5 % MMP in TBS/T	1:5000 in TBS-T +5 % BSA	Overnight at 4 °C	Sigma
FAK	Rabbit 125 kDa	5 % MMP in TBS/T	1:1000 in TBS-T +5 % BSA	Overnight at 4 °C	Cell Signaling

CD47	Sheep 45-70 kDa	5 % MMP in TBS/T	1:200 5 % MMP in TBS/T	Overnight at 4 °C	R&D
Met (D1C2) XP	Rabbit 140,170 kDa	5 % MMP in TBS/T	1:1000 in TBS/T+ 5 % BSA	Overnight at 4 °C	Cell Signaling
CD44	Mouse 80 kDa	5 % MMP in TBS/T	1:1000 in TBS/T +5 % BSA	Overnight at 4 °C	Cell Signaling
p53	Mouse 53 kDa	5 % MMP in TBS/T	1:500 in TBS/T +5 % BSA	Overnight at 4 °C	Santa cruz

Table 13: Secondary Antibody

Antibody	**Supplier**	**Dilution of the Antibody**	**Incubation time**
Anti-Mouse-HRP	Cell signaling	1:2000 in TBS-T	1 h at RT
Anti-Rabbit-HRP	Cell signaling	1:2000 in TBS-T	1 h at RT
Anti-Goat-HRP	Sigma	1:2000 in TBS-T	1 h at RT
Anti-Sheep-HRP	Novus Biologicals	1:500 in TBS-T	1 h at RT

3.10 Breast cancer cell line treatments and assays

3.10.1 Experimental Design

MDM2 was knocked down in the breast cancer cell line ZR-75-1 with siRNA. Untreated cells and non-targeting pool cells served as controls. After treatment, the total cell number was counted and the cells were analyzed on apoptosis. Additionally, western blotting was performed to uncover potential target molecules of MDM2. Moreover, the proliferation was assessed by the measurement of the S-phase fraction (Figure 7). Additionally, the wound-healing of the cells was determined. In order to determine the clinical relevance, ZR-75-1 were treated with AMG232, an MDM2 inhibitor, for 48h and 72h and equally analyzed as MDM2 knockdown cells. Only Western Blotting was skipped in AMG232 treated cells. The detailed protocols for MDM2 knockdown and AMG232 treatment are described in the following passage.

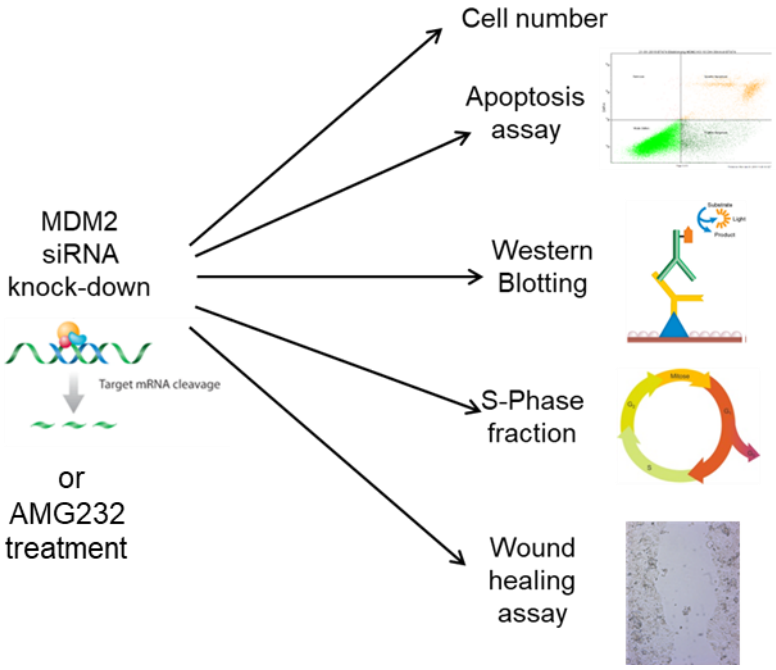

Figure 7: Schematic description of the different assay and analysis after an MDM2 knockdown or an AMG232 inhibition

3.10.2 MDM2 siRNA Knockdown

ZR-75-1 were seeded at a density of 400.000 cells per T25 tissue flask and cultured in RPMI-1640 medium supplemented with 5 % FCS overnight. On the following day, the medium was replaced with 2.5, 2.1 and 2.1 ml (untreated, non-targeting pool siRNA, and anti-MDM2 siRNA) RPMI-1640 medium supplemented with 1 % FCS, respectively. The transfection mix was prepared by incorporation of 10 µl DharmaFECT 1 reagent with 190 µl RPMI-1640 in tube A and 17.5 µl MDM2 siRNA with 182.5 µl RPMI-1640 in tube B. Non-targeting Pool was used as control and prepared in the same matter as the anti-MDM2 siRNA. After a 5 min incubation step at RT, tube A and tube B were pooled and incubated for additional 20 min. Finally, 400 µl of the transfection mixture was added to the appropriate T25 flasks with a final concentration of 70 nM per treatment, MDM2 siRNA and non-targeting Pool, respectively. The transfection reagent was removed after two days, replaced with RPMI-1640 supplemented with 5 % FCS, and incubated for additional two days (Figure 8). On day four after transfection, the cells were either harvested with trypsin-EDTA for further experiments or lyzed with 50 µl lysis buffer (100 µl Cell Lysis Buffer, 10 µl PMSF (1 mM), 10 µl HALT Protease Inhibitor, and 880 µl aqua dest.) and scraped of the flask with a cell scraper for protein biochemical analysis. To determine the protein amount of the lysed cells, the suspension was centrifuged for 10 min at 4 °C at 13000 rpm, the supernatant collected

in a fresh 1.5 ml cup and stored at – 20 °C until BCA assay. A scheme of siRNA knockdown is represented in Figure 8.

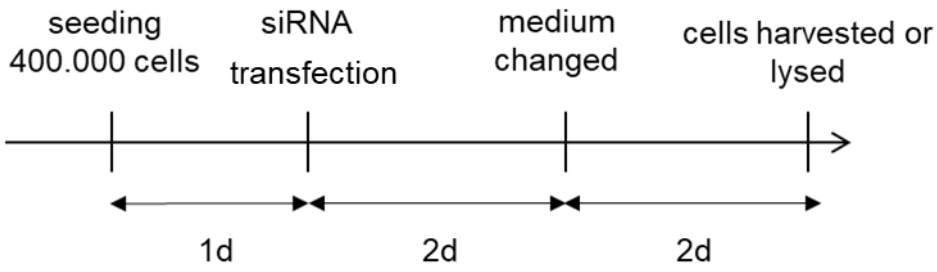

Figure 8: Schematic description of siRNA knockdown procedure
d =day

3.10.3 AMG232 treatment

ZR-75-1 were seeded at a density of 400.000 cells per T25 tissue flask and cultured in RPMI-1640 medium supplemented with 5 % FCS overnight. The next day the medium was changed and the cells treated with DMSO as control or 0.1 M AMG232 inhibitor. Untreated cells served as an additional control. 48h and 72h after AMG232 treatment the cells were harvested with trypsin-EDTA for further experiments (Figure 9).

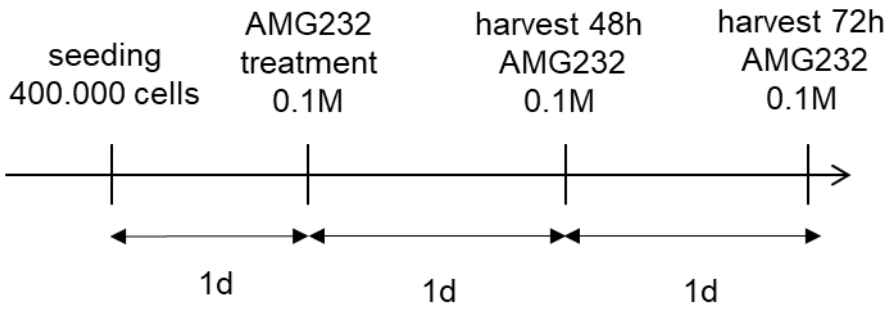

Figure 9: Schematic description of the AMG232 treatment procedure
d =day

3.10.4 Wound Healing Assay

Determination of tumor cell wound closure and migratory properties were analyzed by a wound-healing assay. In brief, 80.000 cells were seeded in each chamber of a 2-Well Culture-Insert (35 mm) (Ibidi) fixed in a 6 -well plate and were allowed to adhere overnight in their appropriate medium. The next day the insert was removed, the cells were washed with PBS to remove cell debris and fresh medium was added to the well. The cell scratch was visualized at 20-fold magnification by light microscopy and documented at the time 0h, 6h,18h, 24h, 48h, 72h, 96h, and 144h after chamber removal. To guarantee the documentation of the same region at each time point the exact coordinates at the microscope were noted at the beginning of the experiment.

For analysis of wound closure, the gap between the two cell layers was marked manually using Axio Vision software and the area of interest was calculated automatically by Axio Vision software in μm^2. For all experiments, untreated cells and cells treated with the corresponding resolvent served as controls.

3.11 Bone Marrow DTC (disseminated cancer cell) single-cell analysis (Cooperation with Christoph Klein and Christoph Irlbeck UKR)

3.11.1 PDX BM staining for DTC detection

500.000 BM cells per HTM or TM of the P model were stained with PanCK (CK8, CK18, CK19) antibody in order to detect DTCs whereas an additional slide with an equal amount of cells was stained to control the isotype positivity. In order to compare the BM DTCs of HTM and TM P model later on with the primary tumor, 500.000 tumor cells from the corresponding primary tumor were stained additionally. In detail, the slides were defrosted and dried 20 min prior to the staining. In order to block unspecific binding, the slides were incubated with PBS (pH: 7.4) supplemented with 10 % AB Serum for 30 min, the buffer was discarded and the primary antibody detecting cytokeratin (CK) 8, CK18, CK19 (A 45 B/B3) diluted in PBS (pH: 7.4) / 10 % AB serum (1:100) was applied to the slides for 60 min. Accordingly, IgG kappa isotype (1:500) diluted in PBS (pH: 7.4) / 10 % AB serum was applied to the isotype control. After incubation time the antibody was discarded, the slides were washed three times in PBS, and incubated with the secondary antibody (Zytomed ZUC077-100) supplemented with 10 % AB serum for 30 min. The solution was discarded, the slides were washed three times for 3 min and the development system BCIP/NBT for alkaline phosphatase enzymatic substrate was added for 15 min. After a washing step, the cells were fixed in 0.5 % formalin (in TBS, pH 7.4) for 5 min and finally washed again. The slides were scored for CK positive DTCs cells that appear in dark violet to black. For each staining, the tumor cell line ZR-75-1 was used as a positive control. The occurrence of CK positive cells in the isotype control excluded the staining from further use.

3.11.2 Single cells isolation and whole genome amplification (WGA) performed by Christoph Irlbeck

The violet stained DTCs (or primary tumor cells) were isolated using a micromanipulator and were directly transferred into a PCR tube containing 2 µl of proteinase K digestion buffer. The DNA of the DTC was amplified according to the manufacturer's protocol of Ampli1™ kit (Silicon Biosystems) resulting in 50 µl WGA

product. The WGA was performed by Christoph Irlbeck as published previously (Klein *et al.*, 1999). The WGA is a multistep process that provides deterministic, i.e. reproducible, amplification of a cell's genome which is beneficial for copy number variation low pass- sequencing or CGH methods. In brief, the DNA solution was subjected to protease digestion to destroy residual proteins or DNases that might have been accidentally introduced. Next, the DNA was digested using the MseI restriction enzyme, which fragments the human genome into pieces that are 150-1500 bp in length. Afterwards, the double-stranded adapter oligonucleotide with one of the strands lacking a phosphate (to prevent its ligation) was ligated to the DNA. Following the ligation, the non-ligated adapter strand was removed by heat denaturation creating an overhang of the so-called Lib1 oligonucleotide. In the last step, the final PCR amplification was performed using the excess Lib1 molecules as a primer. Hence, the polymerase first filled up the previously generated overhangs resulting in a Lib1 complementary sequence on the reverse strand. This provides the exponential amplification of the DNA fragments. Finally, the WGA product is stored at -20° C for further downstream applications.

3.11.3 Control and quality PCR of WGA product

The successful amplification of the genome from the single-cell DTC was confirmed by endpoint PCR (Polzer *et al.*, 2014) (Klein *et al.*, 1999; Stoecklein *et al.*, 2002). For this purpose, two different sets of primers (human and mouse) were used in order to determine that the origin of the DTC is really human and not a mouse BM cell as well as the DNA quality which is reflected by the occurrence of all four human genes. *KRAS*, *KRT19*, *TP53 Exon2/3*, and the polymorphic DNA area D5S2117 on chromosome 5 were used to determine the human origin and DNA quality whereas *Polr2a*, *Taf1b*, *Rps3*, and *Fank1* were used to identify a mouse-derived BM cell. All primer sequences are listed in Table 14 and a master mix for PCR was pipetted according to the scheme in Table 15. In the next step, 9 µl of the master mix was applied to the PCR tube followed by 1 µl template DNA from the WGA product. Each human PCR was performed with a positive control (human: ZR-75-1 cell), a negative control (mouse: BM cell), and a water control in order to verify the reagent purity and functionality of the reaction. For mouse multiplex PCR the control cells served vice versa. The PCR ran according to the program listed in Table 16. The PCR product was loaded onto a 1.5 % agarose gel and the DTC was considered for further analysis if three or four bands occurred in the human PCR and the DTC was tested negative for mouse DNA.

Table 14: Primers for quality PCR of WGA product		
CK19 5'	5' GAAGATCCGCGACTGGTAC 3'	621 bp
CK19 3'	5' TTCATGCTCAGCTGTGACTG 3'	
Exon2/3 5'	5' GAAGCGTCTCATGCTGGATC 3'	299bp
Exon2/3 3'	5' CAGCCCAACCCTTGTCCTTA 3'	
D5S2117 5'	5' CCAGGTGAGAACCTAGTCAG 3'	140 bp
D5S2117 3'	5' ACTGAGTCCTCCAACCATGG 3'	
Kras 5'	5' ATAAGGCCTGCTGAAAAT 3'	91 bp
Kras 3'	5' CTGAATTAGCTGTATCGTCAAGG 3'	
Polr2a 5’	5’-ATTGACTTGCGTTTCCATCC-3’	290 bp
Polr2a 3’	5’-AACAAAAGGCACCCACTGTC-3’	
Taf1b 5‘	5’-GAGCCTTAGCCACTTCATGC-3’	392
Taf1b 3'	5’-AGAGTCAGGCAAGGGGAAAT-3’	
Rps3 5’	5’-TACTGACTGCTGCCGTGTTC-3’	687
Rps3 3'	5’-GGCCCAAGTTTACACAGCAT-3’	
Fank1 5’	5’-GGTCCCCTTGTTTGTCTTCA-3’	148
Fank1 3'	5’-AGTGGCTGTTCTGGGCTAAA-3’	

Table 15: Mastermix for quality PCR of WGA product	
Reagent	**Amount per reaction [µl]**
10x FastStart PCR Buffer (with 20mM $MgCl_2$)	1
Primer mix (8 µM per primer)	1
dNTPs (from FastStart kit)	0.2
BSA (20 mg/ml)	0.2
FastStart Taq Polymerase (5 U/µl)	0.1
PCR-water	6.5

Table 16: PCR program for quality control of the WGA product			
Cycler program	**Temperature**	**Time**	
Step 1	95 °C	04:00 min	
Step 2	95 °C	00:30 min	32 cycles (4-5)
Step 3	58 °C	00:30 min	
Step 4	72 °C	01:30 min	
Step 5	Back to step 2		
Step 6	72 °C	07:00 min	
Step 7	4 °C	forever	

3.11.4 Gel electrophoresis

In order to separate the WGA product according to size 1.5 % gels were cast by dissolving 1.5 g agarose in 1 x TBE buffer, boiled in the microwave and added with 4 µl of ethidium bromide solution. The warm gel was shaken for ethidium bromide distribution, immediately transferred into the gel tray and equipped with two combs of 20 pockets each. After 20 min of polymerization, the gel tray was filled with TBE buffer and 11 µl PCR product containing 3 µl of gel loading dye were pipetted in each pocket.

To identify the size of the bands, the first and the last pocket were loaded with 8 µl of 1 kb DNA ladder. Lastly, the DNA was separated at 160 V for 45 min at 400 mA and the bands were visualized using UV light.

3.11.5 Reamplification

In order to prevent wasting the basic WGA single cell material and in case of potential analysis repetitions, the DNA was reamplified. Therefore, a master mix was pipetted according to the scheme of Table 17 and 1 µl of the WGA product was applied to the reagents resulting in 50 µl reamplified DNA.

Table 17: Mastermix for reamplification of DNA

Reagent	Amount
1x Expand Long Templ.Buffer	5.0 µl
Lib1 (10µM) (5‘AGT GGG ATT CCT GCT GTC AGT)	5.0 µl
dNTPs (10mM)	1.75 µl
BSA (20 mg/ml)	1.25 µl
Pol Mix	0.5 µl
H_2O	35.5 µl

The amplification was performed with the cycler program listed in Table 18.

Table 18: PCR program for Reamplification of DNA

Cycler program	Temperature	Time	
Step 1	94.0 °C	1 min	
Step 2	60.0 °C	30 s	
Step 3	65/68 °C	2 min	
Step 4	94.0 °C	30 s	10 cycles (4-6)
Step 5	60.0 °C	30 s	
Step 6	65/68 °C	2 min (+20 s/c)	
Step 7	4.0 °C	forever	

Before library preparation, the DNA quality has to be reanalyzed using the PCR described at 3.11.3.

3.11.6 Low pass-sequencing for copy number alteration profiling (performed by Christoph Irlbeck)

Low pass-sequencing which includes library preparation, Qubit DNA concentration measurement and bioanalyzer analysis of samples was performed exclusively by my cooperation partner (ITEM, Regensburg, Germany) according to the protocol described in the doctoral thesis of Christoph Irlbeck submitted in November 2019. For Library preparation, the Ampli1™ LowPass kit was used. This kit uses the deterministic nature of Ampli1™ WGA (Menarini Silicon Biosystems, USA) to provide a streamlined,

single-reaction protocol to generate multiplexed, sequencing-ready libraries to detect chromosomal aneuploidies and copy number alteration (CNA) by low-pass whole-genome sequencing. Briefly, starting from purified primary Ampli1™ WGA product, barcoded libraries compatible with Illumina® systems were generated. The libraries were quantified using the Qubit dsDNA HS reagent kit and the Qubit 3.0 Fluorometer. Additionally, the average fragment sizes of the libraries were assessed using the Agilent High Sensitivity DNA Kit on the Agilent 2100 Bioanalyzer. The open-source software Control-FREEC (Control-Free Copy number caller) was used to obtain copy-number calls, using the mode without reference sample and without contamination parameters. For the evaluation of quality metrics, only samples with more than 200,000 reads and a derivative log ratio spread (DLRS) < 0.50 were evaluated.

3.11.7 Preparation of Ref Sequ files and analysis by progenetix software

Progenetix is an online tool for the generation of genome plots and multi-strip plots to summarize user data for further analysis (Baudis and Cleary, 2001). To analyze the DTCs and the tumor cells from the primary tumor the Ref Sequ files were transformed into the format of Progenetix. The data has to be submitted as a tab-delimited segment file with a detailed description of data arrangement at https://info.progenetix.org/uploader.html, where they were finally uploaded. The genomic CNV profiles obtained in the analysis were visualized as scatter plots in which yellow represents genomic gains and blue genomic losses.

3.12 Panel Sequencing (Performed by Nicole Pfarr and Wilko Weichert TUM)

3.12.1 DNA Isolation of FFPE tissue

The panal sequencing was exclusively perfomed by my cooperation partner Nicole Pfarr in Munich. Therefore, eight 8-µm-thick sections of FFPE primary tumor samples or TM tumors were sent for analysis to our cooperation partner in Munich and the panel sequencing procedure was exclusively performed by Nicole Parr. The areas containing exclusively tumor cells were microdissected, deparaffinized and genomic DNA isolation was performed after proteinase K digestion using a fully automated extraction system (Maxwell; Promega, Madison, USA) according to the manufacturers' protocol. The DNA concentration was measured fluorimetrically using the QuBit 2.0 system and the DNA high sensitivity kit (both: Thermo Fisher Scientific, Waltham, USA). Due to the high degradation of DNA retrieved from FFPE material, the amount of amplifiable DNA,

that is, the sequencing grade quality was determined by using a qPCR assay (TaqMan RNAseP detection assay; Thermo Fisher Scientific) (Pfarr *et al.*, 2017).

3.12.2 Sequencing Panels

The Breast Cancer version 3 (BCPv3) panel was designed by the group of Wilko Weichert and consists of three primer pools yielding 617 amplicons covering mutational hotspot regions located in 353 exons of 59 genes that are known to be related to breast cancer. This BCPv3 panel is a modified version from their previously designed panels (Pfarr *et al.*, 2017; Kriegsmann *et al.*, 2014). An overview of the panel of the interrogated gene regions is provided in Table 19 below.

Table 19: Genes and exons included in the breast cancer panel.

AKT1	**CDKN1B**	**FBXW7**	**MDM2**	**PIK3CA**	**SMAD2**
3, 8, 12	1	2, 3, 4, 6, 7, 8, 9, 10	4, 7, 9, 10, 11	2, 5, 8, 10, 14, 21	4, 5, 8, 9, 11
AKT3	**CDKN2A**	**FGFR1**	**MDM4**	**PIK3R1**	**SMAD4**
2, 3, 4, 8	1, 2	4, 13	3, 7, 11	10, 11, 13	2, 3, 4, 6, 8, 9, 10, 12
APC	**CTCF**	**FGFR2**	**MED12**	**PMS2**	**TBX3**
16	3, 4	3, 5, 7, 9, 10, 12, 13, 14	2	6, 10, 11, 14	1, 2
ATM	**DNMT3A**	**FOXA1**	**MSH6**	**PTEN**	**TP53**
35, 37	7, 10, 23	2	3, 5	1-9	2-11
BRAF	**EGFR**	**FOXO3**	**MTOR**	**RB1**	**TSC2**
11, 15	18-21	1, 2	29, 30, 43, 56	2, 3, 4, 6, 8, 11, 13, 14, 16, 17, 18, 19, 20, 21, 22, 23, 25, 26	7, 16, 34
c19orf12	**ELF3**	**GATA3**	**MYC**	**RICTOR**	**URI1**
2	2, 3, 7, 8	2-6	2, 3	3, 23, 25, 31	4, 8
CBFB	**EPCAM**	**GRHL2**	**NCOR1**	**RPS6KA1**	**VHL**
3, 4, 5	3, 5, 7, 9	4, 7, 9, 14	2-12, 14-46	11, 14	1, 2, 3
CCND1	**ERBB2**	**KRAS**	**NF1**	**RPTOR**	**ZNF536**
1, 3, 4	7, 8, 14, 17, 19, 20, 21	2-4	1-57	1, 9, 10, 16, 25	2
CCNE1	**ERBB3**	**MAP2K4**	**PALB2**	**RUNX1**	**ZNF703**
5, 11	2, 3, 7, 8, 9, 17, 23, 25, 28	3-9	4, 5, 10	5, 6, 7, 8, 9	1, 2
CDH1	**ESR1**	**MAP3K1**	**PDL1**	**SF3B1**	
1-16	1-8	4, 9, 10, 13, 14, 17, 18, 19, 20	2-7	14, 15	

Exons included are given below each gene and the genes are printed in bold. BCPv3 (59 genes, 617 Amplikons) adapted from (Kriegsmann *et al.*, 2014; Pfarr *et al.*, 2017)

3.12.3 Massive parallel sequencing

The Library preparation was performed according to the multiplex PCR-based Ion Torrent AmpliSeq™ technology (Thermo Fisher Scientific, Waltham, USA) using the BCPv3 panel and the Ion AmpliSeq Library Kit v2.0. For the amplification of each primer pool, 5 ng of DNA (determined by qPCR) were mixed with 2.5 µl of one of the three primer pool (2x concentrated) and 1µl AmpliSeq HiFi Master mix in a 5µl reaction and transferred to a thermal cycler (Biometra, Göttingen, Germany). 15 ng Total amount of DNA was used. After amplification in a thermal cycler, all three reactions were combined yielding 15 µl for further proceeding. Afterward, the amplicons were partially digested by adding FuPa reagent. This process was followed by the ligation of barcoded sequencing adapters (Ion Xpress Barcode Adapters, Thermo Fisher

Scientific, Waltham, USA) and the purification was finally conducted using AMPure XP magnetic beads (Beckman Coulter, Krefeld, Germany). Subsequently, the library was quantified using the Ion Library Quantitation Kit for qPCR on a StepOnePlus qPCR machine (Thermo Fisher Scientific, Waltham, USA). Individual libraries were diluted to a final concentration of 25 pM and up to 10 of these libraries were pooled and processed using the Ion S5 510/520/530 chef Kit on an Ion Chef instrument where the libraries were processed for sequencing. Sequencing was conducted on an Ion S5XL instrument using the Ion S5 Sequencing chemistry and loaded onto a 530 chip.

3.12.4 Data analysis and prediction of copy number variations

Raw sequencing data analysis and the alignment against the human genome (version hg19) was performed with the Torrent Suite Software (version 5.10.1) using the TMAP algorithm. The build-in plugin „variantCaller“(version 5.8.0.19) was used for mutation analysis. Annotation of the variants was obtained by using ANNOVAR-a custom-built variant annotation pipeline (Wang *et al.*, 2010). The sequencing reads were visualized by the Integrative Genomics Viewer Browser (IGV, http://www.broadinstitute.org/igv/) and variants were analyzed for germline or somatic origin using the COSMIC (catalog of somatic mutations in cancer) database (Forbes *et al.*, 2015), dbSNP, and Exome Variant Server (http://evs.gs.washington.edu/EVS). For each sample and amplicon, a coverage data summary was generated by the Torrent Suite software and used for the identification of copy number variations (CNVs, amplifications, and deletions) that have been ascertained by a four-step algorithm as previously described (Endris *et al.*, 2013; Pfarr *et al.*, 2017)

3.13 Statistical analyses

The overall survival (OS) of the mice was calculated from the date of tumor transplantation to the date of death of any cause. The disease-free survival (DFS) in mouse experiments is designated as the period of time between tumor transplantation and the occurrence of a palpable tumor. OS and DFS curves were estimated using the Kaplan-Meier method and a statistical significance was calculated using the Log-rank (Mantel-Cox) test. For all other experiments either Student's t-test, one-way analysis of variance (ANOVA) with Tukey’s multiple comparison test, two-way ANOVA with Bonferroni post hoc correction, or two-sided Fisher’s exact test was used. The results are represented as mean ± SEM and the animal/patient number is assigned in each experiment respectively. Patient/animals were only excluded from the experiment as a

significant outlier with a p-value > 0.05 using GraphPad quickcalcs https://www.graphpad.com/quickcalcs/Grubbs1.cfm. All *in vitro* experiments were repeated three times. Statistical significance was accepted at *p-value* > 0.05.

4 Results

4.1 Primary tumor patient samples

33 primary or metastatic tumor specimen were obtained from patients of the Caritas Hospital St. Josef Regensburg and were named as primary tumor (PT) in alphabetical order (A-GB) (Table 20). All the biopsies donated from the patients derived either from solid tumors or liquid metastatic specimens from thoracentesis or laparocentesis. The successful PDX, established from primary patient tumor, are highlighted in green. PT P (solid tumor) and PT AB (pleural effusion) are Luminal B/ Her2$^+$ tumors. The TNBCs PT U (pleural effusion) and PT V (solid tumor), as well as the Her2$^+$ PT X (solid tumor), were engrafted to confirm the transplantation method. All of them resulted in a stable and retransplantable PDX. The grey lines mark all the patients that died or suffered from a relapse during enrollment of patient samples from 2015 until February 2019. This overview shows that all of the patients that suffered from metastatic breast cancer and received a thoracentesis or a laparocentesis died within a few months. Moreover, the Luminal B patient PT R relapsed within just a few months further affirming the urgency of markers that subdivide the Luminal B tumors into high and low-risk tumors. Several tumors, especially the patients with ascites or pleural effusions, listed in the table were pretreated, however, detailed information was not available in all cases. The hormone receptor status of each tumor is listed in Table 20 and the detailed Remmele Score (0 -12) (Remmele and Stegner, 1987) assessed by a pathologist of ER and PR expression was provided if possible. In addition to ER and PR expression, the Her2 status (0-3 IHC score), as well as the proliferation index (Ki-67 expression in %) of each tumor according to St. Gallen conference 2011 (Goldhirsch *et al.*, 2011; Cheang *et al.*, 2009), was used to categorize the samples into Luminal A, Luminal B, Luminal B/Her2$^+$, Her2$^+$, or TNBC subtype. The successful propagation of primary tumor cells ex vivo is listed here but a detailed description of primary tumor cell culturing is provided at 4.2.5 Primary tumor culturing.

To bypass the long engraftment duration of the primary tumors in NOD-SCID IL2Rγnull (NSG) mice, already established Luminal B PDX models CTC#288 (Baccelli *et al.*, 2014) and BPE2#0 (dissertation of Dr. Massimo Saini 2017) from Prof. Trumpp, HI-Stem, Heidelberg, Germany were used to generate TM and HTM. CTC#288 derived from circulating tumor cells isolated from the peripheral blood by CellSearch® whereas Bpe2#0 cells were isolated from a pleural effusion specimen of a Luminal B patient.

Moreover, HBCx3, HBCx22, and HBCx34 (Marangoni *et al.*, 2007; Cottu *et al.*, 2012) Luminal B PDX models from Dr. Marangoni (Institute Curie, Paris, France) were used to establish TM and HTM in our laboratory. Already established PDX models and the diagnostic marker expression of the corresponding primary tumor are highlighted in yellow.

Table 20: Overview of all patient samples and the corresponding pathological information, engraftment success, and the survival and relapse status of the patient

Patient/ PDX name	Biopsies donated	Hormone receptor	ER	PR	Her2 status	Proliferation index in %	Disease subtype	PDX successful	Cell culture	Publication	Survival status 08/2019	Relaps
PT A	solid	+	6	6	1	18 %	Luminal B	No	No	unpublished	Alive	No
PT B	Solid	+	+	+	0	30 %	Luminal B	No	No	unpublished	Alive	No
PT C	Solid	+	12	6	3	15 %	Luminal B /Her2$^+$	No	No	unpublished	Alive	No
PT D	solid	+	12	1	0	15 %	Luminal B	No	No	unpublished	Alive	No
PT E	solid	+	12	8	N.A.	5 %	Luminal A	No	No	unpublished	Alive	No
PT F	Solid	+	12	0	1	5 %	Luminal A	No	No	unpublished	Alive	No
PT G	Solid	+	6	9	1	25 %	Luminal B	No	No	unpublished	Alive	No
PT H	Solid	+	12	0	1	6 %	Luminal A	No	No	unpublished	Alive	No
PT I	Solid	+	8	6	1	18 %	Luminal B	No	No	unpublished	Alive	No
PT J	Solid	+	12	9	0	45 %	Luminal B	No	No	unpublished	Alive	No
PT K	Solid	+	12	9	1	10 %	Luminal A	No	No	unpublished	Alive	No
PT L	Solid	+	12	6	1	60 %	Luminal B	No	No	unpublished	Alive	No
PT M	Solid	+	12	4	1	8 %	Luminal A	No	No	unpublished	Alive	No
PT N	Solid	+	12	2	0	25 %	Luminal B	No	No	unpublished	Alive	No
PT O	Solid	+	12	0	1	15 %	Luminal B	No	No	unpublished	Alive	No
PT P	Solid	+	12	0	3	40 %	Luminal B/ Her2$^+$	Yes	No	unpublished	Dead	-
PT Q	solid	+	12	6	1	60 %	Luminal B	No	No	unpublished	Alive	No
PT R	Solid	+	12	9	1	30 %	Luminal B	No	No	unpublished	Alive	yes
PT S	Solid	+	8	8	1	25 %	Luminal B	No	No	unpublished	Alive	No
PT T	Pleural effusion	-	1	0	3	35 %	Her2 $^+$	Yes	No	unpublished	Dead	
PT U	Pleural effusion	-	0	0	0	25 %	TNBC	Yes	No	unpublished	Dead	
PT V	Solid	-	1	1	1	80 %	TNBC	Yes	No	unpublished	Alive	No
PT W	Solid	-	-	-	-	> 14 %	TNBC	No	No	unpublished	Alive	No
PT X	Solid	-	0	0	3	70 %	Her2$^+$	Yes	No	unpublished	Dead	No
PT Y	Solid	+	8	6	1	12 %	Luminal A	No	No	unpublished	Alive	No
PT Z	Solid	+	12	9	1	25 %	Luminal B	No	No	unpublished	Alive	No
PT AB	Pleural effusion	+	12	0	3	>14 %	Luminal B/ Her2$^+$	Yes	Yes	unpublished	Dead	
PT BB	Solid	-	4	0	1	30 %	TNBC	No	No	unpublished	Alive	No
PT CB	Pleural effusion	+	+	+	3	> 14 %	Luminal B/ Her2$^+$	No	No	unpublished	Dead	
PT DB	Pleural effusion	+	+	+	-	> 14 %	Luminal B	No	No	unpublished	Dead	

Results

Patient/ PDX name	Biopsies donated	Hormone receptor	ER	PR	Her2 status	Proliferation index in %	Disease subtype	PDX successful	Cell culture	Publication	Survival status 08/2019	Relaps
PT EB	Pleural effusion	+	+	+	N.A.	> 14 %	Luminal B	No	No	unpublished	Dead	
PT FB	Solid	+	8	12	-	< 14 %	Luminal A	No	No	unpublished	Alive	No
PT GB	Ascitis	+	+	+	N.A.	> 14 %	Luminal B	No	No	unpublished	Dead	
CTC#228	Solid (PDX derived-former peripheral blood CTC derived)	+	+	+	-	> 14 %	Luminal B	Yes	Yes	(Baccelli *et al.*, 2014)	N.A.	N.A.
Bpe 2-0	Solid (PDX derived-former pleural effusion derived)	+	+	+	-	> 14 %	Luminal B	Yes	No	unpublished	N.A.	N.A.
HBCx3	Solid (PDX derived)	+	+	-	-	> 14 %	Luminal B	Yes	No	(Cottu *et al.*, 2012)	N.A.	N.A.
HBCx22	Solid (PDX derived)	+	+	+	-	> 14 %	Luminal B	Yes	No	(Cottu *et al.*, 2012)	N.A.	N.A.
HBCx34	Solid (PDX derived)	+	+	+	-	> 14 %	Luminal B	Yes	No	(Cottu *et al.*, 2012)	N.A.	N.A.

The table shows an overview of all patient samples (A-GB) and the PDX samples from the cooperation partners with the molecular intrinsic marker expression from the primary tumor. HR describes the hormone receptor status in general (ER and PR, ER or PR, PR without ER). ER and PR scores are given as immune reactive score according to Remmele from 0-12. Her2 expression is listed as an IHC score from 0-3. The proliferation is depicted in %. The breast cancer subentities according to the given markers are listed in the disease subtype column. The PDX success, cell culture propagation of the primary tumor and a relapse of the patient is shown as yes or no answer. The survival status is described as dead or alive. The abbreviation N.A. means that the information was not available. Green marked lines show the successful engrafted PDX models from St. Josef, grey marked lines indicate a relapse or the patients' death, and yellow marked lines show the already established PDX models from our cooperation partners.

4.2 Characterization of the primary tumor specimen

4.2.1 Phenotypical characterization of patient Luminal A and B tumor cells using (stem cell FACS) SCF panel

In order to characterize tumors, metastases, or DTCs the SCF panel including CD45, EpCAM, CD44, CD47, cMET, CD24, and Her2 was used as shown in Figure 10. Forward versus side scatter identified the main tumor population, thereby excluding dead tumor cells. Next, the doublet cells were discriminated by the forward scatter width versus forward scatter area. CD45 excluded the immune cells potentially harboring in the tumor cell population. Only EpCAM^{+} cells were then used for further analysis of SCF markers (CD44, CD47, cMET, CD24, and Her2). The EpCAM- population was excluded from the current analysis.

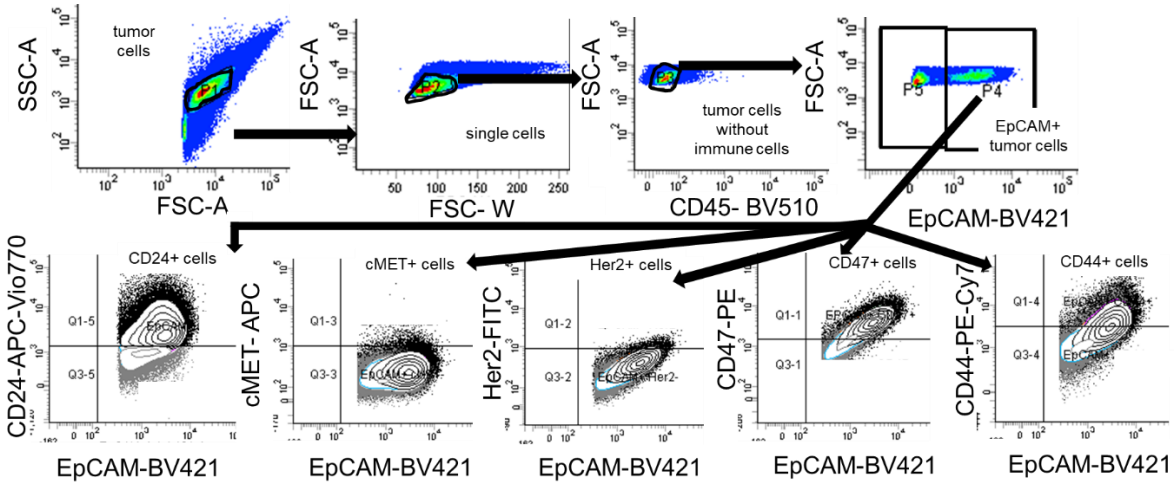

Figure 10: Representative image of the gating strategy for SCF on tumor TM CTC
The population is depicted as a density plot and the gates are shown in bold black. SCF characterization of CD44, CD47, cMET, CD24, and Her2 was performed from gate P4 including the EpCAM $^{+}$ cells.

First, differences regarding stem cell marker expression were compared between Luminal A and Luminal B tumors. Luminal B tumors, as characterized by pathologists according to intrinsic molecular marker (ER status, Ki67, and the grading), revealed a significantly higher expression of CD24, when compared with Luminal A tumors (two-way ANOVA with Bonferroni post hoc correction, $p < 0.05$) (Figure 12 A). All other stem cell markers (CD47, Her2, cMET, CD44, and EpCAM) showed no significant difference in their expression comparing Luminal A with Luminal B tumors. Secondly, the Luminal B cohort was further subdivided to identify specific target molecules for high and low-risk Luminal B tumors. This is based on retrospective analysis subdividing the patients that died, suffered from a relapse, or produced a stable PDX model in the high-risk Luminal B group whereas the patients that were still alive without any relapse and the

tumor did not produce a PDX model were assigned to the low-risk Luminal B group. More specifically, the successful engraftment of a primary tumor in the mouse is per se a poor prognostic indicator for the patients' outcome (Whittle *et al.*, 2015). However, I could not identify a defined stem cell marker signature that could reliably predict a severe progression for Luminal B high-risk tumors (Two-way ANOVA with Bonferroni post hoc correction, $p > 0.05$) (Figure 12 B).

To detect the metastasis initiating cells (MICs) (Baccelli *et al.*, 2013), which are associated with lower overall survival and an increased number of metastatic sites, the FACS gating strategy was performed as described in Figure 11. The $CD44^+$ cells were analyzed in a further gate on CD47 and cMET positivity. This last gate is important because it represents the triple-positive cells ($CD44^+$, $CD47^+$, $cMET^+$) that shows the co-expression of $CD44^+$, $CD47^+$, and $cMET^+$ on a single cell. This co-expression pattern was described previously as the stem cell population called MIC (Baccelli *et al.*, 2013).

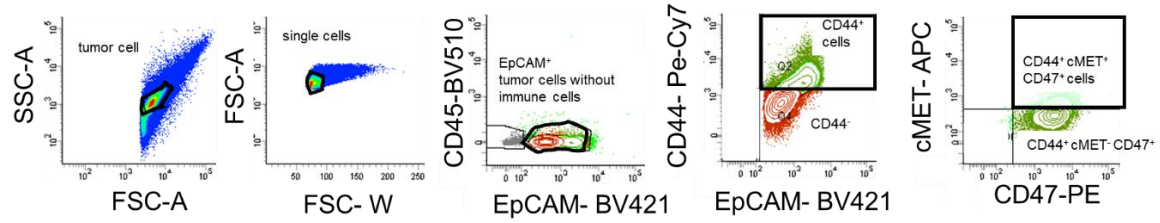

Figure 11: Representative image of the FACS gating strategy for SCF MIC subpopulation.
The gating strategy shows the way to determine the co-expression of $EpCAM^+$, $CD44^+$, $CD47^+$, $cMET^+$ on a single tumor cell. The population is depicted as a density plot and the gates are shown in bold, black edging.

Even though the single stem cell marker expression did not reveal a specific signature for high-risk Luminal B breast cancer, the simultaneous triple positivity of a single cell showed different results. The co-expression of $CD44^+$, $CD47^+$, $cMET^+$ also defined as MICs population were significantly increased in Luminal B high-risk tumors (Student's t-test, $p = 0.035$) (Figure 12 C). In accordance, it has to be emphasized that one patient in the low-risk Luminal B cohort exhibits high co-expression of $CD44^+$, $CD47^+$, $cMET^+$ potentially predicting the further course of the patient as a high-risk Luminal B tumor. This patient is marked with a circle in Figure 12 C.

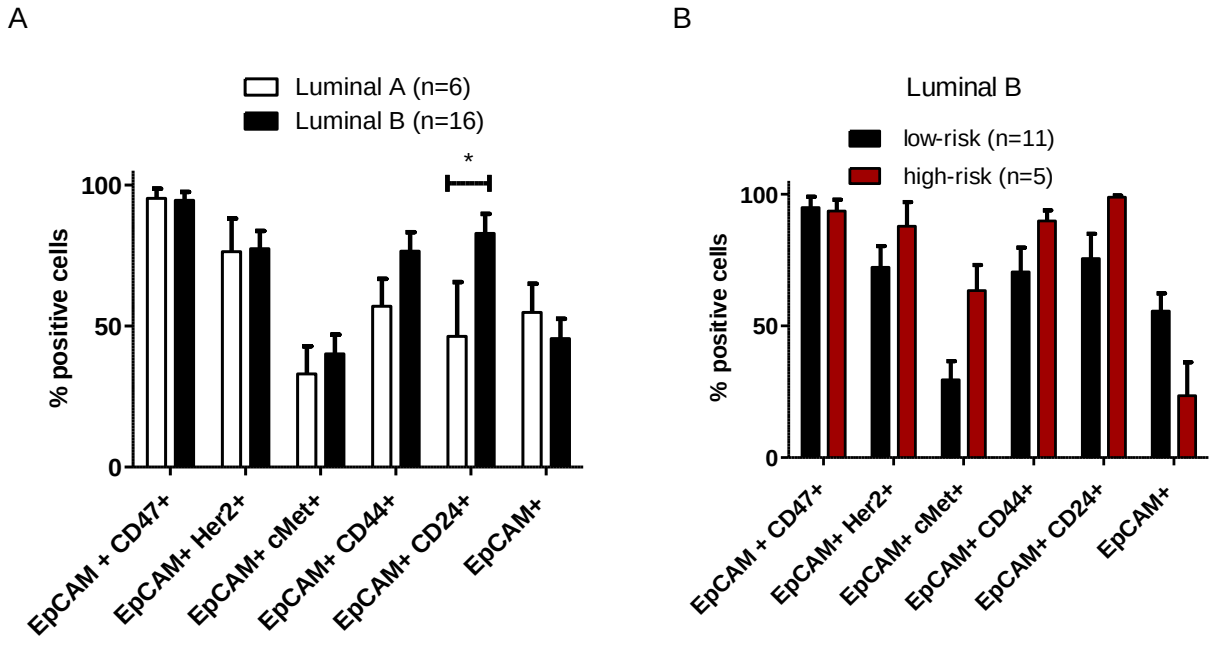

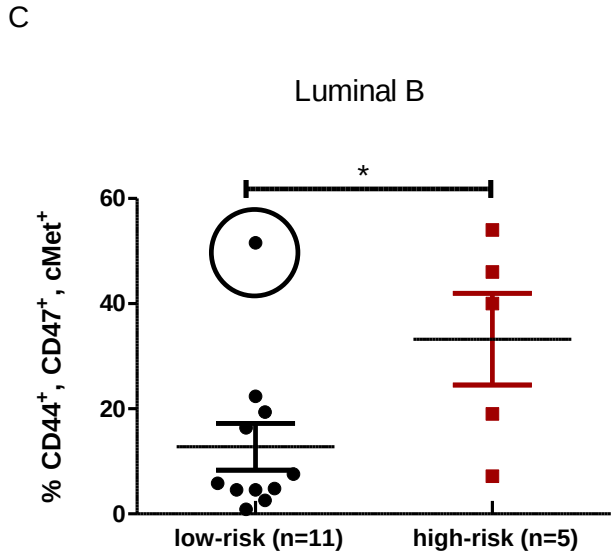

Figure 12 Stem cell marker expression in Luminal breast cancer.
A) Comparison of Luminal A tumors with Luminal B tumors regarding stem cell marker expression based on the intrinsic molecular markers determined by routine pathology. The number of patients is shown in parentheses. The data are represented as mean + SEM. **B)** This figure displays the stem cell marker expression of high and low-risk Luminal B tumors subdivided according to a retrospective survival, relapse, and PDX engraftment. The data are represented as mean + SEM. **C)** The % of the triple-positive population ($CD44^+$, $CD47^+$, $cMET^+$) of high and low-risk Luminal B tumors is shown as mean ± SEM. Each dot displays a single patient. The circle represents a potential high-risk Luminal B individuum. The number of all patients is listed in parentheses. Significances were analyzed using Two-way ANOVA with Bonferroni post hoc correction or Student's t-test (* $p < 0.05$).

4.2.2 Immune cell infiltration in primary Luminal patient tumors

The RECON panel was used to analyze the immune cell infiltration (TIL) into the tumors (Figure 13). To determine human immune cells the gate was set by forward versus side scatter of all living tumor and immune cells, thereby excluding the dead cells seen in the left corner. CD45 as leucocyte common antigen is expressed on all human immune cells and, hence, reflects the immune cell infiltration in tumors. In addition, plotting CD19 versus CD3 could verify the percentage of B and T-cells, respectively. A CD45 drill-down and plotting of CD33 versus side scatter identified on the one hand myeloid cells and on the other hand through side scattering the

granulocytes. However, with the isolation method of the TILs, it is not possible to distinguish between stromal and intratumoral cells.

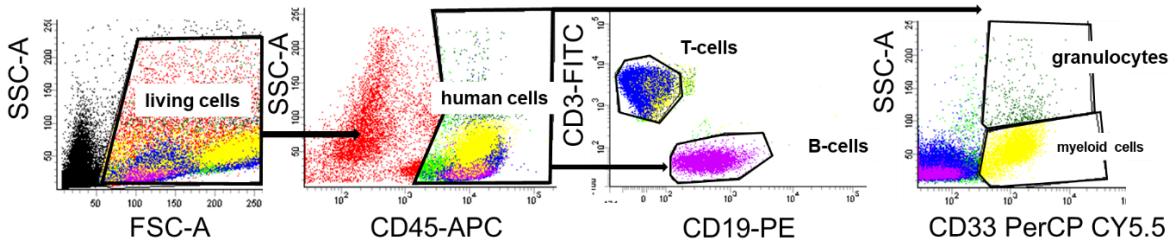

Figure 13: Representative gating strategy of RECON to determine the TILs
The gating strategy is shown as a scatter plot. To determine the T-, B, and myeloid cells and granulocytes the immune cell population were previously gated on CD45. The gates are showed in bold edging.

Solid Luminal tumors in general exhibit between 4.2-6.9 % TILs whereas no difference could be determined between solid Luminal A and solid Luminal B tumors (Figure 14 A). A significant higher immune cell infiltration of ~ 83 % TILs can be found comparing solid Luminal B tumors with Luminal B effusions (One-way ANOVA with Tukey's' multiple comparison test, $p < 0.001$). Nevertheless, only in highly aggressive breast cancer subentities namely Luminal B tumors, but not Luminal A, metastatic effusions can be found. Further analysis of the high and low- risk Luminal B cohort (subdivided as described before) and its TIL subsets (Figure 14 B) revealed no difference regarding T-, B-, myeloid -cells, or granulocytes (Two-way ANOVA with Bonferroni post hoc correction, $p > 0.05$). In detail, there is no distinctive TIL signature that differs between high and low-risk Luminal B tumors and no difference regarding the TIL signature between Luminal A and Luminal B (data not shown).

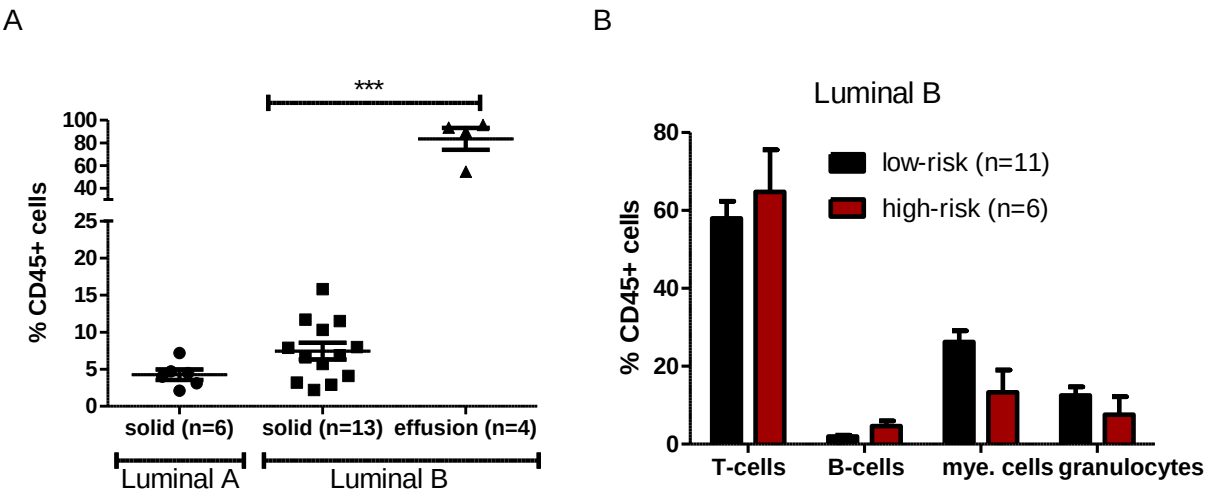

Figure 14: TIL analysis of primary patient tumors
A) The figure shows the % $CD45^+$ cells (immune cells) in Luminal A and Luminal B solid tumors and in the Luminal B metastatic effusion. Each dot displays a single patient and the data are represented as mean ± SEM**.** **B)** The different human immune cell subsets (T-cells, B-cells, myeloid cells, granulocytes) in high and low-risk Luminal B tumors are shown as mean + SEM. The number of patients is listed in parentheses. Significances were analyzed using Two-way ANOVA with Bonferroni post hoc correction or One-way ANOVA using Tukey's' multiple comparison test (*** $p < 0.001$).

4.2.3 T cell phenotyping of TILs in the primary tumors of Luminal patients

Immune cell infiltration in the primary patient tumor was characterized by T-cell marker expression of CD3, CD4, CD8a, CD45RA, CD27, and PD-1, see Figure 15. In brief, forward versus side scatter identified the main immune cell population. The doublet cells were discriminated by forward scatter width versus forward scatter area. All T-cells feature a CD3 receptor by which the T-cells were identified. CD4 versus CD8a as a drill-down of CD3 detected the T-helper cells and the cytotoxic T-cells, respectively. Moreover, the activity state (naïve, effector, effector-memory, or effector memory T-cells re-expressing CD45RA (TEMRA)) of T-helper and cytotoxic T-cells was determined by plotting CD45RA against CD27. In addition, the immune-suppressive PD-1 expression on T-cells was analyzed by plotting PD-1 against CD4 as a CD3 drill-down to analyze the occurrence of PD-1 on T-helper and cytotoxic T-cells. The isolation method of the T-cells does not allow discrimination between stromal and intratumoral T-cells.

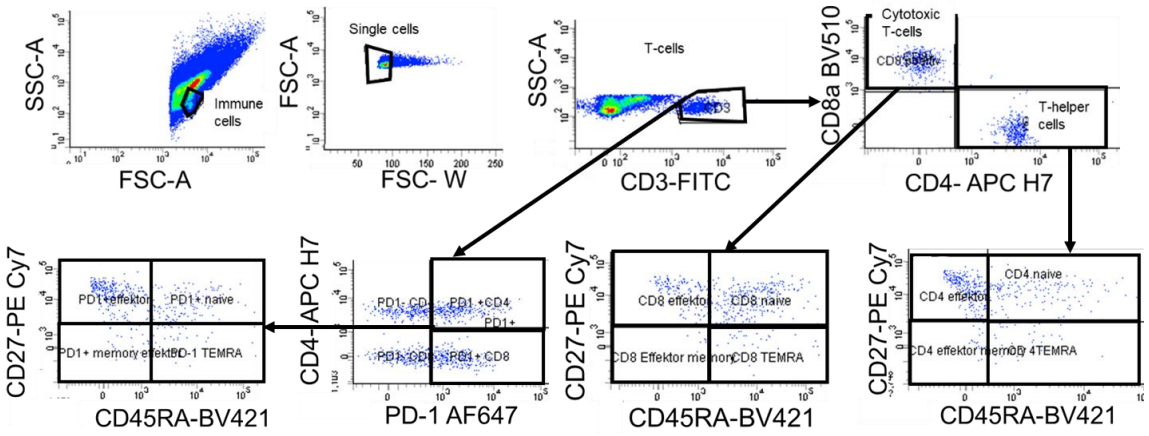

Figure 15: Representative image of the gating strategy that was used for T-cell subset identification
The T-cells were identified by CD3. The drill-down determined the cytotoxic T-cells and the T helper cells. The cytotoxic T-cells and the T-helper cells were analyzed on naive, effector, effector memory and TEMRA state. PD-1 expression as a drill-down of CD3 was analyzed on cytotoxic T-cells and T-helper cells. The whole PD-1 population was further analyzed on naive, effector, effector memory or TEMRA state. The gating strategy is shown with black arrows.

Results

Comparing the CD4/CD8 ratio, the high-risk patients show an increased CD4/CD8 ratio which means the presence of a higher proportion of $CD4^+$ helper cells (Student's t-test, p = 0.0170) (Figure 16 A). No differences were detected regarding the subpopulations of $CD4^+$ and $CD8^+$T cells (effector, naïve, memory-effector, or TEMRA)between high- and low-risk Luminal B patients (Two-way ANOVA with Bonferroni post hoc correction, p > 0.05) (Figure 16 B and C). In general, PD-1 is expressed on T-cells in Luminal B tumors, but neither the whole amount of PD-1 expression nor the PD-1 expression on $CD4^+$ or $CD8^+$ cells differs between high and low-risk Luminal B patients (data not shown).

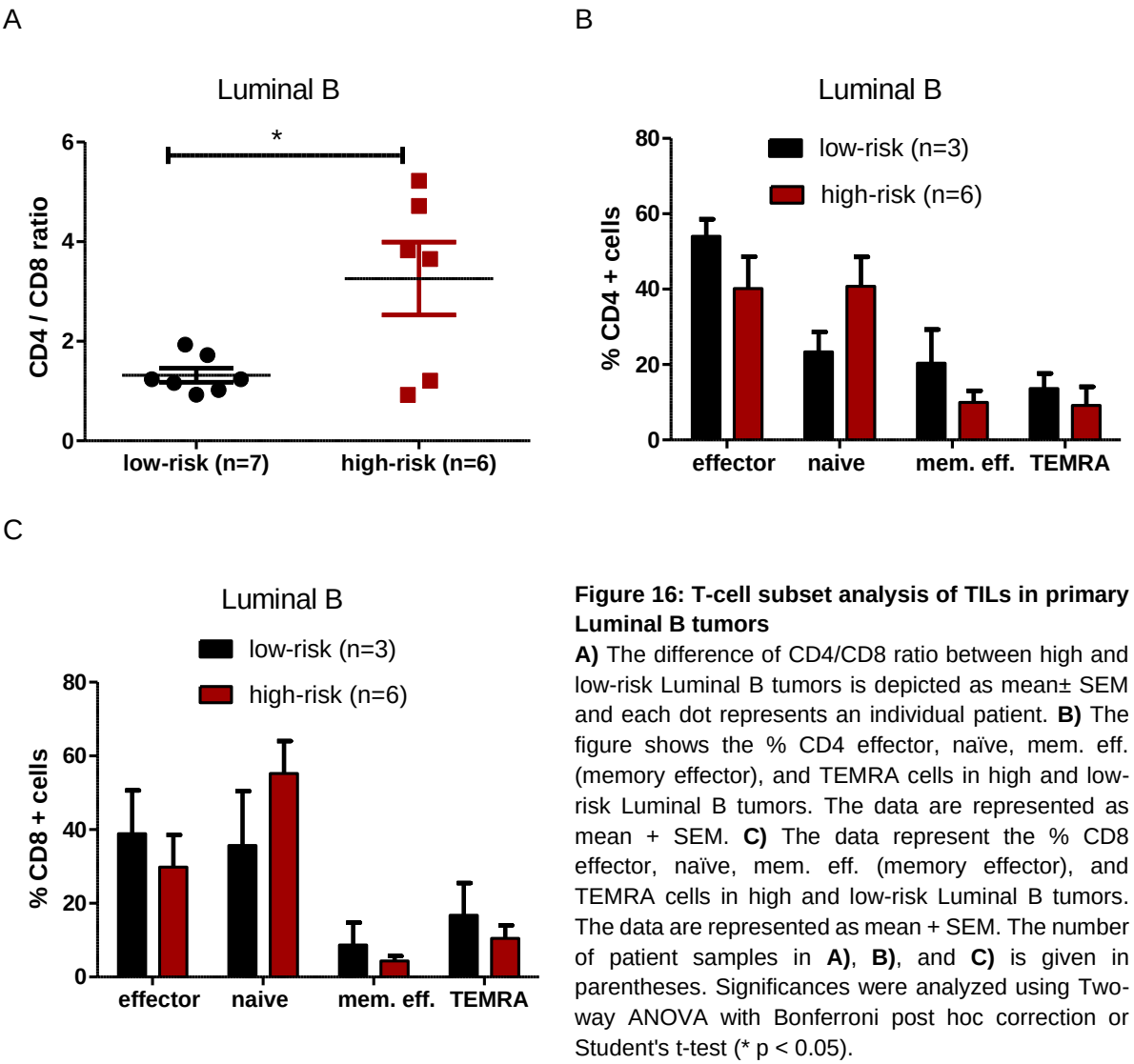

Figure 16: T-cell subset analysis of TILs in primary Luminal B tumors
A) The difference of CD4/CD8 ratio between high and low-risk Luminal B tumors is depicted as mean± SEM and each dot represents an individual patient. **B)** The figure shows the % CD4 effector, naïve, mem. eff. (memory effector), and TEMRA cells in high and low-risk Luminal B tumors. The data are represented as mean + SEM. **C)** The data represent the % CD8 effector, naïve, mem. eff. (memory effector), and TEMRA cells in high and low-risk Luminal B tumors. The data are represented as mean + SEM. The number of patient samples in **A)**, **B)**, and **C)** is given in parentheses. Significances were analyzed using Two-way ANOVA with Bonferroni post hoc correction or Student's t-test (* p < 0.05).

4.2.4 Tumor cell phenotyping and immune cell characterization in solid tumors compared to effusions (metastases) of Luminal B patients.

4.2.4.1 SCF and RECON phenotyping of Luminal B solid tumors and Luminal B effusions

Moreover, it was interesting to elucidate the differences between Luminal B primary tumors and Luminal B effusions in detail. The EpCAM$^+$ cells of the effusions (pleural effusion or ascites) derived from metastasized Luminal B breast carcinoma. EpCAM$^+$ cells in effusions were only present to 2.8 % in the mean (data not shown). In line with the data shown in Figure 14 A, metastatic breast cancer effusions mainly consist of extracellular fluid with immune cells. Despite the other markers (CD47, Her2, CD44, CD24), cMET expression was significantly increased in tumor cells isolated from Luminal B metastatic effusions compared with solid Luminal B tumors (Two-way ANOVA with Bonferroni post hoc correction $p < 0.05$) (Figure 17 A). Interestingly the RECON analysis revealed an increased amount of T-cells in Luminal B breast cancer metastases (Two-way ANOVA with Bonferroni post hoc correction $p < 0.001$), whereas the presence of myeloid cells is decreased in Luminal B breast cancer metastases (Two way ANOVA with Bonferroni post hoc correction $p < 0.001$) (Figure 17 B). In contrast, the number of B-cells and granulocytes did not differ (Two-way ANOVA with Bonferroni post hoc correction $p > 0.05$).

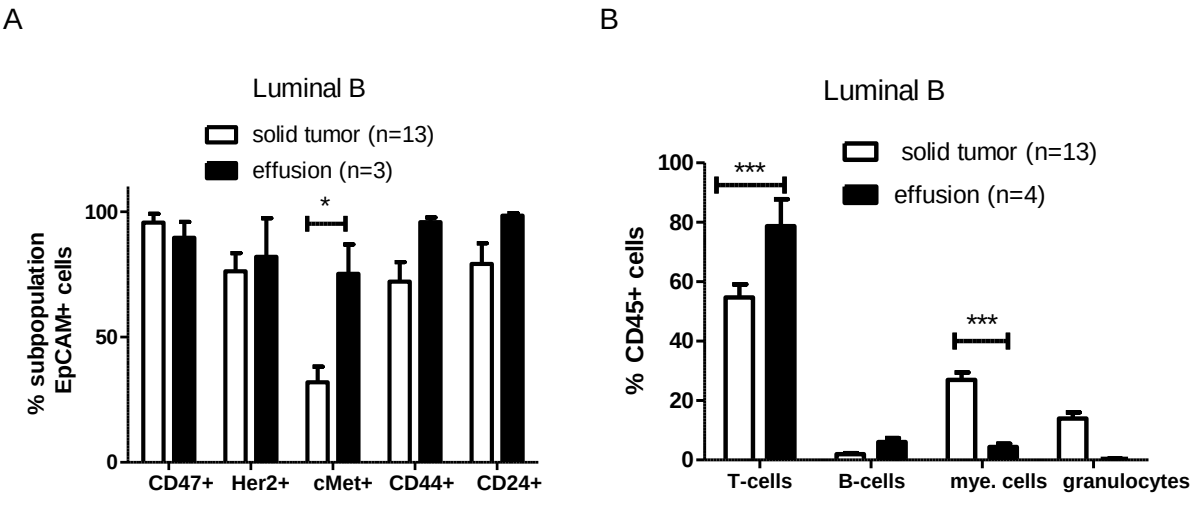

Figure 17: SCF and RECON analysis comparing solid Luminal B tumors with Luminal B effusions
A) Expression profiles of stem cell markers CD47, Her2, cMET, CD44, and CD24 are presented and were previously gated on EpCAM$^+$ cells. **B)** T-cells, the B-cells, the myeloid (mye.) cells, and the granulocytes are shown in solid Luminal B tumors and Luminal B effusion. All data are represented as mean + SEM and the number of patient samples is shown in parentheses. Significances were analyzed using Two-way ANOVA with Bonferroni post hoc correction (* $p < 0.05$, *** $p < 0.001$).

4.2.4.2 Characterization of T cell subsets in the primary tumor compared to the effusion of Luminal B breast cancer patients

T-cell subpopulations were characterized in Luminal B solid tumors and Luminal B effusion. Interestingly, the CD4/ CD8 ratio is shifted significantly towards $CD4^+$ cells in Luminal B effusion (students T-test, $p < 0.0001$) (Figure 18 A). The CD8 effector cells were reduced and naïve $CD8^+$ cells were increased in Luminal B metastatic effusions (Two-way ANOVA with Bonferroni post hoc correction, both (effector and naïve) $p < 0.05$) (Figure 18 B). This phenomenon is also displayed in the CD4 setting. The CD4 effector cells were decreased and the CD4 naïve cells were increased in Luminal B effusions (Two-way ANOVA with Bonferroni post hoc correction, both (effector and naïve) $p < 0.01$) (Figure 18 C). The total PD-1 expression on T-cells was reduced in Luminal B effusions compared to Luminal B solid tumors (Student's t-test, $p = 0.0011$) (Figure 18 D). Detailed analyses revealed that especially the $CD8^+$ T-cells showed decreased PD-1 expression in Luminal B effusion compared with the Luminal B solid tumors (Student's t-test, $p = 0.0003$) (Figure 18 E). $CD4^+$T-cells did not differ in PD-1 expression (data not shown).

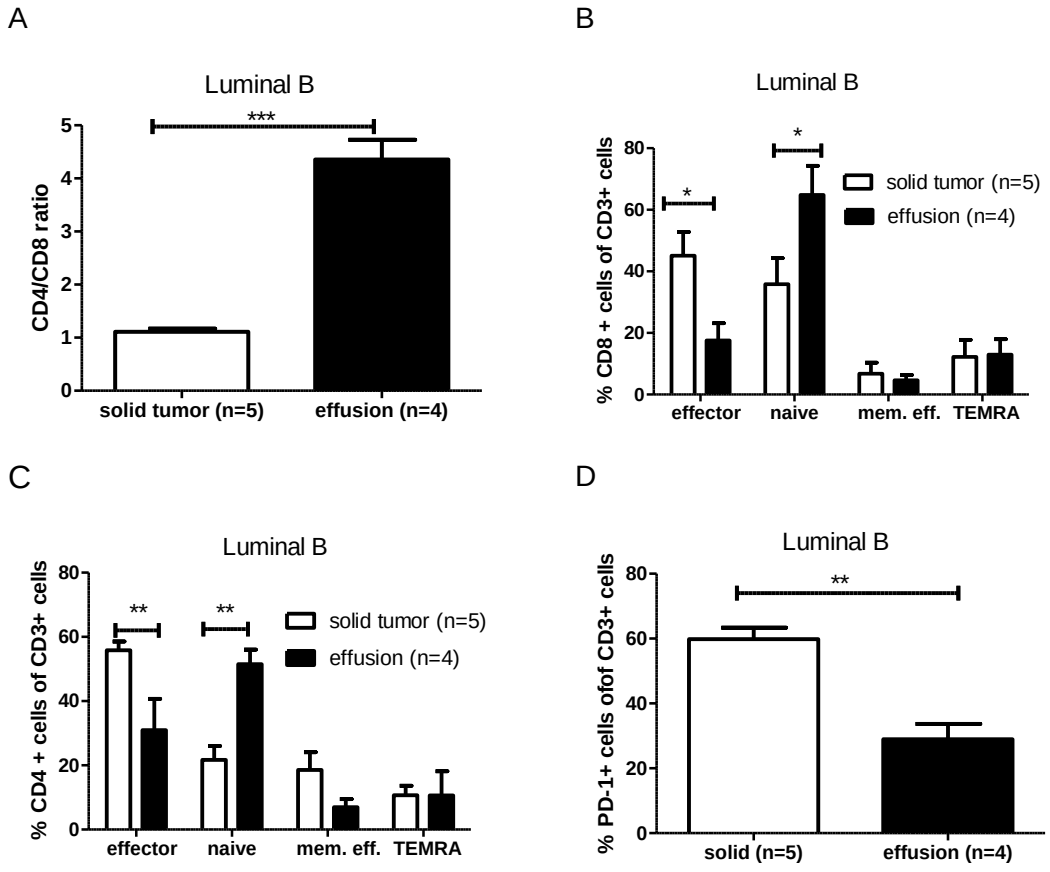

E

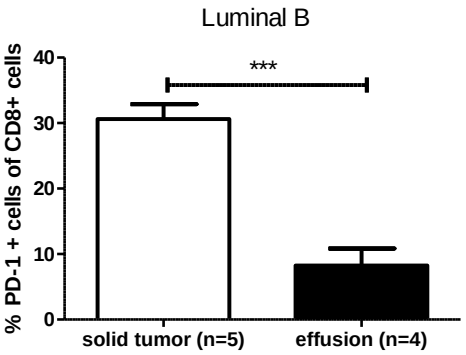

Figure 18: T-cell subpopulations in Luminal B solid tumors compared to Luminal B metastases
A) The figures show the CD4/CD8 ratio of Luminal B solid tumors versus Luminal B effusions. **B)** The data represent the % CD8 effector, naïve, mem. eff. (memory effector), and TEMRA cells in Luminal B solid tumors and effusions. **C)** The figure shows the % CD4 effector, naïve, mem. eff. (memory effector), and TEMRA cells in Luminal B solid tumors and Luminal B effusions. **D)** The data represent the total PD-1 expression on T-cells in solid tumors and effusions in Luminal B breast cancer. **E)** The expression level of PD-1 on $CD8^+$T-cells is presented on Luminal B solid tumors compared to Luminal B effusions. The data are shown as mean + SEM and the group size is indicated in parentheses. Significances were analyzed using Two-way ANOVA with Bonferroni post hoc correction or Student's t-test (*p < 0.05, ** p < 0.01, *** p < 0.001)

4.2.5 Primary tumor culturing

To establish a breast cancer tumor cell line, solid primary tumors were dissociated mechanically or enzymatically, and cultured in DMEM/F12 supplemented with growth factors and nutrients (rhEGF, insulin, hydrocortisone, ß-estradiol). To prevent anoikis of primary cells, 10 µM Rock inhibitor was added for 5 days to enhance the survival of stem cells, prevent dissociation induced apoptosis, and therefore increase the clonal efficiency of the cells (Watanabe *et al.*, 2007). These conditions were not applicable to the primary solid tumor cells from our laboratory and did not result in a successful culturing of a breast cancer tumor cell line (0/32). The tumor cells were often overgrown by fibroblasts. Even though differential trypsinization was performed to remove the fibroblasts, the tumor cells could not be propagated. Tumor cell culturing was stopped at the latest of seven months later calculated from the first day of seeding. However, cells that were isolated from a pleural effusion (PT AB) could be propagated in DMEM + 20 ng/ml EGF + 5 µg/ml Insulin 1 % Amphotericin B + 1 % P/S + 5 % FCS medium, and culturing was successful over five passages (Figure 19 A). It took one month for visible and countable tumor cell proliferation. Moreover, retransplantations of the cultured cells of PT AB resulted in adequate outgrowth of peritoneal tumor cells in 4/4 TM reflecting the equivalent tumor phenotype from the primary tumor. The tumor cells were tested by SCF (EpCAM and Her2 positivity) on the tumor cell origin and by IHC. The tumor cells were positive for CK18, and ER, and negative for Vimentin. In addition, a medium supplemented with 30 different nutrients and growth factors, provided by our cooperation partner in Heidelberg (published in the Ph.D. thesis of Massimo Saini

2017), opened up the opportunity to culture CTC solid tumors for approximately two passages (Figure 19 B).

A

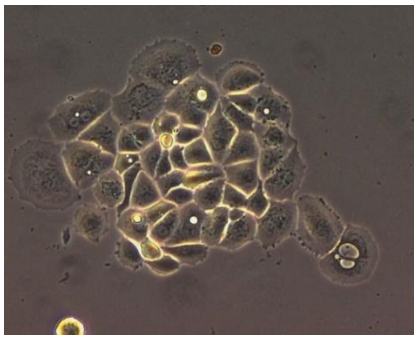

PT AB

B

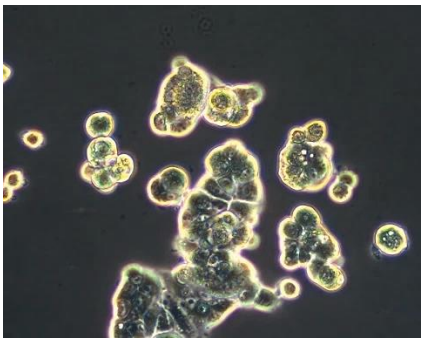

TM CTC

Figure 19: Representative images of the primary tumor cell culture
A) The image shows cultured PT AB tumor cells derived from pleural effusion. **B)** The cultured TM CTC solid tumor cells are displayed. The images were taken in 10-fold magnification.

4.3 Characterization of all Luminal B tumor mice (TM)

4.3.1 Engraftment success of primary tumors in TM (tumor mice)

33 primary tumors were transplanted in 99 NSG mice (n=3 each primary tumor). 16 of the 33 tumors were Luminal B/ $Her2^-$ tumors, 4 Luminal B/$Her2^+$ tumors, 7 Luminal A tumors, 4 TNBC tumors, and 2 $Her2^+$ /HR^- primary tumors. Luminal/ $HER2^-$ tumors did not engraft (0/16; 0%) whereas TNBC (2/4; 50%), $HER2^+$ breast cancer (2/4; 50%), and Luminal B/$HER2^+$ (1/2; 50%) breast cancer were successfully engrafted. In our laboratory settings, only breast cancer single-cells from metastatic effusions engrafted. The solid primary breast cancer fragments, which were mechanically or enzymatically dissociated into single cells, generally failed in engraftment. However, orthotopic tumor fragment transplantations were successful with solid primary breast cancer. The missing engraftment success of Luminal B $HER2^-$ tumors is indicating the general difficulties of the engraftment of HR-positive/$Her2^-$ tumors (Table 21). Moreover, only primary tumors from Caritas Hospital St. Josef Regensburg with either a low PR expression or PR deficiency successfully engrafted in the NSG mice. Additionally, only primary tumors with high Ki67 of > 14 % engrafted in our NSG mice.

Table 21: The Success rate of engrafted PDX models

Successful / total number	Subentity	% engraftment success
1/2	$Her2^+$	50 %
0/7	Luminal A	0 %
0/16	Luminal B $Her2^-$	0 %

2/4	Luminal B Her2$^+$	50 %
2/4	TNBC	50 %

The table represents the number of successful engrafted PDX models versus the received total tumor number (n/n) classified according to the subentity.

4.3.2 Total engraftment numbers of tumors in TM and HTM

Tumor fragments were transplanted in TM CTC, TM Bpe. The idea of simultaneous neonatal tumor cell and hematopoietic stem cell transplantation was realized in the HTM CTC and Bpe model. In all other cases, a neonatal humanization prior to tumor fragment transplantation was necessary as fragments can only be transplanted in adult mice. Single-cell transplantation from the other tumors did not engraft. Hence, tissue fragments were transplanted in TM CTC, TM Bpe, TM P, HTM P, TM V, TM X orthotropy. PT AB was transplanted as a single-cell suspension. PT P resulted in 15 TM and 8 HTM, and PT AB in 5 TM as models of the Luminal B /Her2$^+$ entity. The TNBC PT V was successful in 2 TM and the TNBC PT U engrafted in 5 TM. 8 TM were generated with the Her2$^+$ tumor PT X. As TNBC and Her2$^+$ tumors only served as control of transplantation methods the tumors were not transplanted into humanized mice. Due to the limited time of the project, HTM were not generated out of TM AB mice. The precise passages of the TM and HTM are listed in Table 22.

Table 22: Number of animals with successful tumor engraftment of different tumors from Caritas Hospital St. Josef Regensburg

Solid primary breast cancer St Josef Regensburg					**Pleural effusion (metastasis) St. Josef Regensburg**	
Entity	**Luminal B/Her2$^+$**		**TNBC**	**Her2$^+$**	**TNBC**	**Luminal B/Her2$^+$**
PT	**PT (P)**		**PT (V)**	**PT (X)**	**PT (U)**	**PT (AB)**
TM/HTM	TM	HTM	TM	TM	TM	TM
Number of mice	15	8	2	8	5	5
Passage	P0- P4	P1- P5	P0- P2	P0- P3	P0-P1	P0-P1

PT primary tumor, *TNBC* Triple-negative breast cancer, *Her2* human epithelial growth factor receptor 2, *TM* tumor mouse, *HTM* humanized tumor mouse, *P* passage

5 TM and 4 HTM were generated out of TM PT CTC tumors and TM PT Bpe engrafted successfully in 5 TM and 6 HTM. The tumors derived from our cooperation partner in France resulted in 5 TM and 3 HTM of the HBCx3 tumor, 5 TM and 3 HTM of the HBCx34 tumor, and 11 TM and 2 HTM of the HBCx22 tumor. All TM and HTM were transplanted with a tumor fragment orthotopically into the mammary fat pad of the HBCx tumors. The tumor passages of TM and HTM tumors are depicted in Table 23 below.

Table 23: Number of animals with successful tumor engraftment of different Luminal B PDX tumors from different cooperation partners

Luminal B PDX										
Luminal B PDX (solid primary breast cancer) cooperation Marangoni							Luminal B PDX (CTC/Bpe derived) cooperation Trumpp			
TM	**F TM 3**		**F TM 34**		**F TM 22**		**TM CTC**		**TM Bpe**	
TM/HTM	TM	HTM	TM	HTM	TM	HTM	TM	HTM	TM	HTM
Number of mice	5	3	5	3	11	2	5	4	5	6
Passage	P0-P3	P2-P4	P0-P2	P0-P1	P0-P2	P2-P3	P0-P2	P0-P3	P0-P2	P0-P3

PT primary tumor, *TNBC* Triple-negative breast cancer, *Her2* human epithelial growth factor receptor 2, *TM* tumor mouse, *HTM* humanized tumor mouse, *P* passage, *CTC* circulating tumor cells, *Bpe* pleural effusion, *F* cooperation model from Dr. Marangoni from the Institute Curie, France

4.3.3 Characterization of human origin in PDX tumors

Working with PDX models, it is indispensable to ensure the human origin of the tumors grown in NSG mice. Therefore, DNA was isolated from tumors of TM and tested with species-specific primers for human tissue content using the HuMo PCR. All PDX models generated were shown to be of human and not mouse origin (Table 24). For the PDX model TM X, TM AB, TM P the human DNA content was analyzed even after the first successful engraftment. The PDX models from our cooperation partner were verified on human origin at the end of the experiments as those were analyze by the cooperation partners beforehand. Five NSG mice transplanted with other primary human tumors (at the age of one year or later) were observed to spontaneously develop mouse mammary tumors (data not included in the table). The human origin of these tumors was excluded by HuMo PCR, the lack of $EpCAM^+$ cells in SCF flow cytometry, and IHC negativity for CK18.

Table 24: Percentage of human tissue in tumors isolated from all TM at the end of the experiment after several retransplantations

Tumor	TM X	TM AB	TM P	TM CTC	TM Bpe	F TM 3	FTM 34	F TM 22
% human tissue	96,6	98,6	96,2	91,4	90,1	89,5	96,7	91,1

4.3.4 The immunohistochemical phenotype of the PDX tumor is congruent with the patients' primary tumor

Different tumor passages were analyzed immunohistochemically for H&E, ER, PR, Her2 and Ki67 expression to verify the maintenance of the intrinsic biological Luminal B subtype. The comparison of the different passages of retransplanted tumor fragments into TM revealed the stability of the intrinsic biological markers of the Luminal subtype. ER and Her2 expression remained stable. However, quite a low

expression of PR emerges in passage 4 of the TM compared with the primary tumor and the TM at passage 0. Moreover, the proliferation (Ki67) seems to be increased in passage 4 (Figure 20 A). Noteworthy, the intratumoral heterogeneity of the primary tumor can still be maintained in the PDX model. The intrinsic molecular markers (ER, PR, Her2, Ki67) coincide in the low passages of the PDX models with the primary tumor. This congruency seems to be altered by various passaging of the tumor from TM to TM. The clinical report of the patient AB revealed hepatic, pulmonary, pleural, adrenal, and osseous metastases detected by computer tomography. A report on the occurrence of brain metastases in patient AB was not available. However, the metastatic spread of the primary tumor in the patient is in accordance with the metastatic spread into the lung, the liver, the spleen, and the brain of the TM AB model verified by CK 18 IHC (Figure 20 B). We were not able to determine metastasis in the adrenals as this organ was not stored for analysis.

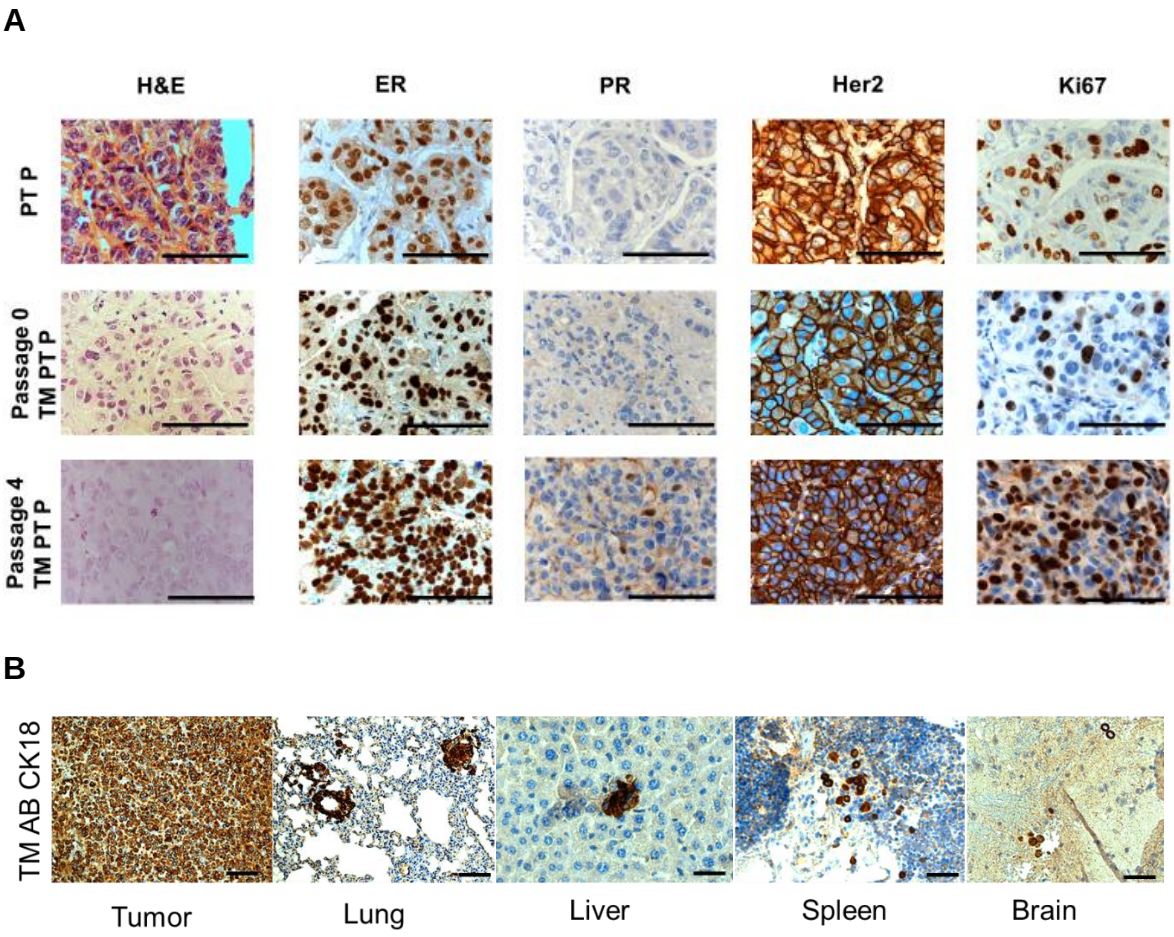

Figure 20: Representative images of the primary tumor compared to TM tumor engraftment and further retransplantations

Results

A) H&E, ER, PR, Her2, and Ki67 were analyzed immunohistochemically. The bars represent 100 µm and the images are taken at 63-fold magnification. **B)** IHC CK18 analysis of TM AB is shown in the tumor and the organs to detect metastases. The bar represents 100 µm and the images are taken at 20-fold magnification.

Additionally, all generated PDX models were analyzed on their morphology (H&E), ER, PR, Her2, Ki67, EpCAM expression (Table 20). Despite the stable ER, Her2, and Ki67 expression (if the primary tumor was $Her2^{+}$) throughout various transplantation, the PR expression was lowered in the TM Bpe, F TM 34, and F TM 3 model compared with the primary tumor. EpCAM positivity was assessed as this was the basis for the gating in flow cytometry in order to detect the tumor cells. In fact, all Luminal tumor PDX models revealed EpCAM expressing cells but with varying intensity (Figure 21 A). Noteworthy, the expression of ER, PR, Her2, Ki67, and EpCAM remained stable even in hematopoietic stem cell cotransplanted HTMs (data not shown). Moreover, all PDX models were CK18 positive. However, the tumors differed in cell morphology. F TM 22 and F TM 3 exhibited huge necrotic areas in the tumor center in contrast to the other PDX models (Figure 21 B).

A

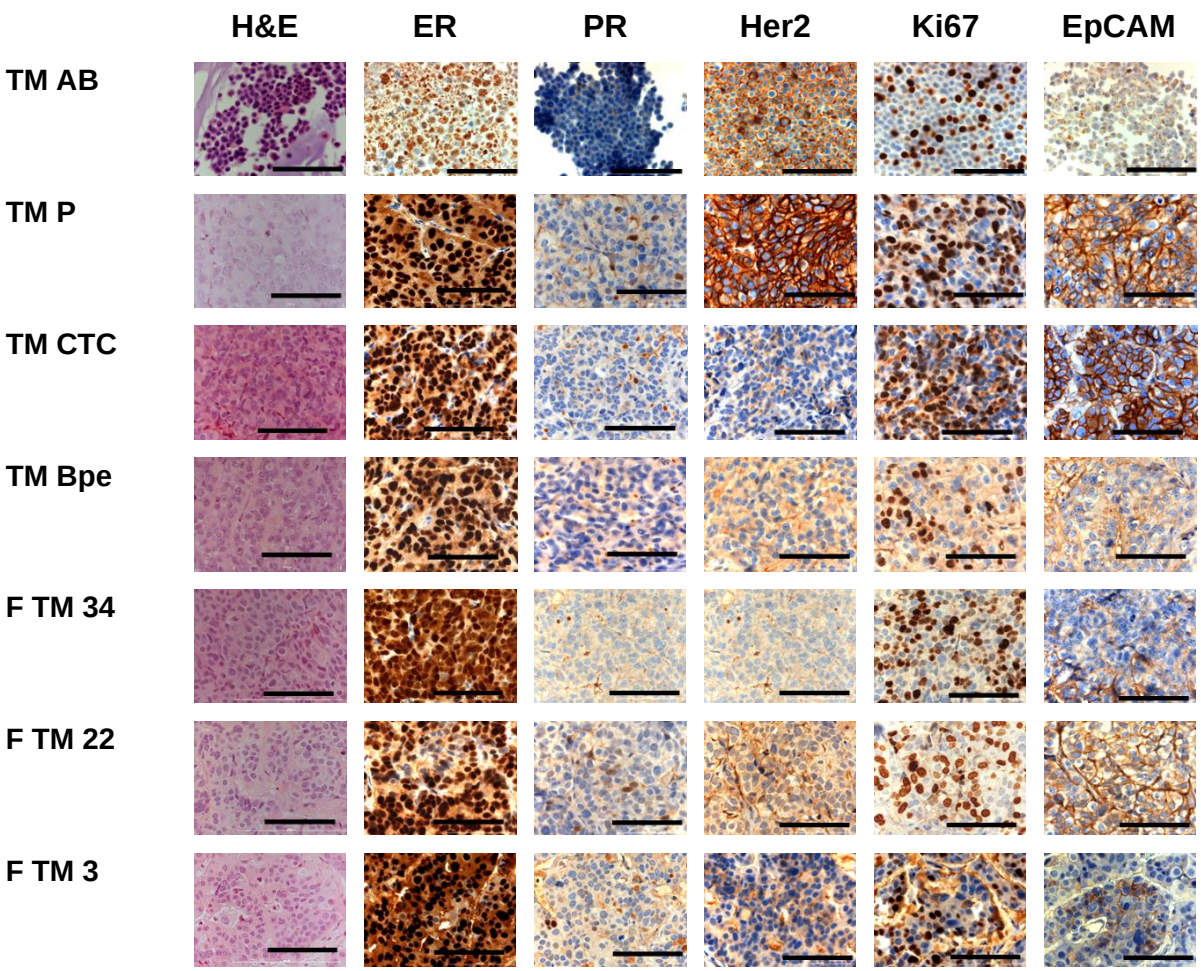

B

Figure 21: Representative images of intrinsic molecular features of all engrafted Luminal B tumors in the TM and the metastatic sites of TM AB model
A) The data show the immunohistochemical staining of H&E, ER, PR, Her2, Ki67, and EpCAM on TM AB, TM P, TM CTC, TM Bpe, F TM 34, F TM 22, and F TM 3 tumors. The images are represented in 63- fold magnification. The bars show 100 µm. **B)** The images show a representative IHC staining of CK18 of all Luminal B TM tumors. The images were taken at 10-fold magnification.

4.4 MDM2 /TP53 /MDM4 alterations in Luminal B breast cancer PDX

4.4.1 Uncovered alterations in Luminal B breast cancer by Panel Sequencing

To characterize the generated PDX and their corresponding tumor in detail, all generated PDX tumors with different subentities were analyzed by panel sequencing by our cooperation partner (Nicole Pfarr, TU Munich) to quantify genomic aberrations. The panel covers 59 genes on different chromosomes that are related to breast cancer (Table 25). Remarkably, all tumors showed alterations in the MDM2/ p53 /MDM4 pathway. Interestingly, TM P, TM Bpe, TM CTC, and F TM 34 of the Luminal B tumors showed an MDM2 amplification. Additionally, TM AB of the Luminal B cohort, as well as TM V of the TNBC group, exhibited an MDM4 amplification. F TM 3 and F TM 22 of the Luminal B cohort displayed a TP53 Mutation. A TP53 mutation is also frequent in the TNBC tumors (TM U and TM V). The analysis revealed that MDM2 amplification and TP53 mutations seem to be mutually exclusive. TM P tumor revealed an MDM2 amplification as well as a TP53 deletion.

For TM X, TM AB, and TM P the Her2 amplification could be confirmed as it was known previously due to the pathological diagnostics and the Her2 FISH performed by the institute of pathology Regensburg. The primary tumor PT P, PT X, and PT V were analyzed equally and revealed the same amplification, mutations, and deletions as the corresponding engrafted TM P, TM X, TM V PDX tumors, indicating that the PDX model genetically reflects the primary tumor (data not shown). However, several other mutations like PIK3CA (TM AB, TM CTC), PTEN (F TM 3, F TM 22), or deletions like CDKN2A (TM AB, TM Bpe, F TM 34, F TM 22) and FOXO3 (TM Bpe, F TM 34), or amplifications like GRHL2 (TM Bpe, F TM 34) or MYC (TM Bpe) were detected by panel sequencing. The detailed aberrations for each TM PDX model are listed in Table 25. Moreover, it was demonstrated by our cooperation partner Prof. Trumpp in

Heidelberg that the PDX models stayed stable in its alterations over several passages in the animals (data not shown).

Based on the alterations described above, Luminal B PDX models were subdivided into groups of MDM2 amplified Luminal B tumors and MDM2 Wildtype (WT) Luminal B tumors in the following chapters.

Table 25: Data from the panel sequencing of all TM tumors analyzed by our cooperation partner in Munich (Nicole Pfarr)

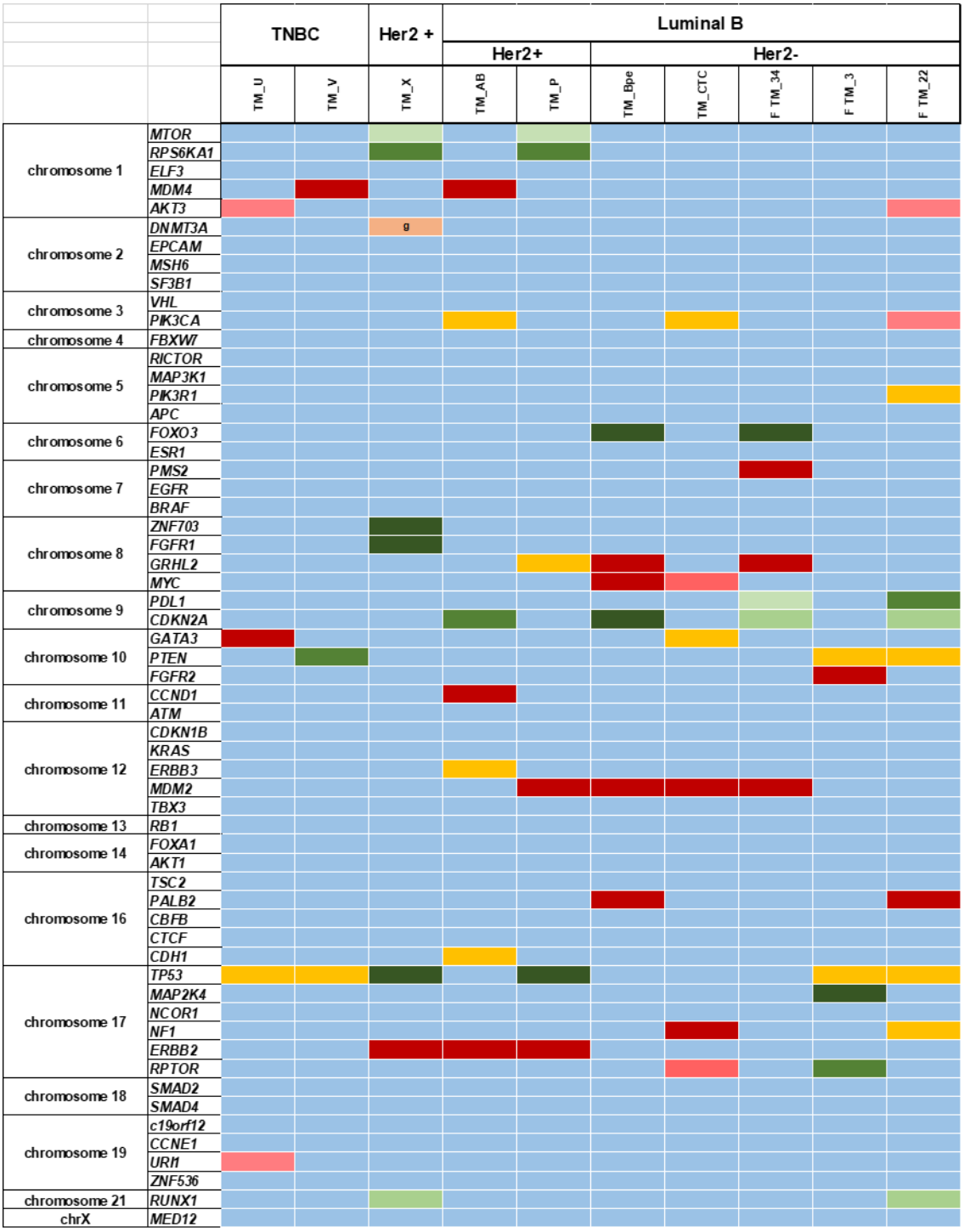

The chromosomes are indicated at the left side with the corresponding genes analyzed. On top, the TM tumors are listed according to their breast cancer entity. The red boxes show an amplification of the gene, the dark green box shows a deletion, and the yellow box indicates a genomic mutation. A germline mutation is marked in pink and a possible deletion is colored in light green.

4.4.2 Classification of PDX models according to chromosomal aberrations of MDM2 and p53

P53, as a product of the TP53 tumor suppressor gene, normally gets ubiquitinylated by MDM2 to be degraded at the proteasome. MDM2 serves therefore as a direct negative regulator of p53. As all Luminal B PDX models exhibited alterations in the MDM2/ p53 axis, it was interesting to determine the Luminal B tumor properties under the aspect of an MDM2 amplification and a TP53 mutation. Based on the results of the panel sequencing the Luminal B PDX models were subdivided into two categories. On the one hand, four PDX models (TM P, TM CTC, TM Bpe, and F TM 34) exhibited an MDM2 amplification and on the other hand F TM 22, FTM 3 and TM AB revealed no amplification in the MDM2 gene but alterations in MDM4 and TP53. The IHC of MDM2 confirmed the expression on protein level in TM P, TM CTC, TM Bpe, and F TM 34 but also showed the expression of MDM2 in TM AB tumors. The latter could be due to the fact that MDM4 stabilizes MDM2 protein expression which was amplified (Stad *et al.*, 2001). The FISH analysis revealed a normal ratio of MDM2 signals versus centromeric signals in TM Bpe, F TM 22, F TM 3 and TM AB and an increased ratio in the TM P and TM CTC model. According to its MDM2 ratio F TM 34 would rather be considered as equivocal. However, the gene signals of MDM2 per cell was increased in TM P, TM CTC, F TM 34 (Table 26).

Table 26: Summary of panel sequencing results and IHC, FISH and the corresponding FISH ratios and gene doses in the different Luminal B PDX models

	MDM2 amplified tumors				MDM2 WT tumors		
Tumor	**TM P**	**TM CTC**	**TM Bpe**	**F TM 34**	**F TM 22**	**F TM 3**	**TM AB**
MDM2 amplification	✓	✓	✓	✓	-	-	-
MDM4 amplification	-	-	-	-	-	-	✓
TP53 mutation	-	-	-	-	✓	✓	-
IHC of MDM2	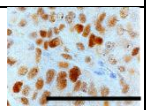	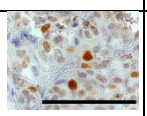	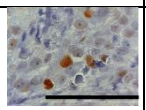	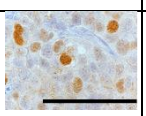	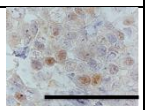	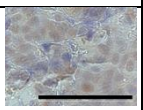	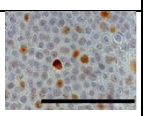
MDM2 FISH	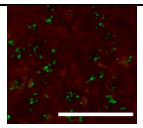	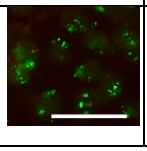	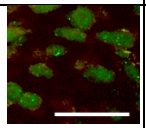	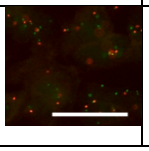	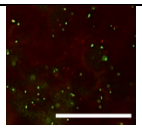	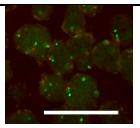	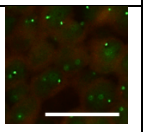

MDM2 FISH ratio	**5,83**	**4,00**	**1,68**	**2,02**	**1,26**	**1,28**	**1,14**
MDM2 gene dose	**< 10**	**< 10**	**3,35**	**5,05**	**3,65**	**3,40**	**1,65**

The table displays the summarized data of all Luminal B PDX models of the panel sequencing regarding MDM2 and MDM4 amplification as well as the TP53 mutations. IHC of MDM2 is shown in 63-fold magnification with a bar of 100 µm. FISH data are represented in 63-fold magnification and the bar shows 25 µm. The FISH ratio is calculated as MDM2 signals per centromeric signal and the single signals per cells of MDM2 are listed as gene dose.

4.4.3 Classification of PDX models according to the MDM2 and p53 protein levels

In order to determine the protein levels of MDM2 and p53 Western Blot analysis of all Luminal B PDX models was performed. Protein levels revealed low expression of p53 in MDM2 amplified tumors (TM P, TM CTC, TM Bpe, and F TM 34), whereas increased p53 expression was observed in F TM 22, and F TM 3 tumors. Interestingly TM AB exhibited an increased expression of p53, whereas the tumor features no TP53 mutation, but an MDM4 amplification. As it was published previously, MDM4 seems to stabilize p53 in TM AB (Stad *et al.*, 2001). The MDM2 antibody recognizes four Isoforms of MDM2 at 90 kDa, 76 kDa, 74 kDa, and 57 kDa. The expression and intensity of the different MDM2 isoforms vary between the different PDX models. In accordance with the IHC data, MDM2 is mainly increased in TM P and F TM 34 but low expression of MDM2 can also be shown in TM CTC, TM Bpe, F TM 22 and F TM 3 (Figure 22).

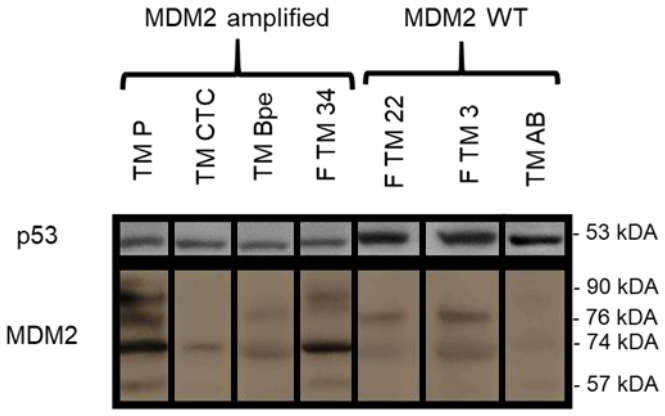

Figure 22: Representative Western Blot of p53 and MDM2 of all Luminal B PDX models
The Blot represents p53 and MDM2 expression of all Luminal B tumors classified according to the results of the panel sequencing in MDM2 amplified and MDM2 wildtype tumors.

Taken together, the data of Table 25, Table 26 and Figure 22 reason the subdivision of the tumors as following: TM P, TM CTC, TM Bpe and F TM 34 are summarized and denoted for all further animal experiments as TM MDM2 Amplified (Amp) whereas F TM 22, F TM 3 and TM AB are summarized as MDM2 wildtype (WT).

4.4.4 MDM2 amplification increased tumor weight and tumor volume over time, decreased the disease-free survival but did not alter the overall survival

The TM were analyzed on tumor weight, tumor volume over time, disease-free survival (DFS) defined as the date of tumor transplantation until the first occurrence of a palpable tumor), and overall survival (OS) (defined as the date of tumor transplantation until death) to determine the impact of the MDM2 amplification on tumor growth *in vivo*. The data include 28 TM P tumors, 6 TM CTC tumors, 7 TM Bpe tumors, 12 F TM 34 tumors which are summarized as TM MDM2 Amp tumors. 10 F TM 3 tumors, 11 F TM 22 tumors, 5 TM AB tumors were summarized as TM MDM2 WT tumors. The data revealed a statistically significant increase in tumor weight of TM MDM2 Amp tumors compared with TM MDM2 WT tumors (Student's t-test, $p = 0.0005$) (Figure 23 A). Moreover, the tumor volume was significantly increased in TM MDM2 Amp tumors compared with TM MDM2 WT tumors, but only at two months after engraftment (Two-way ANOVA with Bonferroni post hoc correction, $p < 0.05$). A tendency towards increased tumor volume of TM MDM2 Amp tumors could be observed at 1.5 months and 2.5 months engraftment whereas the tumor volume converged to a similar volume at 3 and > 4 months after engraftment (Figure 23 B). Noteworthy, the DFS was significantly reduced in TM MDM2 Amp tumors compared with TM MDM2 WT tumors (Log-rank (Mantel-Cox) test, $p < 0.0477$) (Figure 23 C). In contrast, the Kaplan Meyer curves for analysis of overall survival (OS) did not differ between the two groups (Log-rank (Mantel-Cox) test, $p = 0.0876$) (Figure 23 D).

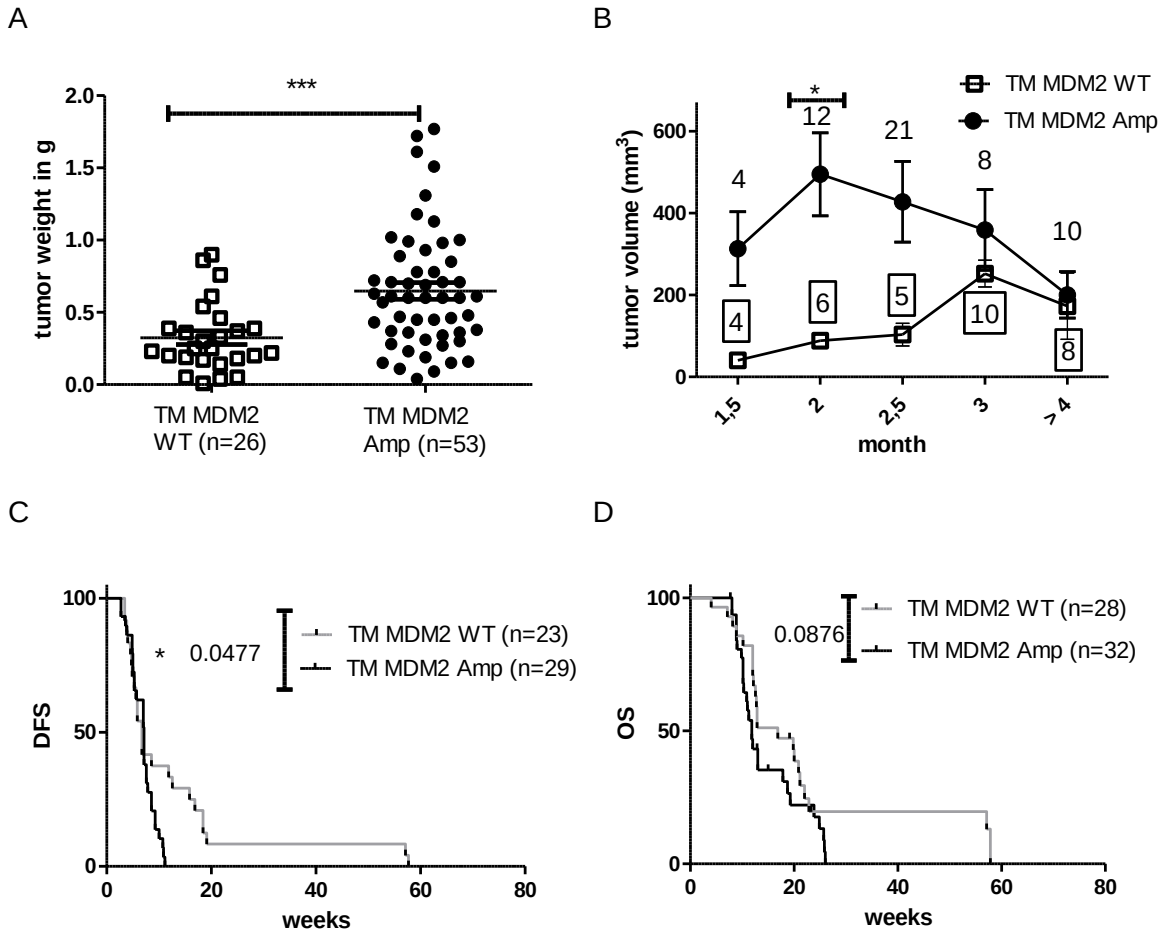

Figure 23: Effect of an MDM2 amplification in TM tumors
A) The figure represents the tumor weight and each dot shows an individual animal. The number of TM is listed in parentheses. **B)** The tumor volume over time is presented in TM MDM2 Amp animals and TM MDM2 WT animals. The number of animals is listed below or above each time point and the black-rimmed numbers belong to TM MDM2 WT tumors. The data are represented as mean ± SEM. **C)** The data show the DFS, and **D)** the OS of TM MDM2 WT tumors compared with TM MDM2 Amp tumors. The number of animals is depicted in parentheses. Significances were analyzed using Two-way ANOVA with Bonferroni post hoc correction, Student's t-test or Log-rank (Mantel-Cox) test (* $p < 0.05$, ***$p < 0.001$).

4.4.5 Phenotypic differences and alterations in the MIC population ($CD44^+/cMET^+/CD47^+$) between TM MDM2 amplified tumors and TM MDM2 WT tumors

Amongst TM MDM2 WT and TM MDM2 Amp tumors, the phenotypic alterations regarding stem cell marker expression were analyzed by flow cytometry and Western Blot to determine the impact of an MDM2 amplification. If two tumors were engrafted in one animal the tumor probe was pooled for flow cytometrical analysis. The exact distribution is given in 4.4.4. In contrast to the expectancies, the TM MDM2 Amp tumors showed a decreased cMET expression compared with TM MDM2 WT tumors, whereas CD47, CD44, and CD24 did not differ in their expression levels (Two-way ANOVA with Bonferroni post hoc correction, $p < 0.01$) (Figure 24 A). These findings could be

confirmed by Western Blot assessment with the highest cMET expression in F TM 22 and F TM 3 belonging to TM MDM2 WT tumors (Figure 24 B). In addition, flow cytometric analysis revealed a significantly decreased expression of the triple-positive MIC population ($CD44^+$, $cMET^+$, $CD47^+$) in TM MDM2 Amp tumors compared with TM MDM2 WT tumors (Student's t-test, $p < 0.0001$) (Figure 24 C). In addition, Western Blot analysis of CD44, cMET, and CD47 confirmed that CD44 and CD47 as single markers do not serve as a prognosticator in TM MDM2 Amp tumors (Figure 24 D). In addition, the EpCAM expression, in general, was shown to be very high (mean 86 - 88 %) and did not differ between the groups (students t-test, $p = 0.5633$) (Figure 24 E).

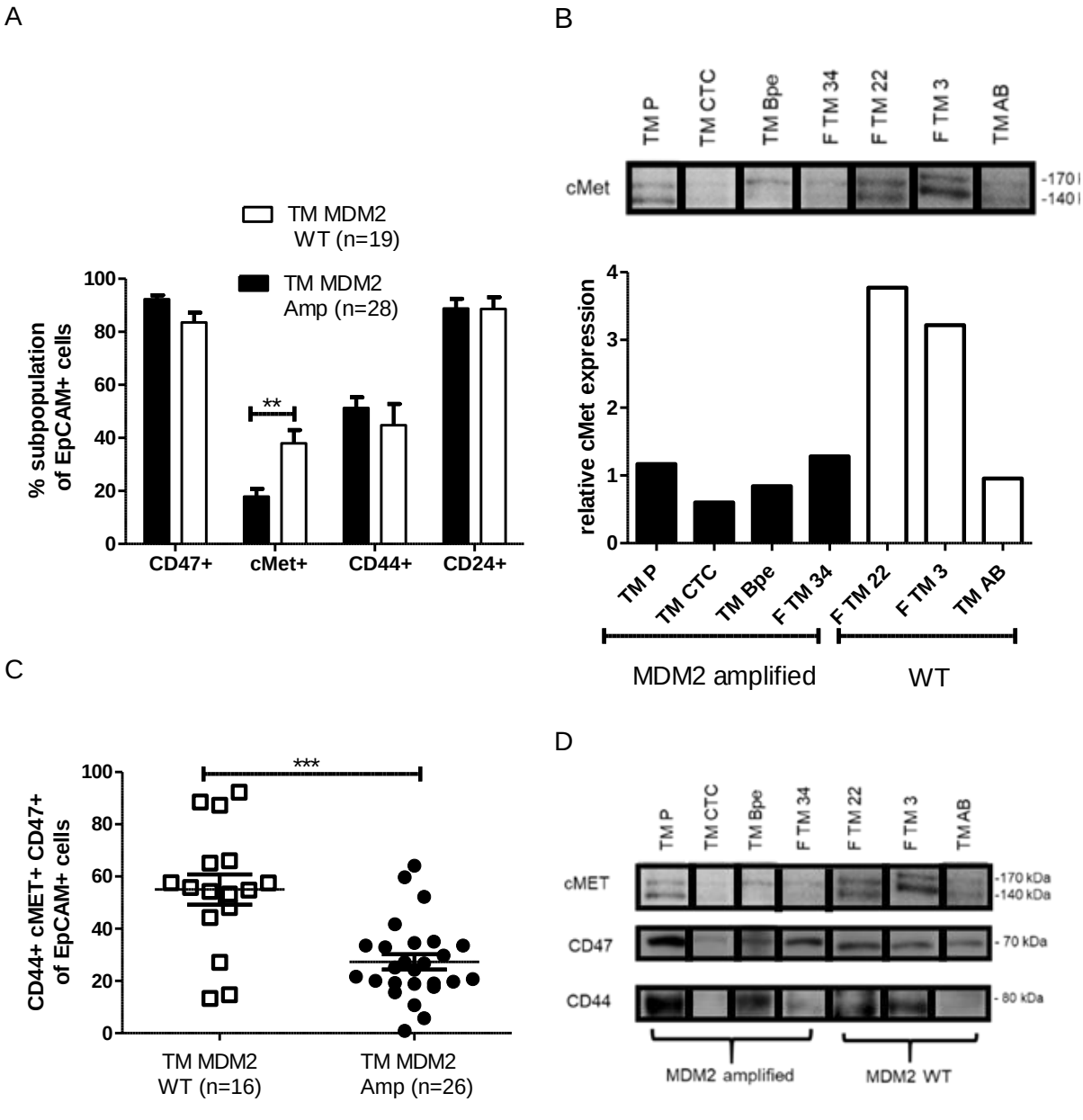

Figure 24: Flow cytometric analysis on stem cell markers comparing TM MDM2 WT with TM MDM2 Amp tumors

A) The figure shows the SCF analysis comparing TM MDM2 WT tumors with TM MDM2 Amp tumors. **B)** The upper panel shows a representative image of the cMET Western Blot. The corresponding densitometric analysis normalized on total protein for each Luminal B PDX model is depicted below. **C)** The MIC population was analyzed by flow cytometry comparing TM MDM2 WT with TM MDM2 Amp tumors. **D)** The Western Blot analysis of cMET, CD47, and CD44 of all Luminal B PDX models is shown in the graph. **E)** The data represent the EpCAM expression of tumor cells comparing TM MDM2 WT with TM MDM2 Amp tumors. The animal numbers are represented in brackets and the Western Blot analysis was performed only once with. The data of **A)** are shown as mean+ SEM and the data in **C)** and **E)** are represented as

mean ± SEM. Each dot represents a single tumor. Significances were analyzed using Two-way ANOVA with Bonferroni post hoc correction or Student's t-test (** p < 0.01, ***p <0.001).

4.4.6 MDM2 amplified tumors promote lung metastases and differ phenotypically from the corresponding tumor

To determine the lung metastasis of TM MDM2 WT compared to TM MDM2 Amp animals, the lungs of the TM were stained for cytokeratin 18 (CK18) and analyzed morphometrically. CK18 as a keratin filament is highly expressed in epithelial cells of Luminal breast cancer and serves as a marker to identify the Luminal breast cancer cells in the periphery. It was shown that the frequency of lung metastases occurrence was significantly increased in TM MDM2 Amp animals compared with TM MDM2 WT animals (Two-sided Fisher's exact test, p < 0.0001) (Figure 25).

TM MDM2 WT **TM MDM2 Amp**

	TM MDM2 WT	TM MDM2 Amp	P value (TM MDM2 Amp versus TM MDM2 WT)
Lung metastases	2/12	22/24	**0.0001**

Figure 25: Lung metastases in TM MDM2 WT compared with TM MDM2 Amp animals
Representative images of lung metastases in TM MDM2 WT and TM MDM2 Amp animals. The images are shown in 20 -fold magnification and the bars represent 100 µm. The incidence for lung metastases was calculated using the two-sided Fisher's exact test and the p-value is listed in the table. The number of animals with detectable CK18 metastases of the total number of animals (n/n) is indicated.

In addition, only the lung metastases of all TM MDM2 Amp animals were analyzed for stem cell marker expression by flow cytometry, because only two animals in the TM MDM2 WT (TM AB tumor) tumor group generated lung metastases. The tumor cells in the lung were detected using EpCAM. The number of $EpCAM^+$ counts in the lung ranges between 200 and 6000 cells per measurement of 0.5 million total lung cells. The TM MDM2 Amp lung metastases revealed an increased level of $cMET^+$ and $CD44^+$ cells, compared to the corresponding tumor (Two- Way ANOVA with Bonferroni post hoc correction, p < 0.001) (Figure 26 A). Moreover, the MIC population ($CD44^+$, $CD47^+$, $cMET^+$) was shown to be increased in TM MDM2 Amp lung metastases, compared to the primary tumor (Student's t-test, p < 0.0001) (Figure 26 B).

A

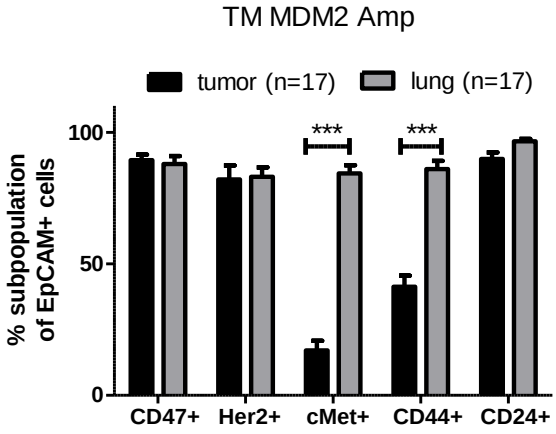

B

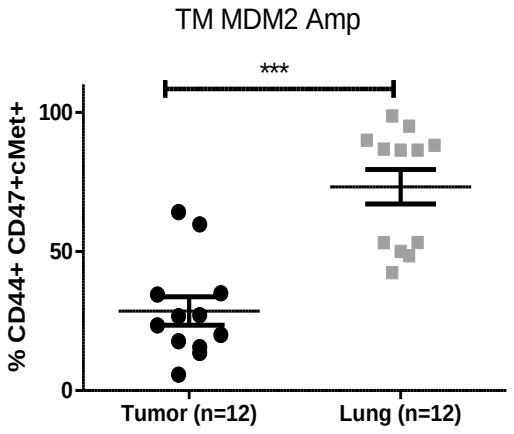

Figure 26: Flow cytometric analysis of lung metastases compared with the corresponding tumor in TM MDM2 Amp animals.
A) The figure shows a comparison of CD47, Her2, cMET, CD44, and CD24 in TM MDM2 Amp tumors vs. TM MDM2 Amp lung metastases. **B)** The MIC population is represented in TM MDM2 Amp tumors and TM MDM2 Amp lung metastases. The data in **A)** are shown as mean + SEM and in **B)** as mean ± SEM whereby each dot represents a single animal. The number of animals and the corresponding lung metastases is indicated in parentheses. Significances were analyzed using Two-way ANOVA with Bonferroni post hoc correction or Student's t-test (*** $p < 0.001$).

4.4.7 MDM2 amplification decreases T-cell infiltration in HTM

In order to determine the influence of the human immune system on Luminal B tumors, HTM of the Luminal B TM were generated. Based on the results of TM (Table 25, Table 26 and Figure 22) HTM tumors were subdivided into two groups for the following examinations: HTM P, HTM CTC, HTM Bpe and F HTM 34 were summarised as HTM MDM2 Amplified (Amp), whereas F HTM 22, F HTM 3 were combined as HTM MDM2 wildtype (WT). HTM AB were not generated and are therefore not included in the HTM MDM2 WT group.

As a prerequisite for successful humanization, the $CD45^+$ cells in the spleen of all HTM were quantified by flow cytometry. All HTM that harbored Luminal B tumors were humanized as shown as % $CD45^+$ cells in the spleen (average: 64 %; range: 18 - 88 % $CD45^+$ cells) (Figure 27 A). The animals that suffered from graft versus host disease (GvHD) were excluded from the analysis, based on the fact that the $CD45^+$ cells in the bone marrow consisted mostly of T-cells, in addition to a bad general condition of the HTM like anemia or extensive skin itchiness. The TIL analysis revealed a lower infiltration rate of $CD45^+$ cells in HTM MDM2 Amp tumors compared with HTM MDM2 WT tumors (Student's t-test, $p = 0.0259$) (Figure 27 B). In general, all Luminal B PDX HTM tumors exhibited a low infiltration and could, therefore, be considered as non-immunogenic. HTM with a CD45 number of < 0.1 % TIL were excluded from the CD3

and CD8 analysis because the number of total cells is not representative. Interestingly, the infiltration of T-cells was also significantly lower in HTM MDM2 Amp tumors (students t-test, p = 0.0454) (Figure 27 C). In addition, the HTM MDM2 Amp tumors tended to be infiltrated by a lower number of cytotoxic T-cells, however, this was not statistically significant (Student's t-test, p = 0.057) (Figure 27 D). About 70 % of the T-cells ($CD4^+$ and $CD8^+$ cells) were shown to express PD-1 on their surface and it was neither influenced by a MDM2 amplification nor dependent on a certain T-cells type (cytotoxic or T-helper cells) (data not shown). In addition, the naïve, effector, effector memory, or TEMRA state of $PD\text{-}1^+$ cells was rather variable (data not shown).

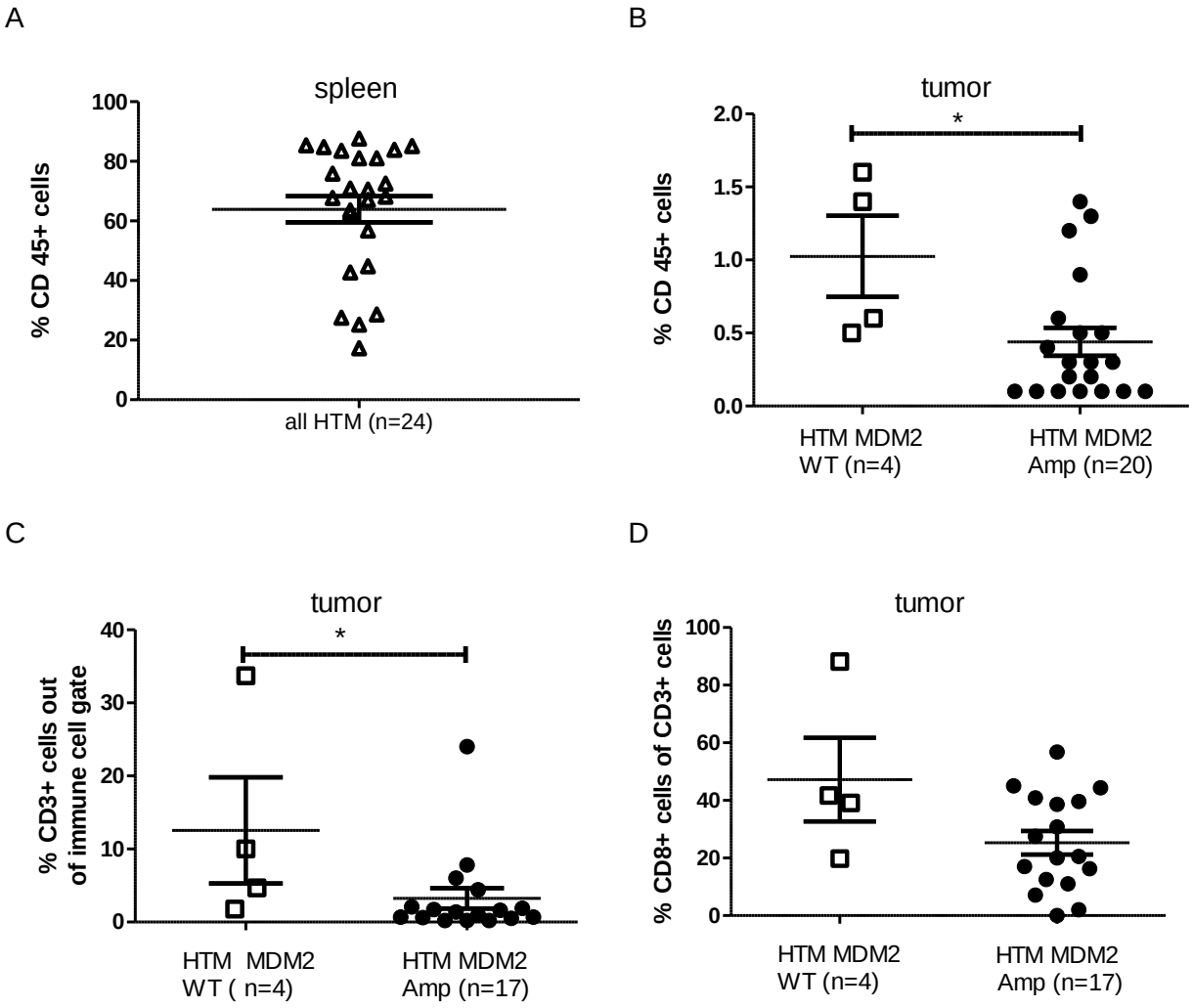

Figure 27: Occurrence of immune cells in the spleen and the tumor of HTM
A) The spleen of the HTM displays the humanization of all HTM. **B)** The data show $CD45^+$ immune cell infiltration in the tumor comparing HTM MDM2 WT with HTM MDM2 Amp tumors. **C)** The figure represents the occurrence of $CD3^+$ cells within the immune cell gate of HTM MDM2 WT tumors and HTM MDM2 Amp tumors. **D)** The % of cytotoxic T-cells are shown in HTM MDM2 WT tumors and HTM MDM2 Amp tumors. All data are represented as mean ± SEM. Each dot shows an individual animal. Significances were analyzed using Student's t-test (* $p < 0.05$).

4.4.8 Effect of MDM2 amplification in Luminal B humanized PDX mice

The data revealed a statistically significant increased tumor weight of HTM MDM2 Amp tumors compared with HTM MDM2 WT tumors (Student's t-test, $p < 0.0119$) (Figure 28 A). The tumor volume over time tended to be increased in HTM MDM2 Amp tumors compared to TM MDM2 WT tumors (Two-way ANOVA with Bonferroni post hoc correction, $p > 0.05$) (Figure 28 B). The DFS as wells as the OS did not differ between HTM MDM2 Amp animals and HTM MDM2 WT animals (Log-rank (Mantel-Cox) test, $p > 0.05$) (Figure 28 C and D). Interestingly, the influence of the human immune system becomes visible, when comparing HTM MDM2 Amp tumors with TM MDM2 Amp tumors that revealed an increased DFS (Log-rank (Mantel-Cox) test, $p = 0.0012$) (Figure 28 E). Nevertheless, comparing the OS of HTM MDM2 Amp with TM MDM2 Amp the OS did not differ (data not shown).

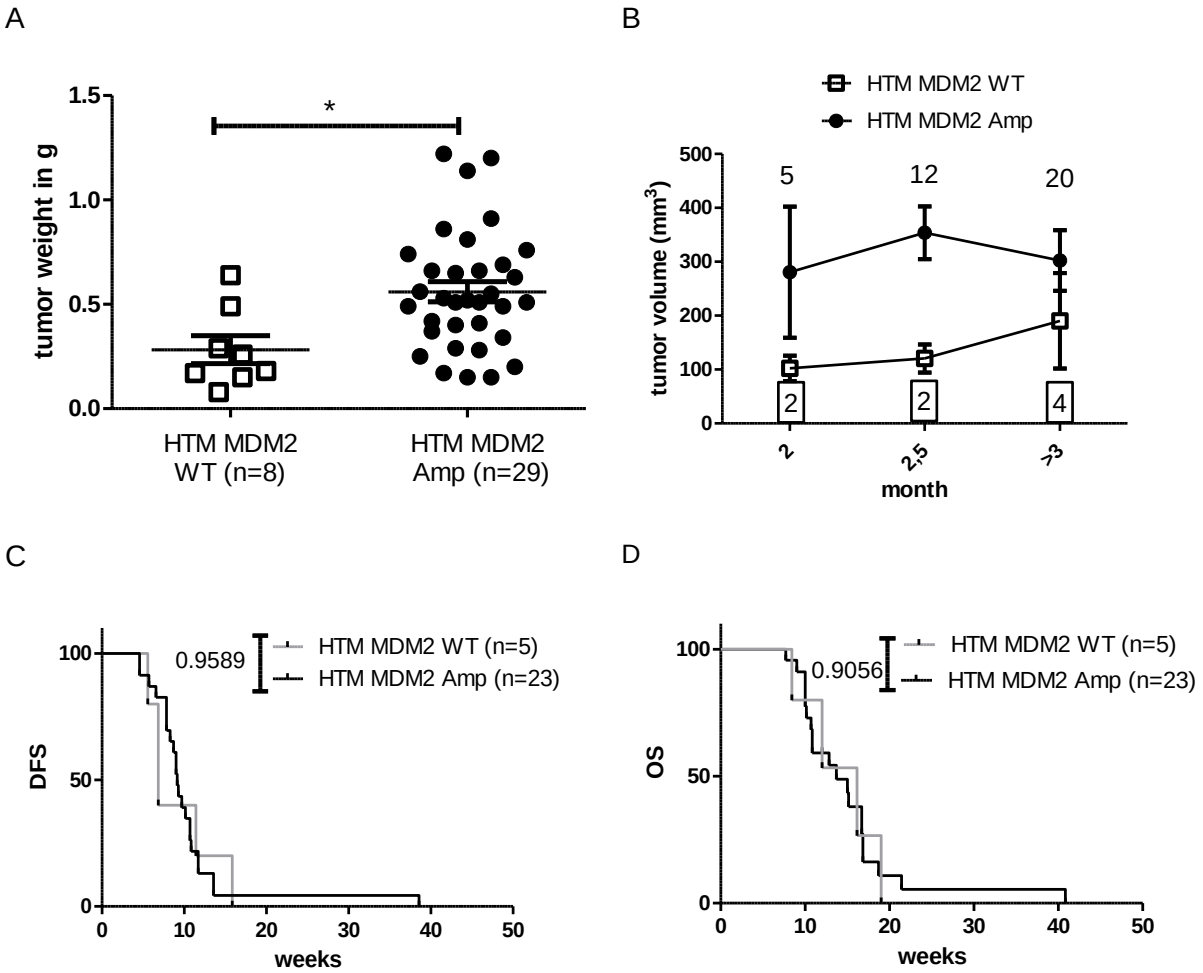

E

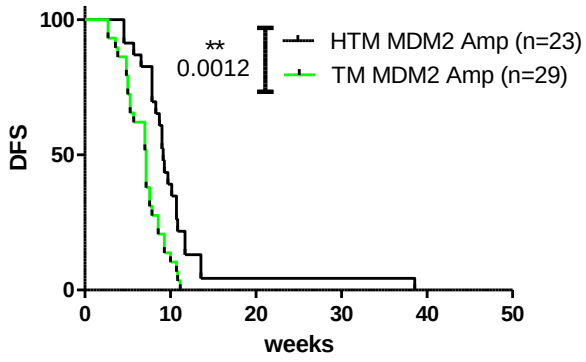

Figure 28: Effect of an MDM2 amplification in HTM A) The *in vivo* data represent the tumor weight of HTM MDM2 WT tumors compared with HTM MDM2 Amp tumors. The data are shown as mean ± SEM. Each dot signs a single tumor. **B)** The tumor volume over time is shown in MDM2 WT tumors compared with HTM MDM2 Amp tumors. **C)** The DFS, and **D)** the OS are represented in HTM MDM2 Amp and HTM MDM2 WT animals. The data are shown as mean ± SEM in **A)** and **B)**. **E)** The data show a comparison of HTM MDM2 WT animals compared with HTM MDM2 Amp animals regarding DFS. The number of animals is indicated in parentheses. Significances were analyzed using Two-way ANOVA with Bonferroni post hoc correction, Student's t-test, or Log-rank (Mantel-Cox) test (* $p < 0.05$, ** $p < 0.01$)

4.4.9 HTM MDM2 amplified tumors promote lung metastases that differ phenotypically from the corresponding tumor

. Similar to the findings obtained in TM, IHC CK18 staining in the lung occurred in a significant higher frequency in HTM MDM2 amp versus HTM MDM2 WT (Two-sided Fisher's exact test, $p = 0.0114$). However, the cotransplantation of a human immune system did not altered the appearance of $EpCAM^+$ tumor cells in the lung (TM MDM2 Amp versus HTM MDM2 Amp Student's t-test, $p = 0.9549$) (Figure 29 B). Hence, the immune system does neither promote nor inhibit the metastatic spread to the lung. Again, as shown for TM MDM2 Amp lung metastases, HTM MDM2 Amp lung metastases revealed an increased level of $cMET^+$ and $CD44^+$ cells, compared to the corresponding tumor (Two- Way ANOVA with Bonferroni post hoc correction, $p < 0.001$) (data not shown). Moreover, lung metastases differed in increased MIC expression pattern from the corresponding primary tumor in the HTM MDM2 Amp animals (Student's t-test, $p = 0.0252$) (Figure 29 C).

A

	HTM MDM2 WT	HTM MDM2 Amp	P value (HTM MDM2 WT versus HTM MDM2 Amp)
Lung metastases	0/4	11/14	**0.0114**

B

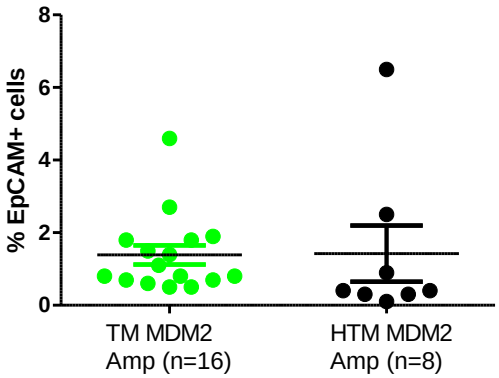

C

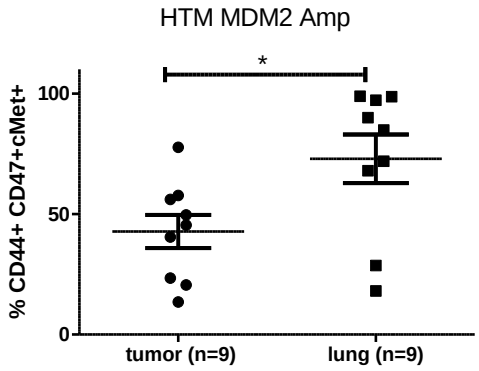

Figure 29: Lung metastases occurrence and MIC population in HTM MDM2 Amp and HTM MDM2 Amp animals and the influence of the human immune system on lung metastases in TM MDM2 Amp versus HTM MDM2 Amp animals

A) The incidence for lung metastases was calculated using the two-sided Fisher's exact test and the p-value is listed in the table. The number of animals with detectable CK18 metastasis of the total number of animals (n/n) is indicated. **B)** The influence of the immune system was assessed by EpCAM staining with flow cytometric analysis in TM MDM2 Amp and HTM MDM2 Amp lungs. **C)** The data show the MIC population in HTM MDM2 Amp animals comparing the tumor with the lung metastases. The data are represented as mean ± SEM and the number of animals is indicated in parentheses. Each dot represents a single animal. Significances were analyzed using two-sided Fisher's exact test or Student's t-test (* $p < 0.05$, ** $p < 0.01$).

4.4.10 MDM2 amplification does not favor colonization of DTCs in the BM

In this context, it was interesting to determine the dissemination of tumor cells to the BM regarding the impact of the human immune system and the influence of an MDM2 amplification of the tumor. The DTCs were verified by a PAN CK staining (CK8, CK18, CK 19) of the BM. It was possible to detect single DTCs as well as DTC clusters in the BM (Figure 30 A). Nevertheless, the DTC existence was neither connected to an MDM2 amplification of the Luminal B tumor in TM or HTM (Fishers' exact test, (TM MDM2 Amp vs TM MDM2 WT: $p = 0.4223$; HTM MDM2 Amp vs HTM MDM2 WT: $p = 0.2929$) (Figure 30 B) nor linked to an influence of the human immune system comparing HTM with TM (Fishers' exact test, (TM MDM2 Amp vs HTM MDM2 Amp: $p = 1.000$; TM MDM2 WT vs HTM MDM2 WT: $p = 1.000$)) (data not shown).

A

B

	TM MDM2 WT	TM MDM2 Amp	P value (TM MDM2 Amp versus TM MDM2 WT)
BM DTC	4/9	13/20	0.4223

	HTM MDM2 WT	HTM MDM2 Amp	P value (HTM MDM2 WT versus HTM MDM2 Amp)
BM DTC	2/5	6/8	0.2929

Figure 30: DTCs in the bone marrow Luminal B breast cancer PDX models
A) The figure shows a representative image of the purple single cells and a DTC cluster in the BM of a TM. **B)** The Fishers' exact test analyzed the occurrence of DTCs and is shown comparing TM MDM2 WT with TM MDM2 Amp and HTM MDM2 WT with HTM MDM2 Amp (not significant). The number of animals with detectable DTCs of the total number of animals (n/n) is indicated.

4.4.11 Copy number variation low pass-sequencing of the Luminal B HTM P and TM P PDX model

In this part, we focused on the analysis of single cells to detect any copy number variations between the primary tumor and the DTCs. The isolated single cell DTCs and the corresponding single-cell tumor cells of the TM P and HTM P PDX model were analyzed by copy number variation low pass- sequencing at the ITEM Regensburg. This study focused only on the TM P and HTM P Luminal B model as the dissemination of tumor cells was confirmed in all animals and the number of animals (TM and HTM) transplanted was the highest including various passages. The Figure 31 shows a representative example comparing the profile of a normal healthy immune cell (isolated from the BM of an HTM), a BM DTC (DCC), and a cell of the corresponding primary tumor cell. The healthy cell represented clearly the normal chromosomal copy number of two genes throughout the genome without any gains or losses. In contrast, the BM DTC showed losses on chromosome 5 whereas the matching primary tumor cell revealed a gain. This demonstrated that the DTC and the matching primary tumor could differ genomically. However, there are still regions like on chromosome 8 were the DTC exhibited the same gain as the primary tumor revealing that some gains (or losses) are stable throughout dissemination.

The whole analysis of all TM P and HTM P DTCs and the corresponding single tumor cells of different passages is displayed as a cluster (Figure 31 B). Here, the copy number gain is shown in yellow and a copy number loss is depicted in blue. With this analysis, the copy number gain or a copy number loss could not be traced back to a certain gene but to a certain area on the chromosome. The human origin of each cell was always confirmed by endpoint PCR. Only cells that were exclusively positive in the human PCR but not in the mouse PCR were included in the sequencing (data not shown). By means of the clustering, the cells could be separated into three groups due to the mapping of the genetic origin of the cell and their genetic similarity (red and blue line). It could be confirmed that the DTCs (in the graph denoted as DCCs) cluster mostly in the upper part (separated through a red line), whereas the tumor cell and just a few DTC could be found in the middle. In the lower part DTCs cluster as a small group that derive mainly from HTM (marked in green boxes) and DTC population is separated through a blue line from the tumor cell population (Figure 31 B). Comparing population 1 (mainly DTCs) with population 2 (mainly tumor cells) the copy numbers vary on chromosome 4 (loss in population 2), chromosome 5 (gain in population 1) and chromosome 6 (gain in population 1). Comparing population 3 (DTCs) with population 2 (mainly tumor cells) the copy number alters on chromosome 4 (loss in population 2), chromosome 6 (gain in the population 2 and loss in population 3) and chromosome 5 (gain in population 2 and loss in population 3). However, several alterations can be detected between DTCs and tumor cells that are not identical. It was also observed that the cell population could harbor converse copy number variations. Noteworthy, a gain on chromosome 17 on the q-arm is present in population 1 and population 2, whereas it is missing in the population 3 were most of the cells derived from HTM. This shows that even the DTC profiles are not genomically congruent with other DTC profiles. In contrast to the HTM DTCs that mainly cluster in the lower part (population 3) DTCs of the TM are located at the upper part (Figure 31 B, population 1).

A

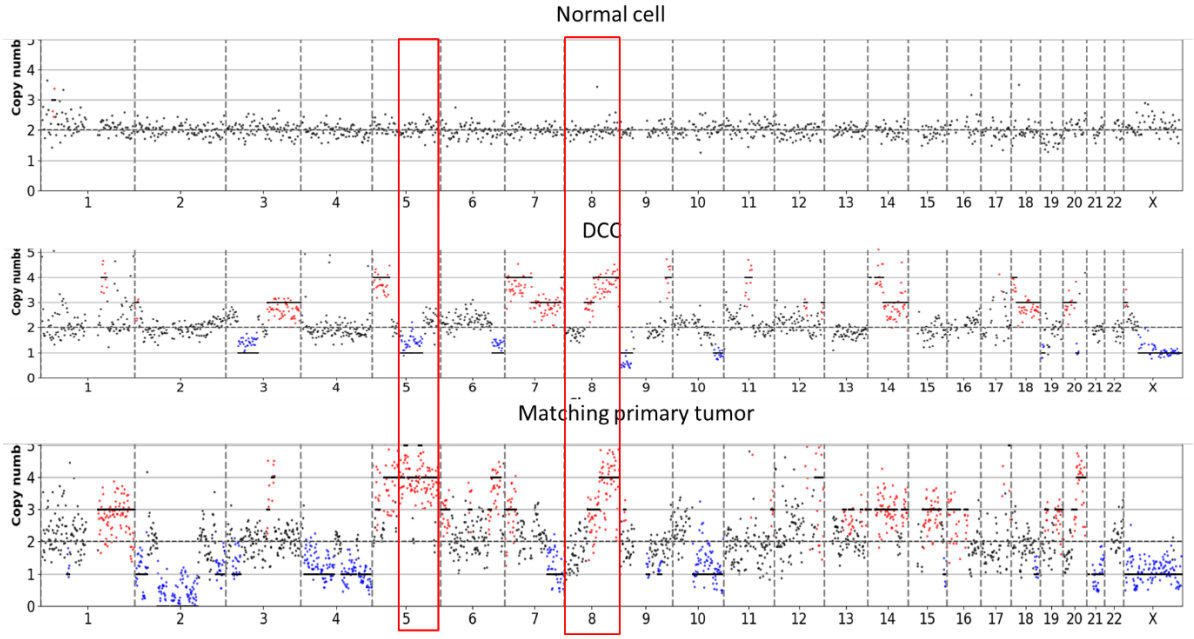

B

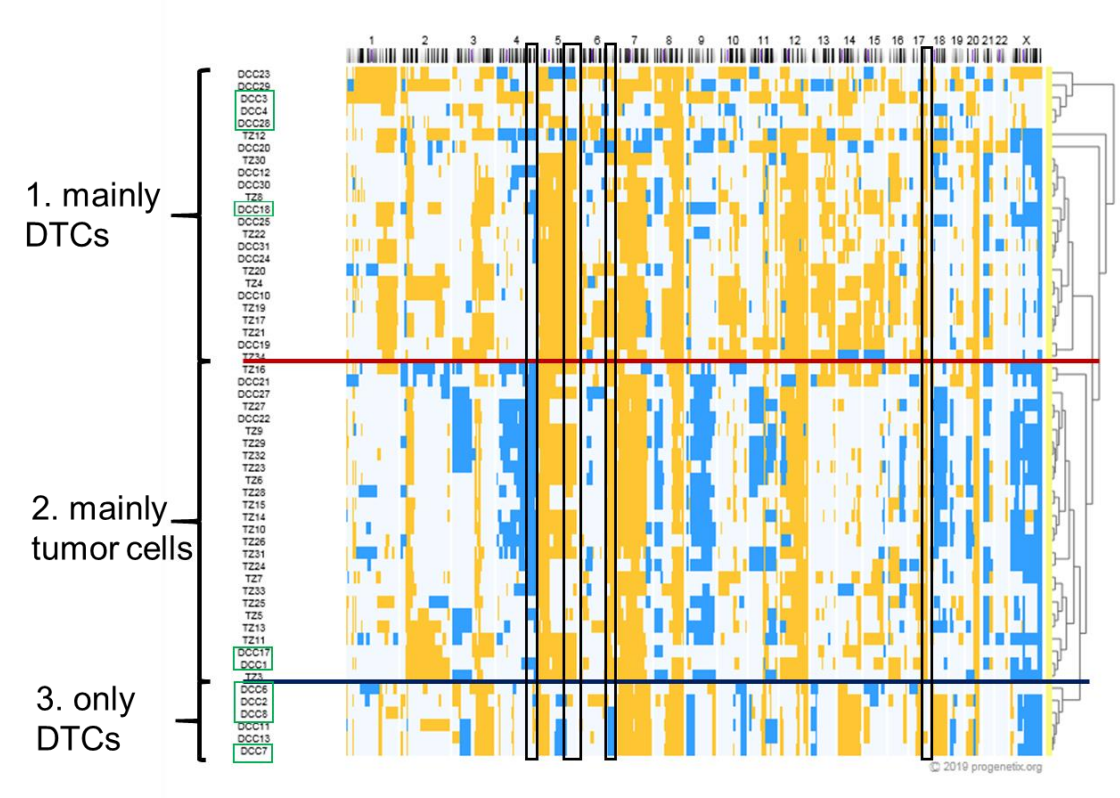

Figure 31: Clustering of DTCs and tumors cells isolated from HTM P and TM P

A) The figure shows exemplarily CNV profiles of a normal cell, a DTC and the corresponding primary tumor. The chromosomes are given at the x-axis and the copy number is depicted on the y-axis. The red boxes mark representative alterations for explanation issues. Genomic gains are depicted in red and genomic losses are shown in blue. **B)** The Affymetrix data of the cell profiles were analyzed on progenetix database. The chromosomes are listed at the x-axis and the different cells (DTCs or tumor cells) are given at the y-axis. The DTCs from HTM are marked with green boxes.DTCs on the y-axis are denoted as DCCs and tumor cells as TZ. The DTCs and some tumor cells that cluster in the upper part are denoted as population 1, followed by the tumor cell population (2.) and in the lower part the DTC population 3. The populations are separated by red and blue

lines. A loss of genomic material is indicated in blue and a gain of genomic material is marked in yellow color. The black boxes mark the regions discussed in the text.

4.4.12 Metastatic potential of generated PDX and the genetic aberrations of HTM and TM tumors

The following table summarizes the findings of the Luminal B breast cancer PDX models in the TM and HTM settings (Table 27). It shows the continuous dissemination of all PDX models to the bone marrow, independent of the human immune system. Due to the fact of continuous dissemination into the BM all of the generated Luminal B PDX models represent a high-risk Luminal B group. Moreover, both, TM and HTM models with an MDM2 amplification, generated lung metastases. In contrast, the TM and HTM tumors with a TP53 mutation did not cause lung metastases. Even though the TM P and HTM P models are MDM2 amplified, the panel sequencing uncovered a deletion in the TP53 gene. The TM AB model is outstanding with the amplification of MDM4 and in these mice, tumor cells were detected in multiple organs such as the bone marrow, lung, liver, and the brain. All other PDX models with either MDM2 amplification or TP53 mutation did not metastasize to the liver or the brain.

Table 27: Summary of the metastatic potential of TM and HTM Luminal B breast cancer PDX models

	BM DTCs	Lung	Liver	Brain	TP53 mut	MDM2 Amp	MDM4 Amp
TM P	✓	✓	-	-	(-)	✓	-
HTM P	✓	✓	-	-	(-)	✓	-
TM CTC	✓	✓	-	-	-	✓	-
HTM CTC	✓	✓	-	-	-	✓	-
TM Bpe	✓	✓	-	-	-	✓	-
HTM Bpe	✓	✓	-	-	-	✓	-
F TM 34	✓	✓	-	-	-	✓	-
F HTM 34	✓	✓	-	-	-	✓	-
F TM 22	✓	-	-	-	✓	-	-
F HTM 22	✓	-	-	-	✓	-	-
F TM 3	✓	-	-	-	✓	-	-
F HTM 3	✓	-	-	-	✓	-	-
TM AB	✓	✓	✓	✓	-	-	✓

The models (TM/ HTM) are indicated at the left and the organs are listed above. ✓ = metastases or genetic alteration is present, - = no metastases or no alterations exists, (-) = deletion, *Amp* =amplification, *mut* =mutation

4.5 The relevance of immune checkpoints (PD-L1) in Luminal breast cancer

As immune checkpoint modulations get more and more attention for therapeutic intervention, it was one aim of this thesis to evaluate the PD-L1 expression in the HTM PDX models, independent of an MDM2 amplification. Overall, the Luminal B HTM

tumors were rather non-immunogenic with just a minor TIL number (Figure 27). In accordance, the PD-L1 expression, as a common defense mechanism of the tumor against TILs, was very low in general. No differences in PD-L1 expression were determined in the context of an MDM2 amplification (Student's t-test, p = 0.3510) (Figure 32 A). Moreover, the data revealed no significant correlation between the PD-1 $CD8^+$ T-cells with the PD-L1 expression on tumor cells (Spearman's rank correlation coefficient r = 0.1943) (Figure 32 B). In addition, a correlation between PD-1 $CD4^+$ T-cells and the PD-L1 expression was also not detected (Spearman's rank correlation coefficient: r = 0,09573) (data not shown). The number of total TILs ($CD45^+$ cells) did also not correlate with the PD-L1 expression on tumor cells (Figure 32 C). Hence, without immune-activating treatments, immune checkpoints play a rather subordinate role in the HTM model of Luminal B breast cancer.

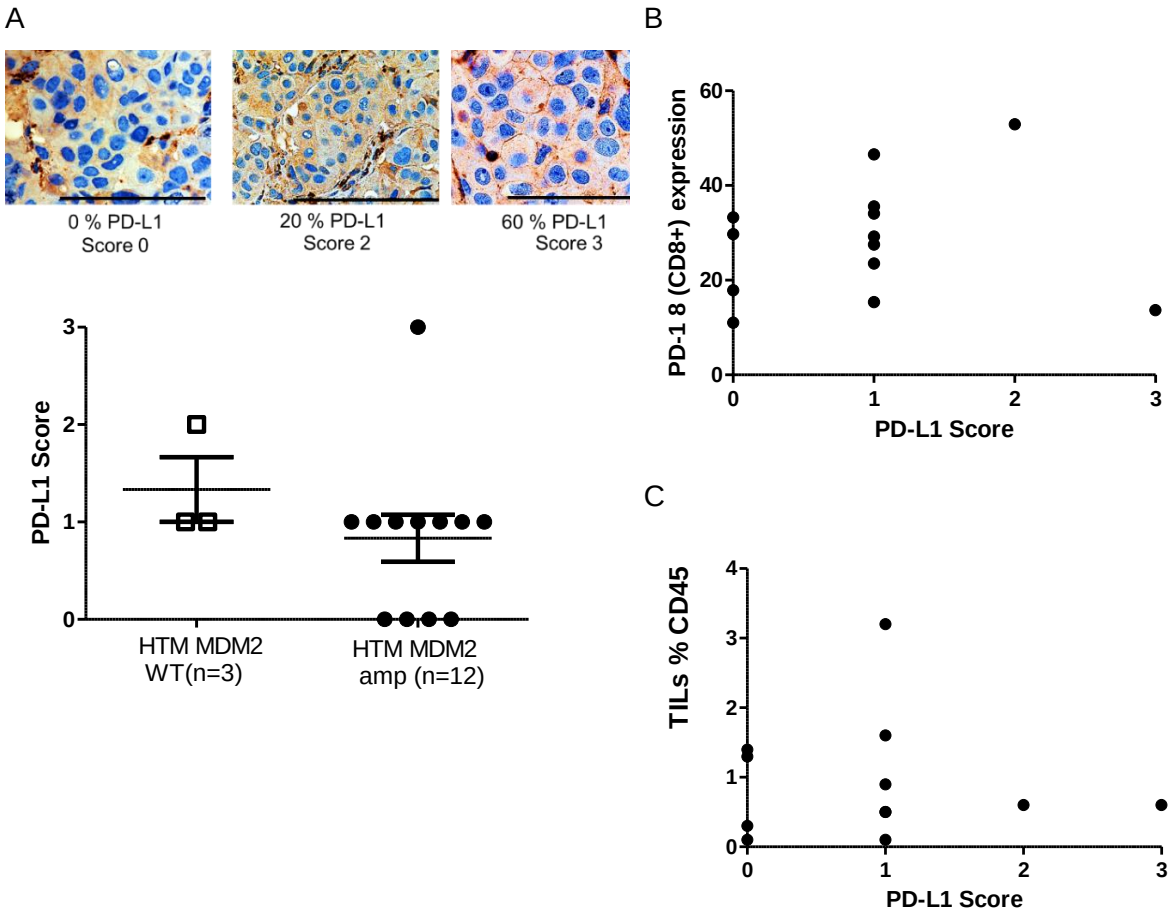

Figure 32: *In vivo* PD-L1 expression in tumors of Luminal B HTM
A) The upper part shows representative images of membrane-bound PD-L1 expression in HTM with 0%, 20 %, and 60 % PD-L1 staining and the corresponding score. The images were taken in 100-fold magnification and the bars represent 100 µm. The Scores 0-3 of HTM MDM2 WT were compared with HTM MDM2 Amp in the figure below. The data are depicted as mean ± SEM and each dot represents an individual animal. **B)** The PD-L1 $CD8^+$ cells determined by flow cytometry were correlated with the IHC PD-L1 Score of all animals. **C**) The number of total TILs in % ($CD45^+$ cells) was correlated with the IHC PD-L1 Score.

In this context, it was necessary to determine the PD-L1 status not only in vivo but also in vitro. Therefore, the constitutive PD-L1 expression of different breast cancer cell lines, cultured under standardized conditions, was analyzed by IHC (Figure 33 A). Immunohistochemical staining verified the highest PD-L1 expression on JIMT-1 ($Her2^+$ breast cancer) breast cancer cells, with 100 % of the cells being $PD\text{-}L1^+$. In contrast, MDA-MB-231 (TNBC breast cancer) and SK-BR-3 ($Her2^+$ breast cancer) breast cancer cell lines showed heterogeneous PD-L1 expression with $PD\text{-}L1^+$ and partially PD-L1- cells. BT-474 (Luminal / $Her2^+$ breast cancer) cells appear as PD-L1- (adapted and modified from (Rom-Jurek et al., 2018)). The FISH data revealed no significant increase of PD-L1 gene copy numbers or alterations of the PD-L1 /centromeric ratio in any of the tested cell lines (Figure 33 B). Additionally, PD-L1 expression was analyzed in an in vivo model based on NSG mice that were transplanted with human breast cancer cell lines (MDA-MB-231, BT-474, SK-BR-3, and JIMT-1) with or without simultaneous intrahepatic transplantation of $CD34^+$ hematopoietic stem cells. The transplanted mice developed either solid tumors subcutaneously (MDA-MB-231, JIMT-1), liver-associated tumors (BT-474), or tumor effusions in the peritoneal cavity (SK-BR-3) and are cell-line derived xenograft models. Moreover, mice transplanted with $CD34^+$ cells developed a functional human immune system up to 12 weeks post-transplant. In line with the in vitro data, the highest PD-L1 expression was found in MDA-MB-231 and JIMT-1 breast cancer cell line transplanted animals, both, in the presence or absence of a human immune system (Figure 33 C). Interestingly, no $PD\text{-}L1^+$ tumor cells isolated from the peritoneal effusion of SK-BR-3 transplanted mice were detectable in vivo in tumor mice (TM) or humanized tumor mice (HTM). However, BT-474, MDA-MB-231, SK-BR-3, and JIMT-1 breast cancer cell line tumors apparently showed diminished PD-L1 expression in vivo compared to in vitro cultured cells. In addition, the expression pattern of PD-L1 in MDA-MB-231 and JIMT-1 TM and HTM tumor tissues was very heterogeneous and not expressed ubiquitously. Apparently, the co-transplantation of a human immune system in HTMs did not affect the PD-L1 expression of the tumor cells in vivo.

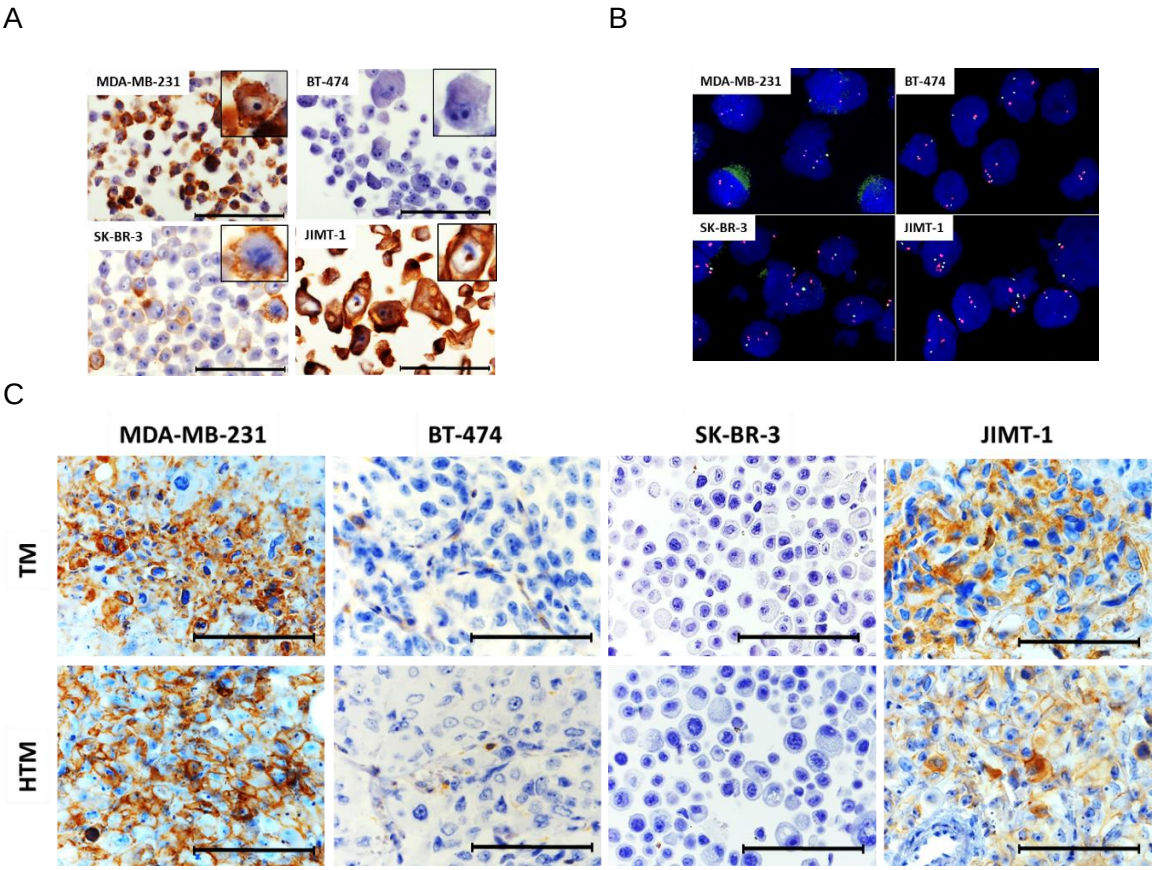

Figure 33: Programmed death ligand 1 (PD-L1) expression on different breast cancer cell lines
A) Immunochemical staining of PD-L1 was performed on FFPE embedded breast cancer cell lines. The bars represent 100 µm. **B)** The data show representative images of FISH analysis in different breast cancer cell lines. MDA-MB-231, BT-474, SK-BR-3, and JIMT-1 cell lines were analyzed for PD-L1 (green) and Cen9 (red) gene copy numbers. **C)** The figure shows *in vivo* PD-L1 expression in tumors of tumor mice (TM) and humanized tumor mice (HTM), transplanted with different breast cancer cell lines. Immunohistochemical staining of PD-L1 is depicted in tumor samples of TM or HTM transplanted with MDA-MB-231, BT-474, SK-BR-3 or JIMT-1 breast cancer cell lines cotransplanted with or without human hematopoietic stem cells (HSC). The bars represent 100 µm.

4.6 Targeting MDM2 in ZR-75-1 breast cancer cell line *in vitro*

4.6.1 Effect of MDM2 knockdown on apoptosis, S-phase fraction, and cell number

Based on the results of MDM2 amplification in TM Luminal B PDX models, the effect of an MDM2 knockdown was analyzed *in vitro*. The experiments were conducted using the Luminal breast cancer cell line ZR-75-1. ZR-75-1 features an increased MDM2 gene dose and belongs to a TP53 wildtype cell line (data not shown). As a prerequisite for all MDM2 knockdown effects, MDM2 knockdown significantly reduced the protein expression of MDM2 compared to ctrl and to NT ctrl in all experiments (One-Way ANOVA with Tukey's multiple comparisons test, $p < 0.05$ (MDM2 KD vs. NT ctrl), $p < 0.01$ (MDM2 KD vs. ctrl)) (Figure 36 A). It was demonstrated that an MDM2 knockdown

reduced the vital cells and lead to increased early apoptosis when compared with the non-target control (Two- way ANOVA with Bonferroni post hoc correction, $p < 0.01$ vital cells and $p < 0.05$ early apoptosis) (Figure 34 A). There was also a significant reduction of vital cells, increased early apoptosis, and increased late apoptosis between the control and MDM2 knockdown cells. For reasons of clarity, the significances are not indicated in the figure. In accordance with this data, the proliferation, which is determined by a high S-phase and low Gap (G1/G2) phase, was decreased by an MDM2 knockdown. Reduced MDM2 levels led to a decreased amount of cells in the S-phase and an accompanying shift towards the G2-phase when compared with the non-target control (Two-way ANOVA with Bonferroni post hoc correction, $p < 0.05$; both, S-phase and G2-phase; Figure 34 B). In addition, the cell number tended to decrease after an MDM2 knockdown without reaching statistical significance even though the reduced confluence is visible under the light microscope (One-Way ANOVA with Bonferroni post hoc correction, $p = 0.2227$) (Figure 34 D). In order to analyze the migratory and proliferative effects of an MDM2 knockdown, a wound-healing assay was performed. The assay revealed that MDM2 knockdown does not alter the migratory properties *in vitro* (Figure 34 C) - a migratory effect would have occurred within the first 12-24 h after chamber removal. Hence, the data of reduced proliferation in the wound healing assay after an MDM2 knockdown 48h after chamber removal, support the results of decreased proliferation determined by S-phase fraction analysis. The proliferation of MDM2 knockdown cells was significantly reduced 48h after chamber removal and lasted until 144h a time point when non-treated control cells and non-target control cells had already closed the wound.

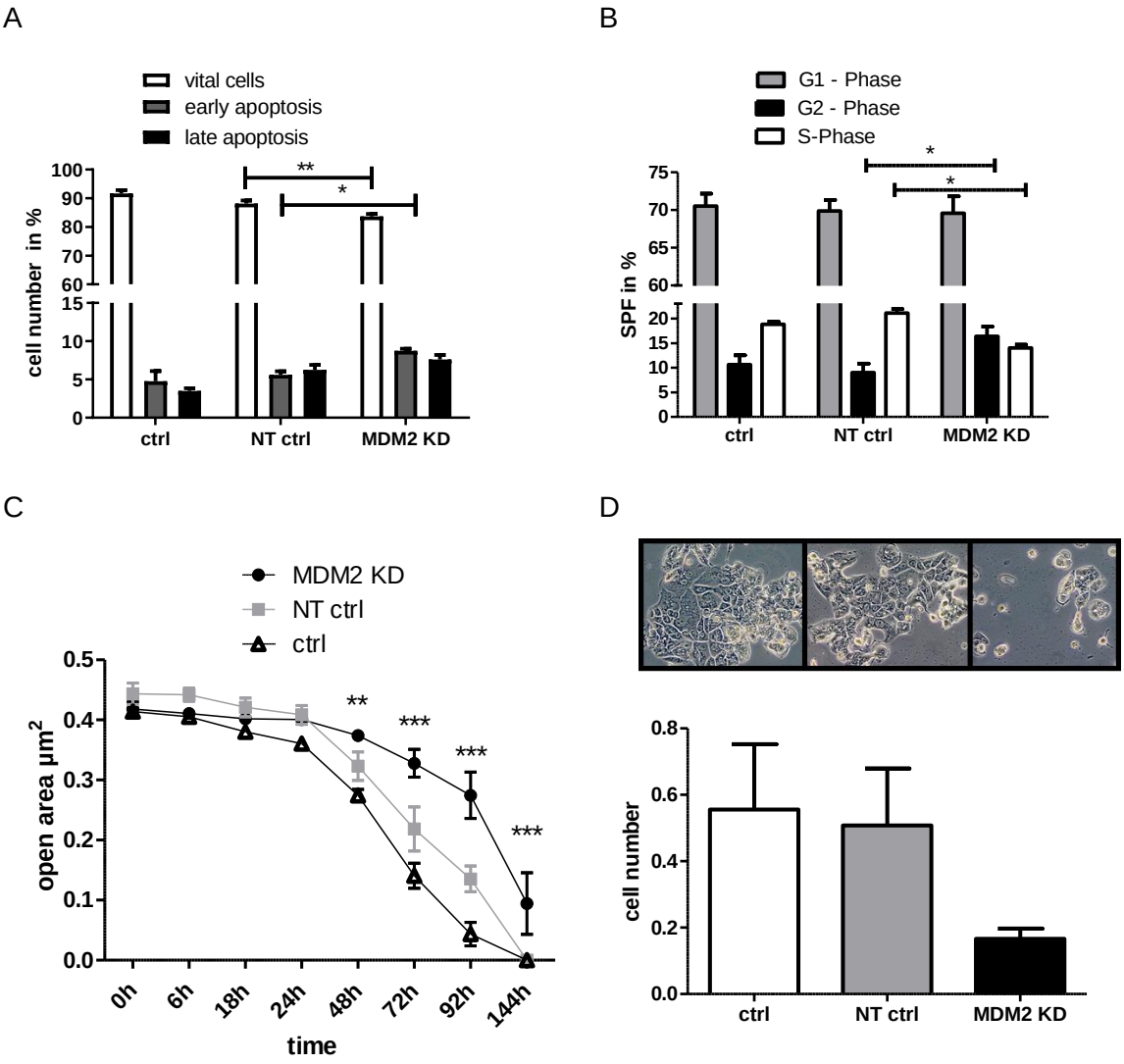

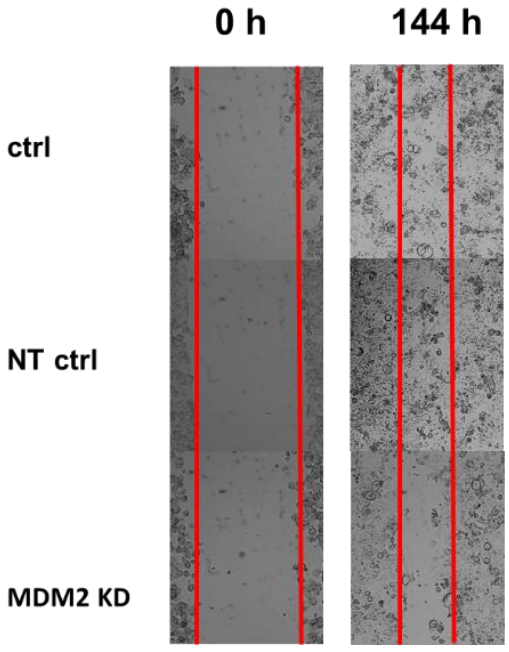

Figure 34: Effects of MDM2 knockdown in ZR-75-1 cells on apoptosis, S-phase fraction, wound healing and cell number

A) The figure displays the effect of MDM2 knockdown on vital cells, early apoptosis, and late apoptosis. **B)** Represents the shifts of S-phase, G1- and G2-phase after an MDM2 knockdown. The data are shown as mean + SEM and the experiments were replicated three times. **C)** The upper panel shows the effect of an MDM2 knockdown on wound healing. The data are presented as mean ± SEM. The image shows the proliferation after 144 h and the red bars mark the gap after chamber removal at point 0h and the gap of MDM2 knockdown cells after 144 h. **D)** The upper panel represents an image of the decreased confluence after an MDM2 knockdown. The lower panel shows the cell number after an MDM2 knockdown, compared with non-treated controls, and non-target siRNA treated controls. The data are shown as mean + SEM and the experiments were replicated three times. Two-way ANOVA with Bonferroni post hoc

correction or One-way ANOVA with Tukey's multiple comparisons test (* $p < 0.05$, ** $p < 0.01$, ***$p < 0.001$).

4.6.2 Effect of AMG232 inhibition on apoptosis, S-phase fraction, and cell number

In order to elucidate the therapeutic aspect of MDM2 inhibition, ZR-75-1 breast cancer cell line was treated with AMG232 *in vitro*. The cells were treated with 0.1 µM AMG232 for 48h or 72h. The optimal concentration of AMG232 was determined in a separate experiment based on the publication of (Werner *et al.*, 2015) (data not shown). The results of an MDM2 inhibition with AMG232 were identical to those of the MDM2 knockdown in ZR-75-1 breast cancer cell line showing a S-phase reduction and a shift towards the G2 phase as well as the prohibited wound closure after AMG232 treatment. In detail, it was demonstrated that an AMG232 inhibition reduced the vital cells 48 h after treatment when compared with the DMSO control (Two- way ANOVA with Bonferroni post hoc correction, $p < 0.05$ vital cells) (Figure 35 A). In contrast, the treatment of AMG232 did not alter the apoptosis 72 h after treatment (Two- way ANOVA with Bonferroni post hoc correction, $p > 0.05$). In accordance with these data, the proliferation, which is determined by a high S-phase and low Gap (G1/G2) phase, was decreased 48 h and 72 h after an AMG232 treatment (Two- way ANOVA with Bonferroni post hoc correction, S-phase 48 h, and 72 h: $p < 0.01$) (Figure 35 B). The AMG232 inhibition led to a decreased number of cells in the S-phase and an accompanied shift towards the G2-phase compared with the DMSO control 72 h after treatment (Two-way ANOVA with Bonferroni post hoc correction, $p < 0.05$; G2-phase). In order to analyze the migratory and proliferative effects of an AMG232 treatment, a wound-healing assay was performed. The assay revealed that AMG232 inhibition did not alter the migratory properties *in vitro* because this would have occurred within the first 12-24h after chamber removal (Figure 35 C). However, the data showed a reduced proliferation 144 h after chamber removal in the wound healing assay after AMG232 treatment. This supports the results of decreased proliferation determined by S-phase fraction analysis. The proliferation of AMG232 treated cells was still reduced 216 h after chamber removal when non-treated control cells and DMSO treated cells had already closed the wound (Two-way ANOVA with Bonferroni post hoc correction, $p < 0.001$) (Figure 35 C). In addition, the cell number was significantly decreased 48 h and 72 h after AMG232 treatment. (Two-way ANOVA with Bonferroni post hoc correction, $p < 0.001$) (Figure 34 D).

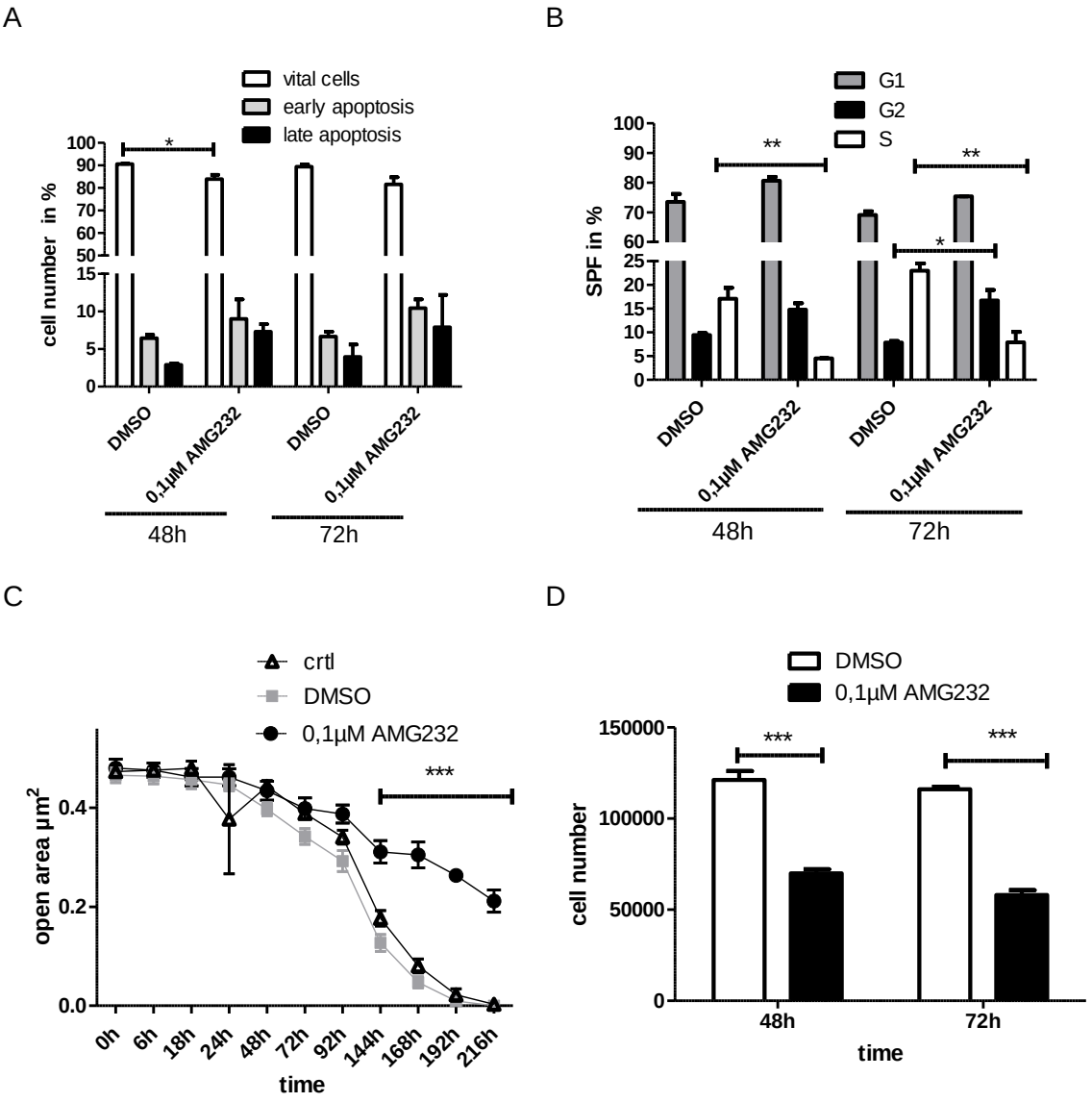

Figure 35 AMG232 treatment effects of ZR-75-1 on apoptosis, SPF, wound healing and cell number
A) Displays the effect of AMG232 treatment on vital cells, early apoptosis, and late apoptosis. **B)** Represents the shifts of S-phase, G1- and G2-phase after an AMG232 treatment. The data are shown as mean + SEM and the experiments were replicated three times. **C)** The upper panel shows the effect of an AMG232 treatment on wound healing. The data are presented as mean ± SEM. The image shows the proliferation after 144h and the red bars mark the gap after chamber removal at point 0h and the gap of AMG232 treated cells after 144h. **D)** It depicts the cell number after an AMG232 treatment, compared with the DMSO treated control. The data are shown as mean + SEM and the experiments were replicated three times. * $p < 0.05$, ** $p < 0.01$, ***$p < 0.001$

.

4.6.3 MDM2 knockdown increases apoptosis *via* the p53 pathway

As demonstrated above, MDM2 knockdown increased apoptosis and reduced proliferation of ZR-75-1 breast cancer cells. These findings were further elucidated by assessing the molecular mechanism that is implicated in MDM2 regulation. For densitometric analysis of the MDM2 Western Blot, only the bands with the protein size of 90 kDa, 76 kDa, and 57 kDa were examined as the 74 kDa band is not affected by an MDM2 knockdown (Figure 36 A). Therefore, it can be concluded that the effect of MDM2 knockdown on apoptosis, SPF, and wound-healing was due to the isoforms 90 kDa, 76 kDa, and 57 kDa of MDM2 protein. In contrast, p53 protein which is normally tagged by MDM2 for protein degradation increased significantly in MDM2 knockdown cells (One -Way ANOVA with Tukey's multiple comparisons test, $p < 0.05$ (MDM2 KD vs. NT ctrl), $p < 0.05$ (MDM2 KD vs. ctrl)) (Figure 36 B). MDM2 knockdown resulted in a decrease of phosphorylated focal adhesion kinase (pFAK) without reaching statistical significance (Figure 36 C and D). The total FAK protein level remained stable (Figure 36 D).

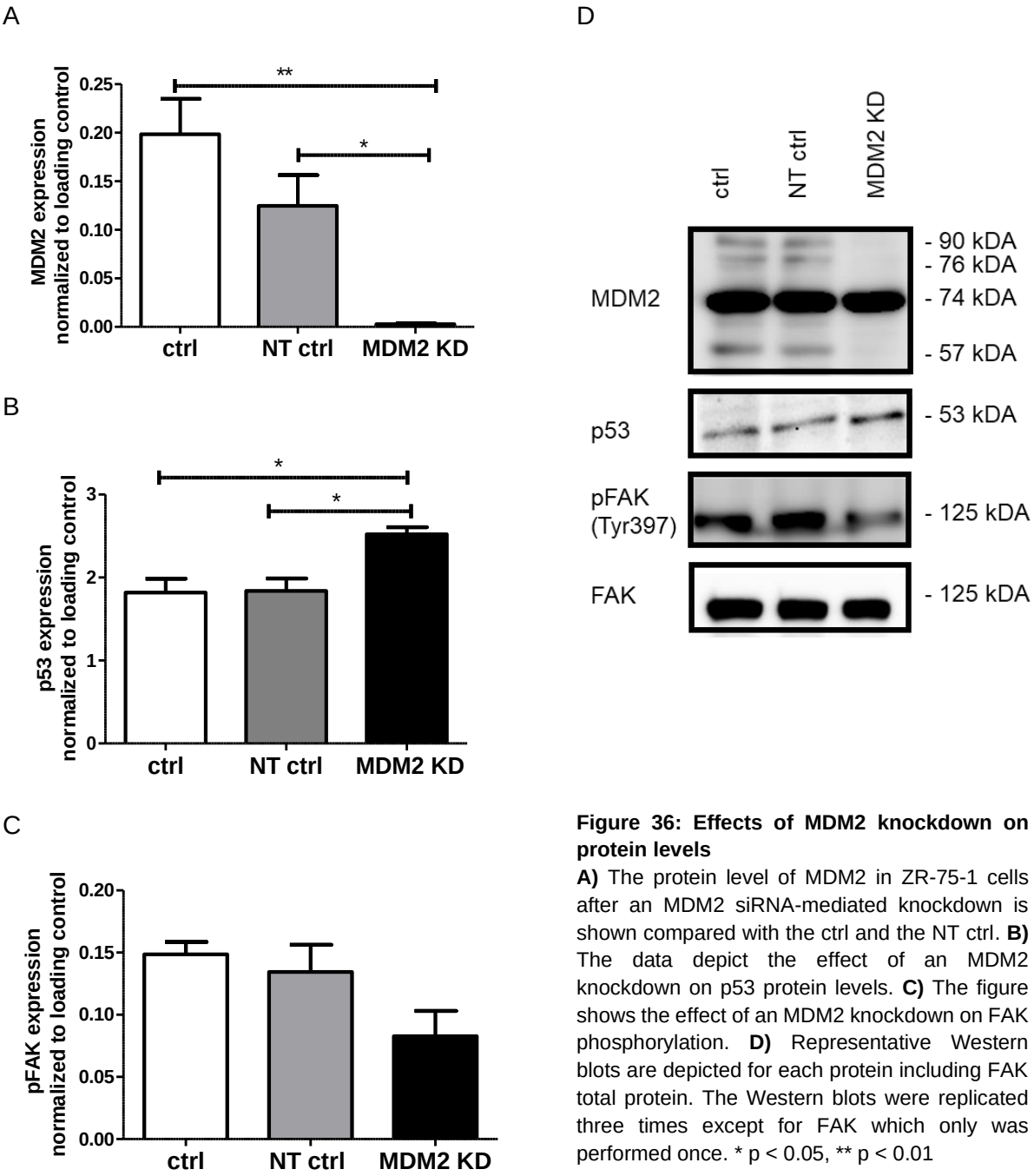

Figure 36: Effects of MDM2 knockdown on protein levels

A) The protein level of MDM2 in ZR-75-1 cells after an MDM2 siRNA-mediated knockdown is shown compared with the ctrl and the NT ctrl. **B)** The data depict the effect of an MDM2 knockdown on p53 protein levels. **C)** The figure shows the effect of an MDM2 knockdown on FAK phosphorylation. **D)** Representative Western blots are depicted for each protein including FAK total protein. The Western blots were replicated three times except for FAK which only was performed once. * $p < 0.05$, ** $p < 0.01$

5. Discussion

The current differentiation between high and low-risk Luminal tumors using the proliferation marker Ki67, the grading, and molecular assays for risk assessment (Goldhirsch *et al.*, 2011; Cheang *et al.*, 2009; Narain and Adcock, 2017) remains unsatisfying. Still, there is a lack of appropriate markers that clearly distinguish between high and low-risk Luminal B tumors. As high-risk Luminal B patients do not necessarily respond to endocrinological therapy compared to low-risk Luminal A patients, the chemotherapy is administered if patients suffer from a Luminal B tumor (Rouzier *et al.*, 2005; Hayes *et al.*, 2007; Goldhirsch *et al.*, 2011). However, it is still disputed if all Luminal B patients profit from chemotherapeutic intervention. Another problem in Luminal B breast cancer is represented by the occurrence of distant metastases. Those metastases do not necessarily coincide with the pheno- or genotype of the primary tumor (Al-Hajj *et al.*, 2003; Baccelli *et al.*, 2013; Schmidt-Kittler *et al.*, 2003). Hence, it is important to elucidate the pheno- and genotype of the corresponding metastases in order to determine potential therapeutic targets for the treatment of metastasized Luminal B breast cancer patients. Therefore, this study focused on the detection of new Luminal B high-risk pheno- and genotypic markers in Luminal B tumors and metastases using the TM and HTM model. With these markers it should be possible to identify the patients that have a high susceptibility to metastasize. In the following chapters the determined geno- and phenotypic markers, as well as the influence of human immune cells in Luminal B breast cancer, will be discussed in detail.

5.1. Luminal B breast cancer PDX models and Luminal B primary tumor cell culturing

Patient-derived xenograft (PDX) models are immunodeficient mice transplanted with malignant tissue or single cells from a patient's primary or metastatic tumor. These PDX mice enable the opportunity to study human cancer biology in a model system which has turned out to be a reliable tool for cancer research. Previously it was demonstrated that those PDX models could predict treatment responses like the PARP inhibitors and mTOR inhibitors that reveled a benefit for TNBC patients (Kawaguchi *et al.*, 2017). Moreover, the PDX models enabled the detection of new targets to fight breast cancer such as the $CD44^+$ tumor cells that are able to initiate tumor growth and the coexpression of $CD44^+$, $cMET^+$, and $CD47^+$ that promote metastases in breast cancer (Al-Hajj *et al.*, 2003; Baccelli *et al.*, 2013). Even if 70% of the breast cancer

tumors belong to the Luminal subentity, the tissue availability for research is limited due to the fact that recent techniques are able to detect breast cancer in a very early stage and low tumor size. Hence, the tissue is only used for diagnostic properties. Moreover, the phenomenon of poor engraftment of Luminal breast cancer tumors in mice has been reported previously (DeRose *et al.*, 2011; Fleming *et al.*, 2010; Vaillant *et al.*, 2013; Oakes *et al.*, 2012; Kabos *et al.*, 2012; Zhang *et al.*, 2013). Vaillant demonstrated 12 % Luminal breast cancer engraftment rate (Vaillant *et al.*, 2013; Oakes *et al.*, 2012), Marangoni: 4 % (Marangoni *et al.*, 2007), Cottu: 2.5 % (Cottu *et al.*, 2012; Marangoni *et al.*, 2007), Zhang: 2 % (Zhang *et al.*, 2013), and 0 % was evaluated by Petrillo (Petrillo *et al.*, 2012). In contrast, other subentities like the highly aggressive TNBC (60.7%: (Vaillant *et al.*, 2013), 100 %: (Petrillo *et al.*, 2012)) and $Her2^+$ breast cancer (35.7 %: (Vaillant *et al.*, 2013)) showed an enhanced take rate in mice. 25 % take rate was reported additionally by Cottu et al. for all non-luminal PDX models (TNBC and $Her2^+$ breast cancer) (Cottu *et al.*, 2012).

In this work, we provided evidence that the molecular intrinsic Luminal subtype of the primary tumor (ER, PR, Her2, Ki67) was maintained in each Luminal PDX model. This is a clear advantage of the PDX models as those were shown previously to recapitulate the individual tumor morphology, gene expression, and drug susceptibility of each patient (Kawaguchi *et al.*, 2017; Marangoni *et al.*, 2007; Zhang *et al.*, 2013). Hence, the models reflect the human situation better than cell line-derived xenograft models making the PDX a powerful tool for translational relevant breast cancer research. In contrast to the PDX models the cell-line derived xenografts are more standardizable due to the unlimited availability to cell line material that can be transplanted simultaneously under equal conditions in several animals (Wege, 2018). With the limited access to primary material and the varying cell number in tumor fragments the PDX model generation remains still challenging.

In this thesis, we were able to successfully establish five PDX models with different breast cancer entities. As published before, in our laboratory settings the aggressive breast cancer tumors, like TNBC (50 %), Luminal B $Her2^+$ (50 %), and hormone receptor-negative $Her2^+$ tumors (50 %) engrafted better in NSG mice compared to Luminal A (0 %) and Luminal B $Her2^-$ tumors (0 %). The low engraftment seems to be dependent on the ER positivity of the tumors, which might be due to the characteristics of the Luminal A and Luminal B $Her2^-$ subentities. A direct mechanism of ER to limit

the engraftment is unknown. It is more likely that the reduced take rate (especially of the low proliferating Luminal A tumors) is evoked by the secondary characteristics of ER^+ tumors. First, ER^+ breast cancer tumors (especially Luminal A tumors) are slowly proliferating and characterized by low grading (Goldhirsch *et al.*, 2011), which could limit the engraftment in NSG mice. Second, Her2 was shown previously to enhance the engraftment in mice as cell survival pathways such as the PI3K/AKT signaling and RAS/ERK pathways were more activated (Kanaya *et al.*, 2017). Moreover, Her2 might serve as a driver for growth due to the constitutive kinase activity that promotes the high proliferative capacity of Her2 amplified tumors (Olayioye, 2001). Hence, the intake rate of Luminal B tumors without Her2 amplification is decreased.

Another reason for the low take rate of ER^+ tumors could be the differences between the hormonal status between mice and women. Although supplementation of estrogen was provided by estrogen pellet transplantation, the supply could be insufficient to mimic the situation in women.

All of the generated PDX models in this study were shown to be either PR negative or expressed PR only to a minor extent. Hence, PR negativity seems to be an additional factor for engraftment success. This could be explained by the regulation of PR that hinders upon high PR expression, the growth-promoting functions of ER and therefore decreases the tumor aggressiveness (Finlay-Schultz *et al.*, 2017). Additionally, PR negativity was shown to be associated with a worse prognosis for the patient (Onitilo *et al.*, 2009; Dunnwald *et al.*, 2007) and the lack of PR expression led to a more aggressive phenotype of the tumor in the PDX model (Bergamaschi *et al.*, 2009). In addition, high PR expression was linked previously to a less aggressive breast cancer entity, namely the Luminal A breast cancer (Lim *et al.*, 2016)

In this study, the transplantation of single cells derived from a solid tumor that was dissociated enzymatically or mechanically was not successful in general. Only single cells that originally derived from circulating tumor cells (TM CTC) or effusions (TM Bpe, and PT AB) were able to successfully engraft. Solid primary tumor samples (PT P, PT X, F TM 3, F TM 22, F TM 34) needed to be transplanted as small tissue fragments. This divergence between the single-cell or tissue fragment transplantation methods might originate from accelerated anoikis during the dissociation process that is employed to create single-cell suspensions. Anoikis, as anchorage-dependent apoptosis prevents the cells from reattaching to other matrices after dissociation from

the extracellular matrix (Frisch and Ruoslahti, 1997). Hence, anoikis hinders the engraftment of tumor cells in the mouse mammary fat pad. The intact extracellular matrix, where the primary tumor cells are embedded in, therefore supports the engraftment success (DeRose *et al.*, 2013; DeRose *et al.*, 2011). Another reason is displayed by the fact that the metastases from pleural effusions or ascites already exist as single cells and do not have to be treated harmful by enzymatical or mechanical dissociation. Another possible scenario is that metastases undergo anoikis resistance if they settle from the primary tumor site into the periphery (Simpson *et al.*, 2008), and therefore feature the ability to reattach to other matrices. Our study revealed that breast cancer metastases, such as pleural effusions or ascites derived tumor cells (PT AB and PT U), or primary solid tumors in an advanced state (as a secondary tumor or relapse) (PT P or PT X), showed an engraftment advantage over untreated primary solid tumors. Moreover, higher engraftment rates of metastases, compared to solid tumors, have also been previously reported by Marangoni and colleagues (Marangoni *et al.*, 2007).

Noteworthy, four out of five patients, where the PDX generation was successful, died within two years after tissue, pleural effusion or ascites removal. This correlation of successful engraftment and patient survival has also been reported previously to be an independent prognostic factor for disease outcome (DeRose *et al.*, 2011; Whittle *et al.*, 2015).

Another aim of the thesis was the culturing of primary breast cancer tumor cells, which resulted in one propagatable cell culture derived from a pleural effusion (PT AB) and a short-term culturing of the TM CTC tumor. All other primary breast cancer tumor cells failed in culturing. A reason for the limited culture success of primary tissue fragments could be the dissociation-induced production of self-inhibiting or suicidal signals of the tumor cells (Simpson *et al.*, 2008; Frisch and Ruoslahti, 1997). This goes along with our observation of limited tumor engraftment in mice after transplantation of dissociated single cells. Another explanation for the failure in primary tumor culturing is that one or more of the key growth factors are missing in cell culture. It was previously shown that mimicking the right physiological conditions (e.g. growth factors or cytokines) of the tumor microenvironment is challenging (Ethier *et al.*, 1993). Moreover, a low tumor cell density and fast proliferating fibroblasts that overgrow the tumor cells could have contributed to the culturing failure (Ip and Asch, 2000). A possible scenario

why PT AB cells were successful in culturing might be that the metastatic cells already existed as single cells. Those single cells did not require enzymatical dissociation or mechanical shearing, which granted a more successful propagation. Moreover, the high number of tumor cells seeded, and the putative low amount of mesothelial cells (in PT AB effusion) that could overgrow the tumor cells (Ip and Asch, 2000) contributed to the successful growth. However, TM CTC, as a tissue fragment, was indeed a special case. The TM CTC tumor was mechanically dissociated and a short-term culturing in a special medium, which contained 30 supplements (dissertation Massimo Saini, 2017), was possible. This medium was kindly provided by our colleges from Heidelberg (HiSTEM, Heidelberg, Germany). The high content of different nutrients and growth factors could have contributed to the culturing success (dissertation Massimo Saini, 2017). Moreover, the TM CTC cells that were cultured and retransplanted several times are used to the medium and might, therefore, be more resistant towards mechanical dissociation as primary tumor cells that are dissociated out of an intact microenvironment for the first time.

Nevertheless, there are several possibilities to improve the primary breast cancer cell culturing. 2D conditions, where the cell surface is coated with collagen I or Geltrex, might be an option, as published previously (Janik *et al.*, 2016). Moreover, feeder cells or conditioned media have already been used to establish primary breast cancer cell cultures (Wang *et al.*, 2001). In addition, different medium supplements like cholera toxin and ethanolamine have been previously shown to contribute to successful culturing (Ethier *et al.*, 1993). Another possibility is to sort the tumor cells for stem cell markers, like $CD44^{high}/CD24^{low}$, as those cells were shown to harbor the capacity for tumor-initiation and self-renewal (Sheridan *et al.*, 2006). Three-dimensional bioprinting would also be an option, because it mimics the perfect microenvironment by incorporating multiple cell types into scaffold-free tumor tissues with defined architecture (Langer *et al.*, 2019). The development of the so-called mini-breast in adherent or non-adherent floating gels could contribute to establish breast cancer cultures. The mini breast is generated from reduction mammoplasty and exhibits the regenerative potential of terminal ductal lobular units (Linnemann *et al.*, 2015). Therefore, the mini-breast could serve as a kind of carrier architecture for culturing breast cancer cells.

5.2. Genomic and phenotypic markers that could identify a high-risk Luminal B tumor

In the clinical practice, Luminal tumors are differentiated according to their molecular intrinsic markers like hormone receptor positivity and Her2 status, and, by means of proliferation and grading, differentiated into Luminal A and B. Further stratification through gene expression profiler assays, such as PAM 50, is time-consuming, cost-intensive. Most importantly, this assay only provides a likelihood for relapse or metastatic spread, which is used as a basis for the decision of chemotherapeutic intervention. Hence, further markers are needed to classify the high-risk luminal tumors. In this study, all the patients that suffered from Luminal B tumors and died, or had a relapse were retrospectively assigned to high-risk Luminal B tumors. Additionally, the primary luminal B tumors that resulted in successful PDX engraftment, which is a separate prognosticator of poor outcome, were dedicated to the high-risk group. The low-risk Luminal B group comprises all other Luminal B patients that are still alive without distant metastases or a relapse. A summary is listed in the table below.

High risk	Low risk
dead	alive
relapse	recurrence-free
tumor engrafted in the mouse	tumor did not engraft in the mouse

5.2.1 Genomic markers

A central finding of the panel sequencing of the primary patient tumors and the TM tumors that engrafted was the significant overlap between the successful engraftment and genomic **MDM2** amplification. This amplification leads to increased MDM2 protein expression in the TM, as confirmed by IHC. According to the MDM2 amplification of the tumor, the TM CTC, TM Bpe, TM P, F TM 34 were assigned to the TM MDM2 amplified group. F TM 22, F TM 3, and TM AB were dedicated to the TM MDM2 WT group, as those tumors exhibited no MDM2 amplification. The following results discussed are based on this subdivision.

In healthy cells, the E3 ligase MDM2 is responsible for the degradation of p53 at the proteasome, which inhibits repair mechanisms after cell damage, or p53 mediated cell death. The overexpression of MDM2 protein, caused by an MDM2 gene amplification, consequently decreases p53, prohibits apoptosis or cell repair, and could cause

uncontrolled cell proliferation (Danovi *et al.*, 2004). Those processes would thereby enhance the engraftment in mice. Moreover, MDM2 amplification has been associated with ER^+ breast cancer and was reported to appear in a varying range of 1.7 % - 32 % in Luminal B breast cancer patients (Network, 2012; Yu *et al.*, 2014; Haupt *et al.*, 2017; Choschzick *et al.*, 2010). MDM2 is able to stimulate the transcription of the ERα gene, which leads to increased levels of ERα, in a p53-independent manner (Kim *et al.*, 2011; Brekman *et al.*, 2011; Swetzig *et al.*, 2016).

Moreover, our data revealed that MDM2 amplification positively correlates with tumor size and tumor volume over time in TM and HTM. As the *in vitro* results in this study demonstrated decreased proliferation, increased apoptosis, and decreased wound healing in a p53 dependent manner after an MDM2 knockdown, the increased tumor size in MDM2 amplified tumors could be explained by uncontrolled proliferation. In support of our *in vivo* findings, another study reported that a decreased tumor size was caused by an MDM2 knockdown in HR-positive breast cancer cell line xenografts (Gao *et al.*, 2019).

The detected upregulation of p53 protein expression after an MDM2 knockdown could act *via* two pathways. The first possibility is the p53-mediated activation of BAX or PUMA, which causes apoptosis. The second possible pathway could be the p53-mediated activation of p21, where the cells will undergo cell cycle arrest (Ozaki and Nakagawara, 2011). P21 activation by the overabundant p53, in turn, inhibits CDK1/ Cyclin B complex formation, leading to a stagnation of the cells in the G2 phase, and consequently, the cells could not enter mitosis and stop proliferation (Khan *et al.*, 2016; Lu *et al.*, 2016). This G2 shift was also determined in this study after an MDM2 knockdown in ZR-75-1 breast cancer cell line.

Noteworthy, the western blot results of ZR-75-1 MDM2 knockdown cells demonstrated an MDM2 isoform-dependent regulation of p53. The knockdown only targeted the MDM2 90 kDa, 76 kDa, and 57kDa, but not the 74 kDa isoform. Hence, all effects of an MDM2 knockdown are attributed to the 90 kDa, 76 kDa or 57kDa isoforms. In line with those data, Alkhalaf 2005 described the MDM2 90kDa isoform to be responsible for the regulation of the p53 protein stability (Alkhalaf *et al.*, 2005).

In order to reverse translate this knowledge of MDM2 downregulation into a clinical therapeutic relevance, a pharmacological MDM2 inhibitor experiment with AMG232 was performed in the ZR-75-1 breast cancer cell line. The inhibitor caused apoptosis,

decreased proliferation, and a shift towards the G2 phase, similar to the MDM2 knockdown. Consequently, the Luminal B breast cancer patients with amplified MDM2 status might benefit from a p53-MDM2 inhibitor treatment, which would reduce tumor cell proliferation. Therefore, the AMG232 treatment could be useful in the future to treat MDM2 amplified tumors and serve optional as an alternative in case of endocrine resistance or additively to chemotherapeutic interventions.

Besides an increased tumor weight and volume, MDM2 amplified PDX showed a decreased DFS in TM MDM2 amplified (Amp) mice compared with TM MDM2 wild type (WT) mice. This might be attributed to the increased proliferative capacity of TM MDM2 amplified tumors. Interestingly, the OS of TM MDM2 Amp animals did not differ from TM MDM2 WT mice. In line with those data is the significant positive correlation between MDM2 amplification and reduced DFS that has been reported previously for breast cancer patients. (Cuny *et al.*, 2000).

Taken together, all the *in vitro* and *in vivo* results demonstrated that an MDM2 amplification in Luminal B tumors is associated with enhanced engraftment in PDX, and therefore with aggressivity of the patients' tumor. Of note, the PAM 50 assay for Luminal risk stratification includes MDM2 gene assessment, however, the information might get lost since multiple genes are included in the risk calculation (Alvarado *et al.*, 2015).

Despite the discussed MDM2 amplification that accounts for high-risk Luminal B tumors, the **TP53 mutation** (FTM 22 and F TM 3 model) and an **MDM4 amplification** (TM AB PDX) were also determined in the panel sequencing in the generated PDX models. Interestingly, MDM2, p53, and MDM4 belong to the same pathway and can regulate each other. TP53 mutation, as a tumor suppressor gene, leads to a loss of function in the p53 protein and therefore hinders apoptosis and promotes uncontrolled proliferation (Lacroix *et al.*, 2006). Hence, similar to how MDM2 hinders the p53 function, the TP53 mutation also leads to a loss of function in the p53 protein and therefore prevents apoptosis of the tumor cells. In turn, this could enhance the engraftment success in mice. TP53 mutations in Luminal B breast cancer were found in 32 % of the patients, but the incidence in non-luminal breast cancer is much higher (TNBC: 84%; $Her2^{+}$ breast cancer: 75% (Network, 2012). TP53 mutations were shown to predict a poor progression-free survival after systemic treatment and additionally, the response to antihormonal therapy was decreased in Luminal breast cancer patients

(Berns *et al.*, 2000; Langerød *et al.*, 2007). The MDM4 protein is structurally homologous to MDM2, but acts differently than MDM2. MDM4 can stabilize p53 and MDM2 protein levels, leading to nuclear accumulation of the p53-MDM2 complex, thereby disabling the p53 function (Stad *et al.*, 2001). In the MDM4 amplified tumor (TM AB) MDM4 stabilizes MDM2, as the IHC of TM AB tumor in this study revealed a high expression of MDM2. However, the MDM2 protein overexpression in MDM4 amplified tumors could block p53 mediated cell death and therefore, result in better engraftment.

Noteworthy, the results of the panel sequencing might give a hint that MDM2 and TP53 seems to be mutually exclusive, even if the number of the analyzed PDX tumors is very low (four MDM2 amplified and two TP53 mutated). However, a TP53 deletion was detected in the TM P PDX model simultaneously with an MDM2 amplification. The phenomenon of the unlikely occasion of simultaneous alteration in TP53 and MDM2 has been published decades ago in osteosarcoma (Lonardo *et al.*, 1997) but was also published recently in breast cancer (Haupt *et al.*, 2017).

5.2.2 Phenotypic markers

In this study, the phenotypic markers EpCAM, CD44, CD47, Her2, cMET, and CD24 were evaluated as they are associated with certain functionalities like stemness, EMT or immune escape. The data of the SCF phenotyping revealed a high expression of **CD24** in Luminal B patient tumors, compared with Luminal A patient tumors. Additionally, all of the engrafted Luminal B PDX models (TM and HTM), which belong to the high-risk Luminal B tumors, exhibited a high CD24 expression. High CD24 expression in Luminal breast cancer and TNBC was previously shown to be associated with a poor prognosis (Kwon *et al.*, 2015). In addition, it was reported previously that high CD24 expression was detected in highly aggressive breast cancer cell lines from the basal subtype (Chekhun *et al.*, 2013). Recently, CD24 expression in breast cancer tumor cells was shown to serve as a potential immune checkpoint through its interaction with the inhibitory receptor sialic-acid-binding Ig-like lectin 10 (Siglec-10) that is expressed by M2-like tumor-associated macrophages (Barkal *et al.*, 2019). Hence, a high CD24 expression forces Siglec-10 binding, thereby inhibiting phagocytosis of the tumor cells by macrophages. Prospectively, CD24-Siglec-10 binding could be another target for an immune modulatory therapy.

In addition, our investigations showed an increased expression of **cMET** in the metastatic effusions of the Luminal B patient samples compared with Luminal B primary tumors. This phenomenon of increased cMET expression was also displayed in the TM MDM2 Amp lung metastases, compared with the corresponding primary tumor. Additionally, the TM MDM2 Amp lung metastases exhibited and increased **CD44** expression, compared with TM MDM2 solid tumors. A possible scenario is that only a few cells of the primary tumor cells express cMET and CD44 and those cells exclusively are able to migrate to other organs and to initiate metastases (Baccelli *et al.*, 2014; Baccelli *et al.*, 2013). Previous studies demonstrated a link between cMET expression in the primary tumor with poor survival, the occurrence of distant metastases, and breast cancer progression (Baccelli *et al.*, 2014; Baccelli *et al.*, 2013; Jia *et al.*, 2018). In detail, cMET serves as an inducer of EMT where the cancer cell reversibly acquires an invasive and motile phenotype (Wallwiener *et al.*, 2013; Polyak and Weinberg, 2009). cMET and CD44, as tumor metastases proteins, were shown to interact by a complex formation of cMET, the CD44v6 isoform, and HGF and as a result enhanced cMET signaling (Orian-Rousseau, 2010; Orian-Rousseau *et al.*, 2002). Hence, in the future other therapeutic targets like cMET inhibitors could be taken into account to treat metastatic breast cancer. There are clinical studies ongoing that evaluate cMET inhibitors and monoclonal antibodies directed against cMET in TNBC patients (Ho-Yen *et al.*, 2015). Additionally, the co-expression of $cMET^+$ and $CD47^+$ CTCs promoted the outgrowth of bone marrow metastases, served as an independent prognostic marker for poor overall survival, and was strongly associated with lymph node metastases in Luminal breast cancer patients (Baccelli *et al.*, 2014). This further emphasizes a responsibility of $cMET^+$/ $CD47^+$ co-expression that enables the tumor cells to colonize other organs.

Additionally, high co-expression of **CD44/cMET/CD47** was determined phenotypically by SCF in high-risk Luminal B primary tumors. Despite the high co-expression of CD44/cMET/CD47 in primary Luminal B patient samples, the TP53 mutated and MDM4 amplified tumors (summarized as TM MDM2 WT in the results part) also exhibited high levels of CD44/cMET/CD47. This triple-positive population has been described as the population that induces metastases in breast cancer so-called MICs (Baccelli *et al.*, 2013). CD47 as “don’t eat me signal” prevents phagocytosis of the tumor cells and thereby evades immune cell recognition (Baccelli et al., 2014). cMET is known to induce EMT and CD44 expression on tumor cells, prevents apoptosis, and

induces angiogenesis and invasion in breast cancer (Orian-Rousseau, 2010). When all those functions merge, the tumor cell is protected against multiple eradication attempts and the tumor cell is empowered to survive even in the periphery and could generate metastases. Hence, the co-expression of CD44/cMET/CD47 serves as a high-risk marker for Luminal B breast cancer. In this context, it is important to note that one patient of the low-risk Luminal B patient samples exhibited a high $CD44^+$, $CD47^+$, and $cMET^+$ expression, potentially predicting relapse or the occurrence of distant metastases in the follow-up care. In support of this data, TM and HTM MDM2 Amp lung metastases exhibited an increased expression level of the triple-positive MICs (CD44/cMET/CD47) compared with the corresponding primary tumor that is also indicative for a high-risk Luminal B tumor.

5.3 Immune cell interactions and immune cell checkpoint relevance in Luminal B breast cancer

In breast cancer research the immunological influence gets more and more in the focus, intending to determine predictive and prognostic factors that account for tumor progression and survival, as well as to target them with therapeutic interventions. Despite the retrospective clinical assessments of patient samples to study the influence of the human immune system, there is a lack of adequate models. To overcome this problem, the humanized PDX turned out to be a good solution to remodel human immune cell and tumor cell interactions.

Supporting the data about **low TILs** in Luminal B breast cancer determined in patient samples (Pruneri *et al.*, 2017), this study revealed a low infiltration of immune cells in the Luminal B breast cancer patients as well as in the humanized PDX models. Hence the humanized PDX model matches with the observation in Luminal B breast cancer patients and again demonstrate the non-immunogenicity of Luminal B tumors. Even if the tumors are infiltrated to a low amount it was demonstrated previously that high TILs in Luminal/$Her2^-$ breast cancer are an adverse prognostic indicator for survival (Denkert *et al.*, 2018). This was explained by the differential immune cell composition in luminal $Her2^-$ breast cancer compared with TNBC and $Her2^+$ breast cancer. The determined T-cells in TNBC were shown to correlate with increased overall survival whereas this was not the case for Luminal breast cancer (Denkert *et al.*, 2018). In contrast, high TILs in TNBC or $HER2^+$ breast cancer rather predicted a survival benefit. Hence, the TIL composition might play a pivotal role. As described in the literature, cytotoxic T-cells, natural killer cells, M1 macrophages, and Th 1- helper cells are

implicated in tumor suppression, whereas Tregs, M2 macrophages or Th 2-helper cells promote tumor progression (Salgado *et al.*, 2015).

An interesting finding in the patient's primary tumors, analyzed by the TCF, is the increased **CD4/CD8 ratio** that was determined in high-risk Luminal B tumors. This means that in our analyzed high-risk Luminal B tumors the predominant immune cell type was $CD4^+$ cells and could, therefore, account as a marker for high-risk Luminal B tumors. In addition, the Luminal B patient effusions also showed an increased CD4/CD8 ratio in this study. In general, $CD4^+$ cells (especially Tregs) are associated with a poor prognosis for Luminal breast cancer patients (Bates *et al.*, 2006). Tregs characterized as $CD4^+$ $CD25^+$ $FOXP3^+$ are known to act immunosuppressive and promote tumor progression by the downregulation of effector T-cells. Previously, Su et al suggested that tumor-infiltrating Tregs arise from chemotaxis of circulating naive $CD4^+$ T-cells being recruited into the tumor that differentiate into Tregs in situ (Su *et al.*, 2017). Hence, it could be speculated the determined $CD4^+$ cells in our Luminal B tumors are Tregs and prohibit therefore an immunologic defense of effector T-cells. This hypothesis could partially be supported by the fact that the $CD4^+$ and $CD8^+$ TILs in the Luminal B patients metastatic effusion were naïve, in contrast to the Luminal B solid patients' tumor.

Interestingly, this study revealed an advantage in DFS of HTM MDM2 Amp animals compared with TM MDM2 Amp animals. Conversely, the HTM MDM2 Amp animals did not differ regarding DFS compared with HTM MDM2 WT mice. First, these data implicate that the human immune cells control tumor cell proliferation. Second, the MDM2 amplification but no other alterations seem to be responsible for the DFS effect, as HTM MDM2 Amp animal and HTM MDM2 WT animals did not differ in DFS. It could be speculated that the TILs in MDM2 amplified tumors control the proliferation for a certain period of time but with increased tumor size the eradication by the limited number of TILs fails. This again would explain the unchanged OS between the groups.

The next level of therapeutic intervention in breast cancer might be represented by immune checkpoint inhibition. This treatment option turned out to be auspicious for the various malignancies. A prerequisite for efficient immune checkpoint inhibition is the expression of, for example, PD-L1 on tumor cells or its counterpart PD-1 on immune cells.

Discussion

The results of the humanized Luminal B PDX models and the already published results of humanized CDX models (Rom-Jurek *et al.*, 2018) coincide with the finding of low or absent **PD-L1** expression in Luminal HTM PDX. As the PDX models in this dissertation were shown to be non-immunogenic, the low impact of immune checkpoints in Luminal B breast cancer was not surprising. This finding in the HTM CDX model is probably due to the co-transplantation of tumor- and immune cells that ensure the development of tolerance of the human immune system towards mouse tissue and allogeneic tumor cells. As a consequence, the immune cells seem not to be activated by the tumor cells and thus, no tumor infiltration and e.g. IFNγ release, as a PD-L1 stimulus, occurred (Rom-Jurek *et al.*, 2018).

Contrary to the Luminal breast cancer, a high PD-L1 expression was determined in aggressive TNBC and one $Her2^{+}$ breast cancer cell line of the HTM CDX model (Rom-Jurek *et al.*, 2018). Enhanced PD-L1 expression in TNBC and HER2 positive tumors *in vivo* seems to be associated with an enhanced load of neoantigens in those cells. Such a phenotype attracts immune cells and triggers a tumor-immune cell interaction that can finally be inhibited by PD-L1/PD-1 interaction. Hence, the PD-L1 negativity might permit T-cell invasion into tumor tissue. However, IFNγ released by activated T-cells can induce PD-L1 expression (Garcia-Diaz *et al.*, 2017) and, vice versa, the PD-L1 expression by tumor cells can impede T-cell activation and IFNγ release that could subsequently entail decreased PD-L1 expression (Garcia-Diaz *et al.*, 2017). Even though, the role of immune cell infiltration and tumor attack in Luminal breast cancer patients is still doubtful, a clinical trial in metastatic hormone receptor-positive women with negative Her2 status has started to treat patients with a combination of Anti-PD-L1 and Anti-CTLA-4 antibody combined with hormone therapy (NCT03430466 https://clinicaltrials.gov/). Moreover, a pilot study that determines the PD-L1 expression during preoperative treatment with Nab-Paclitaxel and Pembrolizumab (PD-1 inhibitor) in hormone receptor-positive breast cancer (NCT02999477 https://clinicaltrials.gov/) is recruiting currently.

As mentioned above, the **PD-1** expression on immune cells, as the counterpart of PD-L1, determines the immunological answer. In the Luminal B HTM PDX model the PD-L1 expression on tumors cells did not correlate with the PD-1 expression or the TIL rate. In this study, increased PD-1 expression was only determined on the cytotoxic T-cells in the Luminal B patient's primary tumor compared with the Luminal B patient

metastatic effusion. However, even though a high PD-1 expression was determined on all TILs no difference in PD-1 expression on T-helper cells was observed comparing Luminal B patient's primary tumor with Luminal B metastatic effusion. Recently it was shown that increased $CD8^+$ $PD\text{-}1^+$ TILs were associated with prolonged DFS (Yeong *et al.*, 2019). The PD-1 expression on immune cells has also been determined to predict a favorable outcome for the patient (Brockhoff *et al.*, 2018; Noske *et al.*, 2019). It could be speculated that the antigen-induced anti-tumor immune pressure provokes the recruitment of immune cells to the tumor and results in successful antitumor defense. Hence, a lack of PD-1 expression on cytotoxic T-cells in Luminal B metastases might explain the unfavorable prognosis for patients.

Another important observation of this study was that the human immune system did not alter the metastatic frequency or the metastatic sites in all Luminal B PDX models. Those remain completely identical to those of the TM PDX. It is tempting to speculate that the geno- and phenotypic configuration of the tumor cell is responsible for the metastatic behavior. Another possibility is the influence of microenvironmental factors of the certain tissue that could contribute to tumor cell colonization like MMPs for lung colonization and IL-6 for bone marrow colonization (Chen *et al.*, 2018).

5.4 Genotypic differences between the primary tumor and bone marrow DTCs

The prevalent metastatic site in Luminal B breast cancer, independent of the Her2 status, is the bone marrow (Wu *et al.*, 2017). In general, the persistence of DTCs predicts a poor outcome with the possibility of a potential relapse for the patient (Janni *et al.*, 2011). However, the biology behind the dissemination of tumor cells is not fully understood. The theory of late dissemination of tumor cells was a long time well accepted in the scientific community (Koscielny *et al.*, 1985) whereas the hypothesis of early dissemination and parallel progression of tumor growth came more and more in the focus (Klein, 2009). Moreover, the primary tumor and the corresponding DTCs could differ genetically (Schmidt-Kittler *et al.*, 2003). Nevertheless, the differences were not yet assigned to a certain breast cancer subentity even with or without the influence of a human immune system.

Low pass-sequencing of primary HTM P and TM P tumors and the matching HTM P and TM P bone marrow DTC genomic profiles were shown to cluster in three populations (1. mainly DTC, 2. mainly tumor cells, 3. DTCs). More precisely, we detected congruent gains and amplification between the single tumor cells, but also

differences in gains and losses on certain genomic regions. The genomic heterogeneity between tumor cells and DTCs might be explained by the early dissemination hypothesis (Klein, 2009). According to that theory, the tumor cells acquire different genomic mutations during differentiation and proliferation, whereas the DTCs that left the primary tumor at a very early time point, only exhibit the genomic aberrations from the initial tumor cells and stay in dormancy (Magbanua *et al.*, 2018).

However, this study is only able to evaluate the endpoint of tumor development, while the alterations a tumor harbors at the beginning cannot be determined. Hence, the differences and concordances of the tumor and DTC profiles cannot distinguish between acquired and initial genetic alterations. The concordance between tumor cell and DTC profiles could rather be due to a late metastatic event. It was reported previously that 30 to 70 % of the patients that harbored DTCs in the bone marrow do not necessarily generate metastases later on (Klein, 2003).

Interestingly, the 3. population mainly consisted of DTCs from HTM PDX tumors and revealed gains and losses in the cell profile that differed from the tumor cell population and the DTCs from the TM. Two scenarios are possible to explain this incongruency. First, it can be speculated that the human immune system promotes a selection pressure on certain genomic aberrations of the tumor cells that migrate through the periphery into the bone marrow and manifest as DTCs other than those of the TM DTCs. Second, the micromilieu in the bone marrow niche of the HTM PDX, which is repopulated with human immune cells and progenitors, releases factors that contribute to the hosting of DTCs with a special genetic constellation. However, treating bone marrow metastases in breast cancer patients still lacks of alternative treatment options other than the chemotherapeutic intervention. However, the chemotherapeutic intervention would not target the dormant cells because only cells that are actively proliferating would be eradicated.

In our TM and HTM Luminal B PDX models not only single DTCs were detected in the bone marrow, but also DTC clusters. Linde 2018 demonstrated that the presence of more than five DTCs in a cluster tended to positively influence proliferation markers, and consequently, were considered as growing micrometastases (Linde *et al.*, 2018). It was reported in CTC clusters that this formation might take advantage of their oligoclonal origin, which enhances their survival in the bloodstream and helps to settle to various organs (Aceto *et al.*, 2014). If the oligoclonality is transferable to DTCs, the

clusters might profit from their inhibition of immunological detection and survive better than single DTCs. However, the functional relevance of DTC clusters in Luminal B breast cancer remains to be elucidated.

5.5 Organotropism in Luminal B breast cancer due to genetic alterations

Breast cancer metastases are frequently found in the distant lymph nodes, the liver, the lung, and the bone marrow, and the brain (Wu *et al.*, 2017). However, different breast cancer subentities were also shown to determine metastases in certain organs, such as the liver, the lung, and the distant lymph nodes, which are the predominant sites in Luminal B breast cancer. This so-called organotropism was shown to be driven by the different breast cancer subentities, different gene signatures, and different signaling pathways of metastatic tumor cells (Chen *et al.*, 2018)

In this study, the tumors that harbored an MDM2 amplification (four different PDX models) promoted metastatic lesions in the lung and bone marrow DTCs, whereas a TP53 mutation (two different PDX models) prevented metastatic lesions in the lung, but caused bone marrow DTCs. This indicates an organotropism that is promoted by the genetic aberration of the different Luminal B tumors. However, different genetic aberrations could account for different phenotypes that drive the metastatic spread. Minn et al. identified a set of genes that mark and mediate breast cancer metastasis to the lung, like MMP1 or VCAM1 (Minn *et al.*, 2005). Moreover, the genetic signature was shown to be tissue-specific (Chen *et al.*, 2018). Interestingly, all Luminal B PDX tumors showed a DTC colonization of the bone marrow. As all of the tumors share a high EpCAM expression in the primary tumor, it could be speculated that EpCAM positivity correlates with bone marrow dissemination. EpCAM positivity and high EpCAM expression was reported to be associated with a CSC phenotype of the tumor cells. Hence, mainly EpCAM positive cells harbor the capacity for self-renewal and differentiation, showing increased sphere formation *in vitro* and tumorigenicity *in vivo* (Hiraga *et al.*, 2016). The occurrence of bone marrow metastasis was previously shown to be associated with a high EpCAM positivity of the primary tumor (Hiraga *et al.*, 2016). In this context, the high EpCAM expression of all Luminal B PDX tumors might be a detrimental factor that promotes the dissemination of the tumor cells to the bone marrow.

This study also revealed that the MDM4 amplification of the tumor in TM AB led to metastases in the lung, the liver, the spleen, the brain, and the bone marrow. The

metastases correlated with those of the primary patient tumor. However, even though the MDM4 amplification of the tumor is supposed to be correlated with the metastatic sites, this organotropism cannot be over-interpreted due to the limited availability of just that one model.

In summary, the MDM2 amplification (four different PDX models), TP53 mutation (two different PDX models) and the MDM4 amplification (one PDX model) of the primary tumor could potentially predict the metastatic sites the tumor cells will colonize. However, the mechanisms have to be further elucidated with an increased number of MDM2 amplified/ TP53 mutated/ MDM4 amplified PDX tumors.

5.6 Conclusion

In this study, we provided evidence for the benefit of using (humanized) PDX models to identify high-risk markers for Luminal B breast cancer. CD24, cMET, CD44 and the co-expression of CD44/cMET/CD47 were determined as phenotypic markers that are able to identify high-risk Luminal B tumors. Moreover, TP53 mutation and especially MDM2 gene amplification seemed to be strongly associated with aggressiveness of Luminal B tumors, which is indicated by increased tumor engraftment, increased tumor size, and metastases in HTM and TM. Potentially, luminal tumors can routinely be scored for a genomic MDM2 gain, *via* in-situ hybridization (ISH), or MDM2 expression *via* IHC, in order to identify high-risk luminal B tumors with increased aggressiveness and an enhanced capacity to metastasize. The analyzed Luminal B PDX models and the primary Luminal B patient tumors were shown to be rather nonimmunogenic. However, even the few determined TILs showed an increased CD4/CD8 expression ratio that additionally accounts as a marker for high-risk Luminal B tumors. Bone marrow DTCs in the TM and HTM P models were shown to differ genetically from the primary tumor, and moreover, the human immune system seems to influence the colonization of bone marrow DTCs with certain genetic aberrations. This further confirms the importance to determine the genetic constitution of the DTCs to ensure a personalized therapy decision in case of recurrence. In summary, our study pointed out different high-risk geno- and phenotypic markers, in addition to a high-risk TIL signature in Luminal breast cancer. This might help to identify patients who might benefit from additional chemotherapeutic intervention or MDM2-specific inhibition.

References

Abubakar, M., Guo, C., Koka, H., Sung, H., Shao, N., Guida, J., Deng, J., Li, M., Hu, N., Zhou, B., Lu, N. and Yang, X.R. (2019), “Clinicopathological and epidemiological significance of breast cancer subtype reclassification based on p53 immunohistochemical expression”, *NPJ breast cancer*, Vol. 5, p. 20.

Aceto, N., Bardia, A., Miyamoto, D.T., Donaldson, M.C., Wittner, B.S., Spencer, J.A., Yu, M., Pely, A., Engstrom, A., Zhu, H., Brannigan, B.W., Kapur, R., Stott, S.L., Shioda, T., Ramaswamy, S., Ting, D.T., Lin, C.P., Toner, M., Haber, D.A. and Maheswaran, S. (2014), “Circulating tumor cell clusters are oligoclonal precursors of breast cancer metastasis”, *Cell*, Vol. 158 No. 5, pp. 1110–1122.

Al-Hajj, M., Wicha, M.S., Benito-Hernandez, A., Morrison, S.J. and Clarke, M.F. (2003), “Prospective identification of tumorigenic breast cancer cells”, *Proceedings of the National Academy of Sciences of the United States of America*, Vol. 100 No. 7, pp. 3983–3988.

Ali, H.R., Glont, S.-E., Blows, F.M., Provenzano, E., Dawson, S.-J., Liu, B., Hiller, L., Dunn, J., Poole, C.J., Bowden, S., Earl, H.M., Pharoah, P.D.P. and Caldas, C. (2015), “PD-L1 protein expression in breast cancer is rare, enriched in basal-like tumours and associated with infiltrating lymphocytes”, *Annals of oncology official journal of the European Society for Medical Oncology*, Vol. 26 No. 7, pp. 1488–1493.

Alkhalaf, M., El-Mowafy, A.M. and Abou-Zeid, L.A. (2005), “Progesterone inhibition of MDM2 p90 protein in MCF-7 human breast cancer cell line is dependent on p53 levels”, *Journal of molecular and genetic medicine an international journal of biomedical research*, Vol. 1 No. 1, pp. 33–37.

Alvarado, M.D., Prasad, C., Rothney, M., Cherbavaz, D.B., Sing, A.P., Baehner, F.L., Svedman, C. and Markopoulos, C.J. (2015), “A Prospective Comparison of the 21-Gene Recurrence Score and the PAM50-Based Prosigna in Estrogen Receptor-Positive Early-Stage Breast Cancer”, *Advances in therapy*, Vol. 32 No. 12, pp. 1237–1247.

Baccelli, I., Schneeweiss, A., Riethdorf, S., Stenzinger, A., Schillert, A., Vogel, V., Klein, C., Saini, M., Bäuerle, T., Wallwiener, M., Holland-Letz, T., Höfner, T., Sprick, M., Scharpff, M., Marmé, F., Sinn, H.P., Pantel, K., Weichert, W. and Trumpp, A. (2013), “Identification of a population of blood circulating tumor cells from breast cancer patients that initiates metastasis in a xenograft assay”, *Nature biotechnology*, Vol. 31 No. 6, pp. 539–544.

Baccelli, I., Stenzinger, A., Vogel, V., Pfitzner, B.M., Klein, C., Wallwiener, M., Scharpff, M., Saini, M., Holland-Letz, T., Sinn, H.-P., Schneeweiss, A., Denkert, C., Weichert, W. and Trumpp, A. (2014), “Co-expression of MET and CD47 is a novel prognosticator for survival of luminal breast cancer patients”, *Oncotarget*, Vol. 5 No. 18, pp. 8147–8160.

Barkal, A.A., Brewer, R.E., Markovic, M., Kowarsky, M., Barkal, S.A., Zaro, B.W., Krishnan, V., Hatakeyama, J., Dorigo, O., Barkal, L.J. and Weissman, I.L. (2019), “CD24 signalling through macrophage Siglec-10 is a target for cancer immunotherapy”, *Nature*, Vol. 572 No. 7769, pp. 392–396.

Bates, G.J., Fox, S.B., Han, C., Leek, R.D., Garcia, J.F., Harris, A.L. and Banham, A.H. (2006), “Quantification of regulatory T cells enables the identification of high-risk breast cancer patients and those at risk of late relapse”, *Journal of clinical oncology official journal of the American Society of Clinical Oncology*, Vol. 24 No. 34, pp. 5373–5380.

Baudis, M. and Cleary, M.L. (2001), “Progenetix.net. An online repository for molecular cytogenetic aberration data”, *Bioinformatics (Oxford, England)*, Vol. 17 No. 12, pp. 1228–1229.

Baumann, P., Cremers, N., Kroese, F., Orend, G., Chiquet-Ehrismann, R., Uede, T., Yagita, H. and Sleeman, J.P. (2005), “CD24 expression causes the acquisition of multiple cellular properties associated with tumor growth and metastasis”, *Cancer research*, Vol. 65 No. 23, pp. 10783–10793.

References

Beckhove, P., Schütz, F., Diel, I.J., Solomayer, E.-F., Bastert, G., Foerster, J., Feuerer, M., Bai, L., Sinn, H.-P., Umansky, V. and Schirrmacher, V. (2003), "Efficient engraftment of human primary breast cancer transplants in nonconditioned NOD/Scid mice", *International journal of cancer*, Vol. 105 No. 4, pp. 444–453.

Bergamaschi, A., Hjortland, G.O., Triulzi, T., Sørlie, T., Johnsen, H., Ree, A.H., Russnes, H.G., Tronnes, S., Maelandsmo, G.M., Fodstad, O., Borresen-Dale, A.-L. and Engebraaten, O. (2009), "Molecular profiling and characterization of luminal-like and basal-like in vivo breast cancer xenograft models", *Molecular oncology*, Vol. 3 No. 5-6, pp. 469–482.

Berns, E.M., Foekens, J.A., Vossen, R., Look, M.P., Devilee, P., Henzen-Logmans, S.C., van Staveren, I.L., van Putten, W.L., Inganäs, M., Meijer-van Gelder, M.E., Cornelisse, C., Claassen, C.J., Portengen, H., Bakker, B. and Klijn, J.G. (2000), "Complete sequencing of TP53 predicts poor response to systemic therapy of advanced breast cancer", *Cancer research*, Vol. 60 No. 8, pp. 2155–2162.

Bertos, N.R. and Park, M. (2011), "Breast cancer - one term, many entities?", *The Journal of clinical investigation*, Vol. 121 No. 10, pp. 3789–3796.

Bill, R. and Christofori, G. (2015), "The relevance of EMT in breast cancer metastasis. Correlation or causality?", *FEBS letters*, Vol. 589 No. 14, pp. 1577–1587.

Blank, C., Gajewski, T.F. and Mackensen, A. (2005), "Interaction of PD-L1 on tumor cells with PD-1 on tumor-specific T cells as a mechanism of immune evasion. Implications for tumor immunotherapy", *Cancer immunology, immunotherapy CII*, Vol. 54 No. 4, pp. 307–314.

Braun, S., Vogl, F.D., Naume, B., Janni, W., Osborne, M.P., Coombes, R.C., Schlimok, G., Diel, I.J., Gerber, B., Gebauer, G., Pierga, J.-Y., Marth, C., Oruzio, D., Wiedswang, G., Solomayer, E.-F., Kundt, G., Strobl, B., Fehm, T., Wong, G.Y.C., Bliss, J., Vincent-Salomon, A. and Pantel, K. (2005), "A pooled analysis of bone marrow micrometastasis in breast cancer", *The New England journal of medicine*, Vol. 353 No. 8, pp. 793–802.

Brekman, A., Singh, K.E., Polotskaia, A., Kundu, N. and Bargonetti, J. (2011), "A p53-independent role of Mdm2 in estrogen-mediated activation of breast cancer cell proliferation", *Breast cancer research BCR*, Vol. 13 No. 1, R3.

Brockhoff, G., Seitz, S., Weber, F., Zeman, F., Klinkhammer-Schalke, M., Ortmann, O. and Wege, A.K. (2018), "The presence of PD-1 positive tumor infiltrating lymphocytes in triple negative breast cancers is associated with a favorable outcome of disease", *Oncotarget*, Vol. 9 No. 5, pp. 6201–6212.

Carreno, B.M., Garbow, J.R., Kolar, G.R., Jackson, E.N., Engelbach, J.A., Becker-Hapak, M., Carayannopoulos, L.N., Piwnica-Worms, D. and Linette, G.P. (2009), "Immunodeficient mouse strains display marked variability in growth of human melanoma lung metastases", *Clinical cancer research an official journal of the American Association for Cancer Research*, Vol. 15 No. 10, pp. 3277–3286.

Cheang, M.C.U., Chia, S.K., Voduc, D., Gao, D., Leung, S., Snider, J., Watson, M., Davies, S., Bernard, P.S., Parker, J.S., Perou, C.M., Ellis, M.J. and Nielsen, T.O. (2009), "Ki67 index, HER2 status, and prognosis of patients with luminal B breast cancer", *Journal of the National Cancer Institute*, Vol. 101 No. 10, pp. 736–750.

Chekhun, S., Bezdenezhnykh, N., Shvets, J. and Lukianova, N. (2013), "Expression of biomarkers related to cell adhesion, metastasis and invasion of breast cancer cell lines of different molecular subtype", *Experimental oncology*, Vol. 35 No. 3, pp. 174–179.

Chen, W., Hoffmann, A.D., Liu, H. and Liu, X. (2018), "Organotropism. New insights into molecular mechanisms of breast cancer metastasis", *NPJ precision oncology*, Vol. 2 No. 1, p. 4.

Choschzick, M., Heilenkötter, U., Lebeau, A., Jaenicke, F., Terracciano, L., Bokemeyer, C., Sauter, G. and Simon, R. (2010), "MDM2 amplification is an independent prognostic feature of node-negative, estrogen receptor-positive early-stage breast cancer", *Cancer biomarkers section A of Disease markers*, Vol. 8 No. 2, pp. 53–60.

References

Christofori, G. (2006), “New signals from the invasive front”, *Nature*, Vol. 441 No. 7092, pp. 444–450.

Cottu, P., Bièche, I., Assayag, F., El Botty, R., Chateau-Joubert, S., Thuleau, A., Bagarre, T., Albaud, B., Rapinat, A., Gentien, D., La Grange, P. de, Sibut, V., Vacher, S., Hatem, R., Servely, J.-L., Fontaine, J.-J., Decaudin, D., Pierga, J.-Y., Roman-Roman, S. and Marangoni, E. (2014), “Acquired resistance to endocrine treatments is associated with tumor-specific molecular changes in patient-derived luminal breast cancer xenografts”, *Clinical cancer research an official journal of the American Association for Cancer Research*, Vol. 20 No. 16, pp. 4314–4325.

Cottu, P., Marangoni, E., Assayag, F., Cremoux, P. de, Vincent-Salomon, A., Guyader, C., Plater, L. de, Elbaz, C., Karboul, N., Fontaine, J.J., Chateau-Joubert, S., Boudou-Rouquette, P., Alran, S., Dangles-Marie, V., Gentien, D., Poupon, M.-F. and Decaudin, D. (2012), “Modeling of response to endocrine therapy in a panel of human luminal breast cancer xenografts”, *Breast cancer research and treatment*, Vol. 133 No. 2, pp. 595–606.

Cristea, S. and Polyak, K. (2018), “Dissecting the mammary gland one cell at a time”, *Nature communications*, Vol. 9 No. 1, p. 2473.

Cuny, M., Kramar, A., Courjal, F., Johannsdottir, V., Iacopetta, B., Fontaine, H., Grenier, J., Culine, S. and Theillet, C. (2000), “Relating genotype and phenotype in breast cancer. An analysis of the prognostic significance of amplification at eight different genes or loci and of p53 mutations”, *Cancer research*, Vol. 60 No. 4, pp. 1077–1083.

Danovi, D., Meulmeester, E., Pasini, D., Migliorini, D., Capra, M., Frenk, R., Graaf, P. de, Francoz, S., Gasparini, P., Gobbi, A., Helin, K., Pelicci, P.G., Jochemsen, A.G. and Marine, J.-C. (2004), “Amplification of Mdmx (or Mdm4) directly contributes to tumor formation by inhibiting p53 tumor suppressor activity”, *Molecular and cellular biology*, Vol. 24 No. 13, pp. 5835–5843.

DeNardo, D.G. and Coussens, L.M. (2007), “Inflammation and breast cancer. Balancing immune response. Crosstalk between adaptive and innate immune cells during breast cancer progression”, *Breast cancer research BCR*, Vol. 9 No. 4, p. 212.

Denkert, C., Minckwitz, G. von, Darb-Esfahani, S., Lederer, B., Heppner, B.I., Weber, K.E., Budczies, J., Huober, J., Klauschen, F., Furlanetto, J., Schmitt, W.D., Blohmer, J.-U., Karn, T., Pfitzner, B.M., Kümmel, S., Engels, K., Schneeweiss, A., Hartmann, A., Noske, A., Fasching, P.A., Jackisch, C., van Mackelenbergh, M., Sinn, P., Schem, C., Hanusch, C., Untch, M. and Loibl, S. (2018), “Tumour-infiltrating lymphocytes and prognosis in different subtypes of breast cancer. A pooled analysis of 3771 patients treated with neoadjuvant therapy”, *The Lancet Oncology*, Vol. 19 No. 1, pp. 40–50.

DeRose, Y.S., Gligorich, K.M., Wang, G., Georgelas, A., Bowman, P., Courdy, S.J., Welm, A.L. and Welm, B.E. (2013), “Patient-derived models of human breast cancer: protocols for in vitro and in vivo applications in tumor biology and translational medicine”, *Current protocols in pharmacology*, Chapter 14, Unit14.23.

DeRose, Y.S., Wang, G., Lin, Y.-C., Bernard, P.S., Buys, S.S., Ebbert, M.T.W., Factor, R., Matsen, C., Milash, B.A., Nelson, E., Neumayer, L., Randall, R.L., Stijleman, I.J., Welm, B.E. and Welm, A.L. (2011), “Tumor grafts derived from women with breast cancer authentically reflect tumor pathology, growth, metastasis and disease outcomes”, *Nature medicine*, Vol. 17 No. 11, pp. 1514–1520.

Duda, V.F. and Schulz-Wendtland, R. (2017), *Mammadiagnostik*, Springer Berlin Heidelberg, Berlin, Heidelberg.

Dunnwald, L.K., Rossing, M.A. and Li, C.I. (2007), “Hormone receptor status, tumor characteristics, and prognosis. A prospective cohort of breast cancer patients”, *Breast cancer research BCR*, Vol. 9 No. 1, R6.

Eirew, P., Steif, A., Khattra, J., Ha, G., Yap, D., Farahani, H., Gelmon, K., Chia, S., Mar, C., Wan, A., Laks, E., Biele, J., Shumansky, K., Rosner, J., McPherson, A., Nielsen, C., Roth,

References

A.J.L., Lefebvre, C., Bashashati, A., Souza, C. de, Siu, C., Aniba, R., Brimhall, J., Oloumi, A., Osako, T., Bruna, A., Sandoval, J.L., Algara, T., Greenwood, W., Leung, K., Cheng, H., Xue, H., Wang, Y., Lin, D., Mungall, A.J., Moore, R., Zhao, Y., Lorette, J., Nguyen, L., Huntsman, D., Eaves, C.J., Hansen, C., Marra, M.A., Caldas, C., Shah, S.P. and Aparicio, S. (2015), "Dynamics of genomic clones in breast cancer patient xenografts at single-cell resolution", *Nature*, Vol. 518 No. 7539, pp. 422–426.

Elston, C.W. and Ellis, I.O. (1991), "Pathological prognostic factors in breast cancer. I. The value of histological grade in breast cancer. Experience from a large study with long-term follow-up", *Histopathology*, Vol. 19 No. 5, pp. 403–410.

Emens, L.A. (2012), "Breast cancer immunobiology driving immunotherapy. Vaccines and immune checkpoint blockade", *Expert review of anticancer therapy*, Vol. 12 No. 12, pp. 1597–1611.

Endris, V., Penzel, R., Warth, A., Muckenhuber, A., Schirmacher, P., Stenzinger, A. and Weichert, W. (2013), "Molecular diagnostic profiling of lung cancer specimens with a semiconductor-based massive parallel sequencing approach. Feasibility, costs, and performance compared with conventional sequencing", *The Journal of molecular diagnostics JMD*, Vol. 15 No. 6, pp. 765–775.

Engel, J., Eckel, R., Kerr, J., Schmidt, M., Fürstenberger, G., Richter, R., Sauer, H., Senn, H.-J. and Hölzel, D. (2003), "The process of metastasisation for breast cancer", *European Journal of Cancer*, Vol. 39 No. 12, pp. 1794–1806.

Ethier, S.P., Mahacek, M.L., Gullick, W.J., Frank, T.S. and Weber, B.L. (1993), "Differential isolation of normal luminal mammary epithelial cells and breast cancer cells from primary and metastatic sites using selective media", *Cancer research*, Vol. 53 No. 3, pp. 627–635.

Felipe Lima, J., Nofech-Mozes, S., Bayani, J. and Bartlett, J.M.S. (2016), "EMT in Breast Carcinoma-A Review", *Journal of clinical medicine*, Vol. 5 No. 7.

Feng, Y., Spezia, M., Huang, S., Yuan, C., Zeng, Z., Zhang, L., Ji, X., Liu, W., Huang, B., Luo, W., Liu, B., Lei, Y., Du, S., Vuppalapati, A., Luu, H.H., Haydon, R.C., He, T.-C. and Ren, G. (2018), "Breast cancer development and progression. Risk factors, cancer stem cells, signaling pathways, genomics, and molecular pathogenesis", *Genes & diseases*, Vol. 5 No. 2, pp. 77–106.

Fiche, M., Scabia, V., Aouad, P., Battista, L., Treboux, A., Stravodimou, A., Zaman, K., Dormoy, V., Ayyanan, A., Sflomos, G. and Brisken, C. (2019), "Intraductal patient-derived xenografts of estrogen receptor α-positive breast cancer recapitulate the histopathological spectrum and metastatic potential of human lesions", *The Journal of pathology*, Vol. 247 No. 3, pp. 287–292.

Fidler, I.J. (2003), "The pathogenesis of cancer metastasis. The 'seed and soil' hypothesis revisited", *Nature reviews. Cancer*, Vol. 3 No. 6, pp. 453–458.

Finlay-Schultz, J., Gillen, A.E., Brechbuhl, H.M., Ivie, J.J., Matthews, S.B., Jacobsen, B.M., Bentley, D.L., Kabos, P. and Sartorius, C.A. (2017), "Breast Cancer Suppression by Progesterone Receptors Is Mediated by Their Modulation of Estrogen Receptors and RNA Polymerase III", *Cancer research*, Vol. 77 No. 18, pp. 4934–4946.

Fleming, J.M., Miller, T.C., Meyer, M.J., Ginsburg, E. and Vonderhaar, B.K. (2010), "Local regulation of human breast xenograft models", *Journal of cellular physiology*, Vol. 224 No. 3, pp. 795–806.

Forbes, S.A., Beare, D., Gunasekaran, P., Leung, K., Bindal, N., Boutselakis, H., Ding, M., Bamford, S., Cole, C., Ward, S., Kok, C.Y., Jia, M., De, T., Teague, J.W., Stratton, M.R., McDermott, U. and Campbell, P.J. (2015), "COSMIC. Exploring the world's knowledge of somatic mutations in human cancer", *Nucleic acids research*, Vol. 43 No. Database issue, D805-11.

References

Friederichs, J., Zeller, Y., Hafezi-Moghadam, A., Gröne, H.J., Ley, K. and Altevogt, P. (2000), "The CD24/P-selectin binding pathway initiates lung arrest of human A125 adenocarcinoma cells", *Cancer research*, Vol. 60 No. 23, pp. 6714–6722.

Frisch, S.M. and Ruoslahti, E. (1997), "Integrins and anoikis", *Current opinion in cell biology*, Vol. 9 No. 5, pp. 701–706.

Gao, C., Xiao, G. and Bargonetti, J. (2019), "Contemplations on MDMX (MDM4) driving triple negative breast cancer circulating tumor cells and metastasis", *Oncotarget*, Vol. 10 No. 49, pp. 5007–5010.

Garcia-Diaz, A., Shin, D.S., Moreno, B.H., Saco, J., Escuin-Ordinas, H., Rodriguez, G.A., Zaretsky, J.M., Sun, L., Hugo, W., Wang, X., Parisi, G., Saus, C.P., Torrejon, D.Y., Graeber, T.G., Comin-Anduix, B., Hu-Lieskovan, S., Damoiseaux, R., Lo, R.S. and Ribas, A. (2017), "Interferon Receptor Signaling Pathways Regulating PD-L1 and PD-L2 Expression", *Cell reports*, Vol. 19 No. 6, pp. 1189–1201.

Ghatak, S., Hascall, V.C., Markwald, R.R. and Misra, S. (2010), "Stromal hyaluronan interaction with epithelial CD44 variants promotes prostate cancer invasiveness by augmenting expression and function of hepatocyte growth factor and androgen receptor", *The Journal of biological chemistry*, Vol. 285 No. 26, pp. 19821–19832.

Ghebeh, H., Mohammed, S., Al-Omair, A., Qattan, A., Lehe, C., Al-Qudaihi, G., Elkum, N., Alshabanah, M., Bin Amer, S., Tulbah, A., Ajarim, D., Al-Tweigeri, T. and Dermime, S. (2006), "The B7-H1 (PD-L1) T lymphocyte-inhibitory molecule is expressed in breast cancer patients with infiltrating ductal carcinoma. Correlation with important high-risk prognostic factors", *Neoplasia (New York, N.Y.)*, Vol. 8 No. 3, pp. 190–198.

Gires, O. (2011), "Lessons from common markers of tumor-initiating cells in solid cancers", *Cellular and molecular life sciences CMLS*, Vol. 68 No. 24, pp. 4009–4022.

Gires, O. and Stoecklein, N.H. (2014), "Dynamic EpCAM expression on circulating and disseminating tumor cells. Causes and consequences", *Cellular and molecular life sciences CMLS*, Vol. 71 No. 22, pp. 4393–4402.

Goldhirsch, A., Wood, W.C., Coates, A.S., Gelber, R.D., Thürlimann, B. and Senn, H.-J. (2011), "Strategies for subtypes--dealing with the diversity of breast cancer: highlights of the St. Gallen International Expert Consensus on the Primary Therapy of Early Breast Cancer 2011", *Annals of oncology official journal of the European Society for Medical Oncology*, Vol. 22 No. 8, pp. 1736–1747.

Haupt, S., Vijayakumaran, R., Miranda, P.J., Burgess, A., Lim, E. and Haupt, Y. (2017), "The role of MDM2 and MDM4 in breast cancer development and prevention", *Journal of molecular cell biology*, Vol. 9 No. 1, pp. 53–61.

Hayat, M.A. (Ed.) (2013), *Tumor Dormancy, Quiescence, and Senescence, Volume 1: Aging, Cancer, and Noncancer Pathologies, Tumor Dormancy and Cellular Quiescence and Senescence, Aging, Cancer, and Noncancer Pathologies*, Vol. 1, Springer, Dordrecht.

Hayes, D.F., Thor, A.D., Dressler, L.G., Weaver, D., Edgerton, S., Cowan, D., Broadwater, G., Goldstein, L.J., Martino, S., Ingle, J.N., Henderson, I.C., Norton, L., Winer, E.P., Hudis, C.A., Ellis, M.J. and Berry, D.A. (2007), "HER2 and response to paclitaxel in node-positive breast cancer", *The New England journal of medicine*, Vol. 357 No. 15, pp. 1496–1506.

Hiraga, T., Ito, S. and Nakamura, H. (2016), "EpCAM expression in breast cancer cells is associated with enhanced bone metastasis formation", *International journal of cancer*, Vol. 138 No. 7, pp. 1698–1708.

Honeth, G., Bendahl, P.-O., Ringnér, M., Saal, L.H., Gruvberger-Saal, S.K., Lövgren, K., Grabau, D., Fernö, M., Borg, A. and Hegardt, C. (2008), "The CD44+/CD24- phenotype is enriched in basal-like breast tumors", *Breast cancer research BCR*, Vol. 10 No. 3, R53.

Ho-Yen, C.M., Green, A.R., Rakha, E.A., Brentnall, A.R., Ellis, I.O., Kermorgant, S. and Jones, J.L. (2014), "C-Met in invasive breast cancer. Is there a relationship with the basal-like subtype?", *Cancer*, Vol. 120 No. 2, pp. 163–171.

References

Ho-Yen, C.M., Jones, J.L. and Kermorgant, S. (2015), "The clinical and functional significance of c-Met in breast cancer. A review", *Breast cancer research BCR*, Vol. 17, p. 52.

Huber, M.A., Kraut, N. and Beug, H. (2005), "Molecular requirements for epithelial-mesenchymal transition during tumor progression", *Current opinion in cell biology*, Vol. 17 No. 5, pp. 548–558.

Huber, S., Wege, A.K., Bernhardt, G., Buschauer, A. and Brockhoff, G. (2015), "Topotecan-induced ABCG2 expression in MCF-7 cells is associated with decreased CD24 and EpCAM expression and a loss of tumorigenicity", *Cytometry. Part A the journal of the International Society for Analytical Cytology*, Vol. 87 No. 8, pp. 707–716.

Ibrahim, T., Leong, I., Sanchez-Sweatman, O., Khokha, R., Sodek, J., Tenenbaum, H.C., Ganss, B. and Cheifetz, S. (2000), "Expression of bone sialoprotein and osteopontin in breast cancer bone metastases", *Clinical & experimental metastasis*, Vol. 18 No. 3, pp. 253–260.

Ip, M.M. and Asch, B.B. (2000), *Methods in Mammary Gland Biology and Breast Cancer Research*, Springer US, Boston, MA.

Jaggupilli, A. and Elkord, E. (2012), "Significance of CD44 and CD24 as cancer stem cell markers. An enduring ambiguity", *Clinical & developmental immunology*, Vol. 2012, p. 708036.

Janik, K., Popeda, M., Peciak, J., Rosiak, K., Smolarz, M., Treda, C., Rieske, P., Stoczynska-Fidelus, E. and Ksiazkiewicz, M. (2016), "Efficient and simple approach to in vitro culture of primary epithelial cancer cells", *Bioscience reports*, Vol. 36 No. 6.

Janni, W., Vogl, F.D., Wiedswang, G., Synnestvedt, M., Fehm, T., Jückstock, J., Borgen, E., Rack, B., Braun, S., Sommer, H., Solomayer, E., Pantel, K., Nesland, J., Friese, K. and Naume, B. (2011), "Persistence of disseminated tumor cells in the bone marrow of breast cancer patients predicts increased risk for relapse--a European pooled analysis", *Clinical cancer research an official journal of the American Association for Cancer Research*, Vol. 17 No. 9, pp. 2967–2976.

Jia, L., Yang, X., Tian, W., Guo, S., Huang, W. and Zhao, W. (2018), "Increased Expression of c-Met is Associated with Chemotherapy-Resistant Breast Cancer and Poor Clinical Outcome", *Medical science monitor international medical journal of experimental and clinical research*, Vol. 24, pp. 8239–8249.

Kabos, P., Finlay-Schultz, J., Li, C., Kline, E., Finlayson, C., Wisell, J., Manuel, C.A., Edgerton, S.M., Harrell, J.C., Elias, A. and Sartorius, C.A. (2012), "Patient-derived luminal breast cancer xenografts retain hormone receptor heterogeneity and help define unique estrogen-dependent gene signatures", *Breast cancer research and treatment*, Vol. 135 No. 2, pp. 415–432.

Kanaya, N., Somlo, G., Wu, J., Frankel, P., Kai, M., Liu, X., Wu, S.V., Nguyen, D., Chan, N., Hsieh, M.-Y., Kirschenbaum, M., Kruper, L., Vito, C., Badie, B., Yim, J.H., Yuan, Y., Hurria, A., Peiguo, C., Mortimer, J. and Chen, S. (2017), "Characterization of patient-derived tumor xenografts (PDXs) as models for estrogen receptor positive (ER+HER2- and ER+HER2+) breast cancers", *The Journal of steroid biochemistry and molecular biology*, Vol. 170, pp. 65–74.

Kareva, I. (2016), "Primary and metastatic tumor dormancy as a result of population heterogeneity", *Biology direct*, Vol. 11, p. 37.

Kawaguchi, T., Foster, B.A., Young, J. and Takabe, K. (2017), "Current Update of Patient-Derived Xenograft Model for Translational Breast Cancer Research", *Journal of mammary gland biology and neoplasia*, Vol. 22 No. 2, pp. 131–139.

Keir, M.E., Butte, M.J., Freeman, G.J. and Sharpe, A.H. (2008), "PD-1 and its ligands in tolerance and immunity", *Annual review of immunology*, Vol. 26, pp. 677–704.

References

Khan, M., Maryam, A., Zhang, H., Mehmood, T. and Ma, T. (2016), “Killing cancer with platycodin D through multiple mechanisms”, *Journal of cellular and molecular medicine*, Vol. 20 No. 3, pp. 389–402.

Kim, K., Burghardt, R., Barhoumi, R., Lee, S.-O., Liu, X. and Safe, S. (2011), “MDM2 regulates estrogen receptor α and estrogen responsiveness in breast cancer cells”, *Journal of molecular endocrinology*, Vol. 46 No. 2, pp. 67–79.

Klein, C.A. (2003), “The Systemic Progression of Human Cancer. A Focus on the Individual Disseminated Cancer Cell—The Unit of Selection”, in *Advances in Cancer Research*, Vol. 89, Elsevier, pp. 35–67.

Klein, C.A. (2009), “Parallel progression of primary tumours and metastases”, *Nature reviews. Cancer*, Vol. 9 No. 4, pp. 302–312.

Klein, C.A., Schmidt-Kittler, O., Schardt, J.A., Pantel, K., Speicher, M.R. and Riethmüller, G. (1999), “Comparative genomic hybridization, loss of heterozygosity, and DNA sequence analysis of single cells”, *Proceedings of the National Academy of Sciences of the United States of America*, Vol. 96 No. 8, pp. 4494–4499.

Klöppel, G., Kreipe, H., Remmele, W. and Dietel, M. (2013), *Pathologie*, Springer Berlin Heidelberg, Berlin, Heidelberg.

Korkaya, H., Paulson, A., Iovino, F. and Wicha, M.S. (2008), “HER2 regulates the mammary stem/progenitor cell population driving tumorigenesis and invasion”, *Oncogene*, Vol. 27 No. 47, pp. 6120–6130.

Korkaya, H. and Wicha, M.S. (2009), “HER-2, notch, and breast cancer stem cells. Targeting an axis of evil”, *Clinical cancer research an official journal of the American Association for Cancer Research*, Vol. 15 No. 6, pp. 1845–1847.

Koscielny, S., Tubiana, M., Lê, M.G., Valleron, A.J., Mouriesse, H., Contesso, G. and Sarrazin, D. (1984), “Breast cancer. Relationship between the size of the primary tumour and the probability of metastatic dissemination”, *British journal of cancer*, Vol. 49 No. 6, pp. 709–715.

Koscielny, S., Tubiana, M. and Valleron, A.J. (1985), “A simulation model of the natural history of human breast cancer”, *British journal of cancer*, Vol. 52 No. 4, pp. 515–524.

Kotiyal, S. and Bhattacharya, S. (2014), “Breast cancer stem cells, EMT and therapeutic targets”, *Biochemical and biophysical research communications*, Vol. 453 No. 1, pp. 112–116.

Kriegsmann, M., Endris, V., Wolf, T., Pfarr, N., Stenzinger, A., Loibl, S., Denkert, C., Schneeweiss, A., Budczies, J., Sinn, P. and Weichert, W. (2014), “Mutational profiles in triple-negative breast cancer defined by ultradeep multigene sequencing show high rates of PI3K pathway alterations and clinically relevant entity subgroup specific differences”, *Oncotarget*, Vol. 5 No. 20, pp. 9952–9965.

Kwon, M.J., Han, J., Seo, J.H., Song, K., Jeong, H.M., Choi, J.-S., Kim, Y.J., Lee, S.-H., Choi, Y.-L. and Shin, Y.K. (2015), “CD24 Overexpression Is Associated with Poor Prognosis in Luminal A and Triple-Negative Breast Cancer”, *PloS one*, Vol. 10 No. 10, e0139112.

Lacroix, M., Toillon, R.-A. and Leclercq, G. (2006), “p53 and breast cancer, an update”, *Endocrine-related cancer*, Vol. 13 No. 2, pp. 293–325.

Landis, M.D., Lehmann, B.D., Pietenpol, J.A. and Chang, J.C. (2013), “Patient-derived breast tumor xenografts facilitating personalized cancer therapy”, *Breast cancer research BCR*, Vol. 15 No. 1, p. 201.

Langer, E.M., Allen-Petersen, B.L., King, S.M., Kendsersky, N.D., Turnidge, M.A., Kuziel, G.M., Riggers, R., Samatham, R., Amery, T.S., Jacques, S.L., Sheppard, B.C., Korkola, J.E., Muschler, J.L., Thibault, G., Chang, Y.H., Gray, J.W., Presnell, S.C., Nguyen, D.G. and Sears, R.C. (2019), “Modeling Tumor Phenotypes In Vitro with Three-Dimensional Bioprinting”, *Cell reports*, Vol. 26 No. 3, 608-623.e6.

References

Langerød, A., Zhao, H., Borgan, Ø., Nesland, J.M., Bukholm, I.R.K., Ikdahl, T., Kåresen, R., Børresen-Dale, A.-L. and Jeffrey, S.S. (2007), "TP53 mutation status and gene expression profiles are powerful prognostic markers of breast cancer", *Breast cancer research BCR*, Vol. 9 No. 3, R30.

Lim, E., Palmieri, C. and Tilley, W.D. (2016), "Renewed interest in the progesterone receptor in breast cancer", *British journal of cancer*, Vol. 115 No. 8, pp. 909–911.

Linde, N., Casanova-Acebes, M., Sosa, M.S., Mortha, A., Rahman, A., Farias, E., Harper, K., Tardio, E., Reyes Torres, I., Jones, J., Condeelis, J., Merad, M. and Aguirre-Ghiso, J.A. (2018), "Macrophages orchestrate breast cancer early dissemination and metastasis", *Nature communications*, Vol. 9 No. 1, p. 21.

Linnemann, J.R., Miura, H., Meixner, L.K., Irmler, M., Kloos, U.J., Hirschi, B., Bartsch, H.S., Sass, S., Beckers, J., Theis, F.J., Gabka, C., Sotlar, K. and Scheel, C.H. (2015), "Quantification of regenerative potential in primary human mammary epithelial cells", *Development (Cambridge, England)*, Vol. 142 No. 18, pp. 3239–3251.

Liu, H., Patel, M.R., Prescher, J.A., Patsialou, A., Qian, D., Lin, J., Wen, S., Chang, Y.-F., Bachmann, M.H., Shimono, Y., Dalerba, P., Adorno, M., Lobo, N., Bueno, J., Dirbas, F.M., Goswami, S., Somlo, G., Condeelis, J., Contag, C.H., Gambhir, S.S. and Clarke, M.F. (2010), "Cancer stem cells from human breast tumors are involved in spontaneous metastases in orthotopic mouse models", *Proceedings of the National Academy of Sciences of the United States of America*, Vol. 107 No. 42, pp. 18115–18120.

Liu, S. and Wicha, M.S. (2010), "Targeting breast cancer stem cells", *Journal of clinical oncology official journal of the American Society of Clinical Oncology*, Vol. 28 No. 25, pp. 4006–4012.

Lonardo, F., Ueda, T., Huvos, A.G., Healey, J. and Ladanyi, M. (1997), "p53 and MDM2 alterations in osteosarcomas. Correlation with clinicopathologic features and proliferative rate", *Cancer*, Vol. 79 No. 8, pp. 1541–1547.

Lønning, P.E. (2012), "Poor-prognosis estrogen receptor- positive disease: present and future clinical solutions", *Therapeutic advances in medical oncology*, Vol. 4 No. 3, pp. 127–137.

Louderbough, J.M.V. and Schroeder, J.A. (2011), "Understanding the dual nature of CD44 in breast cancer progression", *Molecular cancer research MCR*, Vol. 9 No. 12, pp. 1573–1586.

Lu, J., McEachern, D., Li, S., Ellis, M.J. and Wang, S. (2016), "Reactivation of p53 by MDM2 Inhibitor MI-77301 for the Treatment of Endocrine-Resistant Breast Cancer", *Molecular cancer therapeutics*, Vol. 15 No. 12, pp. 2887–2893.

Ma, C.X., Cai, S., Li, S., Ryan, C.E., Guo, Z., Schaiff, W.T., Lin, L., Hoog, J., Goiffon, R.J., Prat, A., Aft, R.L., Ellis, M.J. and Piwnica-Worms, H. (2012), "Targeting Chk1 in p53-deficient triple-negative breast cancer is therapeutically beneficial in human-in-mouse tumor models", *The Journal of clinical investigation*, Vol. 122 No. 4, pp. 1541–1552.

Macias, H. and Hinck, L. (2012), "Mammary gland development", *Wiley interdisciplinary reviews. Developmental biology*, Vol. 1 No. 4, pp. 533–557.

Magbanua, M.J.M., Rugo, H.S., Hauranieh, L., Roy, R., Scott, J.H., Lee, J.C., Hsiao, F., Sosa, E.V., Van't Veer, L., Esserman, L.J. and Park, J.W. (2018), "Genomic and expression profiling reveal molecular heterogeneity of disseminated tumor cells in bone marrow of early breast cancer", *NPJ breast cancer*, Vol. 4, p. 31.

Magnifico, A., Albano, L., Campaner, S., Delia, D., Castiglioni, F., Gasparini, P., Sozzi, G., Fontanella, E., Menard, S. and Tagliabue, E. (2009), "Tumor-initiating cells of HER2-positive carcinoma cell lines express the highest oncoprotein levels and are sensitive to trastuzumab", *Clinical cancer research an official journal of the American Association for Cancer Research*, Vol. 15 No. 6, pp. 2010–2021.

Mahmoud, S.M.A., Paish, E.C., Powe, D.G., Macmillan, R.D., Grainge, M.J., Lee, A.H.S., Ellis, I.O. and Green, A.R. (2011), "Tumor-infiltrating CD8+ lymphocytes predict clinical outcome

in breast cancer", *Journal of clinical oncology official journal of the American Society of Clinical Oncology*, Vol. 29 No. 15, pp. 1949–1955.

Malek, A., Catapano, C.V., Czubayko, F. and Aigner, A. (2010), "A sensitive polymerase chain reaction-based method for detection and quantification of metastasis in human xenograft mouse models", *Clinical & experimental metastasis*, Vol. 27 No. 4, pp. 261–271.

Mani, S.A., Guo, W., Liao, M.-J., Eaton, E.N., Ayyanan, A., Zhou, A.Y., Brooks, M., Reinhard, F., Zhang, C.C., Shipitsin, M., Campbell, L.L., Polyak, K., Brisken, C., Yang, J. and Weinberg, R.A. (2008), "The epithelial-mesenchymal transition generates cells with properties of stem cells", *Cell*, Vol. 133 No. 4, pp. 704–715.

Marangoni, E., Lecomte, N., Durand, L., Pinieux, G. de, Decaudin, D., Chomienne, C., Smadja-Joffe, F. and Poupon, M.-F. (2009), "CD44 targeting reduces tumour growth and prevents post-chemotherapy relapse of human breast cancers xenografts", *British journal of cancer*, Vol. 100 No. 6, pp. 918–922.

Marangoni, E., Vincent-Salomon, A., Auger, N., Degeorges, A., Assayag, F., Cremoux, P. de, Plater, L. de, Guyader, C., Pinieux, G. de, Judde, J.-G., Rebucci, M., Tran-Perennou, C., Sastre-Garau, X., Sigal-Zafrani, B., Delattre, O., Diéras, V. and Poupon, M.-F. (2007), "A new model of patient tumor-derived breast cancer xenografts for preclinical assays", *Clinical cancer research an official journal of the American Association for Cancer Research*, Vol. 13 No. 13, pp. 3989–3998.

Mathiesen, R.R., Fjelldal, R., Liestøl, K., Due, E.U., Geigl, J.B., Riethdorf, S., Borgen, E., Rye, I.H., Schneider, I.J., Obenauf, A.C., Mauermann, O., Nilsen, G., Christian Lingjaerde, O., Børresen-Dale, A.-L., Pantel, K., Speicher, M.R., Naume, B. and Baumbusch, L.O. (2012), "High-resolution analyses of copy number changes in disseminated tumor cells of patients with breast cancer", *International journal of cancer*, Vol. 131 No. 4, E405-15.

Meng, S., Li, L., Zhou, M., Jiang, W., Niu, H. and Yang, K. (2018), "Distribution and prognostic value of tumor-infiltrating T cells in breast cancer", *Molecular medicine reports*, Vol. 18 No. 5, pp. 4247–4258.

Minn, A.J., Gupta, G.P., Siegel, P.M., Bos, P.D., Shu, W., Giri, D.D., Viale, A., Olshen, A.B., Gerald, W.L. and Massagué, J. (2005), "Genes that mediate breast cancer metastasis to lung", *Nature*, Vol. 436 No. 7050, pp. 518–524.

Mittal, D., Gubin, M.M., Schreiber, R.D. and Smyth, M.J. (2014), "New insights into cancer immunoediting and its three component phases--elimination, equilibrium and escape", *Current opinion in immunology*, Vol. 27, pp. 16–25.

Nagahara, M., Mimori, K., Kataoka, A., Ishii, H., Tanaka, F., Nakagawa, T., Sato, T., Ono, S., Sugihara, K. and Mori, M. (2010), "Correlated expression of CD47 and SIRPA in bone marrow and in peripheral blood predicts recurrence in breast cancer patients", *Clinical cancer research an official journal of the American Association for Cancer Research*, Vol. 16 No. 18, pp. 4625–4635.

Naor, D., Nedvetzki, S., Golan, I., Melnik, L. and Faitelson, Y. (2002), "CD44 in cancer", *Critical reviews in clinical laboratory sciences*, Vol. 39 No. 6, pp. 527–579.

Naor, D., Wallach-Dayan, S.B., Zahalka, M.A. and Sionov, R.V. (2008), "Involvement of CD44, a molecule with a thousand faces, in cancer dissemination", *Seminars in cancer biology*, Vol. 18 No. 4, pp. 260–267.

Narain, T. and Adcock, L. (2017), *Gene Expression Tests for Women with Early Stage Breast Cancer: A Review of Clinical Utility and Cost-Effectiveness*, Ottawa (ON).

Network, C.G.A. (2012), "Comprehensive molecular portraits of human breast tumours", *Nature*, Vol. 490 No. 7418, pp. 61–70.

Noske, A., Möbus, V., Weber, K., Schmatloch, S., Weichert, W., Köhne, C.-H., Solbach, C., Ingold Heppner, B., Steiger, K., Müller, V., Fasching, P., Karn, T., van Mackelenbergh, M., Marmé, F., Schmitt, W.D., Schem, C., Stickeler, E., Loibl, S. and Denkert, C. (2019), "Relevance of tumour-infiltrating lymphocytes, PD-1 and PD-L1 in patients with high-risk,

nodal-metastasised breast cancer of the German Adjuvant Intergroup Node-positive study", *European journal of cancer (Oxford, England 1990)*, Vol. 114, pp. 76–88.

Oakes, S.R., Vaillant, F., Lim, E., Lee, L., Breslin, K., Feleppa, F., Deb, S., Ritchie, M.E., Takano, E., Ward, T., Fox, S.B., Generali, D., Smyth, G.K., Strasser, A., Huang, D.C.S., Visvader, J.E. and Lindeman, G.J. (2012), "Sensitization of BCL-2-expressing breast tumors to chemotherapy by the BH3 mimetic ABT-737", *Proceedings of the National Academy of Sciences of the United States of America*, Vol. 109 No. 8, pp. 2766–2771.

Olayioye, M.A. (2001), "Update on HER-2 as a target for cancer therapy. Intracellular signaling pathways of ErbB2/HER-2 and family members", *Breast cancer research BCR*, Vol. 3 No. 6, pp. 385–389.

Onitilo, A.A., Engel, J.M., Greenlee, R.T. and Mukesh, B.N. (2009), "Breast cancer subtypes based on ER/PR and Her2 expression. Comparison of clinicopathologic features and survival", *Clinical medicine & research*, Vol. 7 No. 1-2, pp. 4–13.

Orian-Rousseau, V. (2010), "CD44, a therapeutic target for metastasising tumours", *European journal of cancer (Oxford, England 1990)*, Vol. 46 No. 7, pp. 1271–1277.

Orian-Rousseau, V., Chen, L., Sleeman, J.P., Herrlich, P. and Ponta, H. (2002), "CD44 is required for two consecutive steps in HGF/c-Met signaling", *Genes & development*, Vol. 16 No. 23, pp. 3074–3086.

O'Shaughnessy, J. (2005), "Extending survival with chemotherapy in metastatic breast cancer", *The oncologist*, 10 Suppl 3, pp. 20–29.

Osisami, M. and Keller, E.T. (2013), "Mechanisms of Metastatic Tumor Dormancy", *Journal of clinical medicine*, Vol. 2 No. 3, pp. 136–150.

Ozaki, T. and Nakagawara, A. (2011), "Role of p53 in Cell Death and Human Cancers", *Cancers*, Vol. 3 No. 1, pp. 994–1013.

Paget, S. (1889), "THE DISTRIBUTION OF SECONDARY GROWTHS IN CANCER OF THE BREAST", *The Lancet*, Vol. 133 No. 3421, pp. 571–573.

Pantel, K. and Alix-Panabières, C. (2014), "Bone marrow as a reservoir for disseminated tumor cells. A special source for liquid biopsy in cancer patients", *BoneKEy reports*, Vol. 3, p. 584.

Pellacani, D., Tan, S., Lefort, S. and Eaves, C.J. (2019), "Transcriptional regulation of normal human mammary cell heterogeneity and its perturbation in breast cancer", *The EMBO journal*, Vol. 38 No. 14, e100330.

Perlman, R.L. (2016), "Mouse models of human disease. An evolutionary perspective", *Evolution, medicine, and public health*, Vol. 2016 No. 1, pp. 170–176.

Perou, C.M., Sørlie, T., Eisen, M.B., van de Rijn, M., Jeffrey, S.S., Rees, C.A., Pollack, J.R., Ross, D.T., Johnsen, H., Akslen, L.A., Fluge, O., Pergamenschikov, A., Williams, C., Zhu, S.X., Lønning, P.E., Børresen-Dale, A.L., Brown, P.O. and Botstein, D. (2000), "Molecular portraits of human breast tumours", *Nature*, Vol. 406 No. 6797, pp. 747–752.

Petersen, O.W., Høyer, P.E. and van Deurs, B. (1987), "Frequency and distribution of estrogen receptor-positive cells in normal, nonlactating human breast tissue", *Cancer research*, Vol. 47 No. 21, pp. 5748–5751.

Petrillo, L.A., Wolf, D.M., Kapoun, A.M., Wang, N.J., Barczak, A., Xiao, Y., Korkaya, H., Baehner, F., Lewicki, J., Wicha, M., Park, J.W., Spellman, P.T., Gray, J.W., Van't Veer, L. and Esserman, L.J. (2012), "Xenografts faithfully recapitulate breast cancer-specific gene expression patterns of parent primary breast tumors", *Breast cancer research and treatment*, Vol. 135 No. 3, pp. 913–922.

Pfarr, N., Penzel, R., Endris, V., Lier, C., Flechtenmacher, C., Volckmar, A.-L., Kirchner, M., Budczies, J., Leichsenring, J., Herpel, E., Noske, A., Weichert, W., Schneeweiss, A., Schirmacher, P., Sinn, H.-P. and Stenzinger, A. (2017), "Targeted next-generation sequencing enables reliable detection of HER2 (ERBB2) status in breast cancer and provides ancillary information of clinical relevance", *Genes, chromosomes & cancer*, Vol. 56 No. 4, pp. 255–265.

References

Piccart-Gebhart, M.J., Procter, M., Leyland-Jones, B., Goldhirsch, A., Untch, M., Smith, I., Gianni, L., Baselga, J., Bell, R., Jackisch, C., Cameron, D., Dowsett, M., Barrios, C.H., Steger, G., Huang, C.-S., Andersson, M., Inbar, M., Lichinitser, M., Láng, I., Nitz, U., Iwata, H., Thomssen, C., Lohrisch, C., Suter, T.M., Rüschoff, J., Suto, T., Greatorex, V., Ward, C., Straehle, C., McFadden, E., Dolci, M.S. and Gelber, R.D. (2005), "Trastuzumab after adjuvant chemotherapy in HER2-positive breast cancer", *The New England journal of medicine*, Vol. 353 No. 16, pp. 1659–1672.

Polyak, K. and Weinberg, R.A. (2009), "Transitions between epithelial and mesenchymal states. Acquisition of malignant and stem cell traits", *Nature reviews. Cancer*, Vol. 9 No. 4, pp. 265–273.

Polzer, B., Medoro, G., Pasch, S., Fontana, F., Zorzino, L., Pestka, A., Andergassen, U., Meier-Stiegen, F., Czyz, Z.T., Alberter, B., Treitschke, S., Schamberger, T., Sergio, M., Bregola, G., Doffini, A., Gianni, S., Calanca, A., Signorini, G., Bolognesi, C., Hartmann, A., Fasching, P.A., Sandri, M.T., Rack, B., Fehm, T., Giorgini, G., Manaresi, N. and Klein, C.A. (2014), "Molecular profiling of single circulating tumor cells with diagnostic intention", *EMBO molecular medicine*, Vol. 6 No. 11, pp. 1371–1386.

Pruneri, G., Lazzeroni, M., Bagnardi, V., Tiburzio, G.B., Rotmensz, N., DeCensi, A., Guerrieri-Gonzaga, A., Vingiani, A., Curigliano, G., Zurrida, S., Bassi, F., Salgado, R., van den Eynden, G., Loi, S., Denkert, C., Bonanni, B. and Viale, G. (2017), "The prevalence and clinical relevance of tumor-infiltrating lymphocytes (TILs) in ductal carcinoma in situ of the breast", *Annals of oncology official journal of the European Society for Medical Oncology*, Vol. 28 No. 2, pp. 321–328.

Quadros, R.M., Poluektova, L.Y. and Gurumurthy, C.B. (2016), "Simple and reliable genotyping protocol for mouse Prkdc(SCID) mutation", *Journal of immunological methods*, Vol. 431, pp. 60–62.

Ramakrishnan, R., Khan, S.A. and Badve, S. (2002), "Morphological changes in breast tissue with menstrual cycle", *Modern pathology an official journal of the United States and Canadian Academy of Pathology, Inc*, Vol. 15 No. 12, pp. 1348–1356.

Remmele, W. and Stegner, H.E. (1987), "Vorschlag zur einheitlichen Definition eines Immunreaktiven Score (IRS) für den immunhistochemischen Ostrogenrezeptor-Nachweis (ER-ICA) im Mammakarzinomgewebe", *Der Pathologe*, Vol. 8 No. 3, pp. 138–140.

Reyal, F., Guyader, C., Decraene, C., Lucchesi, C., Auger, N., Assayag, F., Plater, L. de, Gentien, D., Poupon, M.-F., Cottu, P., Cremoux, P. de, Gestraud, P., Vincent-Salomon, A., Fontaine, J.-J., Roman-Roman, S., Delattre, O., Decaudin, D. and Marangoni, E. (2012), "Molecular profiling of patient-derived breast cancer xenografts", *Breast cancer research BCR*, Vol. 14 No. 1, R11.

Rom-Jurek, E.-M., Kirchhammer, N., Ugocsai, P., Ortmann, O., Wege, A.K. and Brockhoff, G. (2018), "Regulation of Programmed Death Ligand 1 (PD-L1) Expression in Breast Cancer Cell Lines In Vitro and in Immunodeficient and Humanized Tumor Mice", *International journal of molecular sciences*, Vol. 19 No. 2.

Rouzier, R., Perou, C.M., Symmans, W.F., Ibrahim, N., Cristofanilli, M., Anderson, K., Hess, K.R., Stec, J., Ayers, M., Wagner, P., Morandi, P., Fan, C., Rabiul, I., Ross, J.S., Hortobagyi, G.N. and Pusztai, L. (2005), "Breast cancer molecular subtypes respond differently to preoperative chemotherapy", *Clinical cancer research an official journal of the American Association for Cancer Research*, Vol. 11 No. 16, pp. 5678–5685.

Salgado, R., Denkert, C., Demaria, S., Sirtaine, N., Klauschen, F., Pruneri, G., Wienert, S., van den Eynden, G., Baehner, F.L., Penault-Llorca, F., Perez, E.A., Thompson, E.A., Symmans, W.F., Richardson, A.L., Brock, J., Criscitiello, C., Bailey, H., Ignatiadis, M., Floris, G., Sparano, J., Kos, Z., Nielsen, T., Rimm, D.L., Allison, K.H., Reis-Filho, J.S., Loibl, S., Sotiriou, C., Viale, G., Badve, S., Adams, S., Willard-Gallo, K. and Loi, S. (2015), "The evaluation of tumor-infiltrating lymphocytes (TILs) in breast cancer. Recommendations by

an International TILs Working Group 2014", *Annals of oncology official journal of the European Society for Medical Oncology*, Vol. 26 No. 2, pp. 259–271.

Schmidt-Kittler, O., Ragg, T., Daskalakis, A., Granzow, M., Ahr, A., Blankenstein, T.J.F., Kaufmann, M., Diebold, J., Arnholdt, H., Muller, P., Bischoff, J., Harich, D., Schlimok, G., Riethmuller, G., Eils, R. and Klein, C.A. (2003), "From latent disseminated cells to overt metastasis. Genetic analysis of systemic breast cancer progression", *Proceedings of the National Academy of Sciences of the United States of America*, Vol. 100 No. 13, pp. 7737–7742.

Sheridan, C., Kishimoto, H., Fuchs, R.K., Mehrotra, S., Bhat-Nakshatri, P., Turner, C.H., Goulet, R., Badve, S. and Nakshatri, H. (2006), "CD44+/CD24- breast cancer cells exhibit enhanced invasive properties. An early step necessary for metastasis", *Breast cancer research BCR*, Vol. 8 No. 5, R59.

Shi, D. and Gu, W. (2012), "Dual Roles of MDM2 in the Regulation of p53. Ubiquitination Dependent and Ubiquitination Independent Mechanisms of MDM2 Repression of p53 Activity", *Genes & cancer*, Vol. 3 No. 3-4, pp. 240–248.

Shultz, L.D., Lyons, B.L., Burzenski, L.M., Gott, B., Chen, X., Chaleff, S., Kotb, M., Gillies, S.D., King, M., Mangada, J., Greiner, D.L. and Handgretinger, R. (2005), "Human lymphoid and myeloid cell development in NOD/LtSz-scid IL2R gamma null mice engrafted with mobilized human hemopoietic stem cells", *Journal of immunology (Baltimore, Md. 1950)*, Vol. 174 No. 10, pp. 6477–6489.

Simpson, C.D., Anyiwe, K. and Schimmer, A.D. (2008), "Anoikis resistance and tumor metastasis", *Cancer letters*, Vol. 272 No. 2, pp. 177–185.

Slamon, D.J., Clark, G.M., Wong, S.G., Levin, W.J., Ullrich, A. and McGuire, W.L. (1987), "Human breast cancer. Correlation of relapse and survival with amplification of the HER-2/neu oncogene", *Science (New York, N.Y.)*, Vol. 235 No. 4785, pp. 177–182.

Smith, S.C., Oxford, G., Wu, Z., Nitz, M.D., Conaway, M., Frierson, H.F., Hampton, G. and Theodorescu, D. (2006), "The metastasis-associated gene CD24 is regulated by Ral GTPase and is a mediator of cell proliferation and survival in human cancer", *Cancer research*, Vol. 66 No. 4, pp. 1917–1922.

Sørlie, T., Perou, C.M., Tibshirani, R., Aas, T., Geisler, S., Johnsen, H., Hastie, T., Eisen, M.B., van de Rijn, M., Jeffrey, S.S., Thorsen, T., Quist, H., Matese, J.C., Brown, P.O., Botstein, D., Lønning, P.E. and Børresen-Dale, A.L. (2001), "Gene expression patterns of breast carcinomas distinguish tumor subclasses with clinical implications", *Proceedings of the National Academy of Sciences of the United States of America*, Vol. 98 No. 19, pp. 10869–10874.

Soysal, S.D., Muenst, S., Barbie, T., Fleming, T., Gao, F., Spizzo, G., Oertli, D., Viehl, C.T., Obermann, E.C. and Gillanders, W.E. (2013), "EpCAM expression varies significantly and is differentially associated with prognosis in the luminal B HER2(+), basal-like, and HER2 intrinsic subtypes of breast cancer", *British journal of cancer*, Vol. 108 No. 7, pp. 1480–1487.

Stad, R., Little, N.A., Xirodimas, D.P., Frenk, R., van der Eb, A.J., Lane, D.P., Saville, M.K. and Jochemsen, A.G. (2001), "Mdmx stabilizes p53 and Mdm2 via two distinct mechanisms", *EMBO reports*, Vol. 2 No. 11, pp. 1029–1034.

Stanton, S.E., Adams, S. and Disis, M.L. (2016), "Variation in the Incidence and Magnitude of Tumor-Infiltrating Lymphocytes in Breast Cancer Subtypes. A Systematic Review", *JAMA oncology*, Vol. 2 No. 10, pp. 1354–1360.

Stoecklein, N.H., Erbersdobler, A., Schmidt-Kittler, O., Diebold, J., Schardt, J.A., Izbicki, J.R. and Klein, C.A. (2002), "SCOMP Is Superior to Degenerated Oligonucleotide Primed-Polymerase Chain Reaction for Global Amplification of Minute Amounts of DNA from Microdissected Archival Tissue Samples", *The American Journal of Pathology*, Vol. 161 No. 1, pp. 43–51.

References

Stoecklein, N.H., Hosch, S.B., Bezler, M., Stern, F., Hartmann, C.H., Vay, C., Siegmund, A., Scheunemann, P., Schurr, P., Knoefel, W.T., Verde, P.E., Reichelt, U., Erbersdobler, A., Grau, R., Ullrich, A., Izbicki, J.R. and Klein, C.A. (2008), "Direct genetic analysis of single disseminated cancer cells for prediction of outcome and therapy selection in esophageal cancer", *Cancer cell*, Vol. 13 No. 5, pp. 441–453.

Stovgaard, E.S., Dyhl-Polk, A., Roslind, A., Balslev, E. and Nielsen, D. (2019), "PD-L1 expression in breast cancer. Expression in subtypes and prognostic significance: a systematic review", *Breast cancer research and treatment*, Vol. 174 No. 3, pp. 571–584.

Su, S., Liao, J., Liu, J., Di Huang, He, C., Chen, F., Yang, L., Wu, W., Chen, J., Lin, L., Zeng, Y., Ouyang, N., Cui, X., Yao, H., Su, F., Huang, J.-D., Lieberman, J., Liu, Q. and Song, E. (2017), "Blocking the recruitment of naive CD4+ T cells reverses immunosuppression in breast cancer", *Cell research*, Vol. 27 No. 4, pp. 461–482.

Swetzig, W.M., Wang, J. and Das, G.M. (2016), "Estrogen receptor alpha (ERα/ESR1) mediates the p53-independent overexpression of MDM4/MDMX and MDM2 in human breast cancer", *Oncotarget*, Vol. 7 No. 13, pp. 16049–16069.

Tomayko, M.M. and Reynolds, C.P. (1989), "Determination of subcutaneous tumor size in athymic (nude) mice", *Cancer chemotherapy and pharmacology*, Vol. 24 No. 3, pp. 148–154.

Toole, B.P. (2009), "Hyaluronan-CD44 Interactions in Cancer. Paradoxes and Possibilities", *Clinical cancer research an official journal of the American Association for Cancer Research*, Vol. 15 No. 24, pp. 7462–7468.

Trusolino, L., Bertotti, A. and Comoglio, P.M. (2010), "MET signalling. Principles and functions in development, organ regeneration and cancer", *Nature reviews. Molecular cell biology*, Vol. 11 No. 12, pp. 834–848.

Vaillant, F., Merino, D., Lee, L., Breslin, K., Pal, B., Ritchie, M.E., Smyth, G.K., Christie, M., Phillipson, L.J., Burns, C.J., Mann, G.B., Visvader, J.E. and Lindeman, G.J. (2013), "Targeting BCL-2 with the BH3 mimetic ABT-199 in estrogen receptor-positive breast cancer", *Cancer cell*, Vol. 24 No. 1, pp. 120–129.

Valastyan, S. and Weinberg, R.A. (2011), "Tumor metastasis. Molecular insights and evolving paradigms", *Cell*, Vol. 147 No. 2, pp. 275–292.

Valdez, K.E., Fan, F., Smith, W., Allred, D.C., Medina, D. and Behbod, F. (2011), "Human primary ductal carcinoma in situ (DCIS) subtype-specific pathology is preserved in a mouse intraductal (MIND) xenograft model", *The Journal of pathology*, Vol. 225 No. 4, pp. 565–573.

van de Wouw, A.J., Janssen-Heijnen, M.L.G., Coebergh, J.W.W. and Hillen, H.F.P. (2002), "Epidemiology of unknown primary tumours; incidence and population-based survival of 1285 patients in Southeast Netherlands, 1984–1992", *European Journal of Cancer*, Vol. 38 No. 3, pp. 409–413.

Visonneau, S., Cesano, A., Torosian, M.H., Miller, E.J. and Santoli, D. (1998), "Growth characteristics and metastatic properties of human breast cancer xenografts in immunodeficient mice", *The American Journal of Pathology*, Vol. 152 No. 5, pp. 1299–1311.

Visvader, J.E. and Stingl, J. (2014), "Mammary stem cells and the differentiation hierarchy. Current status and perspectives", *Genes & development*, Vol. 28 No. 11, pp. 1143–1158.

Wallwiener, M., Hartkopf, A.D., Baccelli, I., Riethdorf, S., Schott, S., Pantel, K., Marmé, F., Sohn, C., Trumpp, A., Rack, B., Aktas, B., Solomayer, E.-F., Müller, V., Janni, W., Schneeweiss, A. and Fehm, T.N. (2013), "The prognostic impact of circulating tumor cells in subtypes of metastatic breast cancer", *Breast cancer research and treatment*, Vol. 137 No. 2, pp. 503–510.

References

Wang, C.S., Goulet, F., Tremblay, N., Germain, L., Auger, F. and Têtu, B. (2001), "Selective culture of epithelial cells from primary breast carcinomas using irradiated 3T3 cells as feeder layer", *Pathology, research and practice*, Vol. 197 No. 3, pp. 175–181.

Wang, K., Li, M. and Hakonarson, H. (2010), "ANNOVAR. Functional annotation of genetic variants from high-throughput sequencing data", *Nucleic acids research*, Vol. 38 No. 16, e164.

Wang, M., Yao, L.-C., Cheng, M., Cai, D., Martinek, J., Pan, C.-X., Shi, W., Ma, A.-H., Vere White, R.W. de, Airhart, S., Liu, E.T., Banchereau, J., Brehm, M.A., Greiner, D.L., Shultz, L.D., Palucka, K. and Keck, J.G. (2018a), "Humanized mice in studying efficacy and mechanisms of PD-1-targeted cancer immunotherapy", *FASEB journal official publication of the Federation of American Societies for Experimental Biology*, Vol. 32 No. 3, pp. 1537–1549.

Wang, X., Teng, F., Kong, L. and Yu, J. (2016), "PD-L1 expression in human cancers and its association with clinical outcomes", *OncoTargets and therapy*, Vol. 9, pp. 5023–5039.

Wang, Z., Zhao, K., Hackert, T. and Zöller, M. (2018b), "CD44/CD44v6 a Reliable Companion in Cancer-Initiating Cell Maintenance and Tumor Progression", *Frontiers in cell and developmental biology*, Vol. 6, p. 97.

Watanabe, K., Ueno, M., Kamiya, D., Nishiyama, A., Matsumura, M., Wataya, T., Takahashi, J.B., Nishikawa, S., Nishikawa, S.-i., Muguruma, K. and Sasai, Y. (2007), "A ROCK inhibitor permits survival of dissociated human embryonic stem cells", *Nature biotechnology*, Vol. 25 No. 6, pp. 681–686.

Wege, A.K. (2018), "Humanized Mouse Models for the Preclinical Assessment of Cancer Immunotherapy", *BioDrugs clinical immunotherapeutics, biopharmaceuticals and gene therapy*, Vol. 32 No. 3, pp. 245–266.

Wege, A.K., Ernst, W., Eckl, J., Frankenberger, B., Vollmann-Zwerenz, A., Männel, D.N., Ortmann, O., Kroemer, A. and Brockhoff, G. (2011), "Humanized tumor mice--a new model to study and manipulate the immune response in advanced cancer therapy", *International journal of cancer*, Vol. 129 No. 9, pp. 2194–2206.

Weilbaecher, K.N., Guise, T.A. and McCauley, L.K. (2011), "Cancer to bone. A fatal attraction", *Nature reviews. Cancer*, Vol. 11 No. 6, pp. 411–425.

Werner, L.R., Huang, S., Francis, D.M., Armstrong, E.A., Ma, F., Li, C., Iyer, G., Canon, J. and Harari, P.M. (2015), "Small Molecule Inhibition of MDM2-p53 Interaction Augments Radiation Response in Human Tumors", *Molecular cancer therapeutics*, Vol. 14 No. 9, pp. 1994–2003.

Whittle, J.R., Lewis, M.T., Lindeman, G.J. and Visvader, J.E. (2015), "Patient-derived xenograft models of breast cancer and their predictive power", *Breast cancer research BCR*, Vol. 17, p. 17.

Wiedswang, G., Borgen, E., Kåresen, R., Kvalheim, G., Nesland, J.M., Qvist, H., Schlichting, E., Sauer, T., Janbu, J., Harbitz, T. and Naume, B. (2003), "Detection of isolated tumor cells in bone marrow is an independent prognostic factor in breast cancer", *Journal of clinical oncology official journal of the American Society of Clinical Oncology*, Vol. 21 No. 18, pp. 3469–3478.

Williams, K., Motiani, K., Giridhar, P.V. and Kasper, S. (2013), "CD44 integrates signaling in normal stem cell, cancer stem cell and (pre)metastatic niches", *Experimental biology and medicine (Maywood, N.J.)*, Vol. 238 No. 3, pp. 324–338.

Wu, Q., Li, J., Zhu, S., Wu, J., Chen, C., Liu, Q., Wei, W., Zhang, Y. and Sun, S. (2017), "Breast cancer subtypes predict the preferential site of distant metastases. A SEER based study", *Oncotarget*, Vol. 8 No. 17, pp. 27990–27996.

Yeong, J., Lim, J.C.T., Lee, B., Li, H., Ong, C.C.H., Thike, A.A., Yeap, W.H., Yang, Y., Lim, A.Y.H., Tay, T.K.Y., Liu, J., Wong, S.-C., Chen, J., Lim, E.H., Iqbal, J., Dent, R., Newell, E.W. and Tan, P.H. (2019), "Prognostic value of CD8 + PD-1+ immune infiltrates and

PDCD1 gene expression in triple negative breast cancer", *Journal for immunotherapy of cancer*, Vol. 7 No. 1, p. 34.

Yu, Q., Li, Y., Mu, K., Li, Z., Meng, Q., Wu, X., Wang, Y. and Li, L. (2014), "Amplification of Mdmx and overexpression of MDM2 contribute to mammary carcinogenesis by substituting for p53 mutations", *Diagnostic pathology*, Vol. 9, p. 71.

Zhang, X., Claerhout, S., Prat, A., Dobrolecki, L.E., Petrovic, I., Lai, Q., Landis, M.D., Wiechmann, L., Schiff, R., Giuliano, M., Wong, H., Fuqua, S.W., Contreras, A., Gutierrez, C., Huang, J., Mao, S., Pavlick, A.C., Froehlich, A.M., Wu, M.-F., Tsimelzon, A., Hilsenbeck, S.G., Chen, E.S., Zuloaga, P., Shaw, C.A., Rimawi, M.F., Perou, C.M., Mills, G.B., Chang, J.C. and Lewis, M.T. (2013), "A renewable tissue resource of phenotypically stable, biologically and ethnically diverse, patient-derived human breast cancer xenograft models", *Cancer research*, Vol. 73 No. 15, pp. 4885–4897.

Zhang, X. and Lewis, M.T. (2013), "Establishment of Patient-Derived Xenograft (PDX) Models of Human Breast Cancer", *Current protocols in mouse biology*, Vol. 3 No. 1, pp. 21–29.

Zöller, M. (2011), "CD44. Can a cancer-initiating cell profit from an abundantly expressed molecule?", *Nature reviews. Cancer*, Vol. 11 No. 4, pp. 254–267.

List of abbreviations

Amp	Amplification
ANOVA	Analysis of variance
BC	Breast cancer
BCA	Bicinchoninic acid
BM	Bone marrow
Bpe	Pleural effusion
CDX	Cell line derived Xenograft
CK	Cytokeratin
CK18	Cytokeratin 18
CSC	Cancer Stem Cell
CTC	Circulating tumor cells
Ctrl	Control
DFS	Disease-free survival
DTC	Disseminated Tumor Cells
EpCAM	Epithelial cell adhesion molecule
ER	Estrogen receptor
F HTM	Humanized tumor mice from the cooperation with France
F TM	Tumor mice from the cooperation with France
FACS	Fluorescence-activated cell scanning analysis
FAK	Focal adhesion kinase
GvHD	Graft versus host disease
H	Hour
HE	Hematoxylin and Eosin Staining
Her2	Human epidermal growth factor receptor 2
HR	Hormone receptor-positive
HTM	Humanized Tumor Mouse (mice)
i.p.	Intraperitoneal
IHC	Immunohistochemistry
KD	Knockdown
kDa	Kilodalton
LN	Lymph node

List of abbreviations

MDM2	MDM2
mfp	Mammary fat pad
MIC	Metastasis initiating cells
Min	Minute
MNC	Mononuclear cells
NSG	NOD-scid IL2Rγnull
NT	Non-target
OS	Overall survival
PD-1	Programmed Death Receptor 1
PD-L1	Programmed Death- Ligand 1
PDX	Patient-derived Xenograft
pFAK	Phosphorylated focal adhesion kinase
PR	Progesterone
PVDF	Polyvinylidene Difluoride
RECON	Reconstitution
RT	Room temperature
s.c.	Subcutaneous
SCF	Stem-cell FACS
s	Second
SPF	S-Phase Fraction
TCF	T-cell FACS
TEMRA	Effector memory T-cells re-expressing CD45RA
TIL	Tumor-infiltrating lymphocytes
TM	Tumor Mouse (mice)
WGA	Whole-genome amplification
WT	Wildtype

List of tables

Table 1: Overview of generated breast cancer PDX models....24
Table 2: List of the amount of anesthesia and antagonist required for the mouse according to the bodyweight....39
Table 3: Transplantation methods for the successfully established PDX models....41
Table 4: Antibody Staining....44
Table 5: Isotype Control....44
Table 6: HuMo PCR Master mix....47
Table 7: HuMo PCR Primer....47
Table 8: RT-PCR program....47
Table 9: Calculation of the standard curve for HuMo PCR....49
Table 10: PD-L1 Score adapted from (Brockhoff *et al.*, 2018)....51
Table 11: Used cell lines and their corresponding media....52
Table 12: Primary antibody....54
Table 13: Secondary Antibody....55
Table 14: Primers for quality PCR of WGA product....60
Table 15: Mastermix for quality PCR of WGA product....60
Table 16: PCR program for quality control of the WGA product....60
Table 17: Mastermix for reamplification of DNA....61
Table 18: PCR program for Reamplification of DNA....61
Table 19: Genes and exons included in the breast cancer panel.....63
Table 20: Overview of all patient samples and the corresponding pathological information, engraftment success, and the survival and relapse status of the patient....68
Table 21: The Success rate of engrafted PDX models....79
Table 22: Number of animals with successful tumor engraftment of different tumors from Caritas Hospital St. Josef Regensburg....80
Table 23: Number of animals with successful tumor engraftment of different Luminal B PDX tumors from different cooperation partners....81
Table 24: Percentage of human tissue in tumors isolated from all TM at the end of the experiment after several retransplantations....81
Table 25: Data from the panel sequencing of all TM tumors analyzed by our cooperation partner in Munich (Nicole Pfarr)....86
Table 26: Summary of panel sequencing results and IHC, FISH and the corresponding FISH ratios and gene doses in the different Luminal B PDX models....87
Table 27: Summary of the metastatic potential of TM and HTM Luminal B breast cancer PDX models....102

List of figures

Figure 1: Anatomy of the human mammary gland 12
Figure 2: Schematic description of the development of distant metastases 16
Figure 3: Graphic presentation of the different layers before and after the density gradient centrifugation....36
Figure 4: Schematic description of the workflow with Luminal B tumors in TM and HTM. 39
Figure 5: Schematic description of tumor passaging from TM to HTM. 42
Figure 6: Example of apoptosis assay analyzed by flow cytometry....46
Figure 7: Schematic description of the different assay and analysis after an MDM2 knockdown or an AMG232 inhibition 56
Figure 8: Schematic description of siRNA knockdown procedure 57
Figure 9: Schematic description of the AMG232 treatment procedure 57
Figure 10: Representative image of the gating strategy for SCF on tumor TM CTC 70
Figure 11: Representative image of the FACS gating strategy for SCF MIC subpopulation. .71
Figure 12 Stem cell marker expression in Luminal breast cancer. 72
Figure 13: Representative gating strategy of RECON to determine the TILs 73
Figure 14: TIL analysis of primary patient tumors 74
Figure 15: Representative image of the gating strategy that was used for T-cell subset identification 74
Figure 16: T-cell subset analysis of TILs in primary Luminal B tumors....75
Figure 17: SCF and RECON analysis comparing solid Luminal B tumors with Luminal B effusions....76
Figure 18: T-cell subpopulations in Luminal B solid tumors compared to Luminal B metastases....78
Figure 19: Representative images of the primary tumor cell culture....79
Figure 20: Representative images of the primary tumor compared to TM tumor engraftment and further retransplantations....82
Figure 21: Representative images of intrinsic molecular features of all engrafted Luminal B tumors in the TM and the metastatic sites of TM AB model 84
Figure 22: Representative Western Blot of p53 and MDM2 of all Luminal B PDX models 88
Figure 23: Effect of an MDM2 amplification in TM tumors....90
Figure 24: Flow cytometric analysis on stem cell markers comparing TM MDM2 WT with TM MDM2 Amp tumors 92
Figure 25: Lung metastases in TM MDM2 WT compared with TM MDM2 Amp animals....93
Figure 26: Flow cytometric analysis of lung metastases compared with the corresponding tumor in TM MDM2 Amp animals. 94
Figure 27: Occurrence of immune cells in the spleen and the tumor of HTM 95
Figure 28: Effect of an MDM2 amplification in HTM 97
Figure 29: Lung metastases occurrence and MIC population in HTM MDM2 Amp and HTM MDM2 Amp animals and the influence of the human immune system on lung metastases in TM MDM2 Amp versus HTM MDM2 Amp animals....98
Figure 30: DTCs in the bone marrow Luminal B breast cancer PDX models 99
Figure 31: Clustering of DTCs and tumors cells isolated from HTM P and TM P 101
Figure 32: *In vivo* PD-L1 expression in tumors of Luminal B HTM 103
Figure 33: Programmed death ligand 1 (PD-L1) expression on different breast cancer cell lines....105

List of figures

Figure 34: Effects of MDM2 knockdown in ZR-75-1 cells on apoptosis, S-phase fraction, wound healing and cell number 107
Figure 35 AMG232 treatment effects of ZR-75-1 on apoptosis, SPF, wound healing and cell number 109
Figure 36: Effects of MDM2 knockdown on protein levels 111

Acknowledgements

Zunächst möchte ich mich vor allem bei meiner Betreuerin Prof. Dr. Anja-Katrin Wege bedanken. Liebe Anja, vielen Dank, dass du mir dies ermöglicht hast. Danke für deine wissenschaftliche Unterstützung, deine konstruktive Kritik und deine Förderung zu jeder Zeit und die schöne Zeit beim „humanized mouse workshop“. Du hast mit deiner Betreuung als meine 1. Mentorin einen großen Beitrag zu meiner wissenschaftlichen und auch persönlichen Entwicklung geleistet.

Zudem geht ein großer Dank an Prof Dr. Gero Brockhoff. Danke Gero, für deine hilfreichen Ratschläge, der Unterstützung meiner in vitro Experimente und, dass du mir stets mit Rat und Tat zur Seite gestanden hast.

Darüber hinaus geht mein Dank vor allem an mein Mentorat Herrn Prof. Dr. Olaf Ortmann, Herrn Prof. Dr. Uwe Ritter und Herrn Prof. Dr. Tobias Pukrop. Vielen Dank für die konstruktive und hilfreiche Kritik und die Vorschläge bei meinen Zwischenberichten. Das hat meine Dissertation und mein weiteres wissenschaftliches Vorgehen immer vorangebracht.

Von ganzem Herzen möchte ich auch meinem „TA-TEAM“ danken. Liebe Teresa, liebe Maria, lieber Gerhard, liebe Anita, liebe Marietta, danke für all eure Unterstützung, das füreinander Dasein auch in schwierigen Situationen, das meistern aller Probleme und den tollen Zusammenhalt. Danke auch für die schöne Zeit, und dass ich so viel von euch lernen konnte und jetzt ein wahrer Excellisten Profi bin. Danke auch für die tollen Stunden, die wir außerhalb des Labors verbracht haben. Es war eine unvergesslich schöne Zeit mit euch!!

Zudem möchte ich mich auch herzlichst bei Peter Ugocsai bedanken – für die unkomplizierten Wege und Lösungen das „Schnabelnurblut“ zu organisieren und das stetige Mitdenken in wissenschaftlichen Fragestellungen.

Danke auch an das ganze Team der Pathologie, Flo, Frau Evert, Frau Utpatel, Bettina, Lisa, Rudi, Heiko, Claudia, Brigitte, Rudi, Silvia, Monika, Antonio, Ingrid. Es war eine wunderschöne Zeit bei euch. Und alle waren immer herzlich, hilfsbereit und kollegial. Ich habe mich sehr wohl gefühlt bei euch.

Ein großes Dankeschön geht auch an all meine Kooperationspartner besonders aus der AG Klein. Danke Christoph Irlbeck für die super Zusammenarbeit, die tolle Zeit beim Zellen picken, wenn wir wieder Metal Bands gehört haben. Danke an Tom, Ana, Courtney, Mani und Christian für die tollen Gespräche beim Mittagessen und die

Acknowledgements

Unterstützung bei allen Experimenten in eurem Labor, wenn ich mal wieder was nicht gefunden habe.

Bedanken möchte ich mich auch bei meinen Kooperationspartnern Prof. Trumpp, Massimo und Corinna in Heidelberg (HiSTEM), Wilko Weichert und Nicole Pfarr in München (TUM) und Elisabetta Marangoni in Frankreich (Institut Curie).

Zudem geht mein Dank an die Masterminds Simone und Katrin aus der Nephro. Ihr habt es mir immer ermöglicht bei euch noch zu mikroskopieren und Paraffinschnitte anzufertigen und nicht zu vergessen die schönen Abende, die wir abseits der Arbeit beim The Thai verbracht haben.

Ein großes Dankeschön geht auch an meine überaus hilfsbereiten und lieben Freunde und Begleiter in meinem Studium und auch darüber hinaus: Richie, Rogi, Kathy, Mone, Dana, Kathi, Babs, Carolin, Joanna, Stefan, Sebastian, Julia, Kicki und Dani, Eva und Xaver, Manuela, David und alle die ich hier an dieser Stelle nicht erwähnt habe. Ohne euch hätte ich das alles nicht geschafft. Ihr habt mich in allen Situationen unterstützt und mit Eurer Freundschaft einen großen Beitrag zum Gelingen dieser Arbeit geleistet.

Das Beste kommt zum Schluss!! Der größte Dank gebührt meiner Mama, meinem Papa und meinem Bruder Constantin. Danke für eure bedingungslose Unterstützung und Motivation. Ich habe es euch nicht immer einfach gemacht, doch Ihr habt es für mich einfacher gemacht. Mama ohne dich hätte ich das nicht geschafft. Du warst immer für mich und meine Kinder da und hast mich aus allen meinen Notlagen manövriert. Ohne dich wäre das undenkbar gewesen. Papa, ohne deine Unterstützung hätte das niemals funktioniert. Soviel Verständnis und Unterstützung, wie ich es von euch bekommen habe ist ein wahres Geschenk.

Meine lieben Kinder, Jonathan und Nicolas, mein lieber Ben. Danke für euer Verständnis, für all die Launen, die ihr ertragen musstet. Danke für all eure Liebe, die es mir immer wieder leichter gemacht hat das Ganze durchzustehen. Ben-Bär, danke für die tollen wissenschaftlichen Gespräche bei einem Glas Rotwein, deine Geduld und deine Ideen. Du hast mich immer inspiriert und motiviert. Du bist das beste was mir je passiert ist. Oder einfacher gesagt: Ein Leben ohne „Bär“ ist möglich, aber sinnlos!

Und natürlich: Danke lieber Kater Elvis - du hast mich fellnasig mit deinem Kopf auf meiner Tastatur bis zuletzt unterstützt und bist jetzt auch verantwortlich für alle sinnfreien Bucxhstaben oder Rechtschreibfähler in dieser Doktorarbeit.

Selbständigkeitserklärung

“Ich, *Rom-Jurek, Eva-Maria;* geboren am 20.08.1986 in *Weiden i. d. Opf.*, erkläre hiermit, dass ich die vorliegende Arbeit ohne unzulässige Hilfe Dritter und ohne Benutzung anderer als der angegebenen Hilfsmittel angefertigt habe.
Die aus anderen Quellen direkt oder indirekt übernommenen Daten und Konzepte sind unter Angabe der Quelle gekennzeichnet. Insbesondere habe ich nicht die entgeltliche Hilfe von Vermittlungs- bzw. Beratungsdiensten (Promotionsberater oder andere Personen) in Anspruch genommen.
Die Arbeit wurde bisher weder im In- noch im Ausland in gleicher oder ähnlicher Form einer anderen Prüfungsbehörde vorgelegt.

Ort, Datum

eigenhändige Unterschrift
des Promovenden

Curriculum vitae

Education and Degree

2015- 2020 Ph.D. in Gynecology and Obstetrics (Prof. Dr. Olaf Ortmann, Supervisor: Prof. Dr. Anja-Katrin Wege) (Experimental Immunology)

‘Evaluation of geno- and phenotypic alterations in Luminal B breast cancer using tumor mice (TM) and humanized tumor mice (HTM)’

2012 - 2015 Master of Science, Biology, University of Regensburg

Master thesis at the Department of Nephrology, University Medical Center Regensburg

2008 - 2012 Bachelor of Science, Biology, University of Regensburg

Bachelor thesis at the Department of Neurobiology, University of Regensburg

Awards and Stipends

10/2017 EMBL Corporate Partnership Fee Waiver for attendance of “Humanized mice in biomedical research” workshop (Travel Grant)

06/2017 Award for the best talk (RIGeL Summer School, Hirschberg)

06/2017 Award for the most scientific questions (RIGeL Summer School, Hirschberg)

10/2016 Award for the most scientific questions (RIGeL Summer School, Nürnberg)